

# **Moistube Irrigation Characterisation and Yield Response of Canola (*Brassica napus*) Under Varied Moistube Irrigation**

**Tinashe Lindel Dirwai**

**215081795**

Submitted in fulfilment of the requirements for the degree of PhD

Bioresources Engineering

School of Engineering

University of KwaZulu-Natal

Pietermaritzburg

May 2021

## **PREFACE**

The research contained in this thesis was completed by the candidate while based in the Discipline of Bioresources Engineering, School of Engineering of the College of Agriculture, Engineering and Science, University of KwaZulu-Natal, Pietermaritzburg, South Africa.

The contents of this work have not been submitted in any form to another university and, except where the work of others is acknowledged in the text, the results reported are due to investigations by the candidate.

---

Dr Aidan Senzanje

Date:

---

Prof Tafadzwanashe Mabhaudhi

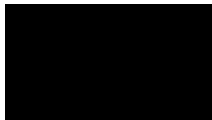
Date:

## DECLARATION OF PLAGIARISM

I, Tinashe Lindel Dirwai, declare that

1. The research reported in this thesis, except where otherwise indicated, is my original research.
2. This thesis has not been submitted for any degree or examination at any other university.
3. This thesis does not contain other persons' data, pictures, graphs or other information, unless specifically acknowledged as being sourced from other persons.
4. This thesis does not contain other persons' writing, unless specifically acknowledged as being sourced from other researchers. Where other written sources have been quoted, then:
  - a. Their words have been re-written but the general information attributed to them has been referenced
  - b. Where their exact words have been used, then their writing has been placed in italics and inside quotation marks, and referenced.

This thesis does not contain text, graphics or tables copied and pasted from the Internet, unless specifically acknowledged, and the source being detailed in the thesis and in the References sections



---

Tinashe Lindel Dirwai

Date: 25 May 2021

## DECLARATION OF PUBLICATIONS

The following are the list of publications in this thesis.

- Dirwai, TL, Mabhaudhi, T, Kanda, EK and Senzanje, A. (2021). Moistube irrigation technology development, adoption and future prospects: A systematic scoping review. *Heliyon* 7 (2): e06213.
- Dirwai, TL, Senzanje, A, Mabhaudhi, T. (2021). Moistube Irrigation Fouling Due to Anaerobic Filtered Effluent (AF) and Horizontal Flow Constructed Wetland (HFCW) Effluent. *Sci Rep* 7124 (2021).
- Dirwai, TL, Senzanje, A, Mabhaudhi, T. (2021). Calibration and Evaluation of the FAO AquaCrop Model for Canola (*Brassica napus*) Under Varied Moistube Irrigation Regimes. *Agriculture* 11 (5): 410.
- Dirwai, TL, Senzanje, A and Mabhaudhi, T. 2020. Moistube irrigation (MTI) discharge under variable evaporative demand. *PloS ONE* 15 (12): e0236211.
- Dirwai, TL, Senzanje, A, Mabhaudhi, T. (Under review). Soil Wetting Geometry under Moistube Irrigation – Model Development and Modelling. *PloS ONE*.
- Dirwai, TL, Senzanje, A, Mabhaudhi, T. (Under review). Two dimensional modelling for canola (*Brassica napus*) grown under varied MTI regimes. *Irrigation Science*.


The following Manuscripts are under preparation and are set for submission to journals

1. Calibration and Evaluation of the SALTMED Model for Canola (*Brassica napus*) Under Varied Moistube Irrigation Regimes  
Dirwai, TL, Senzanje, A, Mabhaudhi, T, & Ragab, R

The following paper was presented at national and international conferences

21<sup>st</sup> WATERNET/WARFSA/GWP-SA SYMPOSIUM, Victoria Falls. Zimbabwe 29 Oct 2020. **Title of paper:** Soil Wetting Geometry under Moistube Irrigation – Model Development and Modelling.

In all the above papers and manuscripts, the conceptualization of the idea was done by TL Dirwai (student), and A Senzanje and T Mabhaudhi (supervisors). TL Dirwai conducted the research and the write up while the supervisors corrected and proof-read the manuscripts.

Signed: 

---

Tinashe Lindel Dirwai



## ABSTRACT

Irrigation technologies such as sub-surface drip irrigation (SDI) save water and further technological advances have resulted in the development new technologies such as Moistube Irrigation (MTI). MTI is a semi-permeable membrane (SPM) and a relatively new technology that comprises of densely spaced nano-pores that act as emitters. This study sought to characterise the MTI technology by (i) investigating the negative pressure discharge capability of MTI, (ii) assessing its performance when irrigating with anaerobic filtered (AF) and horizontal flow constructed wetland (HFCW) effluents and subsequently determining the plugging coefficients, (iii) calibrating and validating soil wetting geometry prediction models under MTI, (iv) investigating solute transport in the vadose zone under MTI, in addition, modelling solute transport using HYDRUS 2D/3D, and (v) calibrating and testing of AquaCrop model for full and deficit irrigated canola.

For the negative pressure experiment, the Moistube tubing was enclosed in a 1 m long PVC conduit. A 20 l water reservoir placed on an electronic balance provided a continuous supply of water whilst a three-speed ( $u_a = 1.2 \text{ m.s}^{-1}$ ,  $2.5 \text{ m.s}^{-1}$ , and  $3.0 \text{ m.s}^{-1}$ ) hot air blower facilitated the radiative factor and advection process. For the second objective which read; assessing MTI performance when irrigating with anaerobic filtered (AF) and horizontal flow constructed wetland (HFCW) effluents and subsequently determining the plugging coefficients, the feed water was supplied from a raised tank (3.5 m) and mass-flow rates were recorded at 15 min intervals using an electronic balance. The effluents were obtained from a decentralised waste water treatment system (DEWATS) in kwaMashu, Durban, South Africa. The effluent feed water concentrations and experimental room temperature ( $25^\circ\text{C} \pm 1^\circ\text{C}$ ) were continuously monitored and kept constant. Hermia's models based on the  $R^2$  coefficient was used to select the best fitting fouling mechanism model and consequently the plugging coefficients. In addition, microbial colony analysis and scanning electron microscopy -energy dispersing x-ray (SEM - EDX) analysis was carried out to assess the composition of the deposited sediment (DS) and adhered bacterial film (ABF) onto the MTI lateral. For the third objective which involved calibrating and validating wetting geometry prediction models under MTI, two independent, but similar experiments, were conducted to calibrate and validate the model using MTI lateral placed at a depth of 0.2 m below the soil surface in a soil bin with a continuous water supply (150 kPa). Soil water content was measured every 5 minutes for 100 h using MPS-2 sensors. Solute movement experiments were conducted in a 20 m by 8 m naturally ventilated greenhouse under three water application regimes namely, (i) full irrigation at 100%  $\text{ET}_c$ , (ii) deficit irrigation (DI) at 75%  $\text{ET}_c$ , and (iii) 55%  $\text{ET}_c$ . Soil samples for fertility analysis were collected at the emitter and 15 cm from the emitter at depths of 20-, 30-, 40-, and 50-cm before and after 2 h, 4 h, 24 h, 48 h, and 72 h of each fertigation exercise. Fertiliser was applied at a rate  $140 \text{ kg.ha}^{-1}$  over two split applications. The AquaCrop model was calibrated and validated for canola (*Brassica napus*) under Moistube irrigation (MTI) and various water regimes [(i) 100%, (ii) 75%, and (iii) 55% of crop water requirement ( $\text{ET}_c$ )] over two seasons, 2019 and 2020. The normalised root mean square ( $n\text{RMSE}$ ), Model Efficiency ( $EF$ ),  $R^2$ , and

the Willmot's index of agreement ( $d$ ) statistics were used to evaluate the model's efficiency in simulating biomass (B), canopy cover (CC), yield (Y) and harvest index (HI).

The negative pressure results revealed that for each of the air velocities, the respective  $E_d$  values obtained were 0.16, 0.31 and 0.36 mm.d<sup>-1</sup>. The recorded discharges ( $q$ ) at normalised time ( $t^*$ ) = 1 h for  $E_d = 0.16$  mm.d<sup>-1</sup> was  $7.67 \times 10^{-3}$  l.hr<sup>-1</sup>.m<sup>-1</sup> length, whilst for  $E_d = 0.31$  mm.d<sup>-1</sup>  $q = 14.5 \times 10^{-3}$  l.hr<sup>-1</sup>.m<sup>-1</sup> length, and for  $E_d = 0.36$  mm.d<sup>-1</sup>  $q = 20.8 \times 10^{-3}$  l.hr<sup>-1</sup>.m<sup>-1</sup> length. The emitter clogging experiment revealed that MTI pore blocking was a complex phenomenon described by complete pore blocking model ( $R^2 \geq 0.50$ ). The  $\alpha$  for each effluent (foulant) were  $\alpha_{AF} = 0.07$  and  $\alpha_{HFCW} = 0.05$  for AF and HFCW respectively. Soil wetting geometry model calibration showed that soil texture influenced water movement ( $p < 0.05$ ) and showed a good fit for wetted widths and depths for both soils ( $nRMSE = 0.5\% - 10\%$ ;  $NSE \geq 0.50$ ; and  $d$ -index  $\geq 0.50$ ). The percentage bias ( $PBIAS$ ) statistic revealed that the models' under-estimated wetted depth after 24 h by 21.9% and 3.9% for silty clay loam and sandy soil respectively. Sensitivity analysis revealed an agreeable models' performance values. This implied the applicability of the models' for estimating wetted distances for an MTI lateral buried at 0.2 m from the surface. AquaCrop was successfully calibrated and tested for canola production under optimal and deficit irrigation regimes. The calibration results indicated the model simulated with accuracy the CC (under 100%  $ET_c$   $R^2 = 0.99$ ,  $EF = 0.92$ ,  $nRMSE = 6.4\%$ ,  $d = 0.98$ ) and 75%  $ET_c$  ( $R^2 = 0.99$ ,  $EF = 0.92$ ,  $nRMSE = 10.3\%$ ,  $d = 0.98$ ). The model simulated CC well for validation for 100%  $ET_c$  ( $R^2 = 0.97$ ,  $EF = 0.93$ ,  $nRMSE = 22.5\%$ ,  $d = 0.98$ ) and 75%  $ET_c$  ( $R^2 = 0.84$ ,  $EF = 0.45$ ,  $nRMSE = 59.2\%$ ,  $d = 0.86$ ) irrigation regimes. Final biomass simulations were reasonably good under 100%  $ET_c$ , 75%  $ET_c$ , and 55%  $ET_c$  irrigation regimes ( $R^2 \geq 0.90$ ,  $d \geq 0.65$ ). The study contributes new knowledge by providing the operationalisation and maintenance (O&M) guidelines for MTI.

The study concluded that MTI is capable of discharging under a negative pressure. The information can be adopted by irrigators for realistic matric potential irrigation scheduling. The study also revealed that the MTI can potentially perform intermittent irrigation under the AF and HFCW effluents. Wetting geometries were successfully modelled for MTI under the fine textured and coarse textured soil. The study recommended the experiment be done under filed (cropped) conditions so as to determine the effect of plant water uptake on wetting patterns. HYDRU 2D/3D successfully simulated the MTI nutrient movement for full and optimal irrigation regimes in the variably saturated zone, hence HYDRUS 2D/3D can successfully simulate solute movement under MTI. In order to avoid nutrient loss MTI should not be adopted for canola fertigation under extreme deficit irrigation regimes (55%  $ET_c$  and lower). In addition, canola grown under extreme deficit MTI regimes incurs yield and biomass penalties. The study strongly recommends that similar experiments be done under field conditions for all the experiments done under controlled conditions (negative pressure, greenhouse and soil box).

## **ACKNOWLEDGEMENTS**

To God Almighty for giving me good health, grace and strength throughout this study.

I would also like to express my sincere gratitude to my supervisors, Dr Aidan Senzanje and Prof Tafadzwanashe Mabhaudhi for their guidance, advice, suggestions and above all the mentorship throughout this journey.

Special thanks go to the University of KwaZulu-Natal (UKZN), for providing access to resources that contributed immensely to the completion of this study.

My heartfelt gratitude to Professor Chris Buckley (RIP) and the Water, Sanitation & Hygiene Research & Development Centre for induction, inoculations and for providing access to wastewater.

I owe my gratitude to the technical staff in Bioresources Engineering of UKZN led by Mr. Alan Hill for facilitating the laboratory and field experiments in this study. I also acknowledge the Center for Water Resources Research, UKZN for lending me some of the equipment used in this study.

I owe sincere gratitude to my family for their steadfast prayers, love and warmth.

Finally, I wish to thank the postgraduate students in the department of Bioresources Engineering for their advice, support and encouragement. Special mention to Dr William Musazura, Takudzwa Mandizvo, Dr Isack Mathew, Dr Admire Shayanowako, Francis Marimbe, Dr Chisenga Mubanga, Dr Daniel Otim, Francis Muga Onyando, Dr Joseph Masanganise Sharon Migeri, and Nqobile Nkomo.

## DEDICATIONS

Dedicated to:

1. **Ruth Dirwai, Loveness Gosha, and Carol Masekesa** - True life's journey companions.

2. This PhD journey, which made me appreciate the Dao Philosophy:

*“What is Kung-Fu: it is supreme skill from hard work. A great poet has achieved kung-fu.*

*The painter, the calligrapher – they can be said to have kung-fu. Even a **PhD scholar** can*

*have kung-fu -*

*Practice,*

*Preparation, and*

*endless reading,*

*until the mind is weary and the bones ache, until the **PhD scholar** is too tired to sweat, too*

*wasted to breathe.*

*That is the way. The only way one acquires kung-fu.”*

*~ Master One Hundred Eyes – Marco Polo*

# TABLE OF CONTENTS

PREFACE .....	ii
DECLARATION OF PLAGIARISM .....	iii
DECLARATION OF PUBLICATIONS .....	iv
ABSTRACT .....	v
ACKNOWLEDGEMENTS .....	vii
DEDICATIONS.....	viii
TABLE OF CONTENTS.....	ix
LIST OF TABLES .....	xiv
LIST OF FIGURES .....	xvi
LIST OF ABBREVIATIONS.....	xix
1 INTRODUCTION .....	22
1.1 More Crop Per Drop Approach Using Efficient Irrigation Technologies.....	22
1.2 Industrial Crop Production Under Irrigation .....	23
1.3 Modelling for Improved Agricultural Water Management (AWM).....	23
1.4 Problem Statement and Research Objectives.....	24
1.5 Thesis Outline and Objectives Flow Map .....	25
1.6 References .....	27
2 MOISTUBE IRRIGATION.....	29
2.1 Introduction .....	30
2.2 Soil Water Dynamics Under Moistube Irrigation .....	30
2.3 Spacing and Depth of Dripline/ Moistube Irrigation Laterals.....	32
2.4 Fertigation Under Moistube Irrigation .....	34
2.5 Simulating Using Numerical Models.....	36
2.5.1 Solute movement.....	37
2.5.2 Modelling tools validation and evaluation .....	38
2.6 Moistube Irrigation Discharge Characteristics.....	39
2.7 Negative Pressure and Evaporative Demand .....	39
2.7.1 Hydrological limit .....	40
2.7.2 Radiative limit .....	40
2.7.3 Advective limit.....	41
2.8 Emitter Clogging .....	42
2.8.1 Waste-water.....	42

2.8.2	Effluent Quality and Emitter Clogging .....	43
2.9	Canola ( <i>Brassica napus</i> L) Crop .....	45
2.9.1	Canola Production .....	47
2.10	Crop Water Use Efficiency (WUE) and Water Productivity (WP) .....	48
2.10.1	Continuous irrigation and crop water use efficiency .....	48
2.11	Crop Water Productivity Modelling .....	49
2.11.1	Radiation driven models .....	50
2.11.2	Carbon driven models .....	51
2.11.3	Water-driven models.....	51
2.12	AquaCrop Model .....	52
2.13	Conclusions and Recommendations .....	54
2.14	References.....	56
3	MOISTUBE IRRIGATION (MTI) DISCHARGE UNDER VARIABLE EVAPORATIVE DEMAND.....	65
3.1	Introduction .....	66
3.2	Materials and Methods .....	67
3.2.1	Experimental Design and Set-up .....	68
3.2.2	ET model selection .....	69
3.2.3	Penman- Monteith model application to compute $E_d$ .....	69
3.2.4	Statistical analyses.....	71
3.3	Results and Discussion.....	71
3.3.1	Air velocity ( $u_a$ ) and evaporative demand ( $E_a$ ).....	71
3.3.2	Evaporative demand ( $E_a$ ) and discharge ( $q_t$ ) relationship.....	72
3.3.3	Discharge ( $q$ ) vs time ( $t$ ) relationship.....	75
3.4	Recommendations .....	77
3.5	Limitations .....	77
3.6	Conclusions .....	77
3.7	References .....	78
4	MOISTUBE IRRIGATION FOULING DUE TO ANAEROBIC FILTERED EFFLUENT (AF) AND HORIZONTAL FLOW CONSTRUCTED WETLAND (HFCW) EFFLUENT .....	80
4.1	Introduction .....	81
4.2	Fundamentals of Fouling.....	84
4.3	Materials and Methods .....	87
4.3.1	Study site and effluent characteristics .....	87
4.3.2	Experimental set-up and procedure .....	88

4.3.3	Method of analysis .....	89
4.4	Results and Discussion.....	91
4.4.1	Degree of clogging ( <b>DC</b> ) and relative discharge $q_{rel}$ .....	92
4.4.2	Permeate flux decline .....	93
4.4.3	Plugging coefficients.....	95
4.4.4	Bacterial activity.....	96
4.4.5	SEM - EDX .....	96
4.5	Irrigation Implication .....	102
4.6	Conclusion and Recommendation.....	102
4.7	References .....	103
5	SOIL WETTING GEOMETRY UNDER MOISTUBE IRRIGATION – MODEL CALIBRATION AND VALIDATION .....	107
5.1	Introduction .....	107
5.2	Materials and Methods .....	111
5.2.1	Model description.....	111
5.3	Experimental Design and Data Collection .....	112
5.3.1	Soil hydraulic parameters and textural characteristics .....	112
5.3.2	Measurement of soil wetted front.....	113
5.3.3	Models' calibration.....	115
5.3.4	Models' validation.....	115
5.3.5	Models' evaluation .....	116
5.4	Results and Discussion.....	117
5.4.1	Model calibration .....	117
5.5	Sensitivity Analysis.....	120
5.5.1	Models' validation.....	122
5.6	Irrigation Implication .....	126
5.7	Limitations .....	127
5.8	Conclusions and Recommendations.....	127
5.9	References .....	128
6	TWO DIMENSIONAL MODELLING OF NITRATE TRANSPORT FOR CANOLA ( <i>BRASSICA NAPUS</i> L.) GROWN UNDER MOISTUBE IRRIGATION USING HYDRUS 2D/3D .....	131
6.1	Introduction .....	132
6.2	Materials and Methods .....	133
6.2.1	Model description.....	133
6.3	Experimental Design.....	134

6.3.1	Study site and soil hydraulic properties .....	134
6.3.2	Field experiment.....	135
6.4	Data Collection.....	136
6.5	Modelling Domain and Nitrogen Reactions.....	137
6.6	Model Calibration .....	137
6.6.1	Parameter values.....	138
6.6.2	Initial and boundary conditions.....	139
6.7	Nitrogen Use Efficiency.....	140
6.8	Model Validation.....	141
6.9	Statistical Analyses and Model Evaluation.....	142
6.10	Results and Discussion .....	143
6.10.1	Effects of different irrigation regimes on solute mobility under canola crop .....	143
6.10.2	Modelling results: MTI solute movement without active root water uptake .....	148
6.11	Second Fertigation Exercise and Model Validation .....	153
6.12	Root Nutrient Uptake.....	155
6.12.1	Partial Factor Productivity (NUE) .....	157
6.13	Conclusion and Recommendations.....	158
6.14	References.....	159
7	<b>CALIBRATION AND EVALUATION OF THE FAO AQUACROP MODEL FOR CANOLA (<i>Brassica Napus. L</i>) UNDER VARIED MOISTURE IRRIGATION REGIMES .....</b>	<b>163</b>
7.1	Introduction .....	164
7.2	Material and Methods.....	167
7.2.1	Model description.....	167
7.2.2	Study site and description of field experiment.....	168
7.3	Model Parameters and Input Data.....	169
7.3.1	Weather data.....	169
7.4	Model calibration .....	173
7.4.1	Model validation and evaluation statistics .....	176
7.5	Results and Discussion.....	177
7.5.1	Effects of water regimes on growth, yield, and water productivity of canola ....	177
7.6	Calibration.....	179
7.7	Model validation .....	183



7.8	Conclusions and Recommendations.....	186
7.9	References .....	187
8	SUMMARY, CONCLUSIONS AND RECOMMENDATIONS.....	191
8.1	Summary .....	191
8.2	Conclusions .....	191
8.2.1	Evaporative demand .....	191
8.2.2	Moistube irrigation plugging.....	192
8.2.3	Moistube soil wetting geometries.....	192
8.2.4	Solute movement.....	192
8.2.5	Calibration and validation of AquaCrop .....	193
8.3	Recommendations .....	193
8.4	Statement of Originality .....	194
9	Appendices.....	195
9.1	Appendix A: Data for the computed $q_{Ave}$ values using Equation 3.7 .....	195
9.2	Appendix B: R Script for DS and ABF from AF and HFCW.....	196
9.3	Appendix C: Irrigation Schedule.....	196

## LIST OF TABLES

Table 2.1 Effluent characterisation modified (after Musazura, 2018).....	43
Table 2.2 Canola production in South Africa (after DAFF, 2016).....	46
Table 2.3 Conservative parameter values for canola grown in a semi-arid region of Australia (after Zeleke et al., 2011).....	53
Table 3.1 $E_d$ formulations and the respective variables applied in the model(s) .....	69
Table 3.2 Air velocity ( $ua$ ) measurements and the corresponding evaporative demand ( $E_d$ ) 72	
Table 3.3 Summarised descriptive statistics for the induced $E_d$ and the observed $q_t$ .....	72
Table 3.4 Normalised time scale ( $t^*$ ) vs $E_d$ for the $q_t$ vs $t^*$ plot.....	75
Table 4.1 3 <sup>rd</sup> generation Moistube membrane properties .....	82
Table 4.2 DEWATS effluent quality characterisation (Musazura, 2018) and the corresponding emitter clogging risks (Bucks et al., 1979). .....	87
Table 5.1 Soil textural and soil hydraulic parameters (van Genuchten-Mualem model) .....	113
Table 5.2 MPS-2 sensors placement depths and lateral spacing for the respective soils .....	114
Table 5.3 Models' inputs .....	114
Table 5.4 The experiments used for models' calibration and validation .....	115
Table 5.5 General performance rating for model evaluation statistics .....	116
Table 5.6 Sensitivity analysis evaluation of $W$ and $Z$ to model parameters.....	121
Table 6.1 Soil textural and soil hydraulic parameters.....	135
Table 6.2 Nutrient composition of the applied fertilisers .....	136
Table 6.3 Summarised model parameter values .....	138
Table 6.4 Irrigation information and model parameters .....	139
Table 6.5 Summarised conservative and non-conservative parameters for model validation .....	141
Table 6.6 General performance rating for model evaluation statistics (Moriassi et al., 2007).....	142
Table 6.7 Plant $NH_4^+ - N, NO_3^- - N$ concentrations and the resultant yields and biomass..	158
Table 6.8 PFP <sub>N</sub> as a proxy to NUE for the respective irrigation regimes.....	158
Table 7.1 Irrigation frequencies and application times.....	168
Table 7.2 Summarised meteorological conditions for the respective growing seasons ( $S_i$ )..	171
Table 7.3 Soil textural and soil hydraulic parameters.....	172
Table 7.4 Conservative and non-conservative parameters for canola. ....	175
Table 7.5 General performance rating for model evaluation statistics .....	177
Table 7.6 Effects of irrigation regime on the soil water content .....	178

Table 7.7 Summarised observed yields and biomass accumulation over two growing seasons .....	179
Table 7.8 Observed and simulated yield and final biomass during calibration .....	183
Table 7.9 Observed and simulated yield and final biomass during validation .....	184

## LIST OF FIGURES

Figure 2.1 Different wetting patterns by a drip emitter at varying flow rates (after GardenSoft, 2009).	32
Figure 2.2 Evaporative demand dynamics around a semi-permeable membrane. The fluxes are in flux units ( $\text{W.m}^{-2}$ ) modified after Hobbins and Huntington (2016).	41
Figure 2.3 The various types of membrane fouling (a) complete pore blocking, (b) internal pore blocking, (c) partial pore blocking, and (d) cake formation (after Field, 2010).	44
Figure 2.4 Canola supply, demand and ending stocks in South Africa (after CEC, 2018; Grain-SA, 2018).	47
Figure 3.1 Experimental set-up	69
Figure 3.2 (a) Moisture discharge ( $q_t$ ) at $0 \leq E_d \leq 7$ and (b) comparison between the simulated $q_t$ vs the observed $q_t$ .	73
Figure 3.3 Discharge vs. normalised time ( $t^*$ ) relationship at (a) $E_d = 0.16 \text{ mm.d}^{-1}$ , (b) $E_d = 0.31 \text{ mm.d}^{-1}$ , (c) $E_d = 0.36 \text{ mm.d}^{-1}$ , and (d) combined $q$ vs $t^*$ plots.	77
Figure 4.1 The various types of membrane fouling (a) complete pore blocking, (b) internal pore blocking, (c) partial pore blocking, and (d) cake formation after Field (2010).	86
Figure 4.2 Experimental set-up	88
Figure 4.3 Sampled DS and ABF points along the MTI lateral for each respective effluent.	91
Figure 4.4 Box plot showing discharge variations between the two types of effluents.	92
Figure 4.5 Degree of clogging (DC) for (a) AF effluent, (b) HFCW effluent, (c) DC vs $q_{Ave}$ for AF and HFCW effluents, and (d) Relative discharge plots for AF and HFCW effluents.	93
Figure 4.6 Flux - time curve for (a) AF and (b) HFCW effluent.	94
Figure 4.7 Linearised flux decline rate for (a) AF effluent and (b) HFCW effluent	95
Figure 4.8 Gel like bacterial colonies progression in selected samples after (a) 3 incubation days and (b) after 7 incubation days	96
Figure 4.9 Bacterial colony growth for deposited sediment (DS) (a) colony growth under AF for lateral 1 (L1), (b) lateral 2 (L2), and (c) lateral 3 (L3). Bacterial growth on adhered sediment (AS) for (a) L1, (b) L2, and (c) L3.	98
Figure 4.10 Bacterial colony growth for deposited sediment (DS) under HFCW effluent (a) for lateral 1 (L1), (b) lateral 2 (L2), and (c) lateral 3 (L3). Bacterial growth on adhered sediment (AS) for (a) L1, (b) L2, and (c) L3.	99

Figure 4.11 SEM-EDX for a pristine MTI lateral (top row), SEM-EDX for deposited sediment (DS) from AF effluent (second row), and SEM-EDX for (DS) from HFCW effluent (bottom row). .....	100
Figure 4.12 SEM-EDX for a pristine MTI lateral (top row), SEM-EDX for adhered biofilm (ABF) from AF effluent (second row), and SEM-EDX for AS from HFCW effluent (bottom row). .....	101
Figure 5.1 Soil bin experimental set-up (a) 3-D view and (b) orthographic top view . Dimensions in cm. ....	115
Figure 5.2 Relationship between (a) dimensionless wetted volume ( $V^*$ ) and dimensionless wetted width ( $W^*$ ) and (b) dimensionless wetted volume ( $V^*$ ) and dimensionless wetted depth ( $Z^*$ ) for silty clay loam (The bars represent a cluster of data points). ....	117
Figure 5.3 Relationship between (a) dimensionless wetted volume ( $V^*$ ) and dimensionless wetted width ( $W^*$ ) and (b) dimensionless wetted volume ( $V^*$ ) and dimensionless wetted depth ( $Z^*$ for sandy soil.....	119
Figure 5.4 Comparison of observed $W_o$ and $Z_o$ vs simulated $W_s$ and $Z_s$ from estimated $V$ for silty clay loam (a and b) and sandy soil (c and d).....	122
Figure 5.5 Observed vs simulated wetted distances for silty clay loam soil. ....	123
Figure 5.6 Observed vs simulated wetted distances for sandy soil.....	124
Figure 5.7 Observed and simulated wetting geometries for silty clay loam under MTI as seen from the front view. ....	125
Figure 5.8 Observed and simulated wetting geometries for sandy soil under MTI as seen from the front view. ....	126
Figure 6.1 Modelling domains for MTI lateral .....	137
Figure 6.2 Boundary conditions adopted from Kanda et al. (2020a).....	140
Figure 6.3 First fertigation exercise: $NH_4^+ - N, NO_3^- - N$ vertical movement at (a) emitter at 100% $ET_c$ , (b) 15 cm away from emitter at 100% $ET_c$ , (c) emitter at 75% $ET_c$ , (d) 15 cm away from emitter at 75% $ET_c$ , (e) emitter at 55% $ET_c$ , and (f) 15 cm away from emitter at 55% $ET_c$ .....	146
Figure 6.4 Cumulative $NH_4^+ - N, NO_3^- - N$ breakthrough curves at (a) 20-, 30 -,40-, 50 cm at emitter at 100% $ET_c$ irrigation regime, (b) 20-, 30 -,40-, 50 cm at 15 cm away from emitter at 100% $ET_c$ irrigation regime, (c) at 20-, 30 -,40-, 50 cm at emitter at 75% $ET_c$ irrigation regime, (d) 20-, 30 -,40-, 50 cm at 15 cm away from emitter at 75%	

ET <sub>c</sub> irrigation regime, (e) 20-, 30 -,40-, 50 cm at emitter at 55% ET <sub>c</sub> irrigation regime, and (f) 20-, 30 -,40-, 50 cm at 15 cm away from emitter at 55% ET <sub>c</sub> irrigation regime. The plots include active root nutrient uptake.....	147
Figure 6.5 Simulated distribution of $NH_4^+ - N, NO_3^- - N$ at 100% ET <sub>c</sub> irrigation regime from $t = 12$ h to $t = 156$ h.....	150
Figure 6.6 Simulated distribution of $NH_4^+ - N, NO_3^- - N$ at 75% ET <sub>c</sub> irrigation regime from $t = 12$ h to $t = 168$ h .....	151
Figure 6.7 Simulated distribution of $NH_4^+ - N, NO_3^- - N$ at 55% ET <sub>c</sub> irrigation regime from $t = 12$ h to $t = 168$ h. ....	152
Figure 6.8 $NH_4^+ - N, NO_3^- - N$ observed vs simulated calibration results for the 55% ET <sub>c</sub> irrigation regime over a 72 h period (a) at emitter and (b) 15 cm away from the emitter. ....	153
Figure 6.9 Second fertigation exercise $NH_4^+ - N, NO_3^- - N$ movement at E and Ae for (a) 100% ET <sub>c</sub> -, (b) 75% ET <sub>c</sub> -, and (c) 55% ET <sub>c</sub> irrigation regimes after $t = 72$ h and observed vs simulated $NH_4^+ - N, NO_3^- - N$ movement at (d) 100% ET <sub>c</sub> -, (e) 75% ET <sub>c</sub> -, and (f) 55% ET <sub>c</sub> irrigation regimes. ....	155
Figure 6.10 $NH_4^+ - N, NO_3^- - N$ concentration (mmol.cm <sup>-3</sup> ) contours during active RNU by plants at (a) 100% ET <sub>c</sub> , (b) 75% ET <sub>c</sub> , and (c) 55% ET <sub>c</sub> .....	157
Figure 7.1 Average maximum and minimum temperatures recorded in the greenhouse during the 2019 growing season.....	170
Figure 7.2 Average maximum and minimum temperatures recorded in the greenhouse during the 2020 growing season.....	170
Figure 7.3 Variation in canopy cover for the (a) 100% ET <sub>c</sub> , (b) 75% ET <sub>c</sub> , and (c) 55% ET <sub>c</sub> irrigation regimes over two seasons (S <sub>i</sub> ). ....	178

## LIST OF ABBREVIATIONS

Abbreviation	Meaning
ABF	Adhered Bacterial Film
AF	Anaerobic Filtered
ANOVA	Analysis of variance
APSIM	Agricultural Production Systems Simulator
AWM	Agricultural Water Management
B	Biomass
BOM	Biodegradable Organic Material
CC	Climate Change
CC <sub>x</sub>	Canopy Cover
CEF	Controlled Environment Facilities
CERES	Crop Environment Resources Synthesis
CI	Continuous irrigation
CU	Christiansen Uniformity Coefficient
CV	Coefficient of Variation
CW	Constructed Wetland
<i>d</i>	Willmot's Index of Agreement
DBPs	Disinfection By-Products
<i>DC</i>	Degree of Clogging
DEWATS	Decentralised Waste-Water Treatment System
DI	Deficit Irrigation
DOM	Dissolved Organic Matter
DS	Deposited Sediment
<i>E<sub>d</sub></i>	Evaporative Demand
EDX	Energy Dispersive X-ray
<i>EF</i>	Model Efficiency
EfOM	Effluent Organic Matter
EPIC	Erosion Productivity Impact Calculator
<i>ET<sub>o</sub></i>	Evapotranspiration
EU	Emission Uniformity
<i>E<sub>w</sub></i>	Wet Environment Evaporation
FC	Field Capacity

FE	Finite Element
Abbreviation	Meaning
FO	Forward Osmosis
HI	Harvest Index
HFCW	Horizontal Flow Constructed Wetland
II	Intermittent Irrigation
ISMZ	Irrigation Management Specific Zones
LAI	Leaf Area Index
MAE	Mean Absolute Error
MSE	Mean Square Error
MTI	Moistube Irrigation
MW	Molecular Weight
N	Nitrogen
<i>nRMSE</i>	Normalised Root Mean Square
NOM	Natural Organic Matter
NSE	Nash-Sutcliffe Efficiency
O&M	Operation and Maintenance
$P_e$	Prediction Efficiency
PFP <sub>N</sub>	Partial Factor Productivity of Applied N
PME	Persistence Model Efficiency
PRD	Partial Root Zone Drying
PV <sub>k</sub>	Performance Virtue Statistic
RH	Relative Humidity
RUE	Radiation Use Efficiency
RMSE	Root Mean Square Error
SDI	Sub-Surface Drip Irrigation
SEM	Scanning Electron Microscopy
SMP	Soluble Microbial Products
SPM	Semi-Permeable Membrane
STICS	Simulator mulTidisciplinary Crop Standard
SOC	Synthetic Organic Compounds
TDS	Total Dissolved Solids
TEM	Transmission Electron Microscopy



TOC	Total Organic Carbon
TSS	Total Suspended Solids
$u_a$	Air Velocity
VPD	Vapour Pressure Deficit
VFCW	Vertical Flow Constructed Wetland
WOFOST	WOrld FOod STudies
WP	Water Productivity
WUE	Water Use Efficiency
Y	Yield

---

# 1 INTRODUCTION

## 1.1 More Crop Per Drop Approach Using Efficient Irrigation Technologies

Climate change (CC) poses a threat to natural water resources. Agriculture consumes 70% of the global fresh-water supply and novel technologies are required to promote water conservation (Zhu et al., 2018). Literature reports that approximately 40% of the fresh water used for agriculture in developing countries is lost to non-beneficial usage such as evapotranspiration, deep percolation and poor conveyance mechanisms (Zhu et al., 2018). Irrigation technology has slowly evolved from less efficient techniques such as flood irrigation to drip irrigation and sub-surface methods. Waste-water has also been considered as an alternative that can potentially reduce the pressure on the fresh-water resources (Singh et al., 2012). A 2001 global estimate asserted that 20 million hectares (ha) of agricultural land is under waste-water irrigation (Hamilton et al., 2007). This proves that recycling has potential to ameliorate the global fresh water demands.

Moistube irrigation (MTI) is a relatively new sub-surface irrigation technology that resembles an upgrade from ceramic pitcher pots, although ceramic pitcher pots are micro-porous. The technology consists of a semi-permeable membrane (SPM) with densely and uniformly spaced nano-pores (100000 nano-pores per square centimetre) and a pore diameter of 10 – 90 nm (Zou et al., 2017; Kanda et al., 2019). Moisture movement is facilitated by soil water potential difference and external system pressure (Yang et al., 2008; Kanda et al., 2019). MTI assumes a line source infiltration mechanism, and it has reported benefits such as improved yields and high water use efficiency (WUE) (Zou et al., 2017; Kanda et al., 2019; Kanda et al., 2020b). MTI is a low pressure discharge irrigation technology hence, it requires minimal pumping requirements that translate to low energy cost for irrigators. A deep understanding on the discharge mechanisms of MTI in the variably saturated zone improves the design process with respect to wetting geometries under various soil textures which, will subsequently inform lateral placement depth and spacing. Furthermore, the MTI discharge mechanisms potentially influence solute movement in the vadose zone.

Knowledge of the design and operation and maintenance (O&M) of MTI irrigation systems equips irrigators with management tools promoting water conservation and minimising yield penalties. Design knowledge such as wetting geometries, performance under waste-water

irrigation and matric potential discharges aid irrigators in determining; (i) optimal lateral spacing and placement depths, (ii) flushing frequency when irrigating with waste-water and (iii) realistic matric potential informed irrigation schedules.

## **1.2 Industrial Crop Production Under Irrigation**

Canola (*Brassica napus*) is a major oil seed crop of economic importance (Barbetti et al., 2012). Current Brassica breeds have been significantly improved to produce less erucic acid and glucosinolate to make them more edible for stock feed and human consumption (Snowdon et al., 2007; Barbetti et al., 2012). Canola is extensively produced in Australia, Asia, Canada, Europe and the USA (Raymer, 2002). Canola is a relatively new crop in South Africa, and the country imports 70% of its oilcake requirements. The main producing provinces in South Africa are Western Cape, Northern Cape, Free State and Eastern Cape. KwaZulu-Natal, North West and Limpopo produce in small quantities.

Industrial crop irrigation is essential for optimal yields and biomass. Informed irrigation management practices are required for efficient and effective industrial crops production i.e., irrigators need not over nor under irrigate (Bilalis et al., 2009). Canola is considered a drought tolerant crop because it's deep tapped roots can extract water from a depth of 1.7 m (Katuwal et al., 2020). Deficit irrigation during canola vegetative and reproductive stages can potentially impose grain yield penalties, however, Katuwal et al. (2020) argued skipping irrigation during vegetative growth maximises water productivity under deficit irrigation scenarios for certain varieties. Therefore, informed irrigation practices are required for canola production to avoid yield penalties.

## **1.3 Modelling for Improved Agricultural Water Management (AWM)**

Empirical models can be adopted to simulate wetted profiles, depths and widths for different irrigation systems. Design and management of sub-surface irrigation systems are essential as it informs the soil moisture movement aspect of irrigation (Singh et al., 2006). Although numerical models are favoured because of their robustness, empirical models are simplistic and can potentially answer design questions around lateral spacing and placement depth.

Kanda et al. (2020c) employed HYDRUS 2D/3D to simulate wetting geometries for sandy clay loam and loamy sand soils under MTI. There exists a gap on empirically developed wetting front predicting models under MTI. Water driven models can be adopted to assess the yield response to differential irrigation regimes. The FAO AquaCrop model can be adopted to predict yields, biomass formation and water productivity footprint for irrigated agriculture (Raes et al., 2009) under MTI. AquaCrop has been used extensively to model yield response for sunflower Todorovic et al. (2009) , maize Ahmadi et al. (2015), cotton Farahani et al. (2009) , canola Safi et al. (2019) and Zeleke et al. (2011), and much recently for cowpea under MTI (Kanda et al., 2020a). Despite the model being applied to a various crops, there is a gap in its application on canola grown under MTI.

#### **1.4 Problem Statement and Research Objectives**

Effective irrigation is facilitated by understanding soil water dynamics of the soil in question, which subsequently informs optimal lateral spacing and correct manifold placement depth. There is limited empirical evidence that documents soil water dynamics of heavy clay and coarse sand soils under Moistube irrigation (MTI). Conceptually, under zero applied pressure a negative pressure induces Moistube discharges. No previous study has investigated Moistube discharge when subjected to negative pressure or an imposed evaporative demand. Whilst Kanda et al. (2018) carried out an experiment assessing the effects of suspended and dissolved solids on the clogging sensitivity of Moistube, there are no empirical investigations into the effects of different wastewater effluents on Moistube clogging sensitivity. The key concern of sub-surface irrigation is water conservation. MTI is a new technology that can potentially save water and boost yields. However, there has been little quantitative analysis of how it performs under fertigation i.e., how effectively it promotes maximum nutrient uptake minimising losses (leaching). Furthermore, no research documents the MTI design for canola crop. This study provides an opportunity to advance the understanding of MTI by seeking to execute the following objectives:

1. Investigating Moistube discharge subjected to negative pressure,
2. Investigating and assessing the effects of anaerobic filtered effluent (AF) and horizontal flow constructed wetland (HFCW) effluent on the clogging characteristics of Moistube,

3. Investigating soil water dynamics of MTI under heavy clay and coarse sandy soils,
4. Determine solute movement under the different irrigation regimes under Moistube irrigation (MTI), and Determine yield response of Canola to different irrigation regimes under Moistube irrigation (MTI) and parameterise the AquaCrop crop module for canola crop (*Brassica napus* L.) grown under South Africa Conditions.

The study was premised on the following hypotheses;

1. An artificially induced evaporative demand ( $E_d$ ) or negative pressure does not impact MTI discharge,
2. AF and HFCW do not degrade MTI membrane performance,
3. Soil hydraulic properties do not influence soil water movement under MTI
4. geometries,
5. MTI has minimal nitrogen (N) leaching, and optimal deficit irrigation strategies are not suitable for canola growth and grain yield development.

## 1.5 Thesis Outline and Objectives Flow Map

This thesis is structured as follows: Chapter 2 presents the review on Moistube irrigation (MTI), MTI discharge under imposed evaporative demand is presented and discussed in Chapter 3. Chapter 4 discusses MTI performance under anaerobic and horizontal flow constructed wetland effluents, whilst Chapter 5 discusses soil wetting geometries under heavy clays and sandy soils. MTI solute movement and the subsequent modelling using HYDRUS 2D/3D is described in Chapter 6. Chapter 7 discusses the parameterisation and testing of AquaCrop model for canola under full and deficit water conditions under MTI. Finally, the conclusions and recommendations are provided in Chapter 8. The thesis objective flow is shown in Figure 1.1.

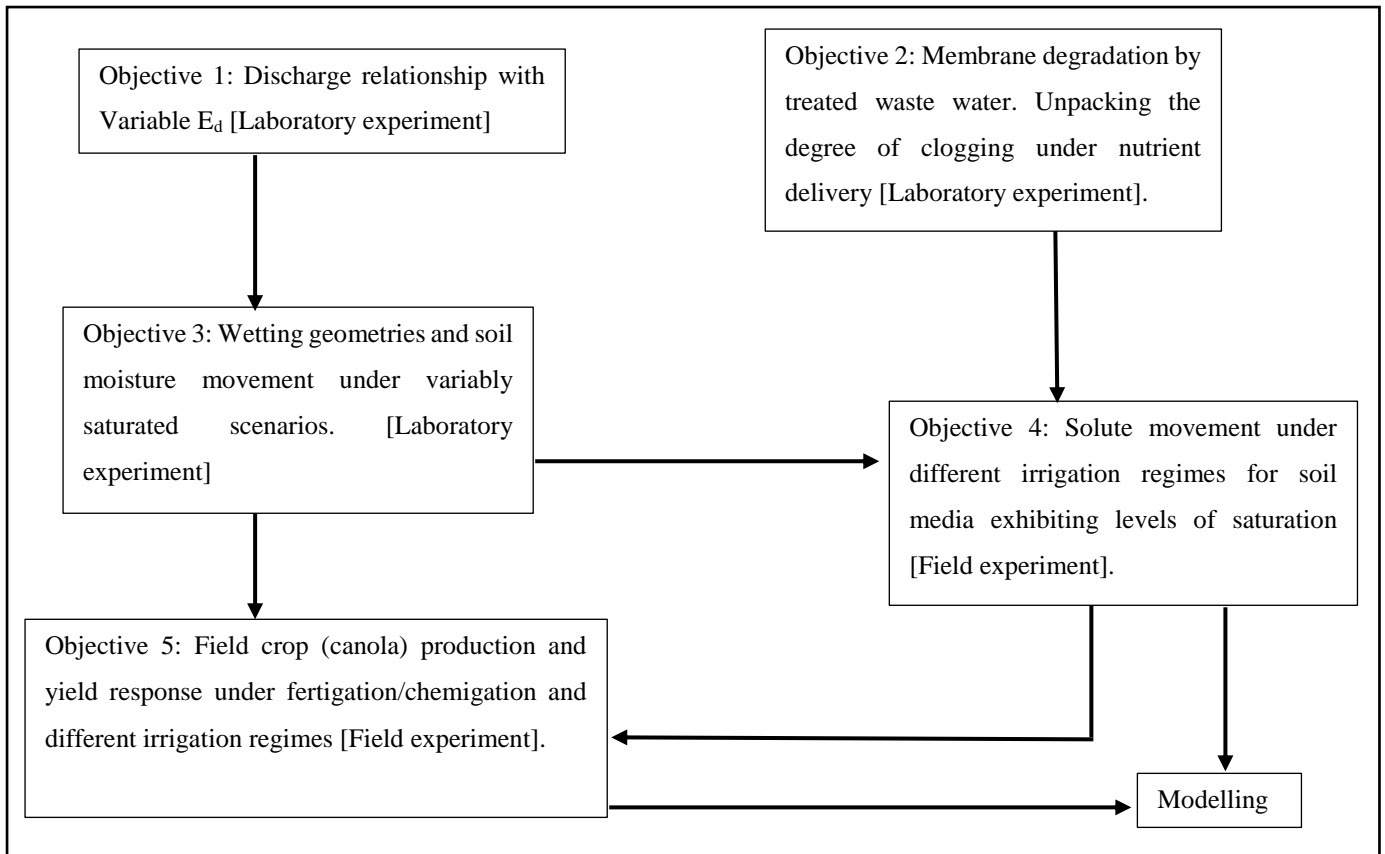


Figure 1.1 Thesis objectives map

This study will contribute to new and additional knowledge aspect of MTI in the following ways:

Firstly, the study will produce an empirical power function for soil water dynamic under heavy clay and coarse sandy soils. This knowledge will aid in the design of MTI for specified soil textures. The study will inform on the irrigation life cycle of MTI using effluent water and subsequently advise on the time taken for pore fouling or plugging. The study will highlight whether or not MTI promotes solute movement thus advising on leaching effects under MTI. Such knowledge is essential, as it will minimise vadose zone contamination. In addition, the study will inform on the fertigation potential of MTI. The study will provide new knowledge on the ability of MTI to satisfy various crop water requirements (CWR) under varying climatic conditions. Furthermore, the study will advise on canola response or performance to continuous and deficit irrigation under MTI. The research will generate knowledge on canola performance under continuous irrigation and the best fertigation regime that produces high yields.

## 1.6 References

- Ahmadi, SH, Mosallaeepour, E, Kamgar-Haghighi, AA and Sepaskhah, AR. 2015. Modeling maize yield and soil water content with AquaCrop under full and deficit irrigation managements. *Water Resources Management* 29 (8): 2837-2853.
- Barbetti, MJ, Banga, SS and Salisbury, PA. 2012. Challenges for crop production and management from pathogen biodiversity and diseases under current and future climate scenarios—case study with oilseed Brassicas. *Field Crops Research* 127 225-240.
- Bilalis, D, Karkanis, A, Efthimiadou, A, Konstantas, A and Triantafyllidis, V. 2009. Effects of irrigation system and green manure on yield and nicotine content of Virginia (flue-cured) Organic tobacco (*Nicotiana tabaccum*), under Mediterranean conditions. *Industrial Crops Products* 29 (2-3): 388-394.
- Farahani, HJ, Izzi, G and Oweis, TY. 2009. Parameterization and evaluation of the AquaCrop model for full and deficit irrigated cotton. *Agronomy Journal* 101 (3): 469-476.
- Hamilton, AJ, Stagnitti, F, Xiong, X, Kreidl, SL, Benke, KK and Maher, P. 2007. Wastewater irrigation: the state of play. *Vadose Zone Journal* 6 (4): 823-840.
- Kanda, EK, Mabhaudhi, T and Senzanje, A. 2018. Hydraulic and clogging characteristics of moistube irrigation as influenced by water quality. *Journal of Water Supply: Research and Technology-Aqua* 67 (5): 438-446.
- Kanda, EK, Niu, W, Mabhaudhi, T and Senzanje, AJAR. 2019. Moistube Irrigation Technology: A Review. *Agricultural Research* 9 (20): 139 -147.
- Kanda, EK, Senzanje, A and Mabhaudhi, T. 2020a. Calibration and validation of the AquaCrop model for full and deficit irrigated cowpea (*Vigna unguiculata* (L.) Walp). *Physics Chemistry of the Earth, Parts A/B/C* 102941 (2020): 102941.
- Kanda, EK, Senzanje, A and Mabhaudhi, T. 2020b. Effect of Moistube and subsurface drip irrigation on cowpea (*Vigna unguiculata* (L.) Walp) production in South Africa. *Water SA* 46 (2): 197-204.
- Kanda, EK, Senzanje, A and Mabhaudhi, T. 2020c. Soil water dynamics under Moistube irrigation. *Physics Chemistry of the Earth, Parts A/B/C* 115 (2020): 102836.
- Katuwal, KB, Cho, Y, Singh, S, Angadi, SV, Begna, S and Stamm, M. 2020. Soil water extraction pattern and water use efficiency of spring canola under growth-stage-based irrigation management. *Agricultural Water Management* 239 (2020): 106232.
- Raes, D, Steduto, P, Hsiao, TC and Fereres, E. 2009. AquaCrop—the FAO crop model to simulate yield response to water: II. Main algorithms and software description. *Agronomy Journal* 101 (3): 438-447.
- Raymer, PL. 2002. Canola: an emerging oilseed crop. In: eds. Janick, J and Whipkey, A, *Trends in new crops new uses*. ASHS Press, Alexandria, Virginia, USA.
- Safi, S, Kamgar-Haghighi, A, Zand-Parsa, S, Emam, Y and Honar, T. 2019. Evaluation of yield, actual crop evapotranspiration and water productivity of two canola cultivars as influenced by transplanting and seeding and deficit irrigation. *International Journal of Plant Production* 13 (1): 23-33.
- Singh, D, Rajput, T, Sikarwar, H, Sahoo, R and Ahmad, T. 2006. Simulation of soil wetting pattern with subsurface drip irrigation from line source. *Agricultural Water Management* 83 (1-2): 130-134.
- Singh, P, Deshbhratar, P and Ramteke, D. 2012. Effects of sewage wastewater irrigation on soil properties, crop yield and environment. *Agricultural Water Management* 103 (2012): 100-104.
- Snowdon, R, Luhs, W and Friedt, W. 2007. Oilseed rape. In: ed. Kole, C, *Genome Mapping and Molecular Breeding in Plants, Oilseeds*. Springer, Heidelberg, Berlin, Germany.

- Todorovic, M, Albrizio, R, Zivotic, L, Saab, MTA, Stöckle, C and Steduto, P. 2009. Assessment of AquaCrop, CropSyst, and WOFOST models in the simulation of sunflower growth under different water regimes. *Agronomy Journal* 101 (3): 509-521.
- Yang, W, Tian, L, Du, T, Ding, R and Yang, Q. 2008. Research Prospect of the Water-saving Irrigation by Semi-permeable Film [J]. *Journal of Water Resources and Water Engineering* 6 016.
- Zeleeke, KT, Luckett, D and Cowley, R. 2011. Calibration and testing of the FAO AquaCrop model for canola. *Agronomy Journal* 103 (6): 1610-1618.
- Zhu, X, Chikangaise, P, Shi, W, Chen, W-H and Yuan, S. 2018. Review of intelligent sprinkler irrigation technologies for remote autonomous system. *International Journal of Agricultural Biological Engineering* 11 (1): 1-8.
- Zou, X, Quan, T, Zhou, M, Yang, Q and Shi, Y. 2017. Progress and Prospects of Moistube Irrigation Technology Research. *Bulletin of Soil and Water Conservation* 37 (4): 150-155.



## 2 MOISTUBE IRRIGATION

This Chapter was published in part as:

**Dirwai, TL**, Mabhaudhi, T, Kanda, EK and Senzanje, A. (2021). Moistube irrigation technology development, adoption and future prospects: A systematic scoping review. *Heliyon* 7 (2): e06213. [DOI: 10.1016/j.heliyon.2021.e06213](https://doi.org/10.1016/j.heliyon.2021.e06213).

### Abstract

Agriculture is the largest consumer of fresh water in the world accounting for almost 70% of the water use. The burgeoning world population and increased demands to feed the world requires novel technologies that reconcile water consumption and food security. Moistube is a polymeric semi-permeable membrane irrigation technology that is known to improve water use efficiency and boost yields. The technology is relatively new, hence a lack of comprehensive literature regarding Moistube irrigation (MTI) technology warrants empirical investigation of the existing literature. The study performed a systematic review guided by the Preferred reporting items for systematic review and meta-analysis protocols (PRISMA-P) and the scoping studies methodological framework to compile an evidence-based literature review on Moistube irrigation. The study performed search queries in the following over-arching and comprehensive databases for grey literature: Google Scholar, Science Direct, Research Gate, CAB direct, All Journals, CNKI, FAO, SCOPUS, Web of Science, and UKZN-EFWE. DistillerSR software was used for screening, data extraction and data charting. Article screening retained 155 (n = 155) articles. Forty-nine articles (n = 49) and information sources were found to be related directly and indirectly to Moistube. Moistube articles (n = 29, 59%) were from China where the technology originated. A bulk of literature reported Moistube irrigation use in the arid regions of China. The review revealed areas for research enquiry into the subject matter. Future research areas were fertigation performance under MTI, effects of waste-water on MTI nano-pore plugging, yield response of industrial crops of economic importance under MTI and soil wetting geometries under MTI. This signified the need to perform further research enquiries into the subject matter to improve literature availability and identify potential research enquiries around MTI. Moistube irrigation technology has a low adoption rate in Africa with reported use in South Africa and Morocco. The technology has massive adoption potential in arid and semi-arid regions of sub-Saharan Africa.

**Keywords:** ceramic pots, semi-permeable membrane, sub-surface irrigation, sub-Saharan Africa, PRISMA-P

## **2.1 Introduction**

Moistube irrigation (MTI) technology can be classified as an upgrade of buried clay pot irrigation. The Moistube is made of a polymeric semi-permeable membrane (SPM) that utilises a soil moisture gradient to facilitate moisture movement or discharge. Similar to the clay pot counter-part, the Moistube releases moisture at the rate at which the plant absorbs water (Anon, 2018). MTI uses membrane technology (Petty et al., 1995) with the inner surface of the Moistube closely simulating the vascular plant tissue. With approximately 100000 nano-pores per square centimetre and a pore diameter of 10 – 900 nm (Zou et al., 2017; Kanda, 2019), the inner membrane uses the soil-moisture gradient for advection (Yang et al., 2008) and it assumes a line source infiltration mechanism during irrigation (Fan et al., 2018a).

The Moistube effectively reduces water consumption by 75%. Water is supplied at a constant rate in small quantities that are consistent with the rate at which plants uptake water (Anon, 2018). Unlike drip irrigation, the Moistube's uniformly and densely spaced nano-pores "sweat" i.e. allow water to ooze to the surrounding porous soil.. The Moistube has a nominal diameter of 16 mm and a wall thickness of 1 mm (Zhang et al., 2002). The next section profiles wetting geometries exhibited by sub-surface irrigation mechanisms and techniques.

## **2.2 Soil Water Dynamics Under Moistube Irrigation**

The two main drivers for uniform irrigation in subsurface irrigation and fertigation are lateral spacing and placement depth (Kandelous and Šimůnek, 2010b). It is imperative that an optimum placement depth is maintained since deep buried conduits will facilitate deep percolation and limit water and nutrients availability to plants (Dukes and Scholberg, 2005; Kandelous and Šimůnek, 2010b). Niu et al. (2017a) performed a study that assessed the effect of placement depth on soil water dynamics for greenhouse-grown tomatoes. The preferred continuous irrigation (CI) technique provided by Moistube prevented soil salinization. Furthermore, the study revealed varying soil moisture patterns in each respective placement depths of 10 cm, 20 cm, and 30 cm. Soil texture also determines the infiltration capacity under MTI. The infiltration effect of vertically placed Moistube under different heads (1 m, 1.5 m, and 2 m) and different soil textures (sand, sandy-loam and red loam) tested by Yu et al. (2017) were consistent with the Horton's empirical model shown in Equation 2.1 (Horton, 1939; Horton, 1941; Beven, 2004):

$$f_p = f_c + (f_0 - f_c)e^{-kt} \quad 2.1$$

where

$f_p$  = instantaneous infiltration capacity ( $\text{m} \cdot \text{s}^{-1}$ ),

$f_c$  = minimum constant infiltration capacity ( $\text{m} \cdot \text{s}^{-1}$ ),

$f_0$  = infiltration capacity at  $t = 0$ , ( $\text{m} \cdot \text{s}^{-1}$ )

$k$  = decay coefficient, and

$t$  = time from beginning of infiltration event (s).

The study revealed that soil-water distribution (vertical and lateral) was higher in red loam and sandy loam ( $R^2 > 0.80$ ), whereas relatively low in sand ( $R^2 < 0.70$ ). Jun et al. (2012) used a soil box to characterise wetted clay-loam soil under MTI and found out that Moistube produced a concentric wetting pattern and maintained soil moisture content of up to 90% of field capacity and exhibited a high irrigation uniformity of 95.62%. Another study by Zhu *et al.* (2018) assessed soil wetting patterns under different heads of 1 m, 1.5 m, and 2 m for *Coffea arabica* under *jujube* shading. The results revealed a direct relationship between wetting geometry/pattern and head; the wetting zones increased with flow rate. Figure 2.1 shows a typical wetting patterns from a drip emitter with varying pressure head (GardenSoft, 2009). Ashrafi et al. (2002) and Siyal and Skaggs (2009) performed a laboratory experiment using a porous pipe in a horizontal configuration, whilst Khan et al. (2015) and Fan et al. (2018a) used a vertically placed Moistube to assess different wetting patterns on silty loam, sandy-loam, and loam soils at a pressure head of 1.5 m. The two porous pipe configurations (horizontal and vertical) exhibited different soil-wetting geometries, with Khan et al. (2015) exhibiting a radial pattern which was a function of pipe diameter and pipe length. From the above, it is evident that few studies have investigated soil-water dynamics of MTI in heavy clay and coarse sand soil.

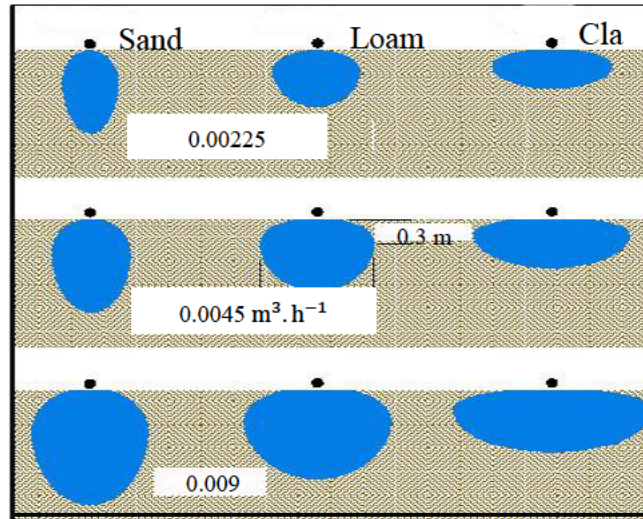


Figure 2.1 Different wetting patterns by a drip emitter at varying flow rates (after GardenSoft, 2009).

### 2.3 Spacing and Depth of Dripline/ Moistube Irrigation Laterals

Emitter spacing and depth are functions of soil hydraulic properties (Bar-Yosef, 1999) and crop root distribution. According to Kandelous and Šimůnek (2010b) water flow in a homogeneous and isotropic soil is governed by Richards equation (Equation 2.2). The equation can model 2-D and 3-D saturated-unsaturated flow in tensor form with anisotropic conductivity (Deng and Wang, 2017).

$$\frac{\partial \theta}{\partial t} = \frac{\partial}{\partial x_i} \left[ K_{ij}(h) \frac{\partial h}{\partial x_j} \right] + \frac{\partial K^{33}(h)}{\partial x^3} + S \quad 2.2$$

where

$\theta$  = volumetric water content ( $\text{m}^3 \text{m}^{-3}$ ),

$h$  = soil water pressure head (m),

$x_i$  = cartesian coordinate (m),

$z$  = vertical space coordinate (m),

$S$  = the source and sink term due to plant water uptake (rainfall or irrigation) ( $\text{s}^{-1}$ )

$t$  = time (s), and

$K^{ij}$  = anisotropic hydrological conductivity tensor, with  $i, j = 1, 2, 3, \dots, n$   
( $\text{m} \cdot \text{s}^{-1}$ ),

Schwartzman and Zur (1986) suggested that the wetted geometry (depth and lateral geometries) exhibited by a point source emitter are dependent on the soil hydraulic conductivity, emitter discharge and duration of application. Dabral et al. (2012) modelled the horizontal width ( $W$ ) and vertical depth ( $Z$ ) from a point source emitter as follows:

$$Z = t^{0.5} Q^{0.25} K^{0.25} \quad 2.3$$

$$W = t^{0.67} Q^{0.5} K^{0.17} \quad 2.4$$

where

$Z$  = vertical depth (m),

$W$  = horizontal soil width (m),

$t$  = elapsed time (s),

$Q$  = discharge rate ( $\text{m}^3 \cdot \text{s}^{-1}$ ), and

$K$  = soil hydraulic conductivity ( $\text{m} \cdot \text{s}^{-1}$ ).

MTI exhibits a line source emission similar to subsurface drip emitters. A study by Singh et al. (2006) developed conceptual model that simulated wetting geometry from a line source SSI drip line. The wetting geometry was a function of soil hydraulic conductivity, emitter discharge, placement depth, and volume applied. The models are shown in Equation 2.5 and 2.6. It can be hypothesised that the MTI vertical ( $Z$ ) and horizontal ( $W$ ) wetting geometry is a function of placement depth ( $D$ ), soil hydraulic conductivity ( $K$ ), total amount of water in soil per unit length ( $V$ ), discharge per unit length of lateral ( $Q$ ), and the matric potential per unit mass of soil ( $\psi$ ).

$$Z = A_1 V^{n_1} \left( \frac{K}{QD} \right)^{(n_1-0.5)} \quad 2.5$$

$$W = A_2 V^{n_2} \left( \frac{K}{QD} \right)^{(n_2-0.5)} \quad 2.6$$

where

$A_i$  = constant of proportionality ( $i = 1, 2$ ),

$D$  = placement depth (L),

$n_i$  = constant obtained graphically from the  $D$  and  $V$  relationship ( $i = 1, 2$ ), and

$V$  = total amount of water in soil per unit length ( $\text{L}^2$ ).

The matric potential induces a negative pressure effect that prompts discharge from the Moistube. The relationship can be modelled using to Equation 2.7.

$$Z, W = f(D, K, V, Q, \psi)$$

2.7

Kanda (2019) investigated the soil-water dynamics of loamy sand and sandy clay loam textures and revealed that lateral and downward distances for loamy sand to be 23 cm and 24.6 cm respectively, whereas for sandy clay loam the lateral and vertical distance was 19 cm in both cases. The Moistube was placed at a depth of 20 cm. Another equally important parameter to consider when determining dripline placement depth is type of crop. Different crops require varying placement depths. For instance Niu et al. (2017a) implemented a depth of 10 cm, 20 cm, and 30 cm on greenhouse tomatoes and recommended a depth of 10 cm. Dukes and Scholberg (2005) investigated yield response for sweet corn in sandy soils using semi permeable membrane (SPM) irrigation placed at depths of 23 cm and 33 cm, respectively. The former had an improved yield over two growing seasons whereas the latter was found to be too deep for optimal nutrient uptake. MTI is a fundamental technology used in China's arid regions. China has adopted MTI for production of crops such as winter wheat, summer sweet corn (Zhang *et al.*, 2017b), vegetables such as tomatoes and onions (Guo *et al.*, 2017; Niu *et al.*, 2017a), and they have extended the usage to orchard irrigation (Han *et al.*, 2015).

Regarding lateral spacing Zhang *et al.* (2017b) empirically investigated yield response of winter wheat and summer sweet corn under MTI in the Lou soil region in China. The lateral spacings adopted were 20 cm, 40 cm, and 60 cm. The results revealed improved water use efficiency and optimal yield response were achieved when Moistubes were 60 cm apart. Both crops exhibited improved water use efficiency under MTI. Researchers have not treated canola crop in much detail in terms of production under MTI.

## 2.4 Fertigation Under Moistube Irrigation

Fertigation is a process whereby plant nutrients are supplied in solute state to plants via an irrigation network system (Hagin and Lowengart, 1996). Fertigation complements irrigation in increasing crop yield and plant biomass. Old fertigation techniques such as broadcasting are still common in developing countries, whilst fertigation practices in the developed world have generally shifted to micro-fertigation (Bar-Yosef, 1999). Incorporating micro-fertigation in crop production has numerous benefits including time saving, avoids nutrient fluctuations in the soil, retards pathogenic activity and improved nutrient absorption capacity by plants (Bar-Yosef, 1999).

Semi-permeable membranes are classified as micro-fertigation technologies and they can potentially improve plant nutrient uptake (Bar-Yosef, 1999; Phuntsho et al., 2011). Subsurface fertigation maximises nutrient uptake since the nutrients are applied in areas where root concentration is high. Empirical investigations by Bar-Yosef (1999) revealed that crop yield in potato and cotton were high under subsurface fertigation than surface fertigation, in addition, the investigation also revealed minimised nitrate leaching whilst maintaining desired crop and fruit yields. Current investigations have not fully exhausted the response of industrial crops, such as canola, to fertigation or chemigation under MTI.

Soluble fertilisers injection in water pumped or gravity driven irrigation systems facilitates precise, controlled, and balanced application of nutrients to plants (Moreira Barradas et al., 2014). Careful consideration has to be taken before micro-fertigation commences. Initial soil nutrient levels need to be noted before fertigation with MTI. The underlying concept of MTI is based on solute transfer via forward osmosis (FO). Phuntsho et al. (2011) performed FO using a SPM to desalinate water. The FO technique, though implemented in desalination, has potential to perform well in MTI. The FO technique can be beneficial in agricultural practices since it does not require high hydraulic pressure (Phuntsho et al., 2011). MTI is yet to be tested for its suitability to use intrinsic osmotic potential difference between the solutes and the surrounding saline or sodic soils.

Fertigation regimes vary depending on grower practices and crop recommendations from industry. Previous studies by Hanson et al. (2006) on evaluating fertigation with SDI adopted fertigation strategies or regimes from industry and growers. There has been little quantitative analysis of the effects of the recommended crop specific fertigation regimes using MTI. Since MTI effectively saves water it can be hypothesised that the technology facilitates effective nutrient uptake with minimal nitrate leaching and minimised soil salinization. According to Moreira Barradas et al. (2014) fine textured soils e.g., clay soils, are susceptible to salinization as compared to coarse textured soils. It is against this backdrop that effects of continuous irrigation by MTI be investigated and assess the degree of salinization in the soil media.

Gärdenäs et al. (2005) suggested that growers' lack the motivation to adopt fertigation strategies since the incentive derived has minimal economic benefit. The economic advantage derived from adopting is a small fraction of the total production costs; however, it is worth

mentioning that effective fertigation strategies lower energy costs. In addition, the improved strategies minimise vadose zone contamination.

## **2.5 Simulating Using Numerical Models**

In order to understand water and chemical movement in the vadose zone, modelling tools become handy (Šimůnek et al., 2008). Numerical modelling is an economic and time saving exercise implemented to monitor and predict solute transport in soils. Various studies have used numerical modelling for various crops under subsurface irrigation. HYDRUS is a model that simulates subsurface multiple solute transport and water movement. The model has undergone upgrades from HYDRUS-1D to HYDRUS-2D and finally HYDRUS 2D/3D, which simulates in both 2D and 3D domains. HYDRUS 2D/3D has incorporated a sink term that accounts for water uptake by plant roots (Šimůnek et al., 2008; Kanda et al., 2018a). Ajdary et al. (2007) used a two-dimensional solute transport model HYDRUS-2D to model nitrogen leaching in permeable soils such as sandy loam. Gärdenäs et al. (2005) used HYDRUS 2D to model nitrate leaching under different fertigation strategies/regimes. Their study revealed how seasonal leaching was significant for coarse textured soils. Furthermore, they identified that lateral movement of nitrates in fine textured soils was enhanced by surface ponding. Ravikumar *et al.* (2011) modelled to evaluate fertigation scheduling for sugarcane.

Another equally powerful numerical model is SALTMED. SALTMED is a relatively powerful physically based modelling tool (Ragab, 2015) that can be used to simulate two dimensional soil-water dynamics and solute transport in porous media. The model is capable of simulating grain yield, and total dry biomass. The model employs established water uptake, water and solute transport, and evapotranspiration equations (Ragab, 2002; Silva et al., 2013). The model has been upgraded to incorporate crop growth according to solar radiation, subsurface irrigation, irrigation techniques such as deficit irrigation (DI) and partial root zone drying (PRD), soil temperature and nitrogen (N) dynamics models to mention a few (Ragab et al., 2016).

A comparative study by Karandish and Šimůnek (2019) investigated the capability of HYDRUS 2D/3D and SALTMED to simulate solute transport, soil salinity, crop N uptake, and water footprints (WF). SALTMED successfully simulated the soil water content more accurately than HYDRUS 2D/3D. The comparison was based on the normalised mean bias error (nMBE). The model successfully simulated with relative accuracy the crop N uptake, and



soil salinity. SALTMed, however, underestimated above ground biomass (DM) and leaf area index (LAI). An added benefit of SALTMed was its capability to estimate crop yield using the relative yield index method (RY) using the crop growth status, and the latter is more precise, where-as HYDRUS 2D/3D estimates yield as a RY ratio of potential to actual evapotranspiration ( $ET_o$ ). Both models utilise the same water and solute equations for simulation (Karandish and Šimůnek, 2019).

### 2.5.1 Solute movement

HYDRUS-2D was used to model the solute movement in the variably saturated soil profile zone. HYDRUS-2D robustness facilitates the simultaneous modelling of multiple independent solutes or nitrogen species whose solutes go through first-order degradation reactions (Hanson et al., 2006). Coupled water flow and solute transport equations were applied. Richards equation (Equation 1) was used to compute the spatially distributed soil moisture and the subsequent volumetric fluxes. For this study, we adopted the  $x$  (lateral)-  $z$  (vertical) spatial directions.

$$\frac{\partial \theta(h)}{\partial t} = \frac{\partial}{\partial x_i} \left[ K_{ij}(h) \frac{\partial h}{\partial x_j} + K_{iz}(h) \right] - S(h) \quad 1$$

Where:  $\theta$  = volumetric water content [ $L^3.L^{-3}$ ],  $h$  = pressure head [L],  $S$  = sink term [ $L^3.L^{-3}.T^{-1}$ ] representing root water uptake as a function of spatial position and time,  $x_i$  = spatial coordinates [L],  $t$  = time [T], and  $K_{ij}$  and  $K_{ij}$  = components of the hydraulic conductivity tensor [ $L.T^{-1}$ ]. The root water uptake was determined by the Vrugt model (Vrugt et al., 2001). Chemical transport of solutes in a variably saturated zone is governed by the linear partial differential Equations 2.8, 2.9 and 2.10.

$$\frac{\partial \theta c_1}{\partial t} + \rho \frac{\partial s_1}{\partial t} = \frac{\partial}{\partial x_i} \left( \theta D_{ij,1} \frac{\partial c_1}{\partial x_j} \right) - \frac{\partial q_i c_1}{\partial x_i} - \mu_{w,1} \theta c_1 - \mu_{s,1} \rho s_1 - S C_{r,1} \quad 2.8$$

$$\frac{\partial \theta c_k}{\partial t} + \rho \frac{\partial s_k}{\partial t} = \frac{\partial}{\partial x_i} \left( \theta D_{ij,k} \frac{\partial c_k}{\partial x_j} \right) - \frac{\partial q_i c_k}{\partial x_i} - \mu_{w,1} \theta c_k - \mu_{s,k} \rho s_k + \mu_{w,k-1} \theta c_{k-1} + \mu_{s,k-1} \rho s_{k-1} - S C_{r,k} \quad 2.9$$

$$S_k = K_{d,k} C_k \quad 2.10$$

Where:  $c_i$  and  $s_i$  = solute concentrations in the liquid [ $M.L^{-3}$ ] and solid [ $M.M^{-1}$ ] phase respectively,  $q_i$  =  $i$ th component of volumetric flux density [ $L.T^{-1}$ ],  $\mu_w$  and  $\mu_s$  = first order rate constants for solutes in the liquid and solid phase [ $T^{-1}$ ] respectively,  $\rho$  = soil bulk density [ $M.L^{-3}$ ],  $S$  = sink term [ $L^3.L^{-3}.T^{-1}$ ] in the water flow equation,  $C_r$  = concentration of the sink term

$[M.L^{-3}]$ ,  $D_{ij}$  = dispersion coefficient tensor  $[L^2.T^{-1}]$  for the liquid phase,  $k = k$ th chain number,  $n_s$  = number of solutes involved in the reaction,  $K_{d,k}$  = distribution coefficient of species  $k$   $[L^3.M^{-1}]$ , and  $c_k$  and  $s_k$  = adsorption isotherms.

### 2.5.2 Modelling tools validation and evaluation

SALTMED and HYDRUS are calibrated using the default values of soil and crop parameters.. The experimentation parameters measured are above ground biomass, LAI, soil water content, soil electrical conductivity, crop yield and the soil  $NO_3^-$  content. The data collection for the next growing season is used to evaluate the model. Model validation and evaluation involves running the model using the measured input parameters from the experimentation process. Statistical and graphical representations are frequently used to evaluate SALTMED, HYDRUS 2D/3D and other related modelling tools. Karandish and Šimůnek (2019) fine-tuned the following crop parameters: crop fraction cover ( $f_c$ ), photosynthesis efficiency, crop coefficients ( $K_c, K_{cb}$ ) and the following soil hydraulic parameters were fine-tuned  $K_s$ ,  $\theta_s$ , air entry value and the pore size distribution index ( $\lambda$ ). The fine-tuning was done using the trial and error approach. Standard regression models such as Pearson's correlation coefficient ( $r$ ) and coefficient of determination ( $R^2$ ) are used to assess the performance of the models. The two evaluation statistical tools measure the degree of collinearity between the measured and the observed data (Moriasi et al., 2007).

Error indices such as mean absolute error (MAE), mean square error (MSE), and root mean square error (RMSE) are employed for model evaluation and testing. The RMSE is the commonly used index and it defines the error in units of the analysed parameter in question. In their study, Karandish and Šimůnek (2019) used the normalised root mean square error (nRMSE), the normalised mean bias error (nMBE) and the relative error (RE) to evaluate the performance of HYDRUS 2D/3D and SALTMED models.

Dimensionless statistical analysis approaches such as the index agreement ( $d$ ), persistence model efficiency (PME), Nash-Sutcliffe efficiency (NSE), prediction efficiency ( $P_e$ ) and the performance virtue statistic ( $PV_k$ ) can also be used for evaluating models. Index agreement ranges from 0 to 1, with 1 indicating the perfect fit and 0 not fit at all (Willmott, 1981). The index agreement, though being overly sensitive due to squared values, can successfully detect additive and proportional differences between the simulated and observed values (Legates and

McCabe Jr, 1999). Nash-Sutcliffe Efficiency (NSE) defines how the observed and simulated plot fits the 1:1 line. NSE ranges between  $-\infty - 1$ , with values in the range 0.5 – 1.0 indicating acceptable performance. The NSE has a limited applicability (Moriasi et al., 2007).  $PV_k$  is the weighted value for NSE and it is adapted for watershed modelling (Wang and Melesse, 2005; Moriasi et al., 2007).

## 2.6 Moistube Irrigation Discharge Characteristics

Moistube irrigation (MTI), like SPMs, require minimal pressure for operation and discharge can be induced by matric potential. MTI can yield a discharge of  $0.24 \text{ L} \cdot \text{hr}^{-1} \cdot \text{m}^{-1}$  at a pressure of 2 bars (Qui et al., 2015). The manufacturers operating pressure of MTI ranges from as low as 2 m to 6 m. In comparison, drip emitters, though described as low-pressure systems have a high-pressure requirement of 17 m to 27.5 m, which is relatively higher than MTI (Lyu et al., 2016). In the absence of applied pressure the MTI discharge is induced by a soil-moisture gradient between the Moistube and the surrounding soil (Kanda et al., 2018b). According to Yang et al. (2008) and Kanda (2019) the pressure-discharge relationship can be characterised by Equation 2.11. When the evaporative demand is reached water oozes through the membrane until the soil water potential ( $\psi$ ) is balanced.

$$q = f(\psi) \tag{2.11}$$

where

$q$  = emitter discharge ( $\text{m}^3 \cdot \text{s}^{-1}$ ), and

$\psi$  = soil water potential ( $\text{kg} \cdot \text{m}^{-1} \cdot \text{s}^{-2}$ ).

## 2.7 Negative Pressure and Evaporative Demand

As explained above, in the absence of applied pressure and under low-pressure situations, discharge can only be induced by negative pressure. An evaporative demand ( $E_d$ ) around the Moistube creates a soil moisture gradient that facilitates water oozing through the membrane. Evaporative demand can be defined as maximum evapotranspiration ( $ET$ ) under ambient conditions and unlimited supply of moisture (Hobbins and Huntington, 2016).  $E_d$  has four physical drivers which are wind speed, net radiation, vapour pressure, and ambient temperature (Donohue *et al.*, 2010a). In addition,  $E_d$  is also characterised by three physical boundaries

namely: hydrological limit, radiative limit and the advective limit (Hobbins and Huntington, 2016).

### 2.7.1 Hydrological limit

The hydrological limit defines the availability of water to evaporate and transpire from plants and soil surfaces. The term can be expressed as a mathematical function shown in Equation 2.12 (Hobbins and Huntington, 2016). For evaporative demand to occur there has to be an infinite water supply to meet the minimum hydrological limit.

$$ET \leq -\left(\frac{\partial\theta}{\partial t}\right)_{max} \quad 2.12$$

where:

$ET$  = evapotranspiration ( $\text{mm.day}^{-1}$ ),

$\frac{\partial\theta}{\partial t}$  = time rate change of moisture availability in units of mass flux ( $\text{kg. m}^{-2}.\text{s}^{-1}$ ), and

$max$  = represents the capillary rise of moisture to the soil surface.

### 2.7.2 Radiative limit

The energy requirement that facilitates the evaporative process can be modelled as indicated by Equation 2.13 (Hobbins and Huntington, 2016):

$$\frac{\partial W}{\partial t} = (1 - SA)R_d + L_d - L_u - \lambda ET - H - G - C - A_d \quad 2.13$$

where:

$\frac{\partial W}{\partial t}$  = time rate change of heat storage in evaporating layer,

$SA$  = surface albedo,

$R_d$  = downward shortwave radiation incident at the surface,

$L_u$  = longwave radiation outward from the surface,

$L_d$  = longwave radiation inward to the surface,

$\lambda ET$  = latent heat flux,

$H$  = sensible heat flux,

$G$  = net heat flux conducted from the evaporating surface into the soil

$C$  = energy absorbed by vegetation in the control volume, and

$A_d$  = heat gained by advection to the control volume.

All terms in Equation 3.4 are in flux units ( $\text{W.m}^{-2}$ ).

### 2.7.3 Advective limit

In evaporation terms the advective limit describes the system boundary's ability to absorb and bear away moisture (Hobbins and Huntington, 2016). A diagram theorizing active fluxes around a semi-permeable membrane is depicted in Figure 2.2. The fluxes involved are active in the surrounding medium. An empirical investigation is required to assess how variations in evaporative demand of different media e.g. soils, effects Moisture discharge in the absence of applied pressure

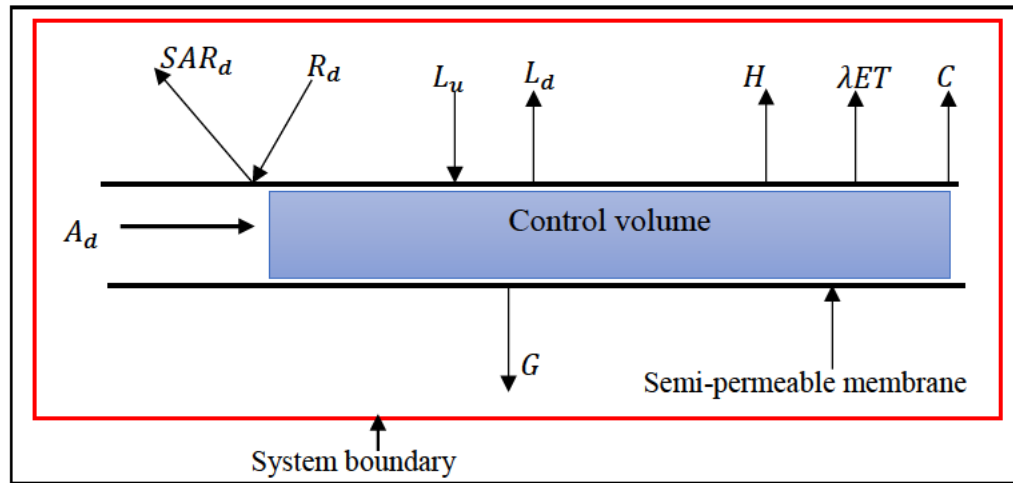


Figure 2.2 Evaporative demand dynamics around a semi-permeable membrane. The fluxes are in flux units ( $\text{W.m}^{-2}$ ) modified after Hobbins and Huntington (2016).

The advection can be modelled as defined in Equation 3.4:

$$E = M(e_{sat} - e_a) \quad 2.14$$

where:

$E$  = evaporation rate ( $\text{mm.day}^{-1}$ )

$e_{sat}$  = saturation vapour pressure at water temperature ( $\text{N.m}^{-2}$ ),

$e_a$  = saturation vapour pressure of air ( $\text{N.m}^{-2}$ ), and

$M$  = mass transfer coefficient.

A laboratory experiment by Khan et al. (2015) on negative pressure difference using a porous pipe made of silty clay and ground rice husks (mix ratio of 4:1) exhibited high water efficiency of up to 97%. The porous pipe was set up in a vertical configuration.

No previous study has investigated Moistube performance under a negative pressure. There is need to assess the Moistube discharge subject to negative pressure or under a laboratory induced evaporative demand, the frontier also offers an opportunity to investigate soil-wetting geometry of Moistube under vertical and horizontal configurations subjected to negative pressure, hence informing on lateral spacing and manifold placement depth.

## **2.8 Emitter Clogging**

Emitter clogging is a challenge when using micro-irrigation techniques. A study by Bucks et al. (1982) cited by Bar-Yosef (1999) revealed that the coefficient of variation of different subsurface emitters increased due to emitter clogging. Emitter clogging is attributed to water quality, i.e. the presence of microfilms from microflora, suspended solids, organic matter in fertigation solutions, and microbes (algae and bacteria) in irrigation water. Emitter clogging is also caused by varying hydraulic pressure. Zhang et al. (2017a) investigated the effect of pulsating and constant pressure on labyrinth clogging, the study revealed how emitters subjected to constant pressure clogged faster than those subjected to pulsating pressure.

The next sections profile waste-water or effluent quality, emitter clogging and the pressure discharge relationships between Moistube and water quality.

### **2.8.1 Waste-water**

Waste-water can be defined as water whose quality has been altered by human action (anthropological activity) (Levy et al., 2011; Musazura, 2018). The use of freshwater for irrigation burdens the already diminishing water sources. Treated waste-water is a suitable alternative to ameliorate the freshwater demand (Puig-Bargués et al., 2005; Liu and Huang, 2009). Treated waste-water can be classified as waste-water that has gone through physical, chemical and biological processing (Pescod, 1992). Three major categories of treated waste-water are industrial, agricultural and domestic (Hussain et al., 2001; Musazura, 2018). Industrial waste-water can be obtained from textile industries, abattoirs just to mention a few; whereas, agricultural treated waste-water comes from piggeries, and chicken farms (Matheyarasu et al., 2015; Musazura, 2018). Domestic waste-water comprises of discharges

from households, learning institutions, health care centres just to mention a few (Levy et al., 2011).

Arid regions in China and Mexico have adopted treated sewage water for irrigation (Friedel et al., 2000; Puig-Bargués et al., 2005; Liu and Huang, 2009). Waste-water reduce the pressures on freshwater bodies, however, the treated waste-water contains heavy metals, pathogen and high nitrate concentrations that can potentially contaminate the environment (Musazura et al., 2019a). Musazura (2018) characterised the treated waste-water effluents (anaerobic filtered (AF) effluent and horizontal flow constructed wetland (HFCW) effluent) from a decentralised waste-water treatment system (DEWATS) in Mashu-Durban, South Africa as per Table 2.1. The DEWATS produces effluent of varying quality, for instance, the AF effluent is produced after secondary anaerobic treatment and HFCW effluent is produced from secondary anaerobic constructed wetland filtering using subsurface filters (Gutterer et al., 2009b).

Table 2.1 Effluent characterisation (after Musazura, 2018)

Effluent				Constituent	Concentration (mg/L)
Anaerobic filtered (AF)				Nitrates	0.1
				Ortho-Phosphate	10.5
				Ammonium	61
				Nitrates	12.7
Horizontal Flow Constructed Wetland (HFCW)				Ortho-Phosphate	4.1
				Ammonium	6.7

\*AF effluent has a high pathogen load as compared to HFCW effluent.

### 2.8.2 Effluent Quality and Emitter Clogging

Membrane fouling is a process whereby soluble fine particles are deposited onto the surface of the membrane, leading to membrane performance degradation (Furuichi et al., 2008). Hermia (1982) in his filtration model clarification characterised cross-flow and dead-end filtration membrane models as in Equation 2.15. The fouling was typified as complete blocking, intermediate blocking, standard blocking, and cake layer formation (Hermia, 1982; Furuichi et al., 2008; Vela et al., 2009b). Understanding semi-permeable membrane (SPM) fouling or plugging mechanisms facilitate deeper knowledge on the capacity and efficiency of the SPM under differential operating conditions such as pressure, flow velocity, and temperature to mention a few (Corbatón-Báguena et al., 2016).

$$\frac{d^2t}{dV^2} = \left(\frac{dt}{dV}\right)^n = \alpha \left(\frac{1}{J}\right)^n \quad 2.15$$

where:

$t$  = filtration time (T),

$V$  = filtrate volume per unit area ( $L^3$ ),

$J$  = filtration velocity (flux) ( $L \cdot T^{-1}$ ),

$\alpha$  = plugging coefficient and,

$n$  = constant of proportionality for constant pressure filtration of a Newtonian fluid.

The  $n$  value ranges from 0 to 2, with complete blocking ( $n = 2$ ), intermediate blocking ( $n = 1$ ), standard blocking ( $n = 3/2$ ), and cake layer ( $n = 0$ ) (Vela et al., 2009b) (see Figure 2.3). The model can be adopted to determine the fouling or plugging coefficient of MTI using different waste-water effluent. The higher the plugging coefficient the rapid the clogging of the membrane.

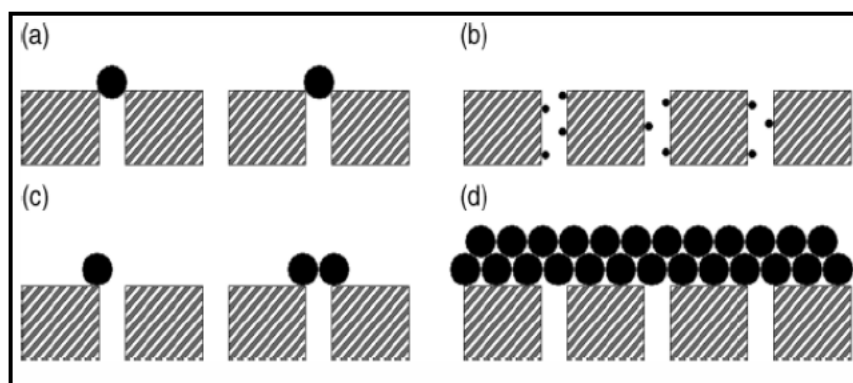


Figure 2.3 The various types of membrane fouling (a) complete pore blocking, (b) internal pore blocking, (c) partial pore blocking, and (d) cake formation (after Field, 2010).

Puig-Bargués et al. (2005) investigated the effects of varying effluent treatment on irrigation uniformity of drip irrigation kits. The study revealed that secondary effluent treatment caused clogging as compared to tertiary treatment. A study by Liu and Huang (2009) revealed that drip emitters subjected to laminar flow were susceptible to clogging compared to emitters having turbulent flow. Defined parameters such as coefficient of variation (CV), emission uniformity (EU), Christiansen uniformity coefficient (CU) are used to evaluate and assess emitter performance (Liu and Huang, 2009). No previous study has investigated the effects of different effluents on the clogging of Moistube nano-pores. Semi-permeable membranes such



as Moistube are sensitive to fine aggregates, for instance Xie et al. (2014) revealed that particle size in the range 37  $\mu\text{m}$  to 74  $\mu\text{m}$  clog the nano-pores.

According to Guo et al. (2012) waste-water can be classified as containing both organic and inorganic foulants. Dissolved organic matter (DOM) found in sewage effluent can be typified as natural organic matter (NOM), synthetic organic compounds (SOC) which is influenced by anthropological activities, soluble microbial products (SMPs) that are introduced during the biological treatment of the raw effluent, and disinfection by-products (DBPs) generated during the disinfection processes of the sewage effluent. After treatment the effluent more often than not contains residual organic matter that is classified as effluent organic matter (EfOM) which comprises of total organic carbon (TOC). EfOM is also characterised by high molecular weight (MW), proteins, enzymes, and low MW compounds that accelerate membrane fouling or blocking. The above-mentioned substances contribute to the formation of biofilms.

Microbiological fouling is accelerated by the presence of microorganism such as vegetative matter, algae, and bacteria. The latter (bacteria) attaches to the polymeric membrane via bio-adsorption, bio-adhesion, and multiplication (Guo et al., 2012). Researchers need to investigate the suitability and efficiency of MTI using waste-water and how various plugging stages form over the course of an irrigation cycle.

## **2.9 Canola (*Brassica napus* L) Crop**

Oilseeds are a major commodity in the global agricultural market. In the period 1987 – 1988, the global oilseed production was 183 million tonnes, with the USA producing 30%, China contributing 16%, Brazil 9%, India 6.1%, Argentina 6.2%, Russia 5.1% and Canada producing 3% (Shahidi, 1990). Oilseed rape is a special type of biotype rapeseed derived from the canola plant (Raymer, 2002a; DAFF, 2016). Originally developed in Canada canola crop has dominant hybrid varieties such as *Brassica napus* L and *B.rapa* L. Other hybrid cultivars have been developed and are under the stewardship of the Canadian Food Inspection Agency (CFIA) (Stringam et al., 2003). The species *B.napus* L and *B.rapa* L have summer and winter varieties. The rapeseeds have an oil profile that ranges from 40% to 45% with the industrial variety yielding the greatest percentage. Common domestic usage are cooking, salad oil and margarine production (Raymer, 2002a). The rapeseed produces oil with 2% erucic acid although improvements have produced seed oil with minimal traces of erucic acid, 5% to 8% saturated fats, 60 to 65% monosaturated fats, and 30% to 35% polysaturated fats (Raymer, 2002a).

Canola oil has high protein content and recently the new breeds produce low erucic acid oil. The seed oil has potential to produce biodiesel and the leaves and stems can be used for forage since they are rich in protein and low in fibre (Bañuelos et al., 2002b). Despite the dietary benefits canola farming is labour intensive and rape seed management is costly (Hu et al., 2017).

Canola is a relatively new crop in South Africa and the country imports 70% of its oilcake requirements. Table 2.2 (DAFF, 2016) and Figure 2.4 (CEC, 2018; Grain-SA, 2018) summarises canola production and consumption in South Africa. The winter form is cultivated extensively in Europe and Asia. According to Li *et al.* (2016) China produces 21% of the global oilseed rapeseed making it the leading global producer of the *B. napus* L seed. The Yangtze River Basin in China has 66.7 M ha under canola cultivation (Li et al., 2015b; Li et al., 2016). South Africa has registered a steady increase in canola crop farming. The Western Cape, Northern Cape, Free State and Eastern Cape are the dominant growers whilst KwaZulu-Natal North West and Limpopo produce in small quantities. Canola farming in South Africa is practised under clay-loam soils since sandy soils are deemed unsuitable because of poor drainage (DAFF, 2016). Little quantitative research has been done on canola farming under MTI in sand and clay soils.

Table 2.2 Canola production in South Africa (after DAFF, 2016)

Production year	Produce (tonnes)
1992 – 1993	400
2003 – 2004	41 000
2007 – 2008	38 150
2011 – 2012	57 340
2013 – 2014	79 000
2015 - 2016	1 690 373
2016 -2017	105 000
2017 - 2018	90 000

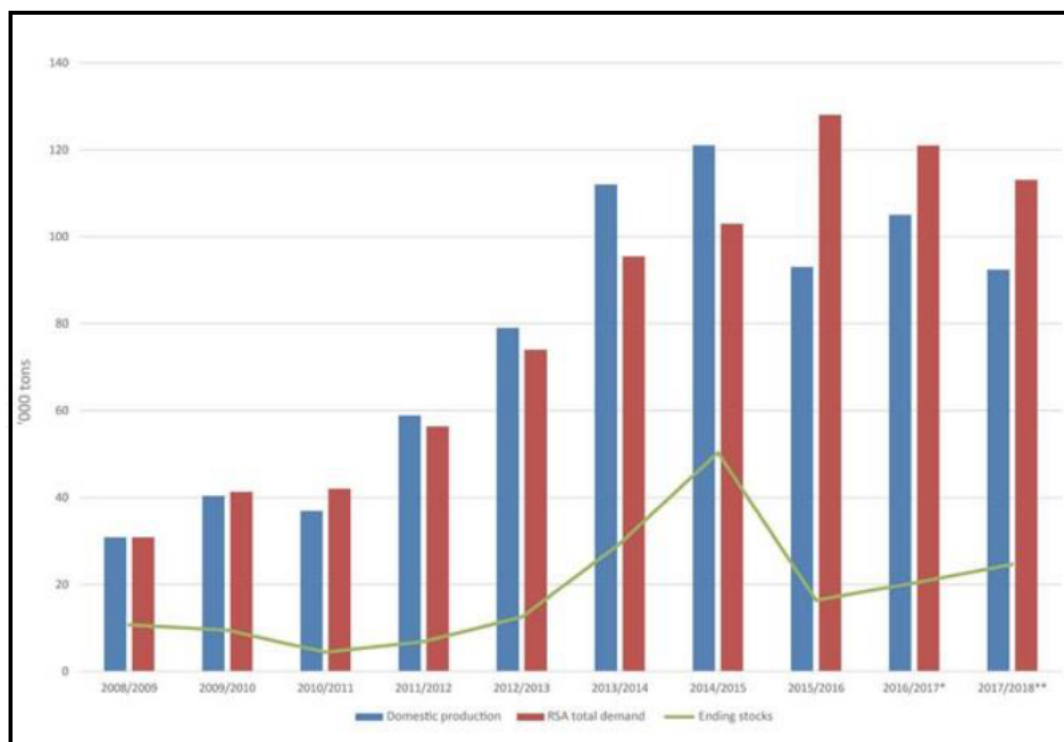


Figure 2.4 Canola supply, demand and ending stocks in South Africa (after CEC, 2018; Grain-SA, 2018)

### 2.9.1 Canola Production

Canola crop has high yields under irrigation. In addition, the crop has high tolerance towards salinity (Bañuelos et al., 1997; Stricker et al., 1997; Bañuelos et al., 2002b). Improved irrigation and fertigation can potentially increase seed yield and maximise vegetative growth. According to Li et al. (2015a) nitrogen fertiliser application improves rapeseed yield by 1.1 to 2.4 tonnes per ha. Canola has a high nitrogen (N) demand even though N increases the production cost of canola (Coetzee, 2017), hence uninformed fertigation strategies will affect profitability. According to Ozer (2003) fertiliser application should differ according to regions. Bañuelos et al. (2002b) investigated yield response under different subsurface drip irrigation regimes of 25, 50, 100, 125, and 150% of  $ET_c$ . The SDI placement depth was 40 cm and the soil type were Handford sandy-loam. The results revealed that dry matter increased with more irrigation and concluded that canola is sensitive to soil moisture availability. Another study by Gu et al. (2018) investigated the effects of ridge furrow film mulching and nitrogen fertilisation of winter oilseed rape. Six nitrogen (N) application rates were adopted namely, 0, 60, 120, 180, 240, and 300 kg.ha<sup>-1</sup> and the resultant yields were an increased average seed yield of 2 904 kg.ha<sup>-1</sup>, water productivity of 8.8 kg.ha<sup>-1</sup>.mm<sup>-1</sup> and economic benefit of \$1 259.60 per ha. The unavailability of optimal fertigation strategies hinders developing guidelines for fertigation and

placement depth that facilitates optimal nutrient uptake using MTI. In addition, there is no quantitative analysis on yield response, nutrient uptake and nutrient use efficiency, and water productivity of canola crop grown under MTI.

## **2.10 Crop Water Use Efficiency (WUE) and Water Productivity (WP)**

Technological development in irrigation systems has enabled water saving, improved water use efficiency (WUE) and water productivity (WP), and increased yield (Levidow et al., 2014). Improving WUE in the face of climate change will ensure food and water security for the growing global population (Kang et al., 2017). Climate change associated risks are anticipated to exacerbate water scarcity, hence threatening global food production (Iglesias and Garrote, 2015). Deficit irrigation as an alternative to conventional irrigation systems has been adopted in water scarce Mediterranean agro-zones. The technique maintains a steady soil moisture stock below field capacity that is necessary for plant growth (Galindo et al., 2018). Water use efficiency (WUE) is a seasonal ratio of harvestable yield or crop biomass ( $Y$ ) to evapotranspiration ( $ET$ ). The index can be estimated on a spatial (yield or leaf level) and temporal scale (seasonal or instantaneous) (Boyer, 1970; Molden et al., 2010; Sun et al., 2018). Water productivity (WP) measures the net positive return from any agricultural activity for every water unit consumed (Molden et al., 2010). Water productivity like WUE can be measured on a temporal and a spatial scale. Water productivity can be categorised as photosynthetic water productivity measured at leaf and canopy scale. The former is the ratio of leaf carbon dioxide assimilation to transpiration and the latter describes the carbon dioxide fluxes and assimilation and transpiration of the crop canopy. Net carbon gains are converted to biomass (Steduto et al., 2007). Various simulation models such as AquaCrop (Raes et al., 2009; Steduto et al., 2009a; Todorovic et al., 2009a), APSIM (Asseng et al., 1998; Farré et al., 2002; Robertson et al., 2002), and SALTMed (Karandish and Šimůnek, 2019), have been developed to simulate crop growth, harvestable yield and biomass with respect to WUE and WP.

### *2.10.1 Continuous irrigation and crop water use efficiency*

Semi-permeable membrane irrigation is an old technology that potentially increases crop yield and WUE. Continuous irrigation (CI) by Moistube minimises water supply fluctuations as experienced in SDI (Sun et al., 2018). The porous emitters reduce non beneficial water losses such as run off, deep percolation and soil evaporation (Cai et al., 2017). According to Khan et al. (2015) WUE lies in the range 0.94 to 0.97 when irrigating using porous pipes. A study by

Zhang et al. (2009) used buried (20 cm) ceramic pitchers to irrigate tomatoes under greenhouse conditions. The results revealed that porous pitchers at 0 cm head increased yield by 1.17 kg/pitcher. However, the zero head irrigation system had low WUE of 24.9 kg.m<sup>-3</sup>. Xue et al. (2013) did a comparative study between CI and intermittent irrigation (II) and quantified WUE during vegetative growth of tomato plants. The WUE was evaluated using the following parameters: stomatal conductance, net photosynthesis rate and leaf transpiration rate. Another study by Isoda et al. (2007) evaluated WUE from three irrigation technologies namely: furrow, drip and semi-permeable membranes. The study revealed that drip and porous tube used 37% less water than furrow. However, the three methods yielded approximately the same throughput of 70 t.ha<sup>-1</sup> of sugar beet. The WUE exhibited by furrow, drip and porous tube were 4.5 g.kg<sup>-1</sup>, 7.2 g.kg<sup>-1</sup>, and 7.5 g.kg<sup>-1</sup> of total dry weight per total irrigated water respectively. Sun *et al.* (2018) investigated WUE of tomato plants at leaf and yield level under MTI and found out that yield response and leaf instantaneous WUE at leaf level was high. Additionally, the study revealed increased irrigation WUE; crop WUE; and normalised WUE (ratio of crop WUE and  $ET_0$ ) at yield level. There is no quantitative analysis on WUE and yield response of canola plant under MTI. Findings by Sun et al. (2018) showed that water use efficiency (WUE) for tomato improved significantly under semi-permeable membrane continuous irrigation.

## 2.11 Crop Water Productivity Modelling

Crop simulation models are increasingly gaining use as alternative to empirical physical models which limit extrapolation beyond their function. Crop simulation models facilitate quantification of crop yield and crop water productivity (Foster et al., 2017). Input parameters for modelling plant resource capture can be simulated by the following; carbon driven models, radiation use efficiency (RUE), and water productivity (WP) or transpiration based (BTR) models (Bauböck, 2014). For example, BioSTAR is a carbon driven model and the primary functionality is an exponential asymptotic light response curve (Bauböck, 2014). Other carbon based models are WOFOST and CROPGRO (Bauböck, 2014). These models use a carbon driven approach to simulate crop growth (Todorovic et al., 2009a). The most common models are the RUE and these include CropSyst, APSIM, CERES, and LINTUL. CropSyst can be classified as hybrid model since it uses water and radiation approaches for crop simulation (Bauböck, 2014). The prominent relatively new water driven approach model is AquaCrop (Todorovic et al., 2009a; Bauböck, 2014). As discussed above, the crop simulation models are classified as: (i) radiation-driven, (ii) carbon-driven, and (iii) water-driven (Steduto, 2003;

Todorovic et al., 2009a). The following sub-sections describe the distinct crop growth simulating modules.

### 2.11.1 Radiation driven models

According to Todorovic et al. (2009a) “*Radiation driven modules derive the biomass directly from the intercepted solar radiation through a single conversion unit ( $\epsilon$ ) called radiation use efficiency*”. The hierarchical nature of radiation use efficiency (RUE) unit synthesises low level modules to process intermediate modules such as leaf quantum efficiency per mole of  $CO_2$  fixed, photorespiration rate and dark respiration leading to biomass accumulation (Todorovic et al., 2009a). Commonly used modules are Crop Environment Resources Synthesis (CERES) (Jones et al., 1986; Hodges et al., 1987; Carberry et al., 1989), Erosion Productivity Impact Calculator (EPIC) (Jones et al., 1991), and Simulator mulTIdisciplinary Crop Standard (STICS) (Brisson et al., 2003) and Agricultural Production Systems Simulator (APSIM) (Keating et al., 2003; Bauböck, 2014). STICS, a daily time step model relies on climatic, soil and crop systems data to simulate crop growth and development, nitrogen and water uptake. The model adapts to various crops e.g. wheat, maize, tomato, rapeseeds to mention a few (Brisson et al., 2003). In addition, it is classified as a robust model because it can simulate climatic-soil data without considerable bias (Brisson et al., 1998; Brisson et al., 2003), the model is versatile and has modularity that facilitates incorporating other modules for coupling. Finally, STICS is user friendly. APSIM was developed in Australia and the system can model and simulate a vast array of scenarios such as irrigated cropping, dryland farming, and agroforestry systems (Holzworth et al., 2006). The model simulates farming systems more than it does crop simulation. APSIM model has crop modules for cotton, canola, lupin, pigeon pea, sorghum, wheat, sunflower, barley and sugarcane (Keating et al., 2003). APSIM is user friendly as compared to its counterparts. Model calibration is made easy by pre-existing databases containing information on tested crop and soil specification. Farré et al. (2002) used APSIM to successfully predict canola (*Brassica napus* L.) yield from irrigation, the observed yield was in the range 0.1 to 3.4 t.ha<sup>-1</sup> whilst simulated yields were in the range 0.4 to 3.0 t.ha<sup>-1</sup>. A study by Albrizio and Steduto (2005) revealed that radiation models are inconsistent and have a constrained robustness.

### 2.11.2 Carbon driven models

Carbon driven models simulate crop growth based on leaf carbon assimilation during photosynthesis (de Wit, 1965). A hierarchical structure where lower level processes integrate to generate higher-level responses underpin the functionality of the models. Simulation is constrained by radiation limit, hydrological limit (water availability), and atmospheric carbon dioxide ( $CO_2$ ) limit. The multi-level interactions and numerous parameter input and constraints renders these models complex (Todorovic et al., 2009a). Carbon driven models include World Food Studies (WOFOST), Wageningen crop models (Bouman et al., 1996), and the American developed CROPGRO (Boote et al., 1998; Boote et al., 2002; Todorovic et al., 2009a).

WOFOST is a hybrid model characterised by remote sensing, crop growth monitoring system (CGMS) and maize simulation modules. The hybrid model has a complex hierarchical structure that requires 49 crop input parameters (Todorovic et al., 2009a). Despite this, the model is versatile as it can simulate crop growth under different approaches namely; (i) potential mode, where by input parameters are temperature and solar radiation, (ii) water-limited mode, where water availability is the only constraint, and (iii) nutrient limit-mode, where simulation requires soil intrinsic characteristics such as macro nutrients in non-fertilised soils (Todorovic et al., 2009a). WOFOST has undergone revision and improvements. Notable improvements include simulating the impact of nutrients limitations, extreme events and climate variability (de Wit et al., 2018). Boote et al. (2002) used CROPGRO to simulate crop growth and yield of faba bean (*Vicia faba* L.). The model simulated a yield excess of 6000 kg.ha<sup>-1</sup>, which was consistent with the observed yield. The process involved model adaption to temperature and crop growth based on specie analogy. Due to their complex structure and hierarchical nature, carbon-driven models are less user friendly. Furthermore, models require numerous parameter inputs for calibration (Todorovic et al., 2009a).

### 2.11.3 Water-driven models

In water-driven models there exists a direct linear relationship between biomass and transpiration through a water productivity (WP) index (Todorovic et al., 2009a). The modelling approach is relatively new and the commonly used simulation models are AquaCrop (Todorovic et al., 2009a; Bauböck, 2014; Foster et al., 2017) and CropSyst (Todorovic et al., 2009a; Bauböck, 2014). CropSyst uses a water-driven approach as a secondary growth engine,

with RUE ( $\epsilon$ ) method as the primary growth model (Bauböck, 2014). This makes AquaCrop the only purely water-driven model. Water-driven models, as compared to their solar driven counterparts, are easy to use and facilitate easy normalisation of WP parameter under different climatic condition (evaporative demand and atmospheric carbon dioxide) (Steduto et al., 2009a; Todorovic et al., 2009a) and this subsequently expands their applicability.

## **2.12 AquaCrop Model**

The main input parameters are crop characteristics, soil and management characteristics that define the environment in which the crop will develop. Todorovic et al. (2009a) posited that the model requires 33 easy to obtain input parameters. For example, it prefers percentage canopy cover to leaf area index (LAI), moisture stress, nutrient input and soil texture that can be observed in the field. The model output has graphical presentations that update at 1 day time steps, this makes the results easy for users to interpret (Raes et al., 2009). AquaCrop primarily simulates harvestable yield, biomass and growth of herbaceous crops. The advantages of AquaCrop over other models are leaf area index (LAI) is not required for simulating percentage canopy cover; rather canopy cover is simulated using proportional green cover. The simulated outputs can be verified against observable data. Another advantage is AquaCrop covers how transpiration is affected by a wide array of water stressors, for example, it accounts for water stress due to stomatal activity, premature senescence and reduced leaf expansion. Finally, AquaCrop factors in climatic dynamics impacts on water productivity (WP) (Foster et al., 2017).

A study by Steduto and Albrizio (2005) compared the performance of RUE ( $\epsilon$ ) models and water-driven model and they posited that water-driven models are robust and efficient in normalising climatic data. In addition, the robustness facilitated extrapolative ability of the water-driven models. Todorovic et al. (2009a) simulated sunflower growth under different water regimes using AquaCrop, WOFOST and CropSyst. All the models gave a satisfactory percentage canopy cover, with CropSyst giving a perfect simulated result at flowering and senescence stages as compared to AquaCrop and WOFOST. Since AquaCrop cannot simulate LAI, WOFOST performed better than CropSyst. When evaluating biomass results AquaCrop produced satisfying results, whereas WOFOST overestimated the biomass. A calibration, validation and testing study on canola (*Brassica napus* L.) using AquaCrop Version 3.1 by Zeleke et al. (2011) revealed the capability of AquaCrop Version 3.1 to accurately predict biomass accumulation, grain yield, and canopy cover (CC<sub>x</sub>). The trial was rainfed and irrigated



using a drip kit. The measured and simulated yield was 3.18 and 3.11 t.ha<sup>-1</sup>, respectively, whereas the accumulated biomass was 21.1 and 19 t.ha<sup>-1</sup>, respectively. The study further determined the conservative parameters (Table 2.3) that can be fine-tuned during simulation to obtain agreeable results between observed and simulated results.

Table 2.3 Conservative parameter values for canola grown in a semi-arid region of Australia (after Zeleke et al., 2011)

Parameters	Value		
	Hyloa 50 Calibration	Skipton Validation	Bin 3343-Co0401 Validation
Base temperature (°C)	0	0	0
Upper temperature (°C)	30	30	30
Cover per seedling (cm <sup>2</sup> .plant <sup>-1</sup> )	5	5	5
Canopy growth coefficient CGC (%.day <sup>-1</sup> )	8.9	8.9	8.9
Canopy decline coefficient CDC (%.day <sup>-1</sup> )	5.2	5.2	5.2
Soil water depletion factor for canopy expansion, upper limit	0.20	0.20	0.20
Soil water depletion factor for canopy expansion, lower limit	0.55	0.55	0.55
Shape factor for Water stress coefficient for canopy expansion	3.5	3.5	3.5
Soil water depletion factor for stomatal closure	0.60	0.60	0.60
Shape factor for Water stress coefficient for stomatal closure	5	5	5
Soil water depletion factor for early canopy senescence	0.70	0.70	0.70
Shape factor for Water stress coefficient for canopy senescence	3	3	3
Normalized water productivity WP* (g.m <sup>-2</sup> )	18.6	18.6	18.6
Adjustment for yield formation (%)	100	100	100
Normalized water productivity during yield formation WP* (g.m <sup>-2</sup> )	18.6	18.6	18.6
Basal crop coefficient (maximum) ( $K_{cb}(x)$ )	0.95	0.95	0.95

According to Zeleke et al. (2011) these conservative parameters can be extend to different cultivars of canola and they are also applicable in different geographical locations and different soil moisture stresses. Conservative parameters need to be adapted for the local South African canola cultivars such as Hyloa 559T (Triazine Tolerant variety) and the Hyloa 557 CL (Clearfield variety). AquaCrop has gone through upgrades, with the new version AquaCrop-OS (Foster et al., 2017) offering flexibility and allows the user to perform parallel execution thereby reducing simulation times. In addition, AquaCrop-OS is versatile i.e., it can be integrated into various development environments such as MATLAB and GNU octave scripts. This renders the ease of coupling AquaCrop-OS with other simulation models.

The model can be calibrated for the following variables: above ground biomass, grain yield, soil water content and canopy cover (CCx). The canopy cover is measured by the canopy cover analyzer LAI 2200. The key aspects for canopy cover adjustment are crop phenology, length of crop cycle and flowering, plant density and maximum canopy at mid-season. In addition,

the parameters to be adjusted for soil water content are soil type, and its related features like soil horizon and the rooting depth. For robust and accurate results, the model should be calibrated, validated and tested over two growing seasons. For instance, for canola (*Brassica napus* L) farming, the model will be calibrated using the data in May 2019 to September 2019 growing season (winter) and validated using data to be obtained in May 2020 to August 2020 growing season (winter).

### **2.13 Conclusions and Recommendations**

This chapter contains the conclusions and recommendations drawn from the reviewed literature.. Moistube irrigation is a relatively new technology developed for use in arid and semi-arid regions. The underlying concept of operation is similar to the age-old technology of buried clay pots whereby plant root suction dictates the moisture movement in the porous media (soil). MTI has been used extensively in China for vegetable and fruit production. Despite all this, many questions on Moistube remain unanswered.

Moistube irrigation is classified as continuous irrigation whereby the plant is supplied by water throughout the growing season, thus avoiding moisture stress. The water supply is subject to uniform water movement from the nanopores to the surrounding soil. Due to water scarcity, domestic and industrial wastewater effluent are considered alternatives for fresh water irrigation. Clogging presents a challenge; literature has analysed the clogging of the nanopores due to total dissolved and suspended solids (TDS and TSS). The TDS and TSS were found to reduce the discharge capability of the Moistube. Evidence of how Moistube discharge characteristics are affected by wastewater effluent is limited. The differential effluent quality presents an opportunity of assessing Moistube clogging sensitivity to anaerobic filtered (AF) effluent and horizontal flow constructed wetland (HFCW) effluent.

In the absence of pressure or zero pressure, Moistube irrigation discharge is driven by matric potential, i.e., soil moisture gradient. The discharge depends on a microclimate that creates an evaporative demand within the surrounding soil. The radiation induces heat fluxes in the surrounding environment that subsequently effects an advection process that bears away with the moisture in the surrounding environment. In arid and semi-arid regions, the evaporation from soil surfaces and transpiration from the plants creates an evaporative demand that will cause the Moistube to discharge water. Previous studies have reported on Moistube discharge

when subjected to a range of positive pressure, however, its discharge performance has never been evaluated under an artificial evaporative demand and under negative pressure.

Moistube is designed to conserve water, i.e., maximise water use efficiency (WUE) and water productivity (WP). The yield response of the tomato and cabbage under MTI was high as compared to subsurface drip irrigation (SDI). MTI has not been used for growing industrial crops such as canola; therefore, it is imperative to empirically investigate the performance of canola crop under varied climatic conditions. Crop modelling is a time saving exercise that can potentially predict crop yields. Model selection is based on potential advantages one modelling tool offers over others. For example, a modelling tool that incorporates and processes a wide array of datasets is preferable since it will be robust. Literature by Tan and Shibasaki (2003) revealed how some FAO global models fail to incorporate soil and climatic data, such input parameters will have to be processed separately. A crop simulation model should be user friendly and easy to couple with other models such as GIS, HYDRUS 2D/3D, SALTMED, and SALTMOD to mention a few (Pauwels *et al.*, 2007; Kanda *et al.*, 2018a). For these reasons, AquaCrop meets the criteria as it is user friendly, requires few input parameters, flexible and estimates yields with certainty and accuracy (Priya and Shibasaki, 2001).

Fertigation facilitates crop growth by supplying much-required nutrients. Fertigation has potential to improve yields and increase plant biomass. Fertigation using inorganic soluble fertilisers is a common practice under micro-irrigation techniques such as micro-sprinklers, subsurface drip and surface drip irrigation. In addition, the aforementioned irrigation techniques have employed fertigation or chemigation on a variety of crops such as strawberry, tomato, and grapes, to mention a few. Fertigation or chemigation poses a challenge of vadose zone contamination due to nutrient leaching. Regarding MTI, there is limited evidence on solute movement and canola crop response to varying fertigation strategies or regimes as prescribed by irrigation equipment manufacturers and grower practices.

Soil texture plays an important role in controlling leaching, as such there is need to investigate the solute movement in selected soils wherein the canola crop is planted. Soil water dynamics under MTI have not been thoroughly analysed, with the conclusions based on SDI. The soil-water dynamics are hypothesised to be symmetrical and asymmetrical in heavy clay and coarse sand soils, respectively. Empirical investigations are required to ascertain the phenomenon.

The use of modelling tools to simulate crop yields, soil water dynamics, and solute transport is an economic and time saving exercise. The use of models like HYDRUS 2D/3D and

SALTMED allows for modelling solute transport and soil water dynamics, however, SALTMED can perform functions that HYDRUS 2D/3D cannot, for instance, SALTMED can estimate crop yield and LAI. Crop modelling tools such as AquaCrop are user friendly and do not require many input parameters. Since these models work independently, model coupling will facilitate accurate, precise and enhanced results regarding crop growth, solute movement, plant nutrient uptake and soil-water dynamics. In addition, model comparison i.e., SALTMED vs AquaCrop in specific areas of yield responses, plant nutrient uptake, and water use efficiency (WUE) and SALTMED vs HYDRUS 2D/3D on solute movement in the vadose zone will provide important information on model performance.

The above conclusions drawn from the review identified research gaps that warrant investigations and add knowledge on Moistube irrigation (MTI) for improved yields, and water productivity. Previous studies have not focused on clogging sensitivity due to microbial activity, fertigation and the subsequent leaching effects of adopted grower fertigation regimes or strategies, yield response of industrial crop canola and the mechanical properties of the Moistube.

## 2.14 References

- Ajdary, K, Singh, D, Singh, AK & Khanna, M. 2007. Modelling of nitrogen leaching from experimental onion field under drip fertigation. *Agricultural Water Management* 89 (1-2): 15-28.
- Albrizio, R & Steduto, P. 2005. Resource use efficiency of field-grown sunflower, sorghum, wheat and chickpea: I. Radiation use efficiency. *Agricultural and Forest Meteorology* 130 (3-4): 254-268.
- Anon. 2018. Moistube. [Internet]. Envirogrower Middle East. Available from: <http://www.moistube.ae/desert.html>. [Accessed: January 22, 2019].
- Ashrafi, S, Gupta, AD, Babel, MS, Izumi, N & Loof, R. 2002. Simulation of infiltration from porous clay pipe in subsurface irrigation. *Hydrological Sciences Journal* 47 (2): 253-268.
- Asseng, S, Keating, B, Fillery, I, Gregory, P, Bowden, J, Turner, N, Palta, J & Abrecht, D. 1998. Performance of the APSIM-wheat model in Western Australia. *Field Crops Research* 57 (2): 163-179.
- Bai, H, Zhou, Y, Wang, X & Zhang, L. 2012. The permeability and mechanical properties of cellulose acetate membranes blended with polyethylene glycol 600 for treatment of municipal sewage. *Procedia Environmental Sciences* 16:346-351.
- Bañuelos, G, Ajwa, H, Mackey, B, Wu, L, Cook, C, Akohoue, S & Zambruzuski, S. 1997. Evaluation of different plant species used for phytoremediation of high soil selenium. *Journal of Environmental Quality* 26 (3): 639-646.
- Bañuelos, GS, Bryla, DR & Cook, CG. 2002. Vegetative production of kenaf and canola under irrigation in central California. *Industrial Crops and Products* 15 (3): 237-245.
- Bar-Yosef, B. 1999. Advances in fertigation. *Advances in Agronomy* 65 (1): 1-77.

- Bauböck, R. 2014. Simulating the yields of bioenergy and food crops with the crop modeling software BioSTAR: the carbon-based growth engine and the BioSTAR ETo method. *Environmental Sciences Europe* 26 (1): 1-9.
- Becker, F. 2017. Effect of seasonal distribution and rate of nitrogen fertilisation on canola production and soil bacterial communities in the Western Cape. Unpublished MSc Thesis. Agronomy, Stellenbosch University, Stellenbosch, South Africa.
- Beven, K. 2004. Robert E. Horton's perceptual model of infiltration processes. *Hydrological Processes* 18 (17): 3447-3460.
- Boote, KJ, Jones, JW, Hoogenboom, G & Pickering, N. 1998. Simulation of crop growth: CROPGRO model. *Agricultural Systems Modeling and Simulation* 18 651-692.
- Boote, KJ, Mínguez, MI & Sau, F. 2002. Adapting the CROPGRO legume model to simulate growth of faba bean. *Agronomy Journal* 94 (4): 743-756.
- Bouman, B, Van Keulen, H, Van Laar, H & Rabbinge, R. 1996. The 'School of de Wit' crop growth simulation models: a pedigree and historical overview. *Agricultural Systems* 52 (2-3): 171-198.
- Boyer, JS. 1970. Differing sensitivity of photosynthesis to low leaf water potentials in corn and soybean. *Plant Physiology* 46 (2): 236-239. DOI: 10.1104/pp.46.2.236
- Brisson, N, Gary, C, Justes, E, Roche, R, Mary, B, Ripoche, D, Zimmer, D, Sierra, J, Bertuzzi, P & Burger, P. 2003. An overview of the crop model STICS. *European Journal of Agronomy* 18 (3-4): 309-332.
- Brisson, N, Mary, B, Ripoche, D, Jeuffroy, MH, Ruget, F, Nicoullaud, B, Gate, P, Devienne-Barret, F, Antonioletti, R & Durr, C. 1998. STICS: a generic model for the simulation of crops and their water and nitrogen balances. I. Theory and parameterization applied to wheat and corn. *Agronomie* 18 (5-6): 311-346.
- Bucks, D, Nakayama, F & Warrick, A. 1982. Principles, practices, and potentialities of trickle (drip) irrigation. In: ed. Hillel, D, *Advances in irrigation*. 219-298. Academic Press, Cambridge, Massachusetts, USA.
- Cai, Y, Wu, P, Zhang, L, Zhu, D, Chen, J, Wu, S & Zhao, X. 2017. Simulation of soil water movement under subsurface irrigation with porous ceramic emitter. *Agricultural Water Management* 192: 244-256.
- Carberry, P, Muchow, R & McCown, R. 1989. Testing the CERES-Maize simulation model in a semi-arid tropical environment. *Field Crops Research* 20 (4): 297-315.
- Castejón, P, Habibi, K, Saffar, A, Ajji, A, Martínez, AB & Arencón, D. 2017. Polypropylene-based porous membranes: influence of polymer composition, extrusion draw ratio and uniaxial Strain. *Polymers* 10 (1): 33-54.
- CEC. 2018. Canola and groundnuts: The past year and the one that lies ahead. [Internet]. Grain-SA. Available from: <https://www.grainsa.co.za/grain-market-overview-16-january-2018>. [Accessed: 23 March 2019].
- Coetzee, A. 2017. Rate and timing of nitrogen fertilisation for canola production in the Western Cape of South Africa. Unpublished MSc Thesis. Agronomy, Stellenbosch University, Stellenbosch, South Africa.
- Corbatón-Báguena, M-J, Vincent-Vela, M-C, Gozávez-Zafrilla, J-M, Álvarez-Blanco, S, Lora-García, J & Catalán-Martínez, D. 2016. Comparison between artificial neural networks and Hermia's models to assess ultrafiltration performance. *Separation and Purification Technology* 170: 434-444.
- Dabral, P, Pandey, P, Pandey, A, Singh, K & Singh, MS. 2012. Modelling of wetting pattern under trickle source in sandy soil of Nirjuli, Arunachal Pradesh (India). *Irrigation Science* 30 (4): 287-292.
- DAFF. 2016. Production guideline for Canola. Department of Agriculture, F, and Fisheries, Pretoria, South Africa.

- de Wit, A, Boogaard, H, Fumagalli, D, Janssen, S, Knapen, R, van Kraalingen, D, Supit, I, van der Wijngaart, R & van Diepen, K. 2018. 25 years of the WOFOST cropping systems model. *Agricultural Systems* 168 (4): 154-167.
- de Wit, CT. 1965. *Photosynthesis of leaf canopies*. Wageningen University, Wageningen, Netherlands.
- Deng, B & Wang, J. 2017. Saturated-unsaturated groundwater modeling using 3D Richards equation with a coordinate transform of nonorthogonal grids. *Applied Mathematical Modelling* 50: 39-52.
- Donohue, RJ, McVicar, TR & Roderick, ML. 2010. Assessing the ability of potential evaporation formulations to capture the dynamics in evaporative demand within a changing climate. *Journal of Hydrology* 386 (1-4): 186-197.
- Dukes, M & Scholberg, J. 2005. Soil moisture controlled subsurface drip irrigation on sandy soils. *Applied Engineering in Agriculture* 21 (1): 89-101.
- Fan, Y-W, Huang, N, Zhang, J & Zhao, T. 2018. Simulation of Soil Wetting Pattern of Vertical Moistube-Irrigation. *Water* 10 (5): 601-621.
- Farré, I, Robertson, M, Walton, G & Asseng, S. 2002. Simulating phenology and yield response of canola to sowing date in Western Australia using the APSIM model. *Australian Journal of Agricultural Research* 53 (10): 1155-1164.
- Field, R. 2010. Fundamentals of fouling. *Membranes for Water Treatment* 4: 1-23.
- Foster, T, Brozović, N, Butler, A, Neale, C, Raes, D, Steduto, P, Fereres, E & Hsiao, TC. 2017. AquaCrop-OS: An open source version of FAO's crop water productivity model. *Agricultural Water Management* 181: 18-22.
- Friedel, J, Langer, T, Siebe, C & Stahr, K. 2000. Effects of long-term waste water irrigation on soil organic matter, soil microbial biomass and its activities in central Mexico. *Biology and Fertility of Soils* 31 (5): 414-421.
- Furuichi, M, Matsumoto, K & Nakamura, K. 2008. Evaluation of water quality using a plugging coefficient based on a pore blocking filtration model in the membrane filtration process. *Membrane* 33 (6): 307-316.
- IGadkaree, KP & Hersh, IS. 1994. Method of making semi-permeable polymer membranes. *New York, USA*. 5275766 (968661). USA.
- Galindo, A, Collado-González, J, Griñán, I, Corell, M, Centeno, A, Martín-Palomo, M, Girón, I, Rodríguez, P, Cruz, Z & Memmi, H. 2018. Deficit irrigation and emerging fruit crops as a strategy to save water in Mediterranean semiarid agrosystems. *Agricultural Water Management* 202: 311-324.
- Gärdenäs, A, Hopmans, J, Hanson, B & Šimůnek, J. 2005. Two-dimensional modeling of nitrate leaching for various fertigation scenarios under micro-irrigation. *Agricultural Water Management* 74 (3): 219-242.
- GardenSoft. 2009. Idealised wetting patterns for drippers in various soil types. [Internet]. GardenSoft. Available from: [http://www.sm.watersavingplants.com/GardenResources/HTML/index.html?types\\_of\\_irrigation\\_systems.htm](http://www.sm.watersavingplants.com/GardenResources/HTML/index.html?types_of_irrigation_systems.htm). [Accessed: 10 March 2019].
- Grain-SA. 2018. Canola and groundnuts: The past year and the one that lies ahead. [Internet]. Grain-SA. Available from: <https://www.grainsa.co.za/grain-market-overview-16-january-2018>. [Accessed: 23 march 2019].
- Gu, X-B, Li, Y-N & Du, Y-D. 2018. Effects of ridge-furrow film mulching and nitrogen fertilization on growth, seed yield and water productivity of winter oilseed rape (*Brassica napus* L.) in Northwestern China. *Agricultural Water Management* 200: 60-70.
- Guo, W, Ngo, H-H & Li, J. 2012. A mini-review on membrane fouling. *Bioresource Technology* 122: 27-34.

- Guo, Y, Shen, L & Zhang, G. 2017. An experimental study on the dynamic growth of onion with moistube irrigation technology in green house. *Water Sav Irrig* 42 (2):9-15
- Gutterer, B, Ulrich, A & Reuter, S. 2009. *Decentralised wastewater treatment systems (DEWATS) and sanitation in developing countries: a practical guide*. WEDC, Loughborough University, BORDA, Loughborough University, United Kingdom.
- Hagin, J & Lowengart, A. 1996. Fertigation for minimizing environmental pollution by fertilizers. In: eds. Stoke, A, Spanos, I, Norris, JE and Cammeraat, E, *Developments in Plant and Soil Sciences*. 23-25. Springer, Dordrecht, South Africa.
- Han, Q, Xiang, L, Jiang, X, Wang, G, Zhou, Y, Gao, T & Lei, C. 2015. Application test of micro-irrigation and fertilization integration technology in citrus orchard. *Modern Gardening*. 65 (7): 1196-1214.
- Hanson, BR, Šimůnek, J & Hopmans, JW. 2006. Evaluation of urea–ammonium–nitrate fertigation with drip irrigation using numerical modeling. *Agricultural Water Management* 86 (1-2): 102-113.
- Hermia, J. 1982. Constant pressure blocking filtration laws-application to power-law non-Newtonian fluids. *Chem. Eng. Res. Des.* 60: 183-187.
- Hobbins, M & Huntington, J. 2016. Evapotranspiration and Evaporative Demand. In: ed. Singh, VP, *Handbook of Applied Hydrology*. 42. 1-18. McGraw-Hill Education, Pennsylvania, USA.
- Hocking, P, Randall, P & DeMarco, D. 1997. The response of dryland canola to nitrogen fertilizer: partitioning and mobilization of dry matter and nitrogen, and nitrogen effects on yield components. *Field Crops Research* 54 (2-3): 201-220.
- Hodges, T, Botner, D, Sakamoto, C & Haug, JH. 1987. Using the CERES-Maize model to estimate production for the US Cornbelt. *Agricultural and Forest Meteorology* 40 (4): 293-303.
- Holzworth, D, Meinke, H, DeVoi, P, Wegener, M, Huth, N, Hammer, G, Howden, M, Robertson, M, Carberry, P & Freebairn, D. 2006. The development of a farming systems model (APSIM) a disciplined approach. *Third International Conference on Environmental Modeling and Software*. Brigham Young University, Burlington, Vermont, USA.
- Horton, RE. 1939. Analysis of runoff-plat experiments with varying infiltration-capacity. *Eos, Transactions American Geophysical Union* 20 (4): 693-711.
- Horton, RE. 1941. An approach toward a physical interpretation of infiltration-capacity 1. *Soil Science Society of America Journal* 5 (C): 399-417.
- Hu, Q, Hua, W, Yin, Y, Zhang, X, Liu, L, Shi, J, Zhao, Y, Qin, L, Chen, C & Wang, H. 2017. Rapeseed research and production in China. *The Crop Journal* 5 (2): 127-135.
- Hussain, I, Raschid, L, Hanjra, MA, Marikar, F & van der Hoek, W. 2001. *A framework for analyzing socioeconomic, health and environmental impacts of wastewater use in agriculture in developing countries*. International Water Management Institute, Colombo, Sri Lanka.
- Iglesias, A & Garrote, L. 2015. Adaptation strategies for agricultural water management under climate change in Europe. *Agricultural Water Management* 155: 113-124.
- Isoda, A, Konishi, H, Wang, P & Li, Z. 2007. *Effects of different irrigation methods on yield and water use efficiency of sugar beet [Beta vulgaris] in the arid area of China*. Horticulture Research, Chiba University, Japan.
- Jones, C, Dyke, P, Williams, J, Kiniry, J, Benson, V & Griggs, R. 1991. EPIC: an operational model for evaluation of agricultural sustainability. *Agricultural Systems* 37 (4): 341-350.
- Jones, CA, Kiniry, JR & Dyke, P. 1986. *CERES-Maize: A simulation model of maize growth and development*. Texas A&M University Press, Texas, USA.

- Jun, Z, Wenquan, N, Linlin, Z & Liyan, S. 2012. Experimental study on characters of wetted soil in moistube irrigation. *Science of Soil and Water Conservation* 10 (6): 32-38.
- Kanda, E. 2019. Soil water dynamics and response of cowpea under Moistube irrigation. Unpublished PhD Thesis. Bioresources Engineering, University of KwaZulu-Natal, Pietermaritzburg, South Africa.
- Kanda, EK, Mabhaudhi, T & Senzanje, A. 2018a. Coupling hydrological and crop models for improved agricultural water management—A review. *Bulgarian Journal of Agricultural Science* 24 (3): 380-390.
- Kanda, EK, Mabhaudhi, T & Senzanje, A. 2018b. Hydraulic and clogging characteristics of moistube irrigation as influenced by water quality. *Journal of Water Supply: Research and Technology-Aqua* 67 (5): 438-446.
- Kandelous, MM & Šimůnek, J. 2010. Numerical simulations of water movement in a subsurface drip irrigation system under field and laboratory conditions using HYDRUS-2D. *Agricultural Water Management* 97 (7): 1070-1076.
- Kang, S, Hao, X, Du, T, Tong, L, Su, X, Lu, H, Li, X, Huo, Z, Li, S & Ding, R. 2017. Improving agricultural water productivity to ensure food security in China under changing environment: From research to practice. *Agricultural Water Management* 179: 5-17.
- Karandish, F & Šimůnek, J. 2019. A comparison of the HYDRUS (2D/3D) and SALTMed models to investigate the influence of various water-saving irrigation strategies on the maize water footprint. *Agricultural Water Management* 213: 809-820.
- Keating, BA, Carberry, PS, Hammer, GL, Probert, ME, Robertson, MJ, Holzworth, D, Huth, NI, Hargreaves, JN, Meinke, H & Hochman, Z. 2003. An overview of APSIM, a model designed for farming systems simulation. *European Journal of Agronomy* 18 (3-4): 267-288.
- Khan, NN, Islam, MM, Islam, S & Moniruzzaman, S. 2015. Effect of porous pipe characteristics of soil wetting pattern in a negative pressure difference irrigation system. *American Journal of Engineering Research (AJER)* 4 (2): 01-12.
- Lamm, FR, Bordovsky, J, Schwankl, L, Grabow, G, Enciso-Medina, J, Peters, R, Colaizzi, P, Trooien, T & Porter, D. 2012. Subsurface drip irrigation: Status of the technology in 2010. *Transactions of the ASABE* 55 (2): 483-491.
- Legates, DR & McCabe Jr, GJ. 1999. Evaluating the use of “goodness-of-fit” measures in hydrologic and hydroclimatic model validation. *Water Resources Research* 35 (1): 233-241.
- Levidow, L, Zaccaria, D, Maia, R, Vivas, E, Todorovic, M & Scardigno, A. 2014. Improving water-efficient irrigation: Prospects and difficulties of innovative practices. *Agricultural Water Management* 146: 84-94.
- Levy, G, Fine, P & Bar-Tal, A. 2011. *Treated Wastewater in Agriculture: Use and Impacts on the Soil Environment and Crops*. John Wiley & Sons, Hoboken, New Jersey, USA.
- Li, H, Cong, R, Ren, T, Li, X, Ma, C, Zheng, L, Zhang, Z & Lu, J. 2015a. Yield response to N fertilizer and optimum N rate of winter oilseed rape under different soil indigenous N supplies. *Field Crops Research* 181: 52-59.
- Li, X, Li, Q, Yang, T, Nie, Z, Chen, G & Hu, L. 2016. Responses of plant development, biomass and seed production of direct sown oilseed rape (*Brassica napus*) to nitrogen application at different stages in Yangtze River Basin. *Field Crops Research* 194: 12-20.
- Li, X, Yang, T, Nie, Z, Chen, G, Hu, L & Wang, R. 2015b. A functional leaf may represent the assimilate accumulation characteristics of the whole seedling plant in winter oilseed rape (*Brassica napus* L.). *Crop and Pasture Science* 66 (8): 849-856.
- Liu, H & Huang, G. 2009. Laboratory experiment on drip emitter clogging with fresh water and treated sewage effluent. *Agricultural Water Management* 96 (5): 745-756.



- Lyu, W, Niu, W, Gu, J, Li, Y, Zou, X & Zhang, R. 2016. Effect of moisture depth and density on tomato yield and quality in solar greenhouse. *Chinese Journal of Eco-Agriculture* 24 (12): 1663-1673.
- Mataram, A, Rizal, S & Pujiono, E. 2018. Physical and mechanical properties of membrane polyvinylidene fluoride with the addition of silver nitrate. *MATEC Web of Conferences*. EDP Sciences, Patra Jasa Hotel in Semarang, Indonesia.
- Matheyarasu, R, Seshadri, B, Bolan, NS & Naidu, R. 2015. Impacts of abattoir waste-water irrigation on soil fertility and productivity. In: ed. Javaid, MS, *Irrigation and Drainage; Sustainable Strategies and Systems*. 3. 55-75. InTech, Croatia.
- Molden, D, Oweis, T, Steduto, P, Bindraban, P, Hanjra, MA & Kijne, J. 2010. Improving agricultural water productivity: Between optimism and caution. *Agricultural Water Management* 97 (4): 528-535.
- Moreira Barradas, J, Abdelfattah, A, Matula, S & Dolezal, F. 2014. Effect of fertigation on soil salinization and aggregate stability. *Journal of Irrigation and Drainage Engineering* 141 (4): 1943-4774.
- Moriasi, DN, Arnold, JG, Van Liew, MW, Bingner, RL, Harmel, RD & Veith, TL. 2007. Model evaluation guidelines for systematic quantification of accuracy in watershed simulations. *Transactions of the ASABE* 50 (3): 885-900.
- Musazura, W. 2018. Crop Fertigation (Nitrogen and Phosphorus) with Decentralised Wastewater Treatment System Effluents and Effects on Soils and Groundwater. Unpublished PhD Thesis. Crop Science, University of KwaZulu-Natal, Pietermaritzburg, South Africa.
- Musazura, W, Odindo, A, Tesfamariam, E, Hughes, J & Buckley, C. 2019. Nitrogen and phosphorus dynamics in plants and soil fertigated with decentralised wastewater treatment effluent. *Agricultural Water Management* 215: 55-62.
- Niu, W, Lü, W, Gu, J, Liang, B, Guo, L & Guan, Y. 2017. Effects of moisture depth and spacing on soil water and salt transports of tomato in solar greenhouse. *Transactions of the Chinese Society of Agricultural Engineering* 33 (19): 131-140.
- Ozer, H. 2003. Sowing date and nitrogen rate effects on growth, yield and yield components of two summer rapeseed cultivars. *European Journal of Agronomy* 19 (3): 453-463.
- Pauwels, V, Verhoest, NE, De Lannoy, GJ, Guissard, V, Lucau, C & Defourny, P. 2007. Optimization of a coupled hydrology–crop growth model through the assimilation of observed soil moisture and leaf area index values using an ensemble Kalman filter. *Water Resources Research* 43 (4): 1-17.
- Pescod, M. 1992. *Wastewater treatment and use in agriculture*. FAO, Rome, Italy.
- Petty, JD, Huckins, JN, Martin, D & Adornato, T. 1995. Use of semipermeable membrane devices (SPMDS) to determine bioavailable organochlorine pesticide residues in streams receiving irrigation drainwater. *Chemosphere* 30 (10): 1891-1903.
- Phuntsho, S, Shon, HK, Hong, S, Lee, S & Vigneswaran, S. 2011. A novel low energy fertilizer driven forward osmosis desalination for direct fertigation: evaluating the performance of fertilizer draw solutions. *Journal of Membrane Science* 375 (1-2): 172-181.
- Priya, S & Shibasaki, R. 2001. National spatial crop yield simulation using GIS-based crop production model. *Ecological Modelling* 136 (2-3): 113-129.
- Puig-Bargués, J, Arbat, G, Barragán, J & De Cartagena, FR. 2005. Hydraulic performance of drip irrigation subunits using WWTP effluents. *Agricultural Water Management* 77 (1-3): 249-262.
- Qui, Z, Jiang, P & Xiao, J. 2015. Experimental study on influence of water temperature on outflows of low pressure Moistube *Water Sav Irrig* 40 (6): 31-38.

- Raes, D, Steduto, P, Hsiao, TC & Fereres, E. 2009. AquaCrop—the FAO crop model to simulate yield response to water: II. Main algorithms and software description. *Agronomy Journal* 101 (3): 438-447.
- Ragab, R. 2002. A holistic generic integrated approach for irrigation, crop and field management: the SALTMED model. *Environmental Modelling & Software* 17 (4): 345-361.
- Ragab, R. 2015. Integrated management tool for water, crop, soil and N fertilizers: the SALTMED model. *Irrigation and Drainage* 64 (1): 1-12.
- Ragab, R, Choukr-Allah, R, Nghira, A & Hirich, A. 2016. SALTMED model and its application on field crops, different water and field management and under current and future climate change. In: eds. Choukr Allah, R, Ragab, R, Bouchaou, L and Barceló, D, *The Souss-Massa River Basin, Morocco*. 227-274. Springer, Cham, Switzerland.
- Ravikumar, V, Vijayakumar, G, Šimůnek, J, Chellamuthu, S, Santhi, R & Appavu, K. 2011. Evaluation of fertigation scheduling for sugarcane using a vadose zone flow and transport model. *Agricultural Water Management* 98 (9): 1431-1440.
- Raymer, PL. 2002. Canola: an emerging oilseed crop. In: eds. Janick, J and Whipkey, A, *Trends in new crops and new uses*. 122-126. ASHS Press, Alexandria, VA, USA.
- Robertson, M, Carberry, P, Huth, N, Turpin, J, Probert, ME, Poulton, P, Bell, M, Wright, G, Yeates, S & Brinsmead, R. 2002. Simulation of growth and development of diverse legume species in APSIM. *Australian Journal of Agricultural Research* 53 (4): 429-446.
- Rost, S, Gerten, D, Bondeau, A, Lucht, W, Rohwer, J & Schaphoff, S. 2008. Agricultural green and blue water consumption and its influence on the global water system. *Water Resources Research* 44 (9): W09405.
- Sangeetha, M & Kandaswamy, A. 2016. Image analysis of pore morphology of hemodialyser membrane using advanced microscopic techniques. *Journal of Medical Imaging and Health Informatics* 6 (7): 1617-1624.
- Schwartzman, M & Zur, B. 1986. Emitter spacing and geometry of wetted soil volume. *Journal of Irrigation and Drainage Engineering* 112 (3): 242-253.
- Shahidi, F. 1990. *Canola and rapeseed: production, chemistry, nutrition, and processing technology*. Van Nostrand and Reinhold, New York, USA.
- Silva, L, Ragab, R, Duarte, I, Lourenço, E, Simões, N & Chaves, M. 2013. Calibration and validation of SALTMED model under dry and wet year conditions using chickpea field data from Southern Portugal. *Irrigation Science* 31 (4): 651-659.
- Šimůnek, J, van Genuchten, MT & Šejna, M. 2008. Development and applications of the HYDRUS and STANMOD software packages and related codes. *Vadose Zone Journal* 7 (2): 587-600.
- Singh, D, Rajput, T, Sikarwar, H, Sahoo, R & Ahmad, T. 2006. Simulation of soil wetting pattern with subsurface drip irrigation from line source. *Agricultural Water Management* 83 (1-2): 130-134.
- Siyal, A & Skaggs, TH. 2009. Measured and simulated soil wetting patterns under porous clay pipe sub-surface irrigation. *Agricultural Water Management* 96 (6): 893-904.
- Smit, B & Skinner, MW. 2002. Adaptation options in agriculture to climate change: a typology. *Mitigation and Adaptation Strategies for Global Change* 7 (1): 85-114.
- Steduto, P. Comparing the growth-engines of crop models. FAO Expert Consultation on Crop Water Productivity Under Deficient Water Supply. 2003. FAO, Rome, Italy.
- Steduto, P & Albrizio, R. 2005. Resource use efficiency of field-grown sunflower, sorghum, wheat and chickpea: II. Water use efficiency and comparison with radiation use efficiency. *Agricultural and Forest Meteorology* 130 (3-4): 269-281.

- Steduto, P, Hsiao, TC & Fereres, E. 2007. On the conservative behavior of biomass water productivity. *Irrigation Science* 25 (3): 189-207.
- Steduto, P, Hsiao, TC, Raes, D & Fereres, E. 2009. AquaCrop—The FAO crop model to simulate yield response to water: Concepts and underlying principles. *Agronomy Journal* 101 (3): 426-437.
- Stricker, J, Prine, G & Riddle, T. 1997. *Yield of kenaf grown on two soils at two locations in Florida*. 0096-4522. Soil and Crop Science Society of Florida, Florida, USA.
- Stringam, G, Ripley, V, Love, H & Mitchell, A. 2003. Transgenic herbicide tolerant canola—the Canadian experience. *Crop Science* 43 (5): 1590-1593.
- Stucki, M, Loepfe, M & Stark, WJ. 2018. Porous Polymer Membranes by Hard Templating—A Review. *Advanced Engineering Materials* 20 (1): 1700611.
- Sun, Q, Wang, Y, Chen, G, Yang, H & Du, T. 2018. Water use efficiency was improved at leaf and yield levels of tomato plants by continuous irrigation using semipermeable membrane. *Agricultural Water Management* 203: 430-437.
- Tan, G & Shibasaki, R. 2003. Global estimation of crop productivity and the impacts of global warming by GIS and EPIC integration. *Ecological Modelling* 168 (3): 357-370.
- Todorovic, M, Albrizio, R, Zivotic, L, Saab, M-TA, Stöckle, C & Steduto, P. 2009. Assessment of AquaCrop, CropSyst, and WOFOST models in the simulation of sunflower growth under different water regimes. *Agronomy Journal* 101 (3): 509-521.
- Vela, MCV, Blanco, SÁ, García, JL & Rodríguez, EB. 2009. Analysis of membrane pore blocking models adapted to crossflow ultrafiltration in the ultrafiltration of PEG. *Chemical Engineering Journal* 149 (1-3): 232-241.
- Wang, X & Melesse, A. 2005. Evaluation of the SWAT model's snowmelt hydrology in a northwestern Minnesota watershed. *Transactions of the ASAE* 48 (4): 1359-1376.
- Willmott, CJ. 1981. On the validation of models. *Physical Geography* 2 (2): 184-194.
- Xie, X, Qi, S, Guohong, L, Wang, Z & Ma, X. 2014. Effects of silt content and particle size in irrigation water on Moistube outflow. *Journal of Irrigation and Drainage* 33 (6): 38-40.
- Xue, W, Niu, W, Zhang, Z & Zhang, K. 2013. Effects of the tomato growth and water use efficiency in sunlight greenhouse by Moistube-irrigation. *Agricultural Research in the Arid Areas* 25 (6): 61-66.
- Yang, W-j, Tian, L, Du, T-s, Ding, R-s & Yang, Q. 2008. Research prospect of the water-saving irrigation by semi-permeable film [J]. *Journal of Water Resources and Water Engineering* 6: 16.
- Yu, X, Liu, X, Zhu, Y, Qi, Y, Yang, Q & Tang, J. 2017. Effects of soil texture and water pressure on moistube infiltration in vertical inserting mode. *Journal of Drainage and Irrigation Machinery Engineering* 35: 71-79.
- Zeleeke, KT, Luckett, D & Cowley, R. 2011. Calibration and testing of the FAO AquaCrop model for canola. *Agronomy Journal* 103 (6): 1610-1618.
- Zhang, J, Niu, W, Zhang, L, Shi, L & Wu, Z. 2014. Effects of soil initial water content on line-source infiltration characteristic in moisture irrigation. *Journal of Drainage Irrigation Machinery Engineering* 34 (11): 72-78.
- Zhang, J, Saito, H & Kato, M. 2009. Study on subsurface irrigation using ceramic pitcher on tomato cultivation in greenhouse. *J. Arid L. Stud.* 19: 265-267.
- Zhang, L, Wu, P, Zhu, D & Zheng, C. 2017a. Effect of pulsating pressure on labyrinth emitter clogging. *Irrigation Science* 35 (4): 267-274.
- Zhang, M, Niu, W, Lu, Z, Yuan, L, Wang, J & Qui, X. 2017b. Effect of moistube-irrigation on crop yield and water use efficiency. *Chinese Journal of Eco-Agriculture* 11 (25): 1671-1683.

- Zhang, P, Chen, G & Zheng, X. 2010. Preparation and mechanical property of polymer-based biomaterials. *Journal of Physics: Conference Series*. 240 (1): 12152.
- Zhang, S, Lei, T, Ding, Y & Xu, C. 2002. Finite element modeling of soil water movement under subsurface irrigation with porous pipe and its application. *Nongye Gongcheng Xuebao(Transactions of the Chinese Society of Agricultural Engineering)* 18 (4): 1-5.
- Zhang, Z, Niu, W, Xu, J & Zhang, K. 2015. Effect of tube depth of Moistube-Irrigation under plastic film mulching on soil water and salt transports of greenhouse tomato *Chinese Journal of Eco-Agriculture* 23 (9): 1112-1121.
- Zhu, Y, Liu, X, HE, H, Yang, Q & Sui, L. 2018. Effects of moistube irrigation on growth and moisture-radiation use of coffea arabica under jujube shading cultivation. *Journal of Drainage and Irrigation Machinery Engin* 36 (9): 806-811.10.3969/j.issn.1674-8530.18.1019
- Zou, X, Quan, T, Zhou, M, Yang, Q & Shi, Y. 2017. Progress and prospects of moistube irrigation technology research. *Bulletin of Soil and Water Conservation* 37 (4): 150-155.

### 3 MOISTUBE IRRIGATION (MTI) DISCHARGE UNDER VARIABLE EVAPORATIVE DEMAND

This Chapter was published as:

**Dirwai, TL**, Senzanje, A, Mabhaudhi, T (2020). Moistube Irrigation (MTI) Discharge Under Variable Evaporative Demand. *PLoS ONE* 15(12):1 – 12. <https://doi.10.1371/journal.pone.0236211>

#### Abstract

We investigated the conceptual capability of Moistube irrigation (MTI) to discharge under zero applied positive pressure and under varied climatic conditions by inducing an artificial evaporative demand ( $E_d$ ) or negative pressure around Moistube tubing. This study was premised on the null hypothesis that an artificially induced  $E_d$  or negative pressure does not impact MTI discharge. Moistube tubing was enclosed in a 1 m long PVC conduit. A 20 l water reservoir placed on an electronic balance provided a continuous supply of water whilst a three-speed hot air blower simultaneously supplied a heat flux and facilitated the advection process. The procedure was conducted under varied climatic conditions with three air velocity ( $u_a$ ) treatments namely; 1.2 m.s<sup>-1</sup>, 2.5 m.s<sup>-1</sup>, and 3.0 m.s<sup>-1</sup> and the experiment run times were 159 h, 134 h and 10 h, respectively. The average temperature ( $T_{ave}$ ) and relative humidity (RH) data for  $u_a = 1.2$  m.s<sup>-1</sup> were 53°C and 7.31%, whilst for  $u_a = 2.5$  m.s<sup>-1</sup>,  $T_{ave}$  was 56°C and RH = 7.19%, and for  $u_a = 3.0$  m.s<sup>-1</sup>,  $T_{ave}$  was 63°C and RH = 6.16%. The experimental data was input into the four variable Penman-Monteith method to compute the evaporative demand ( $E_d$ ). For each  $E_d$ , the instantaneous mass flow rate ( $\dot{m}$ ) was recorded using an electronic balance and subsequently converted to volumetric flow rates. For each of the air velocities, the respective  $E_d$  values obtained were 0.16, 0.31 and 0.36 mm.d<sup>-1</sup>. The Bowen ratios ( $r$ ) were well below 1 ( $r < 1$ ), which suggested a sufficient supply of moisture to evaporate. For  $E_d = 0.16$  mm.d<sup>-1</sup> the vapour pressure deficit (VPD) was 113.08 mbar, whilst for  $E_d = 0.31$  mm.d<sup>-1</sup> and for  $E_d = 0.36$  mm.d<sup>-1</sup> the VPD were 129.93 mbar and 150.14 mbar, respectively. The recorded discharges ( $q$ ) at normalised time ( $t^*$ ) = 1 h for  $E_d = 0.16$  mm.d<sup>-1</sup> was  $7.67 \times 10^{-3}$  l.hr<sup>-1</sup>.m<sup>-1</sup> length, whilst for  $E_d = 0.31$  mm.d<sup>-1</sup>  $q = 14.5 \times 10^{-3}$  l.hr<sup>-1</sup>.m<sup>-1</sup> length, and for  $E_d = 0.36$  mm.d<sup>-1</sup>  $q = 20.8 \times 10^{-3}$  l.hr<sup>-1</sup>.m<sup>-1</sup> length.. This phenomenon allows MTI to be used for deficit irrigation purposes and allows irrigators to capitalize on realistic soil matric potential irrigation scheduling approach.

**Keywords:** Bowen ratio; negative soil water potential, semi-permeable membrane, vapour pressure deficit

### 3.1 Introduction

Moistube irrigation (MTI) is a relatively new semi-permeable membrane (SPM) irrigation technology. A typical third generation Moistube pipe has an outer protective membrane and an inner membrane that constitutes of densely and uniformly spaced nano-pores whose pore-diameter ranges from 10 – 900 nm. The technology utilises nano-technology such that the inner membrane imitates plant water uptake, which facilitates discharge according to crop water requirements (Zou et al., 2017; Kanda et al., 2019). MTI is a low pressure discharge sub-surface irrigation technology whose functionality is similar to ceramic pitcher pots. Under a negative pressure, or in the absence of applied pressure, the discharge is a function of matric potential ( $\psi$ ) (Yang et al., 2008; Zou et al., 2017; Kanda et al., 2019). Negative pressure irrigation (NPI) is when water supply pressure is regulated by soil matric potential (Wang et al., 2019). NPI can be classified as a precision irrigation technique which offers benefits such as continuous regulation of soil moisture thus improving crop yield, reduction of non-beneficial water use such as water loss by evaporation and runoff (Khan et al., 2013; Zheng et al., 2013; Wang et al., 2019). Conceptually, when water potential ( $\psi_{water}$ ) is greater than the matric potential of the surrounding soil ( $\psi_{soil}$ ), the MTI discharge rate is high and vice versa (Yang et al., 2008; Kanda et al., 2019). There exists a number of issues in need of research answers, for example, how MTI discharge varies with imposed evaporative demand ( $E_d$ ). The  $E_d$  mimics changing soil water conditions thus exploring MTI applicability to deficit irrigation.

According to FAO (2002), evapotranspiration ( $ET$ ) is a combination of water loss from soils and transpiration by plants; the water loss mechanisms occur simultaneously under ambient conditions. A simpler method of estimating  $ET$  is by using evaporative demand ( $E_d$ ), which is defined as the upper boundary for  $ET$  under ambient conditions with an uncapped hydrological limit or unlimited water supply.  $E_d$  is used in irrigation scheduling as a proxy for plant water consumptive use wherein crop coefficients or factors such as phenology and soil stress are used to estimate the  $ET_o$  (Hobbins and Huntington, 2016). There exists a correlation between rate and amount of plant water use and  $E_d$  (Clark, 1992), thus since MTI discharge is a function of soil matric potential a high  $E_d$  potentially increases MTI discharge. Currently there is a dearth in literature concerning MTI discharge under variable  $E_d$ . What is known is how rate and amount of water uptake correlates with  $E_d$  (Hobbins and Huntington, 2016).

$E_d$  has three drivers, which are the hydrological, radiative and the advective limits (Donohue et al., 2010b; Hobbins and Huntington, 2016). For evaporative demand to occur there has to be

an adequate water supply to meet the minimum hydrological limit, hence, the hydrological limit defines the availability of water to evaporate and transpire from plants and soil surfaces. According to Hobbins and Huntington (2016), the radiative limit is the energy required to facilitate the evaporative process. Under field conditions, the radiative limit is influenced by variables such as surface albedo ( $\alpha$ ), and shortwave and longwave radiation. For a buried MTI lateral the soil heat fluxes are also involved. Advection is a critical component for  $E_d$ . The advective limit describes the system boundary's ability to absorb and bear away moisture.

Limited research efforts have been made to model  $E_d$  under controlled and varied micro-climatic conditions. For example, Donohue et al. (2010b) used five evapotranspiration formulations namely Penman, Priestley–Taylor, Morton point, Morton areal and Thornthwaite to model and assess the best proxy for  $E_d$ . Abu-Zreig et al. (2018) modelled an artificially induced pan evaporation scenario in order to measure the discharge rates of ceramic pitchers under negative head. The theoretical discharge design aspects of the MTI technology have not been tested. Understanding negative pressure discharge capability of MTI tubing can potentially aid irrigators to inform deficit irrigation strategies and save on energy costs that otherwise drive positive head irrigation systems, and more importantly assess MTI ability to satisfy the irrigation requirements of high water demand crops such as sugar cane.

The study investigated the conceptual discharge mechanism of Moistube irrigation when subjected to a negative pressure or in the absence of a positive driving pressure. The study hypothesized that the presence of an imposed negative pressure or an artificial  $E_d$  cannot induce MTI discharge. This study adds to knowledge by providing answers around the conceptual zero pressure head discharge capability of MTI. The  $E_d$  was used to simulate low matric potential or negative soil water tension conditions whilst monitoring the subsequent discharge performance of a buried Moistube tubing.

## **3.2 Materials and Methods**

### **Study Site**

The experiment was carried out at the University of KwaZulu-Natal Hydrology Laboratory (29.626044, 30.403325). The laboratory had a controlled room temperature of  $22^{\circ}\text{C} \pm 1^{\circ}\text{C}$  and a measured relative humidity (RH) of  $55\% \pm 5\%$ . Controlled conditions helped to eliminate the variations in atmospheric temperature and humidity.

### 3.2.1 Experimental Design and Set-up

The experiment was a single factor experiment: air velocity ( $u_a$ ) with three controlled air velocities namely  $1.2 \text{ m.s}^{-1}$ ,  $2.5 \text{ m.s}^{-1}$  and  $3.0 \text{ m.s}^{-1}$ . Each air velocity level was replicated three times and it was dictated by the default hot air blower settings. The experiment comprised five recorded variables, namely, relative humidity (RH), air velocity ( $u_a$ ), net heat flux from the hot air blower ( $R_n$ ), water mass flow rate ( $\dot{m}$ ), and micro-climate temperature ( $T_a$ ). For each  $u_a$ , the subsequent  $T_a$  and  $R_n$ , were recorded at five-minute intervals for 159 hr, 134 hr and 10 hr, respectively. The last experimental run was limited to 10 hr because the experienced temperatures exceeded realistic temperature scenarios that a buried MTI lateral can experience. The VPD expressed as the difference between actual vapour pressure of the air ( $e_a$ ) and the observed vapour pressure ( $e$ ) was derived from the recorded  $T_a$  and  $R_n$ . Each replicated  $u_a$  yielded values that were used to compute the resultant average  $E_d$  and the corresponding average  $\dot{m}$  values. The  $\dot{m}$  was converted to discharge ( $q$ ) by multiplying the recorded values by the density of water ( $\rho_w$ ).

The equipment was assembled as shown in Figure 3.1. Air was blown axially to the suspended 1 m long Moistube lateral tubing in the PVC conduit. The flow of hot air was provided by a three speed 1800 W hot air blower. The water mass flow ( $\dot{m}$ ) was measured using a GFK 75H electronic balance with a resolution of 0.001 kg (Adam Equipment, South Africa). The water level in the reservoir was kept constant and at the same elevation as the MTI lateral to eliminate the effect of water pressure head on discharge. The relative humidity (RH) was measured using the HCT01-00D sensor (E + E ELEKTRONIC <sup>TM</sup>, Austria) with a 5 - 95% RH working range, resolution of  $\pm 2.5\%$  RH, 2% RH accuracy, and a temperature dependency of  $\pm 0.03\%$  RH/ $^{\circ}\text{C}$ , meaning the measured values were  $\pm 0.02$  close to the actual value and a limit of detection of  $\pm 0.025$ . The temperature was measured using thermocouples (J-type) and a Pt1000 sensor (E + E ELEKTRONIC <sup>TM</sup>, Austria) with a resolution of  $\pm 0.3^{\circ}\text{C}$  and an accuracy of  $0.1^{\circ}\text{C}$ . Air velocity was measured using a hot film anemometer (EE 65 Series, Austria) with a working range of  $0 \text{ m.s}^{-1} - 20 \text{ m.s}^{-1}$  and a resolution and accuracy of  $\pm 0.2 \text{ m.s}^{-1}$ . The sensors were connected to a five terminal unit and 12 channel VGR-B100 (RKC Instrument <sup>TM</sup>, Japan) data logger. The logger was programmed to record average data every five-minute interval for each experimental  $u_a$  and the subsequent replications. The experimental setup is shown in Figure 3.1.



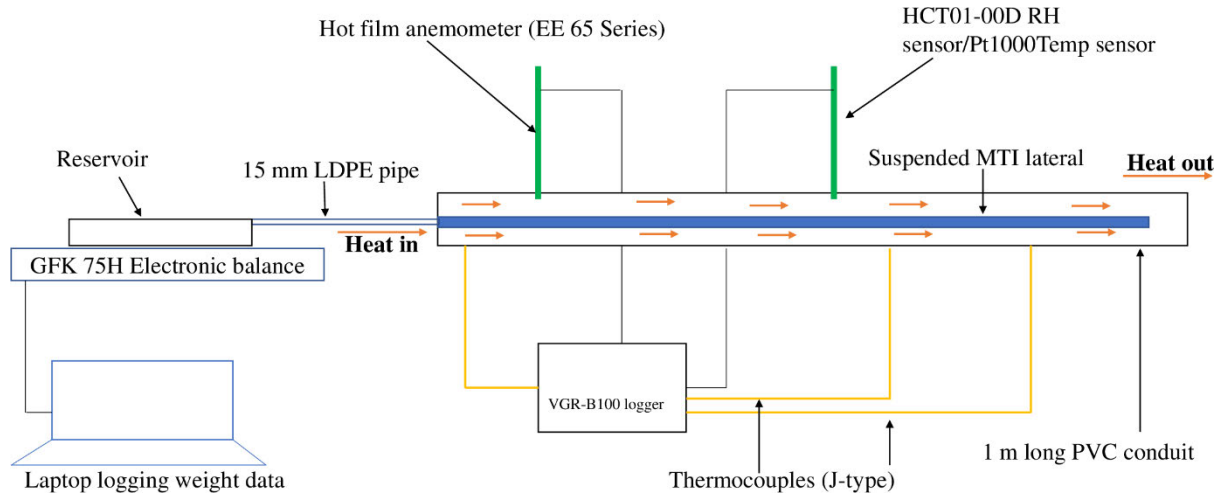


Figure 3.1 Experimental set-up

### 3.2.2 *ET model selection*

The following *ET* models were assessed as proxies for determining  $E_d$ : (i) Morton areal, (ii) Morton point, (iii) Penman-Monteith, (iv) Priestley–Taylor, and (v) Thornthwaite (*Table 3.1*). These models are considered as universal standards for estimating *ET* (Luo et al., 2014). Model selection was based on the ability to accommodate all measured variables. The Penman-Monteith model proved satisfactory since the model could accommodate the input data variables obtained from the experimental data i.e.,  $T_a$ ,  $(e_a - e)$ ,  $R_n$ , and  $u_a$ .

Table 3.1  $E_d$  formulations and the respective variables applied in the model(s)

Formulation	Variables	Reference
Morton areal	$T_a$ , $(e_a - e)$ , $R_n$	(Morton, 1983;Donohue et al., 2010b)
Morton point	$T_a$ , $(e_a - e)$ , $R_n$	(Morton, 1983;Donohue et al., 2010b)
Penman-Monteith	$T_a$ , $(e_a - e)$ , $R_n$ , $u_a$	Penman (1948) cited by Donohue et al. (2010b)
Priestley–Taylor	$T_a$ , $R_n$	Priestley and Taylor (1972) cited by Donohue et al. (2010b)
Thornthwaite	$T_a$	Thornthwaite (1948) cited by (Donohue et al., 2010b)

### 3.2.3 *Penman- Monteith model application to compute $E_d$*

The standardized ASCE Penman-Monteith model was used to compute  $E_d$ . Standardized formulation aided in retaining data accuracy yet simplifying applicability. The model is defined by Equation 3.1 (Penman, 1948; Monteith, 1965; FAO, 2002; Itenfisu et al., 2003):

$$E_d = \frac{0.408\Delta(R_n - G) + \gamma \frac{C_n}{T+273} u_a (e_a - e)}{\Delta + \gamma(1 + C_d u_a)} \quad 3.1$$

where:  $\Delta$  = slope of the saturation vapour-pressure curve at air temperature (kPa.°C),  $R_n$  = net radiation (W.m<sup>-2</sup>),  $e_a - e$  = vapour-pressure deficit (mbars),  $e$  = actual vapour pressure of air (mbars),  $\gamma$  = psychometric constant of proportionality (kPa.°C<sup>-1</sup>),  $T$  = hourly air temperature (°C),  $C_n$  = numerator constant for reference type and calculation time step ( $C_n = 900$ ), and  $C_d$  = denominator constant for reference type and calculation time ( $C_d = 0.34$ ) (Itenfisu et al., 2003).

The energy balance equation was used to determine the evaporation energy. The  $R_n$  was determined by Equation 3.2 and it was recorded in five-minute intervals:

$$R_n = R_i - R_r - L_u - R_c - R_s + R_a \quad 3.2$$

where:  $R_i$  = short wave solar radiation,  $R_r$  = reflected part of the solar energy,  $R_c$  is the conduction energy in air,  $R_s$  = incremental stored energy in the conduit, and  $R_a$  = advective energy.  $R_i$ ,  $R_c$ ,  $R_s$  and  $R_a$  are measured in flux units (W.m<sup>-2</sup>). Parameters  $R_i$ ,  $R_r$ ,  $L_u$ , and  $R_c$  were neglected because the experiment was conducted in the laboratory. According to Cross [17] when  $R_s$  and  $R_a$  are measured in five-minute intervals which constitute “short intervals” the two parameters can be neglected since they are negligible. Furthermore, considering that the experiment was not a closed air system, it therefore invalidated the relevance of  $R_s$ . In addition, the parameter  $R_s$  is dependent on duration of sunshine hours (DS) and maximum possible sunshine hours available whilst the parameter  $R_a$  utilises the  $d_r$  function which is the distance between the earth and the sun (Najmaddin et al., 2017), thus providing further evidence in their exclusion in Equation 7. Therefore  $R_n$  was computed as per Equation 3.3:

$$R_n = \frac{Q_{in}}{\rho_w * L * (1+r)} \quad 3.3$$

where  $Q_{in}$  = energy from the heater (J) (Equation 3.4),  $\rho_w$  = density of water (kg.m<sup>-3</sup>),  $L$  = latent heat of evaporation (J.kg<sup>-1</sup>), and  $r$  = Bowen ratio (Equation 3.5):

$$Q_{in} = \rho_{air}(\dot{v}A) * C_p(\Delta T) + \varepsilon\sigma\Delta T^4 + hA\Delta T \quad 3.4$$

where  $A$  = area of the blower duct (m<sup>2</sup>),  $\dot{v}$  = air volumetric flow rate (m<sup>3</sup>.s<sup>-1</sup>) (product of the cross-sectional area ( $A$ ) of hot air blower duct and the average flow velocity  $u_i$ ),  $C_p$  = specific heat capacity of air (J.kg<sup>-1</sup>. °C<sup>-1</sup>),  $\varepsilon$  is the emissivity coefficient of the PVC conduit (0.92) (Anon, 2020),  $\sigma$  = Stefan-Boltzmann Constant (5.670367\*10<sup>-8</sup> W.m<sup>-2</sup>.°C<sup>-4</sup>),  $h$  = convective

heat transfer coefficient ( $\text{W.m}^{-2}.\text{°C}^{-1}$ ),  $\rho_{air}$  = density of air ( $\text{kg.m}^{-3}$ ), and  $\Delta T$  = change in temperature along the PVC conduit heating surface ( $\text{°C}$ ). The Bowen ratio was determined as follows:

$$r = \frac{6.1 \cdot 10^{-4} \cdot \rho_{air} \cdot \Delta T}{e_a - e} \quad 3.5$$

The  $q$  vs  $t$  relationship was established on a normalised time-scale ( $t^*$ ). The  $t^*$  was calculated according to Equation 3.6.

$$t^* = \frac{t - t_{min}}{t_{max} - t_{min}} \quad 3.6$$

where:  $t^*$  = normalised time,  $t$  = time variable to be normalised,  $t_{max}$  and  $t_{min}$  = maximum and minimum experimental run times respectively.

### 3.2.4 Statistical analyses

A normality test was undertaken on the three discharge data sets ( $q_t$ ) obtained from the respective  $E_d$  experiments using the Shapiro-Wilk normality test followed by a non-parametric Kruskal-Wallis one-way ANOVA test. All statistical analyses were done using R Studio© (R-Core-Team, 2017). A linear regression of observed and simulated values was plotted and tested for goodness of fit using the  $R^2$  value. To evaluate the functional relationship's performance the study employed the PBIAS statistics (Equation 3.6). The PBIAS statistic measured the degree of over or under-estimation by the simulation model.

$$PBIAS = \frac{\sum_{i=1}^x (O_i - P_i) \cdot 100}{\sum_{i=1}^x O_i} \quad 3.6$$

Where  $O_i$  and  $P_i$  = observed and predicted value(s), respectively,  $\bar{O}_i$  = mean observed data, and  $x$  = number of observations.

## 3.3 Results and Discussion

### 3.3.1 Air velocity ( $u_a$ ) and evaporative demand ( $E_d$ )

The  $E_d$  values for each air velocity are presented in Table 3.2. The Bowen ratios ( $r$ ) (Equation 3.5) were significantly low, which means the system had a sufficient water supply. This concurs with Hobbins and Huntington (2016) and Cross (2019) who posited that a Bowen ratio ( $r$ ) of

less than one signifies an unlimiting hydrological supply i.e., the MTI tubing, which is a non-water surface was relatively wet and had ample moisture to evaporate.

Table 3.2 Air velocity ( $u_a$ ) measurements and the corresponding evaporative demand ( $E_d$ )

Air velocity ( $u_a$ ) (m.s <sup>-1</sup> )	Bowen ratio ( $r$ )	VPD ( $e_a - e$ ) (mbars)	$E_d$ (mm.d <sup>-1</sup> )
1.2	$3.502 \times 10^{-6}$	113.081	0.16
2.5	$3.221 \times 10^{-6}$	129.934	0.31
3.0	$3.135 \times 10^{-6}$	150.144	0.36

The results (Table 3.2) revealed a positive correlation amongst the variables  $u_a$ ,  $r$ , VPD and  $E_d$ . A high air velocity ( $u_a$ ) effected a high VPD, which subsequently induced a high  $E_d$ . The observation concurs with Donohue *et al.* (2010b) whose study attributed high evaporation rates to increased air temperatures.

### 3.3.2 Evaporative demand ( $E_d$ ) and discharge ( $q_t$ ) relationship

The normality test (Table 3.3) was carried out on the evaporative demand results ( $E_d = 0.16 \text{ mm.d}^{-1}$ ,  $0.31 \text{ mm.d}^{-1}$  and  $0.36 \text{ mm.d}^{-1}$ ) and the respective discharge data. The sample data revealed high data skewness ( $p < 0.05^*$ ). The statistical analysis revealed that there were no significant differences among the means across the three  $E_d$  categories ( $p > 0.05^{**}$ ). Moisture discharge reaches a constant beyond a certain threshold time under the imposed negative pressure.

Table 3.3 Summarised descriptive statistics for the induced  $E_d$  and the observed  $q_t$

Evaporative Demand ( $E_d$ ) (mm.d <sup>-1</sup> )	0.16	0.31	0.36
Mean Discharge ( $q_t$ ) (l.h <sup>-1</sup> .m <sup>-1</sup> )	0.00139	0.0014	0.0015
$p^*$	$p < 0.05$	$p < 0.05$	$p < 0.05$
$p^{**}$	$p > 0.05$	$p > 0.05$	$p > 0.05$

$p^*$  represents the Shapiro  $p$ -value at 95% confidence interval (CI) and  $p^{**}$  represents the non-parametric Kruskal-Wallis one-way ANOVA test.

The effect of the negative pressure was determined by establishing a relationship between mass flow rates ( $\dot{m}$ ) against the recorded  $E_d$ . The MTI discharge under variable  $E_d$  was characterized by a power function ( $R^2 = 0.62$ ) as shown in Figure 2 over selected time scales.

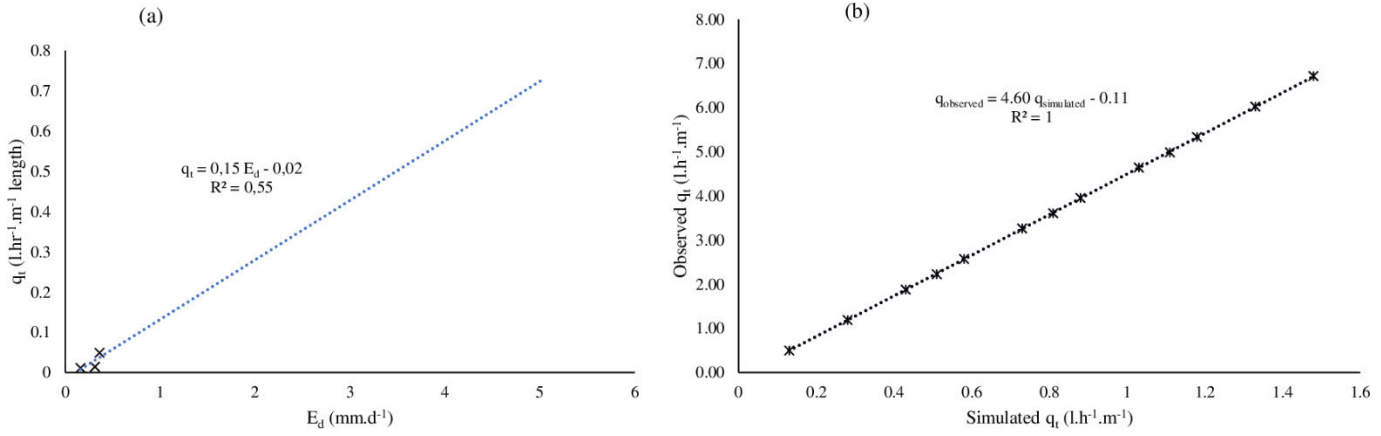


Figure 3.2 (a) Moistube discharge ( $q_t$ ) at  $0 \leq E_d \leq 7$  and (b) comparison between the simulated  $q_t$  vs the observed  $q_t$ .

The overall average  $q_t$  vs  $E_d$  was modelled as in Equation 12. The equation ( $R^2 = 0.55$ ) represented average discharge ( $q_t$ ) value for each respective  $E_d$  sessions, i.e., the  $E_d = 0.16 \text{ mm.d}^{-1}$  had 1908 data points, whilst  $E_d = 0.31 \text{ mm.d}^{-1}$  had 1608 data points, and  $E_d = 0.36 \text{ mm.d}^{-1}$  had 120 data points. For comparative analysis purposes a normalized time scale ( $0 \leq t^* \leq 1$ ) was used because the last  $E_d = 0.36 \text{ mm.d}^{-1}$  experimental conditions exceeded realistic temperature scenarios that a buried MTI lateral can experience.

$$q_t = 0.15E_d - 0.02 \quad 3.7$$

where:  $q_t$  = average discharge ( $\text{l.h}^{-1}.\text{m}^{-1}$ ) across the respective  $E_d$  sessions. A linear increase in  $q_t$  relationship is observed as  $E_d$  increases and under humid conditions where  $E_d = 0$ , MTI discharge  $q_t = -0.02 \text{ l.h}^{-1}.\text{m}^{-1}$  length, which amounts to zero discharge. Abu-Zreig et al. (2006) in their study with ceramic pitcher pots recorded a linear discharge-evaporative demand relationship ( $R^2 = 0.98$ ). MTI functionality closely resembles that of ceramic pitcher pots. Equation 12 characterizes laminar flow through a porous media (MTI) and it is a function of membrane surface area ( $A$ ), flow path length ( $L$ ), flow duration (irrigation interval) ( $t$ ) (Keller and Karmeli, 1974; Karmeli, 1977), and MTI hydraulic properties such as effective porosity of MTI lateral ( $\phi$ ), and inertial coefficient of MTI ( $\delta$ ) (Antohe et al., 1997). The functional relationship is characterised by Equation 3.8. Equation 3.9 shows that at  $E_d = 0$ , MTI experiences zero discharge ( $q_t = -0.02$ ), that is the MTI inertial coefficient facilitates an undisturbed fluid force.

$$q_{Ave} = f(A, \phi, L, t, \delta) \quad 3.8$$

The established relationship (Equation 3.9) is characterized by a one-sided  $E_d$  sensitive limit as in Equation 3.9. The limits were informed by the FAO evaporating power scale (FAO, 2002). The simulated  $q_t$  data had a significant difference ( $p < 0.05$ ) across the respective regions (humid, semi-arid and arid regions).

$$\lim_{E_d \rightarrow 10} 0.15E_d - 0.02 = q_t \quad \text{for } 0 \leq E_d \leq 0.36 \quad 3.9$$

The observed ( $q_o$ ) (including the extrapolated values) and the simulated ( $q_{sim}$ ) (see Appendix A) were plotted on a linear regression plot and yielded a correlation value of  $R^2 = 1$  (Figure 3.2b). The model overestimated the  $q_t$  ( $PBIAS = 77\%$ ), thus, the limits for Equation 3.7 applicability were defined by Equation 3.9.

A higher  $E_d$  resulted in high discharge rates. To assess the effects of  $E_d$  on  $q$  the study employed the relative discharge approach defined by Equation 3.10:

$$q_{rel} = \frac{(q_i - q_o)}{q_o} * 100 \quad 3.10$$

where  $q_{rel}$  = average relative discharge (%),  $q_i$  = average discharge ( $\text{l.h}^{-1}.\text{m}^{-1}$ ) at  $t^* = 0 \leq t^* \leq 1$  h and  $q_o$  = average initial discharge obtained at the beginning of the experiment.,  $t = 0$  ( $\text{l.h}^{-1}.\text{m}^{-1}$ ).

For  $E_d = 0.31 \text{ mm.d}^{-1}$  there was a 10% decline in relative discharge ( $q_{rel}$ ) whilst  $E_d = 0.36 \text{ mm.d}^{-1}$  recorded a 67% decline in  $q_{rel}$  over a  $t^* = 1$  period. These observed variations in  $q_{rel}$  between  $E_d = 0.31 \text{ mm.d}^{-1}$  and  $E_d = 0.36 \text{ mm.d}^{-1}$  are attributed to high  $E_d$  values due to increased drying power of the air in the conduit, hence effecting high discharges. Yang et al. (2008) postulated that in the absence of a driving pressure MTI discharge is a function of matric potential or a negative pressure. Under  $E_d = 0.16 \text{ mm.d}^{-1}$ , it was observed that over 10 h the discharge rose from  $0.043 \text{ l.h}^{-1}.\text{m}^{-1}$  to  $0.077 \text{ l.h}^{-1}.\text{m}^{-1}$ . This effect can be attributed to a slow and gradual increase in VPD ( $e_a - e$ ) within the PVC conduit that effected continuous and gradual discharges. A near saturation scenario was observed from  $t^* = 0.1$  hr to  $t^* = 1$  hr under  $E_d = 0.16 \text{ mm.d}^{-1}$  which signified a protracted equilibrium scenario whereby  $e_a \geq e$ . For a buried Moistube lateral, continuous discharge is observed until water potential between soil-moisture and the water inside the MTI equilibrates. For applicability, to ensure continuous discharge

beyond equilibrium points a net positive pressure is required to effect discharge as stated in studies (Niu et al., 2017a; Kanda et al., 2019).

### 3.3.3 Discharge ( $q$ ) vs time ( $t$ ) relationship

The  $q$  vs  $t$  relationship was established on a normalised time-scale ( $t^*$ ) (Figure 3.3). Statistical analysis revealed significant differences ( $p < 0.05$ ) in  $q$  over different  $E_d$  scenarios. The normalised run-times for each experiment are shown in Table 3.4. The study established a functional relationship between  $q$  and  $t^*$  characterized by Equation 3.11.

$$q_t = K_t e^{-\beta t^*}, \text{ for } 0 < t < a_i \quad 3.11$$

where:  $q_t$  = time dependent discharge,  $K_t$  = constant of proportionality dependent on MTI hydraulic properties, MTI surface area ( $A$ ) flow path length ( $L$ ), (Bucks et al., 1982) and,  $\beta$  = discharge exponent,  $t^*$  = normalised time for a specific induced  $E_d$ , and  $a_i$  = normalised upper limit time range for each subsequent  $E_d$ , value. The relationship revealed that  $q_t$  is time sensitive i.e. if MTI is continuously exposed to an imposed  $E_d$ , MTI discharges exhibits an exponentially decreasing trend to a point of stability at each respective normalised time.

Table 3.4 Normalised time scale ( $t^*$ ) vs  $E_d$  for the  $q_t$  vs  $t^*$  plot

$E_d$ session (mm.d <sup>-1</sup> )	Normalised time scale ( $t^*$ )		
	0	0.5	1
	Actual run-times (h)		
0.16	0.1	79.5	159
0.31	0.1	67	134
0.36	0.1	5	10

For  $E_d = 0.36$  mm.d<sup>-1</sup> there was a steady decline in discharge (Figure 3.3). The recorded flow rate variations were approximately 0.129 l.h<sup>-1</sup>.m<sup>-1</sup> length from  $t^* = 0$  to  $q = 0.021$  l.h<sup>-1</sup>.m<sup>-1</sup> length at  $t^* = 1$ . Whereas for  $E_d = 0.16$  mm.day<sup>-1</sup> and  $E_d = 0.31$  mm.d<sup>-1</sup> discharge reached a stable steady state ranging from  $q = 0.011$  l.h<sup>-1</sup> length.m<sup>-1</sup> to 0.014 l.h<sup>-1</sup>.m<sup>-1</sup> length at  $t^* = 0.45$  and  $t^* = 0.8$ , respectively. These low discharge variations mimic a buried Moistube lateral experiencing minimal to zero discharge at low soil-water potential. Niu et al. (2017b) posited that at zero driving head a buried Moistube lateral reaches a stable steady state discharge after 48 hours.

The discharge for  $E_d = 0.16$  mm.d<sup>-1</sup> at 10% of the normalised time ( $q = 1.2 \times 10^{-2}$  l.hr<sup>-1</sup>.m<sup>-1</sup> length) compared well with the discharge for  $E_d = 0.31$  mm.d<sup>-1</sup> at 95 % of the normalised time

( $q = 1.3 \times 10^{-2} \text{ l.hr}^{-1} \cdot \text{m}^{-1} \text{ length}$ ) (Figure 3.3). Flow rates reached steady state at  $t^* = 0.9$  for both  $E_d = 0.16 \text{ mm.d}^{-1}$  and  $E_d = 0.31 \text{ mm.d}^{-1}$ . The stable flow rates describe a near saturation phenomenon within the PVC enclosure, thus the suction effect of the imposed negative pressure had little effect on the Moistube discharge since the observed discharges were lower than the nominal MTI discharge of  $0.3 \text{ l.hr}^{-1} \cdot \text{m}^{-1} \text{ length}$ . Yang et al. (2008) asserted that discharge from a buried Moistube lateral reduces or stops when the matric potential of the surrounding soil approaches saturation i.e. when  $\psi_{\text{water}} \leq \psi_{\text{soil}}$  less seepage from the Moistube tubing is anticipated and when  $\psi_{\text{water}} = \psi_{\text{soil}}$  there is zero seepage. Once MTI is in equilibrium with its surrounding, discharge stops and only a positive driving pressure will induce discharge. A similar observation was made by Abu-Zreig et al. (2006).

For  $E_d = 0.16 \text{ mm.d}^{-1}$  it was observed that there was uniform and steady decline in discharge rates from  $t = 0.1 \text{ hrs}$  to  $t^* = 0.5$  (33% decrease in relative discharge rate), thereafter there was a steady state discharge rate ( $t^* = 0.5$  vs  $t^* = 1$ ) where the discharge varied from  $0.0121 \text{ l.h}^{-1} \cdot \text{m}^{-1} \text{ length}$  to  $0.0117 \text{ l.h}^{-1} \cdot \text{m}^{-1} \text{ length}$  resulting in a  $q_{\text{rel}} = 2.5\%$ . The phenomenon can potentially be attributed to a stagnating VPD ( $e_a - e$ ) over time. The steady state discharge rates were also observed on the  $E_d = 0.31 \text{ mm.d}^{-1}$  after  $t^* = 0.5$ . This phenomenon indicates a situation where VPD stabilizes such that evaporation occurs over an extensively wet MTI tubing i.e. wet environment evaporation ( $E_w$ ) (Hobbins and Huntington, 2016). For a buried MTI tubing the slow stable irrigation water release would occur in a near saturation MTI –  $\psi_{\text{soil}}$  continuum. From Figure 5, the  $E_d = 0.36 \text{ mm.d}^{-1}$  discharge decreased rapidly due to the high drying power of the air which increased the VPD ( $e_a - e$ ) resulting in a high  $E_d$  that induces discharge. The findings concur with Abu-Zreig et al. (2018) experiment with pitcher pots under constant head. The seepage rate of both buried pitcher pots and those in a controlled environment had a steady decrease as soil water increase. All three plots plateaued signifying a saturated micro-environment within the PVC conduit and consequently a decreased air suction effect.



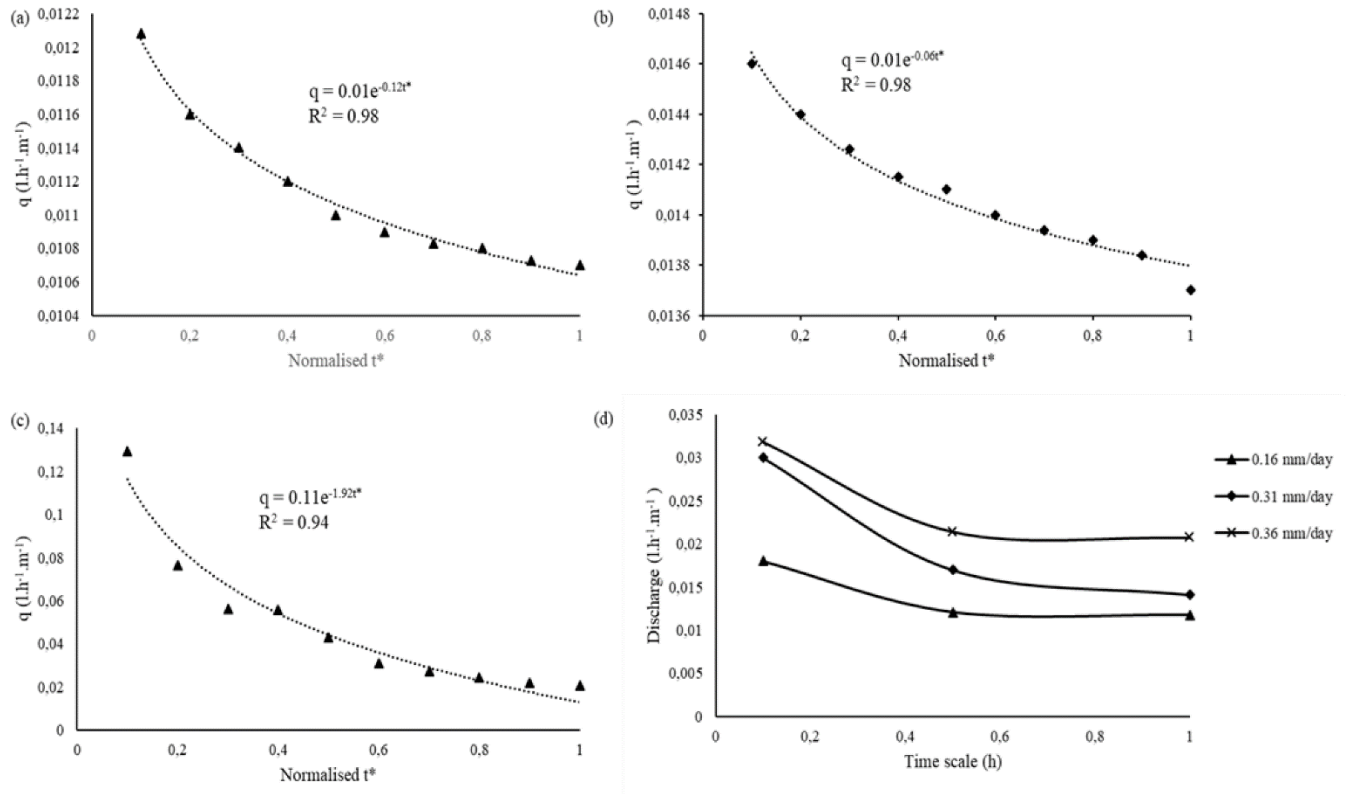


Figure 3.3 Discharge vs. normalised time ( $t^*$ ) relationship at (a)  $E_d = 0.16$  mm.d<sup>-1</sup>, (b)  $E_d = 0.31$  mm.d<sup>-1</sup>, (c)  $E_d = 0.36$  mm.d<sup>-1</sup>, and (d) combined  $q$  vs  $t^*$  plots.

### 3.4 Recommendations

The study was an open-air experiment; hence it is recommended that the study be carried on an actual buried MTI tubing wherein the soil matric potential ( $\psi$ ) are present and influence soil-moisture movement. The  $E_d$  vs  $q_t$  relationship should be experimentally explored to define the actual limits of the MTI operation and  $q$  variations for high evaporating ( $ET_o$ ) power of the atmosphere.

### 3.5 Limitations

The study was a laboratory experiment, hence the evaporative demand values obtained were lower than those experienced under field conditions. However, findings of the study can be used as a guideline on MTI negative pressure irrigation scheduling under field conditions.

### 3.6 Conclusions

The study mimicked a buried MTI tubing, wherein the VPD represented the soil matric potential. At various evaporative demand scenarios, the MTI tubing released moisture at

diminishing rates, thus rejecting the null hypothesis. An increase in  $E_d$  subsequently resulted in an increased MTI discharge, a characteristic likely to be observed under arid climatic conditions. The steady plateauing discharge curve under low  $E_d$  ( $0.16 \text{ mm.d}^{-1}$ ) represented a humid environment where evaporation was occurring on a relatively wet surface. The functional  $E_d - q_t$  relationship revealed that at  $E_d = 0$  there is no MTI discharge scenario, therefore, in humid regions there is need to incorporate pumping units to drive irrigation water and effect MTI discharge. Likewise, in arid regions where  $E_d > 7 \text{ mm.d}^{-1}$  irrigators can capitalise on the MTI negative pressure discharge capability thus minimising energy costs. . The approach can be used to model irrigation schedules based on soil matric potential ( $\psi$ ), which subsequently avails irrigation water as per crop water requirements (CWRs); thus, improving water use efficiency (WUE). MTI tubing performs according to the conceptual design, where it releases moisture at zero positive pressure head.

### 3.7 References

- Abu-Zreig, MM, Abe, Y and Isoda, H. 2006. The auto-regulative capability of pitcher irrigation system. *Agricultural Water Management* 85 (3): 272-278.
- Abu-Zreig, MM, Zraiqat, AM and Abd Elbaset, M. 2018. Seepage Rate from Ceramic Pitchers under Positive and Negative Hydraulic Head. *Applied Engineering in Agriculture* 34 (4): 707-714.
- Anon. 2020. Emissivity coefficients of some common materials [Internet]. <https://analytical-testing.ie/blog/emissivity-coefficients/>. [15 January 2020].
- Antohe, B, Lage, J, Price, D and Weber, R. 1997. Experimental determination of permeability and inertia coefficients of mechanically compressed aluminum porous matrices. *Journal of Fluids Engineering* 119 (2): 404-412.
- Bucks, D, Nakayama, F and Warrick, A. 1982. Principles, practices, and potentialities of trickle (drip) irrigation. In: *Advances in irrigation*. pp 219-298 Elsevier, Amsterdam, Netherlands.
- Clark, G. 1992. Drip irrigation management and scheduling for vegetable production. *HortTechnology* 2 (1): 32-37.
- Cross, I. 2019. Measurement or Estimation of Evaporation [Internet]. <https://slideplayer.com/slide/13217255/>. [25 December 2019].
- Donohue, RJ, McVicar, TR and Roderick, MLJJoH. 2010. Assessing the ability of potential evaporation formulations to capture the dynamics in evaporative demand within a changing climate. 386 (1-4): 186-197.
- FAO. 2002. Planning, Development, Monitoring and Evaluation of Irrigated Agriculture with Farmer Participation. In: *Water Requirements and Irrigation Scheduling*. FAO, Harare, Zimbabwe.
- Hobbins, M and Huntington, J. 2016. Evapotranspiration and Evaporative Demand. In: ed. Singh, VP, *Handbook of Applied Hydrology*. McGraw-Hill Education, Pennsylvania, USA.
- Itenfisu, D, Elliott, RL, Allen, RG, Walter, IAJJoI and Engineering, D. 2003. Comparison of reference evapotranspiration calculations as part of the ASCE standardization effort. 129 (6): 440-448.

- Kanda, EK, Niu, W, Mabhaudhi, T and Senzanje, A. 2019. Moistube Irrigation Technology: A Review. *Agricultural Research* 9(2): 139-147.
- Karmeli, D. 1977. Classification and flow regime analysis of drippers. *Journal of Agricultural Engineering Research* 22 (2): 165-173.
- Keller, J and Karmeli, D. 1974. Trickle irrigation design parameters. *Transactions of the ASAE* 17 (4): 678-684.
- Khan, JN, Jain, AK, Sharda, R, Singh, N, Gill, PS and Kaur, S. 2013. Growth, yield and nutrient uptake of guava (*Psidium Guavaja* L.) affected by soil matric potential, fertigation and mulching under drip irrigation. *Agricultural Engineering International: CIGR Journal* 15 (3): 17-28.
- Luo, Y, Chang, X, Peng, S, Khan, S, Wang, W, Zheng, Q and Cai, X. 2014. Short-term forecasting of daily reference evapotranspiration using the Hargreaves–Samani model and temperature forecasts. *Agricultural Water Management* 136: 42-51.
- Monteith, J. 1965. Evaporation and environment. In: *The state and movement of water in living organisms*. Cambridge University Press, Cambridge, United Kingdom.
- Morton, F. 1983. Operational estimates of areal evapotranspiration and their significance to the science and practice of hydrology. *Journal of Hydrology* 66 (1-4): 1-76.
- Najmaddin, PM, Whelan, MJ and Balzter, H. 2017. Estimating daily reference evapotranspiration in a semi-arid region using remote sensing data. *Remote Sensing* 9 (8): 779.
- Niu, W, Lü, W, Gu, J, Liang, B, Guo, L and Guan, Y. 2017a. Effects of moistube depth and spacing on soil water and salt transports of tomato in solar greenhouse. *Transactions of the Chinese Society of Agricultural Engineering* 33 (19): 131-140.
- Niu, W, Zhang, M, Xu, J, Zou, X, Zhang, R and Li, Y. 2017b. Prediction methods and characteristics of flow for Moistube. *Trans. Chin. Soc. Agric. Mach* 48: 217-224.
- Penman, HL. 1948. Natural evaporation from open water, bare soil and grass. *Proceedings of the Royal Society of London. Series A. Mathematical and Physical Sciences* 193 (1032): 120-145.
- Priestley, CHB and Taylor, R. 1972. On the assessment of surface heat flux and evaporation using large-scale parameters. *Monthly Weather Review* 100 (2): 81-92.
- R-Core-Team. 2017. *R: A language and environment for statistical computing*. R Foundation for Statistical Computing, Vienna, Austria.
- Thornthwaite, C. 1948. An approach toward a rational classification of climate. *Geographical Review* 38 (1): 55-94.
- Wang, J, Long, H, Huang, Y, Wang, X, Cai, B and Liu, W. 2019. Effects of different irrigation management parameters on cumulative water supply under negative pressure irrigation. *Agricultural Water Management* 224: 105743.
- Yang, W, Tian, L, Du, T, Ding, R and Yang, Q. 2008. Research Prospect of the Water-saving Irrigation by Semi-permeable Film [J]. *Journal of Water Resources and Water Engineering* 6 016.
- Zhang, S, Lei, T, Ding, Y and Xu, C. 2002. Finite element modeling of soil water movement under subsurface irrigation with porous pipe and its application. *Nongye Gongcheng Xuebao(Transactions of the Chinese Society of Agricultural Engineering)* 18 (4): 1-5.
- Zheng, J, Huang, G, Jia, D, Wang, J, Mota, M, Pereira, LS, Huang, Q, Xu, X and Liu, H. 2013. Responses of drip irrigated tomato (*Solanum lycopersicum* L.) yield, quality and water productivity to various soil matric potential thresholds in an arid region of Northwest China. *Agricultural Water Management* 129: 181-193.
- Zou, X, Quan, T, Zhou, M, Yang, Q and Shi, Y. 2017. Progress and Prospects of Moistube Irrigation Technology Research. *Bulletin of Soil and Water Conservation* 37 (4): 150-155.

## 4 MOISTUBE IRRIGATION FOULING DUE TO ANAEROBIC FILTERED EFFLUENT (AF) AND HORIZONTAL FLOW CONSTRUCTED WETLAND (HFCW) EFFLUENT

This Chapter was published as:

**Dirwai, TL**, Senzanje, A, Mabhaudhi, T, Buckley, CA. (2021). Moistube Irrigation Fouling Due to Anaerobic Filtered Effluent (AF) and Horizontal Flow Constructed Wetland (HFCW) Effluent. *Scientific Reports* (2021) 11:7124. <https://doi.org/10.1038/s41598-021-86737-7>

### Abstract

The study assessed the suitability of two effluent types, namely anaerobic filtered (AF) and horizontal flow constructed wetland (HFCW) effluent for Moistube irrigation (MTI). Secondary to this, the study determined the plugging coefficients ( $\alpha$ ) on MTI for the respective effluents. The feed water was supplied from a raised tank (3.5 m), and mass-flow rates were recorded at 15 min intervals using an electronic balance. The effluent feed water concentrations and experimental room temperature ( $25^{\circ}\text{C} \pm 1^{\circ}\text{C}$ ) were continuously monitored and kept constant. Hermia's models based on the  $R^2$  coefficient was used to select the best fitting fouling mechanism model and consequently, the plugging coefficients. In addition, microbial colony analysis and scanning electron microscopy with energy dispersive x-ray (SEM - EDX) analysis was carried out to assess the composition of the deposited sediment (DS) and adhered bacterial film (ABF) onto the MTI lateral. The study revealed that MTI pore blocking was a complex phenomenon described by complete pore-blocking model ( $R^2 \geq 0.50$ ). Discharge followed an exponential decay with early fouling observed on AF effluent because of a high concentration of total suspended solids (TSS) and dissolved organic matter (DOM). Discharge declined by 50% after 20 and 10 h of intermittent operation for AF and HFCW effluent, respectively. The  $\alpha$  for each effluent (foulant) were  $\alpha_{AF} = 0.07$  and  $\alpha_{HFCW} = 0.05$ , respectively, for AF and HFCW. The microbial analysis revealed bacterial aggregation structures that contributed to pore blocking. SEM imaging revealed complete surface coverage by deposited sediment. It is concluded that water quality determines the operation life span of MTI and the two effluents promote accelerated MTI pore fouling or blocking. Continuous use without flushing the MTI will promote membrane degradation and reduced discharge efficiency. Additional filtration can potentially mitigate the membrane degradation process.

**Keywords:** dissolved organic matter (DOM), plugging coefficient, total soluble solids (TSS)

## 4.1 Introduction

Agriculture consumes approximately 70% of the global blue water (Rost et al., 2008). This exacerbates water scarcity in the wake of erratic rainfall fuelled by climate variability and change. Domestic wastewater can be a suitable alternative for irrigated agriculture. Wastewater is defined as water that has gone through anthropological change (Kijne, 2011). Wastewater treatment plants such as the decentralised wastewater treatment system (DEWATS) produce different types of effluents; for example, there is anaerobic filtered (AF) effluent and horizontal flow constructed wetland (HFCW) effluent. AF and HFCW effluents have varying degrees of microbial activity, total suspended solids (TSS) and total dissolved solids (TDS). AF is obtained after the effluent passes through the anaerobic baffled reactor (ABR) chamber, removing suspended solids and biodegradable organic material (BOM). The AF chamber further removes additional suspended solids, colloidal solids and further reduces BOM. For tertiary filtration, a combination of anaerobic filtration and constructed wetlands (CWs) filtration is applied. For example, the HFCW effluent is obtained by passing the AF effluent through a vertical flow constructed wetland (VFCW) which consists of planted gravel filters that aid in further filtration and removal of pathogens. The horizontal flow constructed wetland removes additional pathogens and suspended solids (Gutterer et al., 2009b). CWs are considered tertiary wastewater treatment mechanisms, and they significantly process wastewater for reuse (Thalla et al., 2019).

Although wastewater relieves pressure on freshwater bodies, the treated wastewater from a decentralised wastewater treatment system (DEWATS) contains heavy metals, pathogen and high nitrate concentrations that can contaminate the environment (Scott et al., 2010; Musazura, 2018; Musazura et al., 2019b). A combination of wastewater usage and water use efficient irrigation technologies such as Moistube irrigation (MTI) can potentially relieve the pressure on freshwater bodies and improve water use efficiency for crop production. According to Trooien et al. (2000) potential benefits such as replenishing phosphorous in the soil, minimal human contact, and improved nutrient control, to mention a few, are derived from using wastewater from animal lagoons. Also, micro-irrigation systems offer an opportunity to effectively control pollution by wastewater and simultaneously promoting agricultural production (Hills and Brenes, 2001).

MTI is a new technology which uses semi-permeable membrane (SPM) to emit water continuously in response to the soil matric potential and the applied pressure. The SPM membrane is made from inorganic filler material mixed with surfactant ethylene oxide/oxirane (AEO-7) aliphatic alcohol polyethenoxy. The filler material facilitates the carboxymethylation reaction of the aliphatic alcohol polyethenoxy (Yang, 2017). The SPM is characterised by nano-pores uniformly and densely distributed for maximised irrigation uniformity (Jun et al., 2012; Fan et al., 2018). MTI is a low-pressure continuous irrigation method whose discharge is controlled by soil matric potential. The inner membrane closely simulating the vascular plant tissue and uses the soil-moisture gradient for advection (Yang et al., 2008), and it assumes a line source infiltration mechanism during irrigation (Fan et al., 2018). Table 4.1 summarises the membrane properties. The technology optimises irrigation field water use efficiency (fWUE) since it utilises on-demand water application (Jun et al., 2012; Kanda et al., 2019).

Table 4.1 3<sup>rd</sup> generation Moistube membrane properties

Property	Information
Material	Polymeric
Thickness ( <i>mm</i> )	1.1
Inside / outside diameter ( <i>mm</i> )	15.87 / 17.28
Area ( $\text{m}^2 \cdot \text{m}^{-1}$ length)	0.1043
Pore size ( <i>nm</i> )	500 (average)
Nominal discharge ( $\text{L} \cdot \text{h}^{-1} \cdot \text{m}^{-1}$ length)	0.489

When used in irrigation, depending on irrigation technology, wastewater accelerates emitter clogging and fouling. Emitter fouling and clogging can be caused by physical, chemical and biological processes and components or particles (Bucks et al., 1982; Kanda et al., 2018). Fouling is characterised by four elementary phenomena: deposition, re-entrainment or re-suspension, agglomeration and clogging (Henry et al., 2012). Clogging can be classified as “later stages” of fouling, leading to blockage (Henry et al., 2012). Membrane fouling is a process whereby fine soluble particles deposit on the surface of an SPM facilitating pore narrowing and subsequently pore blocking. MTI, as like other membranes, is susceptible to membrane fouling.

A study by Bucks et al. (1982) revealed how wastewater increased the coefficient of variation of micro-irrigation emitters. Puig-Bargués et al. (2005) investigated the effects of effluents on drip irrigation kits. They found that drip-kits exposed to secondary treated effluent clogged faster than those exposed to wastewater that underwent tertiary treatment. Li et al. (2015) investigated biofilms' formation around drip emitters and conclusively recommended

prescribed frequent lateral flushings to remove bio-films that accumulate from sewage water. Another study by Song et al. (2017) tested various chlorination techniques to eliminate bio-clogging caused by reclaimed water. Kanda et al. (2018) revealed that total suspended solids (TSS) had a significant effect on MTI clogging as compared to total dissolved solids (TDS).

Technology has facilitated the means to perform microscopy analysis on irrigation emitters. Emitter clogging has over the years been analysed by high-resolution microscopy methods such as scanning electron microscopy (SEM), energy dispersive x-ray (EDX), transmission electron microscopy (TEM) (Xu and Van Deventer, 2002) scanning tunnelling microscopy (STM), and the atomic force microscopy (AFM) (Risović and Pavlović, 2013). Energy-dispersive X-ray (EDX) is a powerful tool for breaking down sediment compounds into elemental composition (Brodowski et al., 2005). Also, fractal analysis is made possible by grey-scale SEM imagery, thus allowing the analysis of sediment's physical make-up (Risović and Pavlović, 2013).

DEWATS effluent undergoes multiple filtration stages; this provides an opportunity to irrigate with “least” expensive water. Wastewater promotes emitter clogging, thus, determining the plugging coefficients aids in understanding MTI degradation process and the SPM’s capacity to perform irrigation effectively under varied effluent quality (Corbatón-Báguena et al., 2016). There is no empirical evidence on the performance and the fouling of MTI under selected wastewater effluents. Kanda et al. (2018) investigated the clogging effect of suspended solids and dissolved solids on MTI; however, the study did not quantify the extent of clogging due to wastewater. Furthermore, the study did not quantitatively determine the plugging coefficients. This study sought to address the following questions: (1) how does different effluent type influence the irrigation performance of MTI and (2) what is the degree of clogging and the subsequent plugging coefficient associated with flux decline in the different effluents used for the study. The study offers significant insights into MTI degradation due to wastewater irrigation, subsequently providing information on operation and maintenance (O&M) of MTI when used wastewater is used for irrigation. The study further determined the plugging coefficients ( $\alpha$ ) for AF and HFCW effluents using MTI. The plugging coefficients can be adopted for the emitter discharge equation for MTI. The study hypothesised that wastewater effluent degraded MTI discharge capacity. A study by Bhattacharjee and Datta (2003) developed pore blocking models exclusively for gel formation, which limits its applicability on generating knowledge around MTI performance under permeate flux decline

## 4.2 Fundamentals of Fouling

Fouling diminishes a membrane's permeability (Janus and Ulanicki, 2015). The model formulated by Hermia (1985), forms the basis of other modified fouling models (Vela et al., 2009; Chang et al., 2011; Guo et al., 2012; Corbatón-Báguena et al., 2015), defined various membrane clogging stages as standard blocking, intermediate blocking, complete blocking and cake formation and characterised them according to Equation 4.1:

$$\frac{d^2t}{dV^2} = \left(\frac{dt}{dV}\right)^n = \alpha \left(\frac{1}{J}\right)^n \quad 4.1$$

Where:  $t$  = filtration time (s),  $V$  = filtrate volume per unit area ( $\text{m}^3 \cdot \text{m}^{-2}$ ),  $J$  = filtration velocity (permeate flux) ( $\text{m} \cdot \text{min}^{-1}$ ),  $\alpha$  = plugging coefficient and,  $n$  = constant of proportionality for constant pressure filtration of a Newtonian fluid.

Permeate flux decline is caused by pore blocking and cake deposition (Ho and Sung, 2009). Field (2010) posited that membrane fouling occurs in stages, and there exist empirical functions that define each plugging or fouling stage (Figure 4.1). For instance, the modified Equations 4.1 to 4.5 define standard, intermediate, complete fouling and cake formation, respectively (Field, 2010; Corbatón-Báguena et al., 2016).

Standard blocking or pore narrowing occurs when the effluent soluble molecules have a lower diameter than the membrane pores (Furuichi et al., 2008). The effluent molecules adhere to the emitting pores of the membrane and subsequently diminish its discharge. Standard blocking is characterised by Equation 4.2 (Corbatón-Báguena et al., 2016)

$$J_p = \frac{J_o}{(J_o + J_o^{0.5} \cdot \alpha_s \cdot t)^2} \quad 4.2$$

Where:  $J_p$  = instantaneous permeate flux ( $\text{m}^3 \cdot \text{m}^{-2} \cdot \text{min}^{-2}$ ),  $J_o$  = permeate flux ( $\text{m}^3 \cdot \text{m}^{-2} \cdot \text{min}^{-2}$ ) at time  $t = 0$ , and  $\alpha_s$  = phenomenological standard blocking coefficient.

Corbatón-Báguena et al. (2016) defined intermediate blocking as a phenomenon that occurs when the effluent soluble molecules equal to the membrane's pore diameter. The corresponding function for the phenomenon is characterised by Equation 4.3:

$$J_p = \frac{J_o J_{pss} (e^{\alpha_i J_{pss} t})}{J_p + J_o (e^{\alpha_i J_{pss} t} - 1)} \quad 4.3$$

Where:  $J_{pss}$  = permeate flux ( $\text{m}^3 \cdot \text{m}^{-2} \cdot \text{min}^{-2}$ ) at steady-state flow, and  $\alpha_i$  = phenomenological intermediate blocking coefficient.



Complete blocking or pore sealing entails the complete blocking of the membrane pores (Guo et al., 2012). The blocking mechanism is defined by Equation 4.4 (Corbatón-Báguena et al., 2016).

$$J_p = J_{pss} + (J_o - J_{pss}) \cdot e^{-\alpha_c \cdot t \cdot J_o} \quad 4.4$$

Where:  $\alpha_c$  = phenomenological complete blocking coefficient.

Cake formation or gel layer formation occurs after complete blocking. The effluent solutes cannot pass through the membrane layer and they form a cake layer. The mechanism has the general equation as in Equation 4.5:

$$t = \frac{1}{\alpha_{gl} \cdot J_{pss}^2} \cdot \ln \left[ \left( \frac{J_p}{J_o} \cdot \frac{J_o - J_{pss}}{J_p - J_{pss}} \right) - J_{pss} \left( \frac{1}{J_p} - \frac{1}{J_o} \right) \right] \quad 4.5$$

Where:  $\alpha_{gl}$  = phenomenological gel layer or cake formation coefficient.

The nano-pore size characteristics of MTI SPM has a cross-flow filtration effect on the AF and HFCW effluent, thus the Hermia model was adopted since it characterises cross-flow and dead-end filtration. Studies by Chang et al. (2011), Abdelrasoul et al. (2013), and Corbatón-Báguena et al. (2016) just to mention a few, successfully adopted the Hermia's filtration model on various membranes.

Drip irrigation emitter discharge is described by Equation 4.6 and when there is emitter clogging, the discharge equation is modified as in Equation 4.7 (Keller and Karmeli, 1974; Gil et al., 2008):

$$q_e = kH^x \quad 4.6$$

$$q_e = (1 - \alpha)kH^x \quad 4.7$$

Where  $q_e$  is the emitter discharge (L.min<sup>-1</sup>),  $k$  is the emitter proportionality constant,  $H$  is the emitter operating pressure (m), and  $x$  is the emitter exponent and characterises the type of emitter.

According to Kanda et al. (2018b), MTI discharge follows the general emitter discharge equations and is characterised by Equation 4.8 ( $R^2 = 0.978$ ), and the presence of clogging reduces the discharge capacity by a factor  $\alpha_i$  giving rise to Equation 4.9:

$$q = 0.1116h^{1.1948} \quad 4.8$$

$$q = (1 - \alpha_i)0.1116h^{1.1948} \quad 4.9$$

Where:  $q$  = discharge,  $h$  = pressure head from the feed water supply, and  $\alpha_i$  = plugging coefficient.

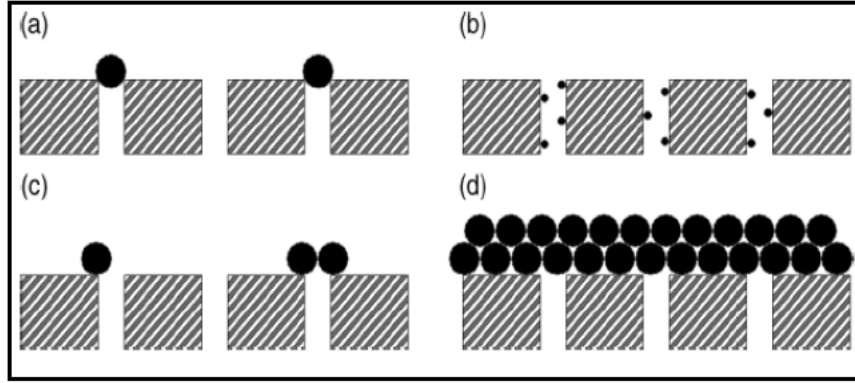


Figure 4.1 The various types of membrane fouling (a) complete pore blocking, (b) internal pore blocking, (c) partial pore blocking, and (d) cake formation after Field (2010).

Technology has facilitated the means to perform microscopy analysis on irrigation emitters. Emitter clogging has over the years been analysed by high resolution microscopy methods such as scanning electron microscopy (SEM), SEM- energy dispersive X-ray (EDX), transmission electron microscopy (TEM) (Xu and Van Deventer, 2002) scanning tunnelling microscopy (STM), and the atomic force microscopy (AFM) (Risović and Pavlović, 2013). Energy-dispersive X-ray (EDX) is a powerful tool for breaking down sediment compounds into elemental composition (Brodowski et al., 2005), also, fractal analysis is made possible by grey-scale SEM imagery, thus allowing the analysis of the physical make-up of sediment (Risović and Pavlović, 2013).

Determining the plugging coefficients aids in understanding MTI degradation process and the SPM's capacity to perform irrigation effectively under varied effluent quality (Corbatón-Báguena et al., 2016). There is no empirical evidence on the performance and the fouling of MTI under selected wastewater effluents. Kanda *et al.* (2018b) investigated the clogging effect of suspended solids and dissolved solids on MTI, however the study did not quantify the extent of clogging due to wastewater. Furthermore, the study did not quantitatively determine the plugging coefficients. This study determined the plugging coefficients ( $\alpha$ ) for AF and HFCW effluents using MTI. DEWATS effluent undergoes multiple filtration stages, this, provides an

opportunity to irrigate with “least” expensive water. the study hypothesised that wastewater effluent degraded MTI discharge capacity. A study by Bhattacharjee and Datta (2003) developed pore blocking models exclusively for gel formation, which limits its applicability on generating knowledge around MTI performance under permeate flux decline.

### 4.3 Materials and Methods

#### 4.3.1 Study site and effluent characteristics

The laboratory experiment was carried out at the University of KwaZulu-Natal Ukulinga Research Farm in Pietermaritzburg, KwaZulu-Natal, South Africa (29°39'44.8"S 30°24'18.2"E). AF and HFCW effluents were used to determine the plugging coefficients. AF has a high microbial load whilst HFCW is produced after the secondary filtered AF passes through sub-surface filters. The effluent was obtained from a decentralised wastewater treatment system (DEWATS) in KwaMashu, Durban, South Africa (29°45'49.0"S 30°58'34.6"E). DEWATS is a modular water sanitation system consisting of settler, anaerobic baffled reactor (ABR) + anaerobic filter (AF) and planted gravel filters (Gutterer et al., 2009a; Musazura et al., 2019a). Other experiments such as microbial analysis and scanning electron microscopy (SEM) were done at the University of KwaZulu-Natal (Pietermaritzburg) plant pathology laboratory and microbiology and microscopy unit (MMU) respectively. Musazura (2018) characterised the two types of effluents as per Table 4.2. The on-site laboratory analysed for  $NH_4^+ - N$ ,  $NO_3^- - N$ , and  $PO_4^{3-} - P$  using a NOVA 60 Merck Spectroquant (Merck Millipore, Germany) following standard methods for water and wastewater analysis (APHA, 2012). According to Capra and Scicolone (2007), the tabled parameters (Table 4.2) can be used to evaluate emitter fouling exclusively.

Table 4.2 DEWATS effluent quality characterisation (Musazura, 2018) and the corresponding emitter clogging risks (Bucks et al., 1979).

Constituent	concentration		Emitter clogging risk Hazard rating		
	AF	HFCW	Minor	Moderate	Severe
Ammonium (mg/l)	61	01			
Chemical Oxygen Demand (mg/l)	360	38			
Electrical Conductivity (mS/m)	95	65			
E. coli (CFU per 100 ml)	$3.5 \times 10^{05}$	508		✓	✓
Nitrates (mg/l)	0.1	4.1			
Ortho-Phosphates (mg/l)	10.5	6.7			
pH	7.5	7.2		✓	
Total Dissolved Solids (mg/l)	476	543		✓	
Total Suspended Solids (mg/l)	579	575			
Total Soluble Solids (mg/l)	21	12.7	✓		

The above listed characterised effluent can further be classified according to the severity of pore blocking by the active foulants in the effluent. Bucks et al. (1979) hazard rating scale was adopted to explain how the physical, chemical and biological characteristics of each effluent influenced pore narrowing and the subsequent pore blocking.

#### 4.3.2 Experimental set-up and procedure

The experiment equipment (Figure 4.2) consisted of two 250 L tanks placed at a height of 3.5 m to facilitate enough head for fluid flow (Kanda et al., 2018). Each tank had a different effluent type. MTI lateral tubing of length 0.6 m were assembled in manifold arrangement and replicated three times. Each MTI lateral end was sealed by a 15 mm nylon end plug. Pressure head was kept at 3.5 m; thus, there were minimal fluctuations in permeate flux velocity ( $0.49 \text{ l.h}^{-1}.\text{m}^{-1} \text{ length}$ ). According to Kanda et al. (2018), there are no guidelines for manifold length, but standard practice dictates selecting a length that minimises frictional losses.

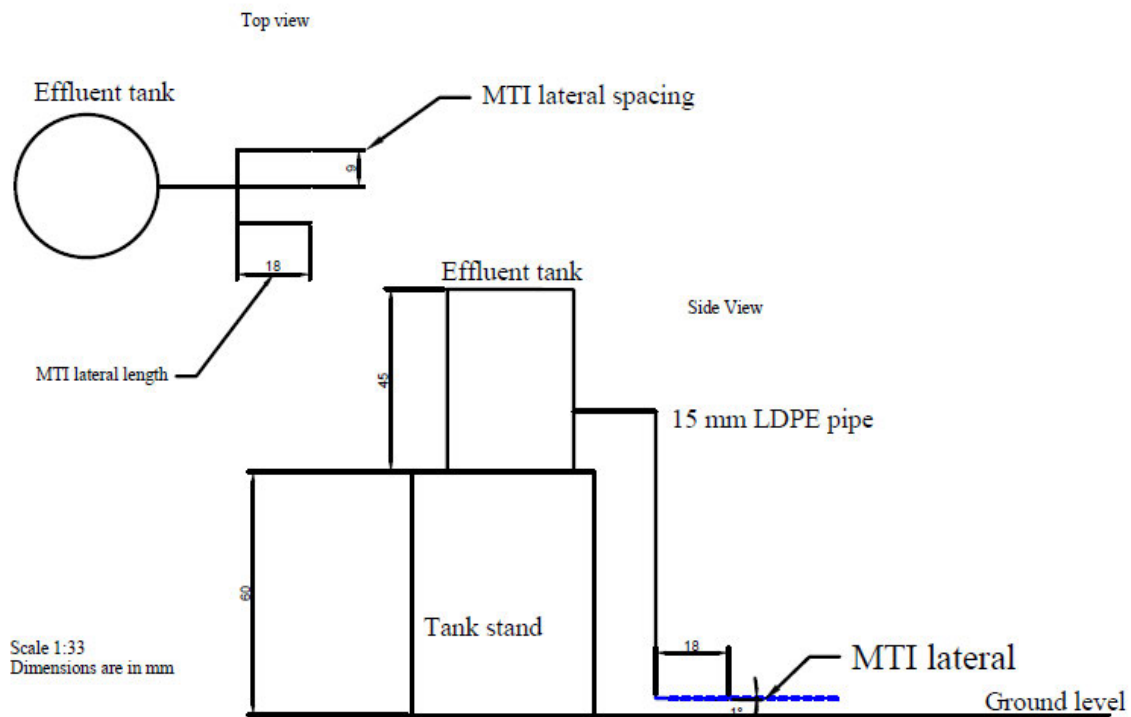


Figure 4.2 Experimental set-up.

The lateral spacing was 0.3 m (Kanda et al., 2018), and the MTI laterals were placed in gutters laid at a gentle slope of 1% for ease of collection of the MTI discharge. The experiment was operated intermittently (Puig-Bargués et al., 2005) for approximately 60 hrs with start and end times of 08h30 and 16h00 culminating to  $7.5 \text{ h.d}^{-1}$  for 8 consecutive days, respectively. No

MTI flushing happened during the experimental period. The mass-flow rate collected in each gutter was recorded at 15-minute intervals using a 1 kg full capacity electronic balance with a 1 g resolution.

The experiment was carried in a closed room where conditions were kept at room temperature ( $24\text{ }^{\circ}\text{C} \pm 1^{\circ}\text{C}$ ) and atmospheric pressure to minimise evaporation effects. The effluent feed water quality was periodically tested for uniformity throughout the experiment using portable handheld TSS meter from HACH industries (TSS resolutions of 0.1 at 10–99.9 g.L<sup>-1</sup> and 1 at greater than 100 g.L<sup>-1</sup>), and HI98129 combo tester for pH/EC/TDS/temperature from Hanna Industries (resolutions of 0.01 pH, 1  $\mu\text{S.cm}^{-1}$ , 1 ppm of TDS, 0.1 $^{\circ}\text{C}$ ). To avoid settling suspended solids, a low-head submersible pump was placed at the bottom of the tank for continuous mixing. Water levels were periodically checked at 5-minute intervals using a graduated dip-meter. The effluent was periodically topped up to maintain the constant head.

#### 4.3.3 Method of analysis

##### Statistical analysis

R Studio (R-Core-Team, 2017) was used for statistical analyses. The one-way ANOVA was applied to assess differences in discharges among laterals of the same treatment and the discharges from the different wastewater treatments.

##### Mass flow rates

The mass flow rates were converted to discharge by multiplying the weight per unit time by the density ( $\rho_w$ ) of water. The permeate flux ( $J_o$ ) was obtained from Equation 4.10:

$$J_o = \frac{Q}{A \Delta t} \quad 4.10$$

Where:  $J_o$  = effluent permeate flux ( $\text{m}^3 \cdot \text{m}^{-2} \cdot \text{h}^{-2}$ ),  $Q$  ( $\text{m}^3 \cdot \text{min}^{-1}$ ) = discharge at time  $\Delta t$  (min),  $A$  ( $\text{m}^2$ ) = membrane total surface area determined by Equation 4.11, surface area of a hollow cylinder:

$$A = 2\pi l_{MTI}(R + r) + 2\pi(R^2 - r^2) \quad 4.11$$

Where:  $l_{MTI}$  = MTI lateral length,  $R$  = MTI external radius,  $r$  = MTI internal radius.

##### Relative discharge and Degree of clogging

The other selected criteria or measures for assessing emitter clogging were, relative discharge ( $q_{rel}$ ), and time taken for discharge to reduce from 95% to 50% (Liu and Huang, 2009) and degree of clogging ( $DC$ ) (Cararo et al., 2006). The relative discharge ( $q_{rel}$ ) and  $DC$  was calculated by Equations 4.12 and 4.13 as follows:

$$q_{rel} = \frac{q_{ini} - q_t}{q_{ini}} * 100 \quad 4.12$$

$$DC = \left(1 - \frac{q_t}{q_{ini}}\right) * 100 \quad 4.13$$

Where:  $q_t$  = instantaneous discharge at time  $t$  (h), and  $q_{ini}$  = initial discharge ( $\text{l.h}^{-1}.\text{m}^{-1}$ ).

### **Bacterial quantity**

The study assessed the bacterial colonies that formed along the MTI lateral walls, hereafter referred to as adhered bacterial biofilm (ABF) and the bacteria that was deposited at the bottom section of the MTI lateral, hereafter referred to as deposited sediment (DS). The bacterial agar consisted of a mixture of 12 g Agar No.2 Bacteriological (Neogen Company, Heywood, Lancashire, UK) and 16 g of nutrient broth (Biolab Modderfontein, South Africa). The reagents were mixed to a solution of 1000 ml and stirred till boiling for 15 min. Considering that the irrigation intervals were intermittent, i.e., the laterals were allowed to drain during non-irrigating hours, hence the bacterial culture used catered for both aerobic and anaerobic bacteria. The culture mixture was then autoclaved at  $150^{\circ}\text{C}$  for 1 h before being transferred to petri-dishes. The stock solution was obtained by cutting sections of the MTI laterals into  $1\text{ cm} \times 1\text{ cm}$  coupons. The coupons were allowed to soak for 72 h in de-ionised water. The sample to be tested was then diluted to  $1 \times 10^{-5}$  and  $1 \times 10^{-6}$  dilution from the stock solution of dispersed bacteria. A 0.1 ml diluted solution was then applied to the medium and cultured in a  $28\text{--}30^{\circ}\text{C}$  incubator for 48 h. A sterilised inoculating loop was dipped into each bacterial solution to collect bacteria from the dispersed bacteria sample and then streaked into each petri dish. The number of bacterial colonies was detected by the plate counting method (Zhang et al., 2020). For both the AF and HFCW effluents, all three laterals were sampled three times for DS and ABF. The laterals were sampled on three segments which were the start (S) of the lateral, mid-section (M) and the end section (E) of the lateral (Figure 4.3).

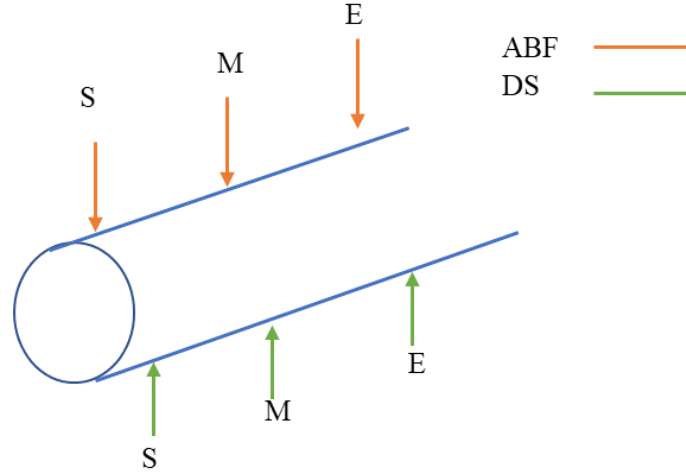


Figure 4.3 Sampled DS and ABF points along the MTI lateral for each respective effluent

### Scanning Electron Microscopy (SEM) with Energy Dispersive X-Ray (EDX)

For sediment analysis the scanning electron microscopy with energy dispersive x-ray (SEM - EDX) was employed to analyse the elemental composition in the two sediments (ABF and DS). The sediment sample to be analysed was cut into small pieces measuring approximately 1 cm  $\times$  1 cm and mounted on stub and secured using insulated carbon double sided tape. To facilitate conductivity the samples were sputter coated by gold using the Quorum Q150R ES machine. The viewing was done on a Zeiss EVO LS 15 machine with a resolution of up to 3072  $\times$  2304 pixels. The samples were subjected to observational fractal analysis to assess the space occupied on MTI inner surface by the irregular and potentially clogging particles (Zhang et al., 2020). For both effluents, material for DS and AS sediment analysis was taken from the mid-section of each MTI lateral.

## 4.4 Results and Discussion

A one-way ANOVA revealed no significant differences ( $p > 0.05$ ) in discharges amongst the laterals for the respective effluents. The discharge from individual MTI laterals from AF and HFCW had approximately equal means and medians (Figure 4.4) revealing a constant discharge from the respective laterals and replicates. The one-way ANOVA analysis however revealed a significant difference ( $p < 0.05$ ) in clogging due to AF and the HFCW effluent. This meant that effluent quality influenced degree of clogging.

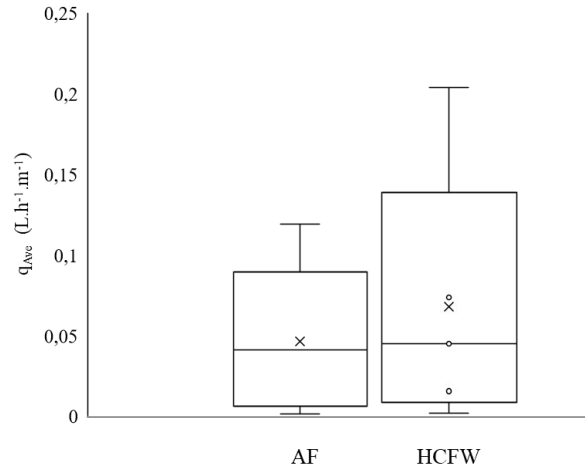


Figure 4.4 Box plot showing discharge variations between the two types of effluents.

#### 4.4.1 Degree of clogging ( $DC$ ) and relative discharge $q_{rel}$

The degree of clogging increased with operation time (Figure 4.5 a, b, and c). AF presented a high clogging risk for the MTI laterals. AF had approximately 60 %  $DC$  from  $t = 0$  h to  $t = 5$  h whilst HFCW had approximately 40 %  $DC$  over the same time period. The phenomenon was potentially attributed to physical bore blocking caused by a high concentration of total suspended solids (TSS) in both effluents. A high TDS concentration ( $476 - 543 \text{ mg.L}^{-1}$ ) potentially contributed to the constriction of the MTI nano-pores. A high concentration of TSS in sewage sludge promotes complete pore blocking and subsequently cake formation (Charfi et al., 2012).

There was a significant difference in  $q_{rel}$  between AF and HFCW effluent (Figure 5 d) ( $p < 0.05$ ). The significant drops in  $q_{rel}$  during the beginning stages of the experiment were attributed to the presence of active and effective MTI pores as the SMP gradually wets, this concurs with the observations by Kanda et al. (2018b). The time required for  $q_{rel}$  to get to 50 % ( $T_{q_{rel}} \leq 50\%$ ) under HFCW was low at 5 hours as compared to AF at 15 hours. This rapid decline for the HFCW effluent could be attributed to the high concentration of TSS in the effluent which according to the Bucks et al. (1979) hazard risk rating scale causes severe pore narrowing or clogging risk.



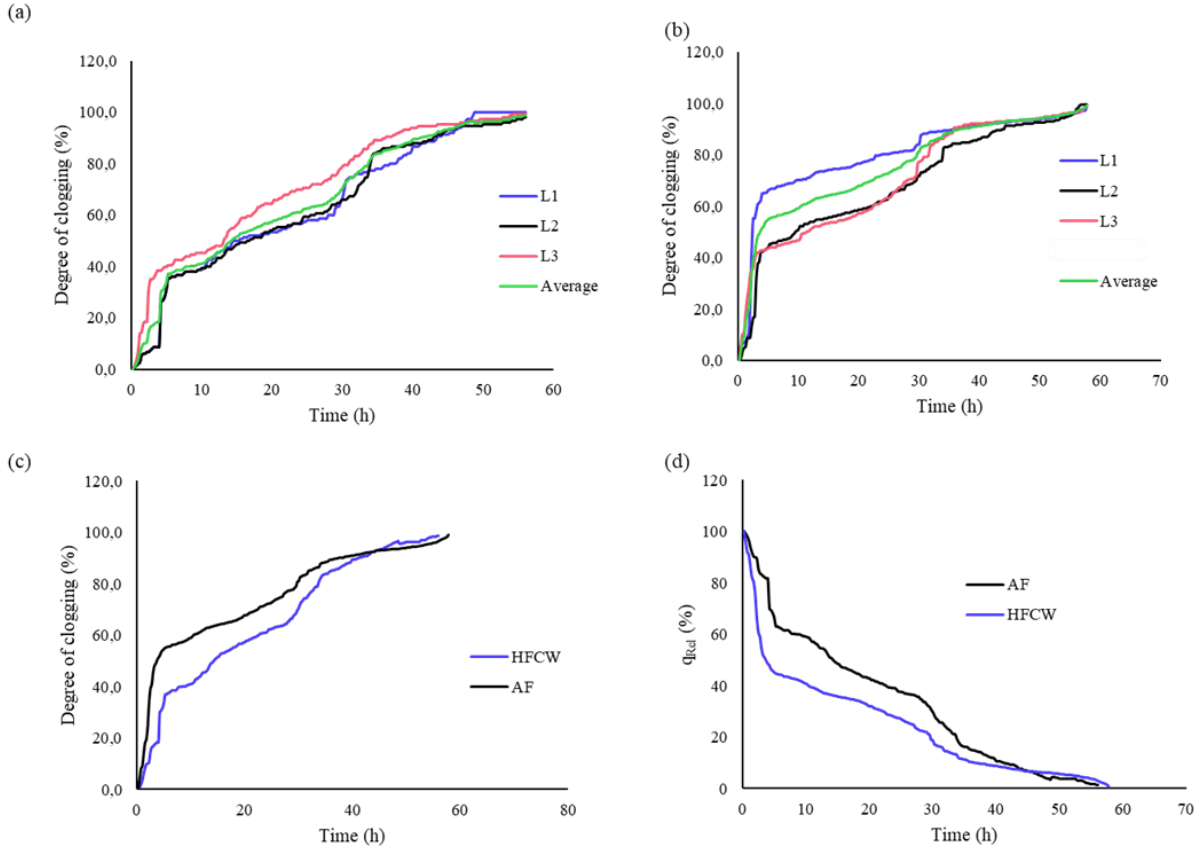


Figure 4.5 Degree of clogging ( $DC$ ) for (a) AF effluent, (b) HFCW effluent, (c)  $DC$  vs  $q_{Ave}$  for AF and HFCW effluents, and (d) Relative discharge plots for AF and HFCW effluents.

$T_{q_{rel}} \leq 10\%$  for HFCW effluent was  $t = 37$  h and for AF effluent was  $t = 41$  h after which, both MTI discharges reached steady state (Figure 4.5d). Pore blocking for AF effluent occurred at about  $t = 47.5$  h with  $q_{rel}$  of approximately 4%, whereas for HFCW there was a steady decline with a seemingly asymptotic relative discharge of  $q_{rel} = 10\%$  from  $t = 51$  h to  $t = 56$  h. The HFCW effluent  $q_{rel}$  declined steadily again from 10 % to approximately 8% from  $t = 56$  h to  $t = 57.75$  h.

#### 4.4.2 Permeate flux decline

Flux decline for AF and HCFW effluent followed an exponential decay function with  $R^2 = 0.93$  and  $R^2 = 0.95$ , respectively (Figure 4.6). The flux decline exemplified a typical flux vs time curve wherein the first stage showed a rapid decline in flux (Stage I), followed by a protracted gradual flux decline (Stage II), and a steady state flux decline (Stage III). The sharp decline in flux is reported in Lim and Bai (2003) where a hollow membrane used for micro-filtration of activated sludge wastewater showed reduction in discharge over time. The flux – time data were modelled against the linear, logarithmic, polynomial and exponential functions,

and the exponential function produced satisfactory results based on the respective  $R^2$  values. Satisfactory  $R^2$  values range from  $R^2 \geq 0.50$  (Moriassi et al., 2007; Van Liew et al., 2007). Previous membrane clogging studies have modelled their experimental results against different functions and reported that the power function produced satisfactory  $R^2$  values (Hwang and Lin, 2002; Yuan et al., 2002; Lim and Bai, 2003). Similar to previous studies (Hwang and Lin, 2002; Yuan et al., 2002; Lim and Bai, 2003), the selected power function encompassed the collective flux – time data points.

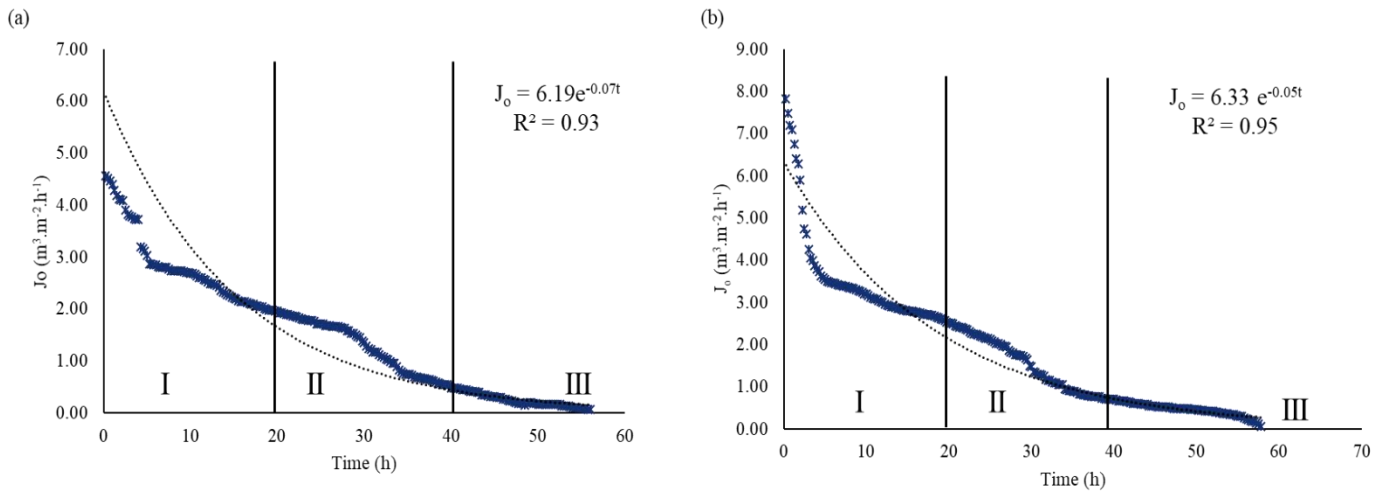


Figure 4.6 Flux - time curve for (a) AF and (b) HFCW effluent.

The various stages in membrane fouling were characterized by the functional relationships as in Equations 4.13 and 4.14.

$$J_o = 6.19e^{-0.07t} \quad 4.13$$

$$J_o = 6.33e^{-0.05t} \quad 4.14$$

Maximum permeate flux was observed from  $t = 0$  h to  $t = 10$  h for both effluents because all MTI pores were available for discharging the effluents. The long-term gradual flux decline (II) was attributed to the high concentration of suspended solids. Extended MTI pore blockage (III) resulted in a steady-state permeate flux discharge for AF at  $t = 45$  h and  $t = 50$  h (approx.) for HFCW effluent.

The accelerated pore narrowing of AF effluent is attributed to the high concentration of TSS (49 mg/l) compared to HFCW (TSS = 20  $\text{mg} \cdot \text{L}^{-1}$ ) as well as to a high concentration of ortho-phosphates in AF effluent (10.5  $\text{mg} \cdot \text{L}^{-1}$ ) and ammonium (61  $\text{mg} \cdot \text{L}^{-1}$ ). Ortho-phosphates and nitrates can be classified as dissolved inorganic matter (DOM) and Tang et al. (2010) reported

that DOM contributes 26% – 52% to membrane fouling. The findings also concur with Capra and Scicolone (2007) whose study revealed that a high concentration of TSS and organic matter caused accelerated clogging of drip emitters. Effluent quality influences MTI fouling as dictated by the Bucks et al. (1979) hazard rating scale.

#### 4.4.3 Plugging coefficients

In practice, pore blocking occurs in stages (Judd and Jefferson, 2003; Ho and Sung, 2009). The linear relationship derived from the flux vs time curve yielded a functional relationship shown in Figure 4.7. Effluent quality influences the plugging process. It is worth noting that pore blocking occurs in stages thus the complexity of membrane plugging makes it difficult for one model to fit one plugging model.

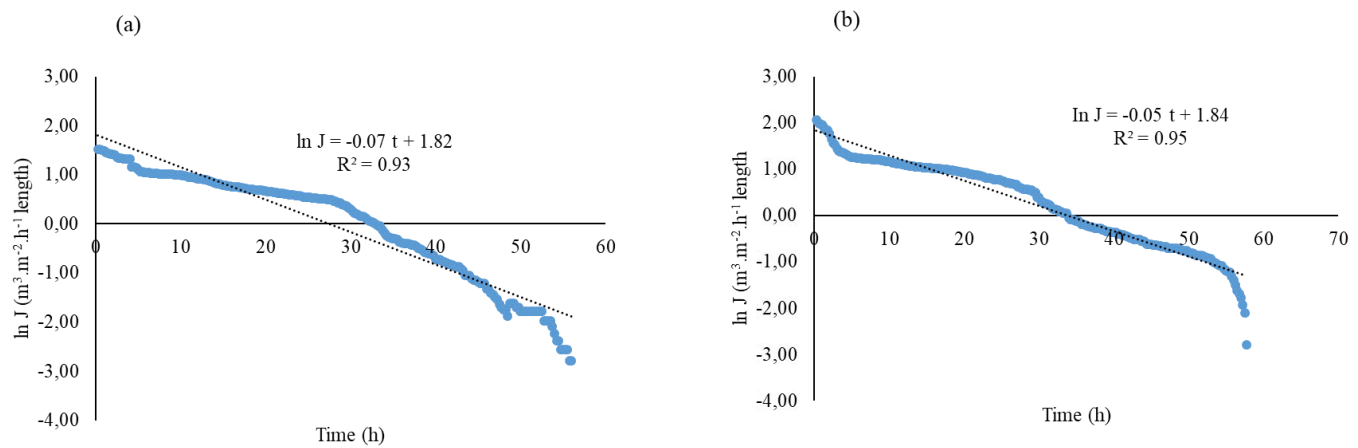


Figure 4.7 Linearised flux decline rate for (a) AF effluent and (b) HFCW effluent

The derived plugging coefficients from the respective effluents were;  $\alpha_{AF} = 0.07$  and  $\alpha_{HFCW} = 0.05$ . The resultant MTI discharge function were then characterised by Equation 4.15 and 4.16 as follows:

$$q_{AF} = (0.93)0.116h^{1.1948} \quad 4.15$$

$$q_{HFCW} = (0.95)0.116h^{1.1948} \quad 4.16$$

The marginal difference in  $\alpha$  under the two effluents permits for low ( $t = 0$  h to approx.  $t = 60$  h) intermittent MTI intervals. An intermittent drip irrigation experiment using urban wastewater by Capra and Scicolone (2007) that operated for 4-6 hours for 60 hours revealed that emitters with low discharge rates clogged faster as compared to high discharge rate emitters. Continued MTI usage over  $t = 60$  h resulted in 95 % decline in flux.

#### 4.4.4 Bacterial activity

The bacterial colonies increased significantly over the course of five days (Figures 4.8, 4.9, and 4.10). The microbial activity in deposited sediment (DS) approximately equalled that in the adhered bacterial biofilm (ABF). Hence the bacteria films formed by the DS and ABF potentially caused microbial fouling hence contributing to flux decline. Microbes contribute to formation of biofilms that resulted in stables bacterial matrices that form around the active MTI discharge nano-pores. Flux decline in membranes are due to biofilms formed after aggregated microbial communities produce a stable mechanical structure around active pores over an irrigation span Kerdi et al. (2019).

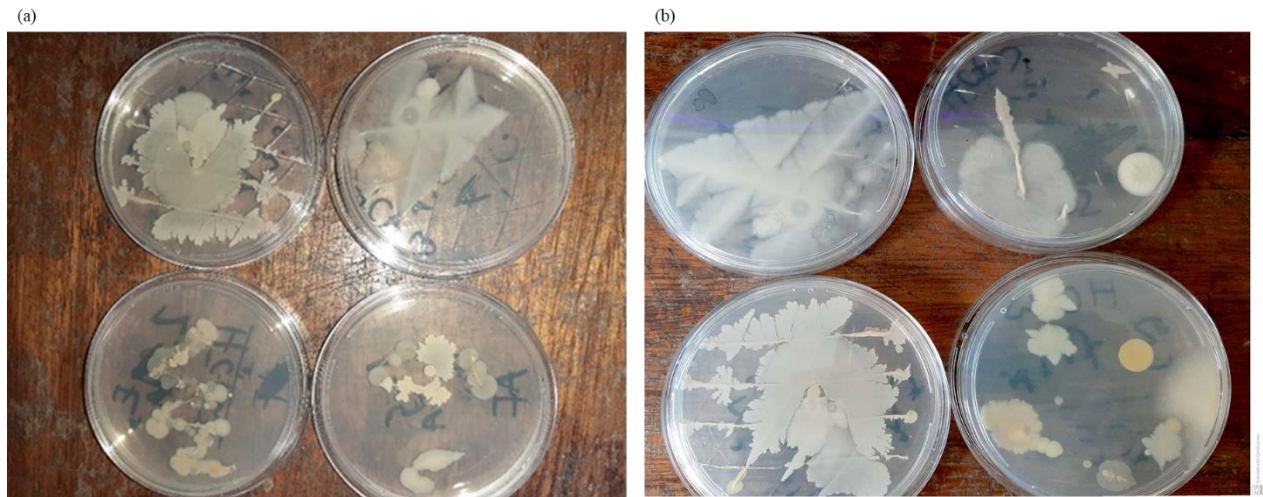


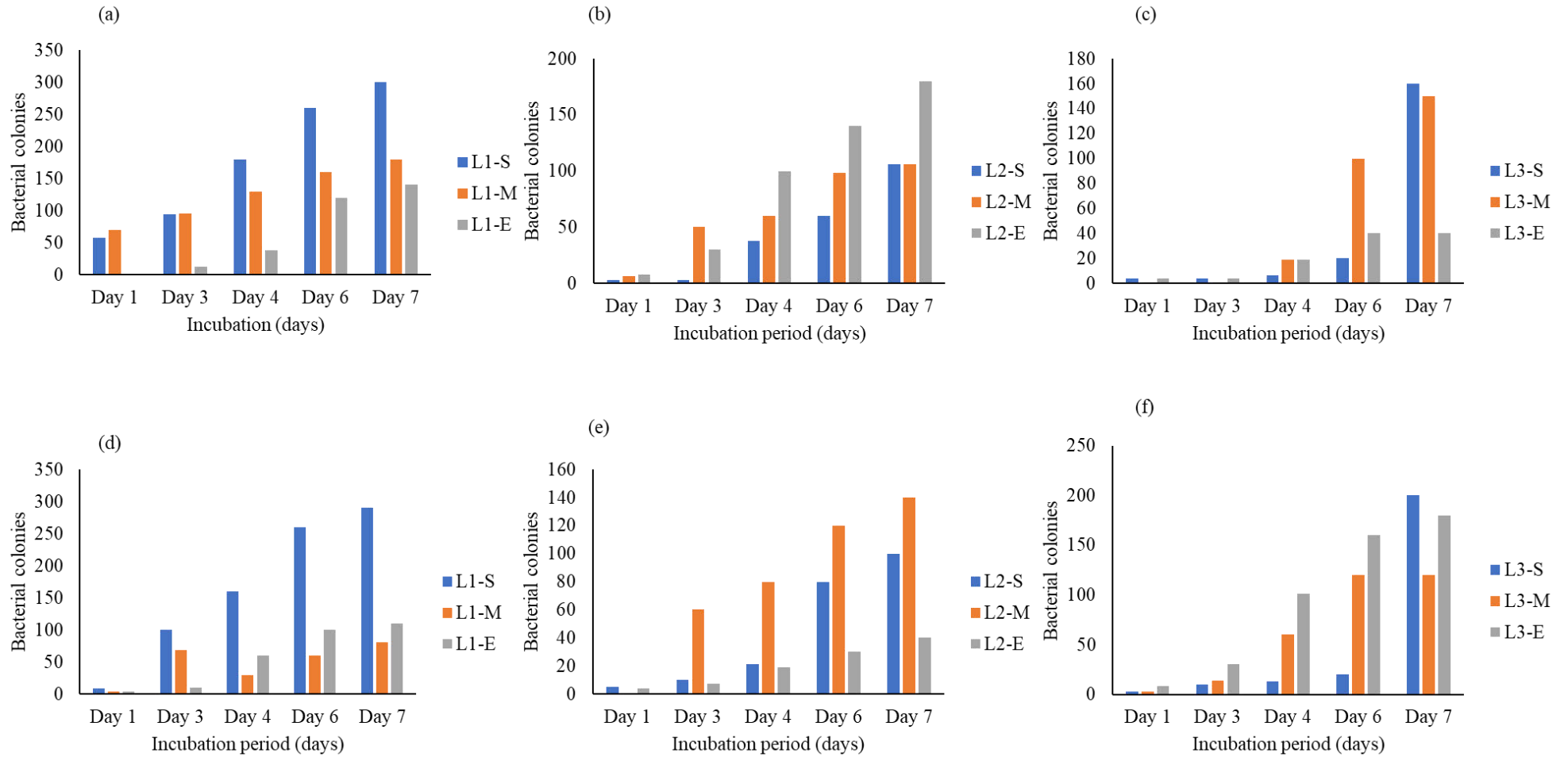
Figure 4.8 Gel like bacterial colonies progression in selected samples after (a) 3 incubation days and (b) after 7 incubation days

#### 4.4.5 SEM - EDX

Deposited sediment (DS) and adhered biofilm (ABF) SEM-EDX images (Figures 4.10 and 4.11) revealed a dry gelatinous layer forming on the surface of the MTI. AF effluent deposited sediment covered a significant MTI surface area as compared to HFCW. ABF for both effluents formed a thin yellow layer which the imaging software could not present. The effluent produced gel layers in the MTI tubing thus causing resistance, consequently leading to flux decline

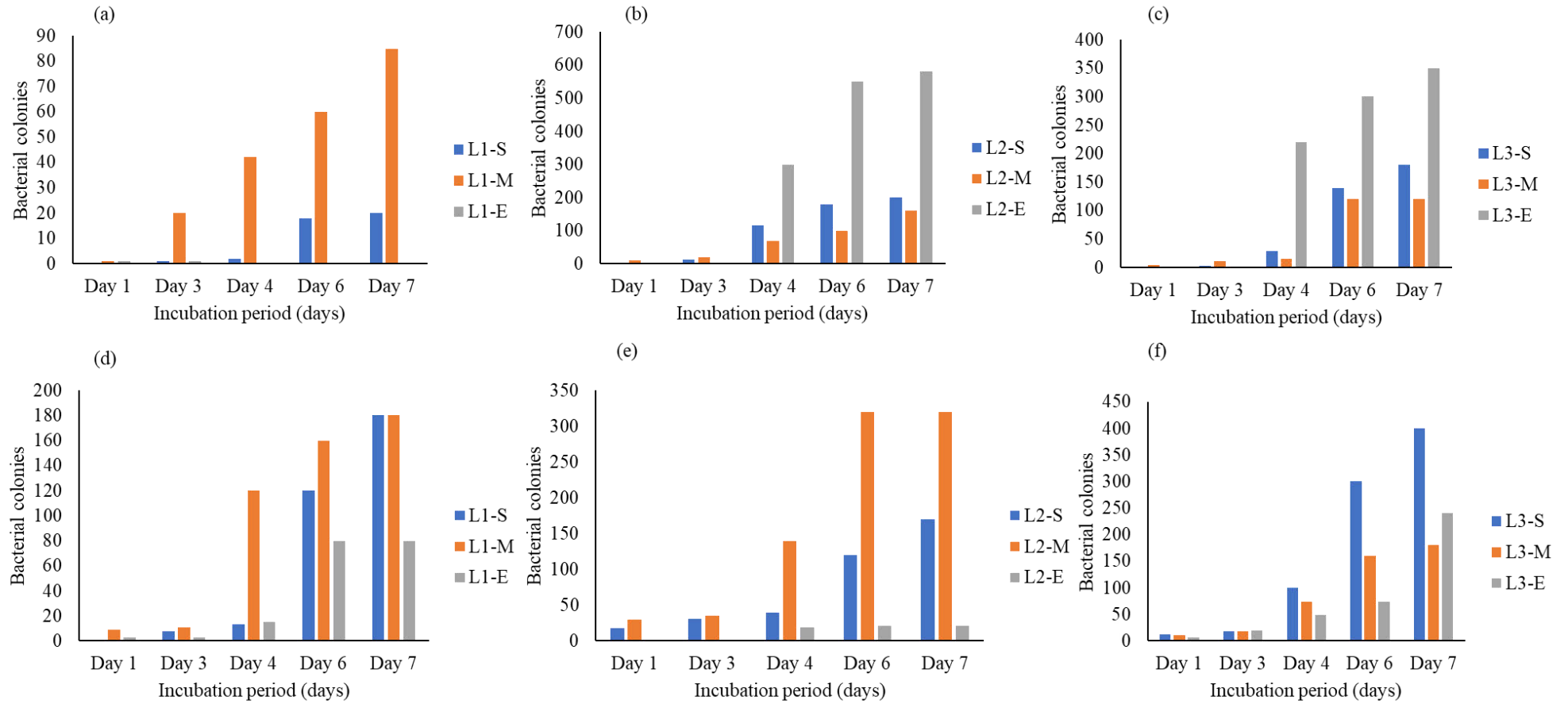
EDX analysis revealed that the DS from the AF and HFCW effluents contained inorganic elements. The decline in discharge for the AF and HFCW effluent could be attributed to a high

concentration of TDS. A one-way ANOVA test revealed there was a statistical difference between the DS and ABF from AF and that from HFCW ( $p > 0.05$ ) (see R-script in Appendix B). The DS from AF had a significantly high amount of heavy metals. The pH level 7 facilitates precipitation and long-term flocculation which consequently cause partial or complete pore blocking for instance, Kanda et al. (2018b) cited how inorganic compounds such as  $\text{NaHCO}_3$ ,  $\text{MgSO}_4$ , and  $\text{CaCl}_2$  precipitate at  $\text{pH} \geq 7$  and flocculate and partially block MTI pores. The experiment by Kanda et al. (2018b) a TSS concentration of  $150 \text{ mg.L}^{-1}$  caused an approximately 60% decrease in MTI relative discharge over 300 h of operation whilst a TDS concentration of  $2500 \text{ mg.L}^{-1}$  caused a 60% decline in relative discharge over an approximately 325 h of operation. The findings also concur with Lili et al. (2016) who posited that chemical precipitation caused emitter clogging.



\*L ( $i = 1, 2, 3$ ) -S = start section of lateral, M = mid-section of lateral, E = end section of lateral.

Figure 4.9 Bacterial colony growth for deposited sediment (DS) (a) colony growth under AF for lateral 1 (L1), (b) lateral 2 (L2), and (c) lateral 3 (L3). Bacterial growth on adhered sediment (AS) for (a) L1, (b) L2, and (c) L3.



\*L ( $i = 1, 2, 3$ ) -S = start section of lateral, M = mid-section of lateral, E = end section of lateral.

Figure 4.10 Bacterial colony growth for deposited sediment (DS) under HFCW effluent (a) for lateral 1 (L1), (b) lateral 2 (L2), and (c) lateral 3 (L3). Bacterial growth on adhered sediment (AS) for (a) L1, (b) L2, and (c) L3.



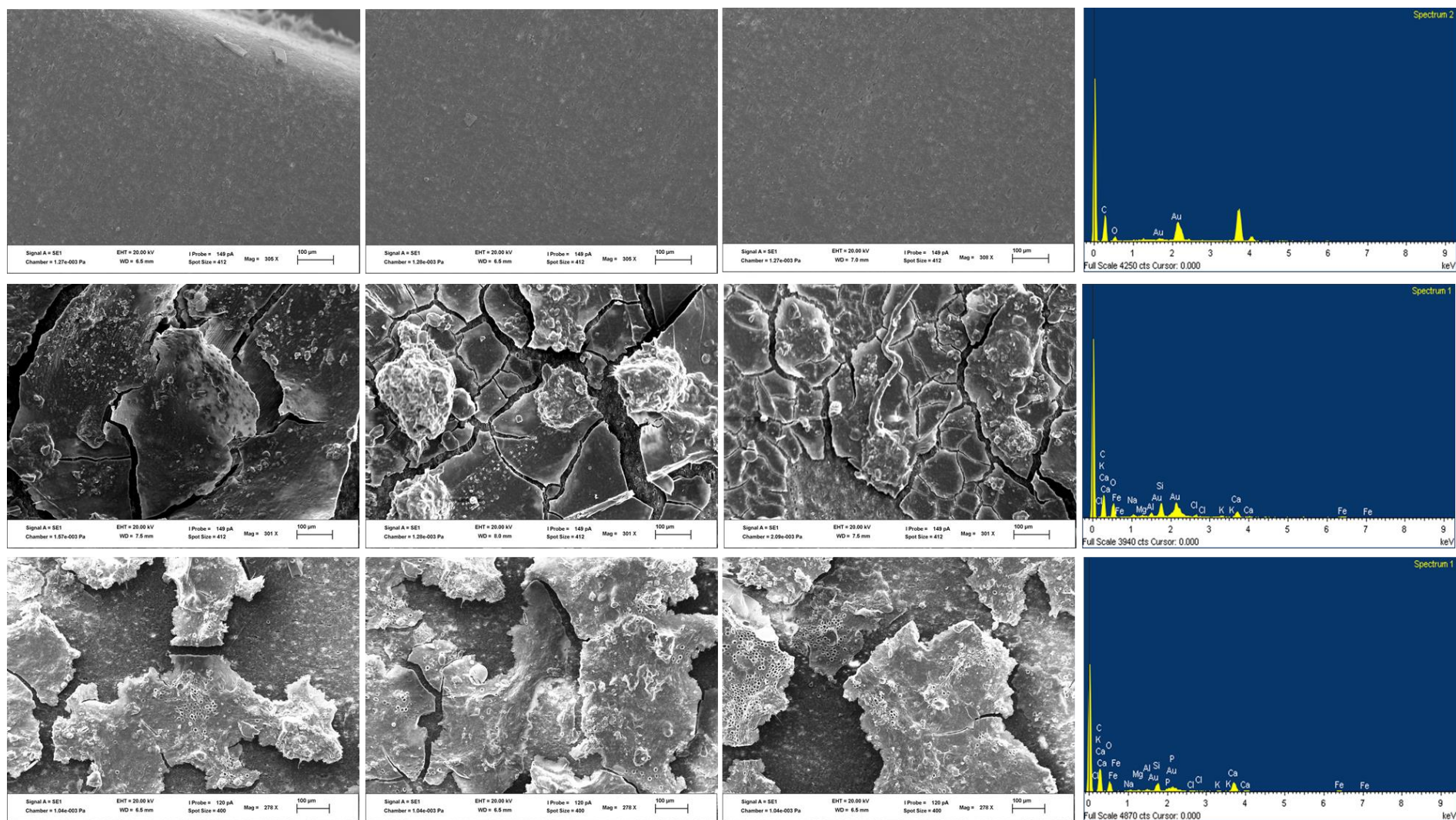


Figure 4.11 SEM-EDX for a pristine MTI lateral (top row), SEM-EDX for deposited sediment (DS) from AF effluent (second row), and SEM-EDX for (DS) from HFCW effluent (bottom row).



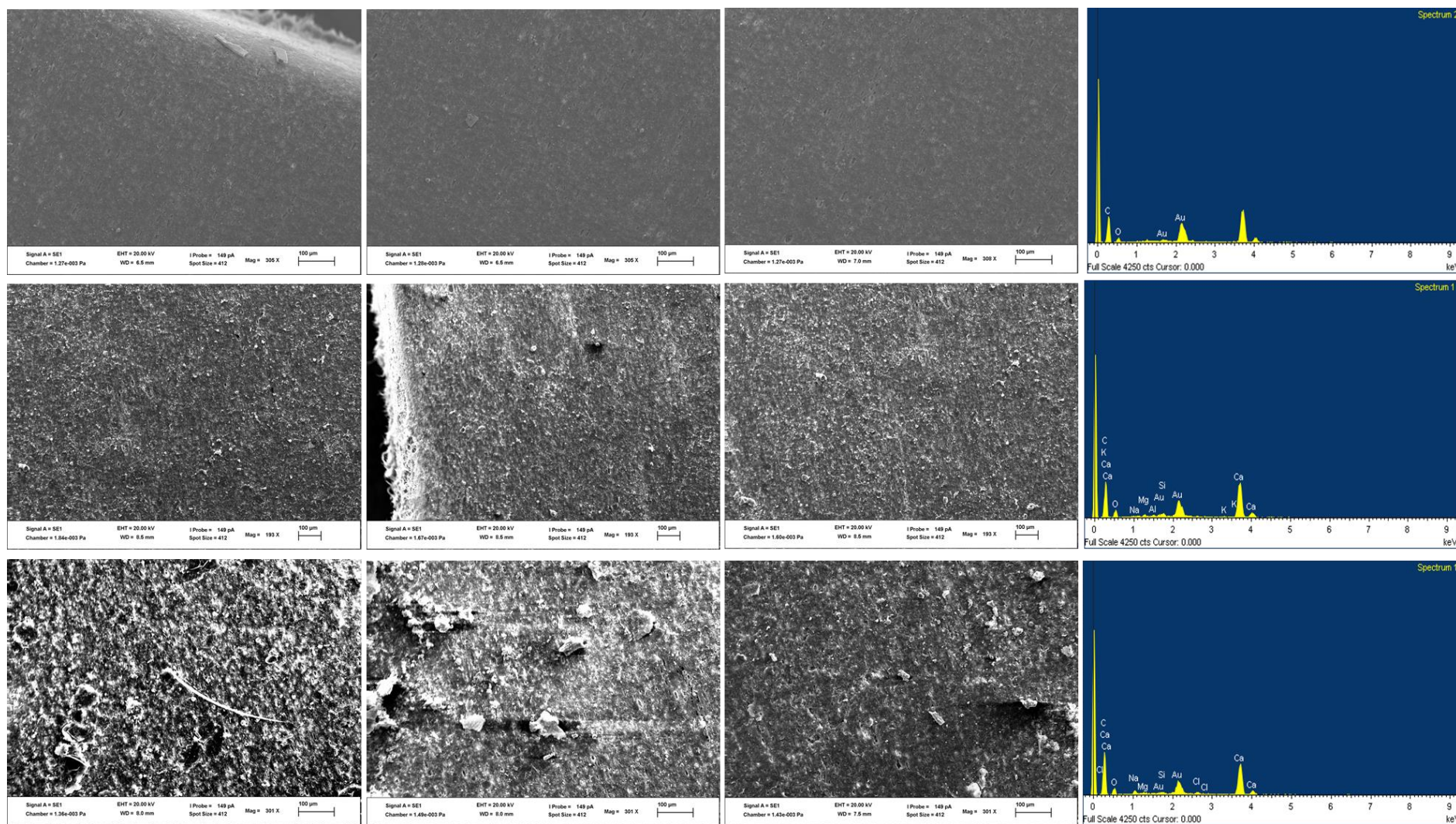


Figure 4.12 SEM-EDX for a pristine MTI lateral (top row), SEM-EDX for adhered biofilm (ABF) from AF effluent (second row), and SEM-EDX for AS from HFCW effluent (bottom row).

#### 4.5 Irrigation Implication

Wastewater as an alternative for freshwater irrigation has gained traction. As such research on the effects of different effluents on irrigation technologies' performance informs operation and management (O&M) procedures. The AF and HFCW effluents significantly degraded the discharge efficiency of MTI over intermittent operation. Caution must be taken when irrigating with the respective effluents. For example, to reduce the risk of early fouling, the irrigators should perform a flushing exercise after irrigation intervals. Although this research did not perform flushing during the experiment, the exercise can potentially minimise fouling rate. Suspended solids posed a significant risk of clogging as they were deposited on the MTI tubing surface. This negative outcome can be countered by additional filtration although pumping systems will be required to give the irrigation water sufficient head to maintain a uniform emission. The plugging coefficients have a minute difference; however, HFCW is suitable for irrigation because of the low TSS volume. Considering that pore constriction occurs in phases, different pore locking fractals contribute differently to permeate flux reduction. Thus, phased fractal analysis will aid in understanding the pore constriction and the consequent degree of flux decline.

#### 4.6 Conclusion and Recommendation

The study assessed the pore blocking effects of AF and HFCW effluent. From the findings of the study the following conclusions can be drawn:

- Effluent quality influences MTI pore blocking.
- AF has more pronounced pore-blocking as evidenced by the high degree of clogging ( $DC$ ) and quick decline in relative discharge ( $q_{rel} = 0$ ).
- A high concentration of TSS and bacteria accelerate pore blocking. This was evidenced by a high  $DC$  and quick decline in  $q_{rel}$  (AF,  $q_{rel} = 0$  at  $t = 57$  h and HFCW,  $q_{rel} = 0$  at  $t = 60$  h)
- MTI permeate flux decline follows a typical time vs flux curve
- For both AF and HFCW effluents, MTI plugging coefficients were 0.07 and 0.05, respectively.
- The SEM revealed cake formation layer under AF effluent that covered a significant surface area, thus reducing active MTI pores for discharge.

Additional filtering of irrigation water can potentially mitigate the effects of MTI plugging by wastewater effluent. Future research is required to assess the actual performance of a buried MTI lateral under wastewater irrigation with filtration. Also, the researchers recommend the experiment be run under continuous irrigation scenarios. It is worth noting that MTI pore locking happens in phases depending on the characteristic effluent. Stage by stage fractal analysis will help determine the build-up to the eventual pore-blocking coefficients. Thus, a future study is recommended to determine the characteristic fractal formation of the different effluents and their effects on MTI fouling.

#### 4.7 References

- Abdelrasoul, A, Doan, H and Lohi, A. 2013. A mechanistic model for ultrafiltration membrane fouling by latex. *Membrane Science* 433: 88-99.
- APHA. 2012. *Wpcf-Standard methods for the examination of water and wastewater*. Washington DC, USA.
- Bhattacharjee, C and Datta, S. 2003. Analysis of polarized layer resistance during ultrafiltration of PEG-6000: an approach based on filtration theory. *Separation and Purification Technology* 33 (2): 115-126.
- Brodowski, S, Amelung, W, Haumaier, L, Abetz, C and Zech, W. 2005. Morphological and chemical properties of black carbon in physical soil fractions as revealed by scanning electron microscopy and energy-dispersive X-ray spectroscopy. *Geoderma* 128 (1-2): 116-129.
- Bucks, D, Nakayama, F and Warrick, A. 1982. Principles, practices, and potentialities of trickle (drip) irrigation. In: *Advances in irrigation*. Elsevier, Amsterdam, Netherlands.
- Bucks, DA, Nakayama, F and Gilbert, R. 1979. Trickle irrigation water quality and preventive maintenance. *Agricultural Water Management* 2 (2): 149-162.
- Capra, A and Scicolone, B. 2007. Recycling of poor quality urban wastewater by drip irrigation systems. *Journal of Cleaner Production* 15 (16): 1529-1534.
- Cararo, D, Botrel, T, Hills, D and Leverenz, H. 2006. Analysis of clogging in drip emitters during wastewater irrigation. *Applied Engineering in Agriculture* 22 (2): 251-257.
- Chang, E-E, Yang, S-Y, Huang, C-P, Liang, C-H and Chiang, P-C. 2011. Assessing the fouling mechanisms of high-pressure nanofiltration membrane using the modified Hermia model and the resistance-in-series model. *Separation and Purification Technology* 79 (3): 329-336.
- Charfi, A, Amar, NB and Harmand, J. 2012. Analysis of fouling mechanisms in anaerobic membrane bioreactors. *Water Research* 46 (8): 2637-2650.
- Corbatón-Báguena, M-J, Álvarez-Blanco, S and Vincent-Vela, M-C. 2015. Fouling mechanisms of ultrafiltration membranes fouled with whey model solutions. *Desalination* 360: 87-96.
- Corbatón-Báguena, M-J, Vincent-Vela, M-C, Gozávez-Zafrilla, J-M, Álvarez-Blanco, S, Lora-García, J and Catalán-Martínez, D. 2016. Comparison between artificial neural networks and Hermia's models to assess ultrafiltration performance. *Separation and Purification Technology* 170: 434-444.
- Fan, Y-W, Huang, N, Zhang, J and Zhao, T. 2018. Simulation of soil wetting pattern of vertical moistube-irrigation. *Water* 10 (5): 601.
- Field, R. 2010. Fundamentals of fouling. *Membranes for Water Treatment* 4: 1-23.

- Furuichi, M, Matsumoto, K and Nakamura, K. 2008. Evaluation of Water Quality Using a Plugging Coefficient Based on a Pore Blocking Filtration Model in the Membrane Filtration Process. *Membrane* 33 (6): 307-316.
- Gil, M, Rodríguez-Sinobas, L, Juana, L, Sanchez, R and Losada, A. 2008. Emitter discharge variability of subsurface drip irrigation in uniform soils: effect on water-application uniformity. *Irrigation Science* 26 (6): 451-458.
- Guo, W, Ngo, H-H and Li, J. 2012. A mini-review on membrane fouling. *Bioresource Technology* 122: 27-34.
- Gutterer, B, Sasse, L, Panzerbieter, T and Reckerzügel, T. 2009a. *Decentralised wastewater treatment systems (DEWATS) and sanitation in developing countries: a practical guide*. Loughborough University & Bremen Overseas Research (BORDA), Loughborough University, UK, United Kingdom.
- Gutterer, B, Ulrich, A and Reuter, S. 2009b. *Decentralised wastewater treatment systems (DEWATS) and sanitation in developing countries: a practical guide*. WEDC, Loughborough University, BORDA, Loughborough University, United Kingdom.
- Henry, C, Minier, J-P and Lefèvre, G. 2012. Towards a description of particulate fouling: From single particle deposition to clogging. *Advances in Colloid Interface Science* 185: 34-76.
- Hermia, J. 1985. Blocking filtration. Application to non-Newtonian fluids. In: *Mathematical models and design methods in solid-liquid separation*. Springer, Dordrecht, Netherlands.
- Hills, D and Brenes, M. 2001. Microirrigation of wastewater effluent using drip tape. *Applied Engineering in Agriculture* 17 (3): 303.
- Ho, J and Sung, S. 2009. Effects of solid concentrations and cross-flow hydrodynamics on microfiltration of anaerobic sludge. *Membrane Science* 345 (1-2): 142-147.
- Hwang, K-J and Lin, T-T. 2002. Effect of morphology of polymeric membrane on the performance of cross-flow microfiltration. *Journal of Membrane Science* 199 (1-2): 41-52.
- Janus, T and Ulanicki, B. 2015. A behavioural membrane fouling model for integrated simulation of membrane bioreactors for wastewater treatment. *Procedia Engineering* 119: 1328-1337.
- Judd, S and Jefferson, B. 2003. *Membranes for industrial wastewater recovery and re-use*. Elsevier Science Ltd, United Kingdom.
- Jun, Z, Wenquan, N, Linlin, Z and Liyan, S. 2012. Experimental study on characters of wetted soil in moistube irrigation. *Science of Soil and Water Conservation* 10 (6): 32-38.
- Kanda, EK, Mabhaudhi, T and Senzanje, A. 2018. Hydraulic and clogging characteristics of moistube irrigation as influenced by water quality. *Journal of Water Supply: Research and Technology-Aqua* 67 (5): 438-446.
- Kanda, EK, Niu, W, Mabhaudhi, T and Senzanje, A. 2019. Moistube Irrigation Technology: A Review. *Agricultural Research* 9 (2): 139-147.
- Keller, J and Karmeli, D. 1974. Trickle irrigation design parameters. *Transactions of the ASAE* 17 (4): 678-684.
- Kerdi, S, Qamar, A, Alpatova, A and Ghaffour, N. 2019. An in-situ technique for the direct structural characterization of biofouling in membrane filtration. *Membrane Science* 583: 81-92.
- Kijne, JW. 2011. Treated Wastewater in Agriculture. Use and Impacts on the Soil Environment and Crops. . In: eds. Levy, G, Fine, P and Bar-Tal, A, *Experimental Agriculture*. Wiley-Blackwell, Chichester, United Kingdom.

- Li, Y, Song, P, Pei, Y and Feng, J. 2015. Effects of lateral flushing on emitter clogging and biofilm components in drip irrigation systems with reclaimed water. *Irrigation Science* 33 (3): 235-245.
- Lim, A and Bai, R. 2003. Membrane fouling and cleaning in microfiltration of activated sludge wastewater. *Membrane Science* 216 (1-2): 279-290.
- Liu, H and Huang, G. 2009. Laboratory experiment on drip emitter clogging with fresh water and treated sewage effluent. *Agricultural Water Management* 96 (5): 745-756.
- Musazura, W. 2018. Crop Fertigation (Nitrogen and Phosphorus) with Decentralised Wastewater Treatment System Effluents and Effects on Soils and Groundwater. Unpublished thesis, Crop Science, University of KwaZulu-Natal, University of KwaZulu-Natal, Pietermaritzburg, South Africa.
- Musazura, W, Odindo, A, Tesfamariam, E, Hughes, J and Buckley, C. 2019a. Nitrogen and phosphorus fluxes in three soils fertigated with decentralised wastewater treatment effluent to field capacity. *Journal of Water Reuse and Desalination* 9 (2): 142-151.
- Musazura, W, Odindo, AO, Tesfamariam, EH, Hughes, JC and Buckley, CA. 2019b. Nitrogen and phosphorus dynamics in plants and soil fertigated with decentralised wastewater treatment effluent. *Agricultural Water Management* 215: 55-62.
- Puig-Bargués, J, Arbat, G, Barragán, J and De Cartagena, FR. 2005. Hydraulic performance of drip irrigation subunits using WWTP effluents. *Agricultural Water Management* 77 (1-3): 249-262.
- R-Core-Team. 2017. *R: A language and environment for statistical computing*. R Foundation for Statistical Computing, Vienna, Austria.
- Risović, D and Pavlović, Ž. 2013. Performance assessment of methods for estimation of fractal dimension from scanning electron microscope images. *Journal of Scanning Microscopies* 35 (6): 402-411.
- Rost, S, Gerten, D, Bondeau, A, Lucht, W, Rohwer, J and Schaphoff, S. 2008. Agricultural green and blue water consumption and its influence on the global water system. *Water Resources Research* 44 (9): W09405.
- Scott, CA, Drechsel, P, Raschid-Sally, L, Bahri, A, Mara, D, Redwood, M and Jiménez, B. 2010. *Wastewater irrigation and health: challenges and outlook for mitigating risks in low-income countries*. Earthscan, IWMI, IDRC, Colombo, Sri Lanka.
- Song, P, Li, Y, Zhou, B, Zhou, C, Zhang, Z and Li, J. 2017. Controlling mechanism of chlorination on emitter bio-clogging for drip irrigation using reclaimed water. *Agricultural Water Management* 184: 36-45.
- Tang, S, Wang, Z, Wu, Z and Zhou, Q. 2010. Role of dissolved organic matters (DOM) in membrane fouling of membrane bioreactors for municipal wastewater treatment. *Journal of Hazardous Materials* 178 (1-3): 377-384.
- Thalla, AK, Devatha, CP, Anagh, K and Sony, E. 2019. Performance evaluation of horizontal and vertical flow constructed wetlands as tertiary treatment option for secondary effluents. *Applied Water Science* 9 (6):1-9.
- Trooien, T, Lamm, F, Stone, L, Alam, M, Rogers, D, Clark, G and Schlegel, A. 2000. Subsurface drip irrigation using livestock wastewater: Dripline flow rates. *Applied Engineering in Agriculture* 16 (5): 505-508.
- Van Liew, MW, Veith, TL, Bosch, DD and Arnold, JG. 2007. Suitability of SWAT for the Conservation Effects Assessment Project: Comparison on USDA Agricultural Research Service Watersheds. *Journal of Hydrologic Engineering* 12 (2): 173-189.
- Vela, M, Blanco, S, García, J and Rodríguez, E. 2009. Analysis of membrane pore blocking models adapted to crossflow ultrafiltration in the ultrafiltration of PEG. *Chemical Engineering Journal* 149 (1-3): 232-241.

- Xu, H and Van Deventer, JS. 2002. Microstructural characterisation of geopolymers synthesised from kaolinite/stilbite mixtures using XRD, MAS-NMR, SEM/EDX, TEM/EDX, and HREM. *Cement Concrete Research* 32 (11): 1705-1716.
- Yang, W, Tian, L, Du, T, Ding, R and Yang, Q. 2008. Research Prospect of the Water-saving Irrigation by Semi-permeable Film [J]. *Journal of Water Resources and Water Engineering* 6:16.
- Yuan, W, Kocic, A and Zydney, AL. 2002. Analysis of humic acid fouling during microfiltration using a pore blockage–cake filtration model. *Journal of Membrane Science* 198 (1): 51-62.
- Zhang, W, Niu, W, Li, G, Wang, J, Wang, Y and Dong, A. 2020. Lateral inner environment changes and effects on emitter clogging risk for different irrigation times. *Agricultural Water Management* 233: 106069.

## 5 SOIL WETTING GEOMETRY UNDER MOISTUBE IRRIGATION – MODEL CALIBRATION AND VALIDATION

This chapter is under review with the Scientific Reports Journal.

**Dirwai, TL**, Senzanje, A, Mabhaudhi, T (Under review). Soil Wetting Geometry under Moistube Irrigation – Model Development and Modelling. *Sci Reports*.

### Abstract

We developed an empirical soil wetting geometry model for silty clay loam and coarse sand soils under a semi-permeable porous wall line source Moistube Irrigation (MTI) lateral irrigation. The model was developed to simulate vertical and lateral soil water movement using the Buckingham pi ( $\pi$ ) theorem. This research was premised on a hypothesis that soil hydraulic properties influence soil water movement under MTI. Two independent, but similar experiments, were conducted to calibrate and validate the model using MTI lateral placed at a depth of 0.2 m below the soil surface in a soil bin with a continuous water supply (150 kPa). Soil water content was measured every 5 minutes for 100 h using MPS-2 sensors. Model calibration showed that soil texture influenced water movement ( $p < 0.05$ ) and showed a good fit for wetted widths and depths for both soils ( $nRMSE = 0.5\% - 10\%$ ;  $NSE \geq 0.50$ ; and  $d\text{-index} \geq 0.50$ ). The percentage bias ( $PBIAS$ ) statistic revealed that the models' under-estimated wetted depth after 24 h by 21.9% and 3.9% for silty clay loam and sandy soil respectively. Sensitivity analysis revealed an agreeable models' performance values. This implies the applicability of the model for estimating wetted distances for an MTI lateral placed at 0.2 m. However, further experimentation under varying scenarios for which MTI would be used, including field conditions, is needed to further validate the model and establish robustness. MTI wetting geometry informs placement depth for optimal irrigation water usage.

**Keywords:** Buckingham  $\pi$  theorem, MTI, model evaluation, porous wall line source

### 5.1 Introduction

Novel irrigation technologies such as sub-surface irrigation and porous pipes promote water conservation (Besharat et al., 2020). Moistube irrigation (MTI) is a line source semi-permeable porous pipe that has reported improved water use efficiency (WUE) (Keller and Bliesner, 1990;



Kanda et al., 2020). MTI is a sub-surface irrigation technology whose discharge is facilitated by an applied pressure or at zero pressure it utilizes soil water matric potential ( $\psi$ ) that causes a pull effect thus facilitating discharge. Soil water movement under various irrigation technologies has informed irrigators on the effective placement depth and lateral spacing that promote water use efficiency (WUE).

There is limited empirical knowledge on models that facilitate estimation of wetted perimeters under porous wall emitters. Knowledge on soil wetting geometry is critical in optimizing MTI irrigation system design (lateral placement depth and spacing) and operation (discharge rates, irrigation set times and satisfying irrigation water requirements). To maximize the advantages offered by sub-surface irrigation, knowledge of soil wetting geometries aids in irrigation network design i.e., emitter spacing and placement depths, which subsequently improve irrigation schedules (Provenzano, 2007), minimize run-off losses, promotes higher irrigation uniformity (Lamm et al., 2002; Lamm et al., 2006), increases water productivity (WP) and fWUE (Lamm, 2005; Kanda et al., 2020).

Soil wetting geometries can be determined either experimentally or using modelling tools. The former is expensive and time consuming. Modelling is a time saving exercise and numerical models have gained wide applicability over their counterparts (analytical and empirical models) because of their robustness and use of finite element boundary approximation techniques (Kandelous and Šimůnek, 2010; Kanda et al., 2020). Experimental and simulation models for line source semi-permeable emitters can potentially shed light on robust installation and management guidelines for MTI (Cote et al., 2003).

Kandelous and Šimůnek (2010a) conducted a comparative research on analytical (WetUp), numerical (HYDRUS-2D) and empirical models' performance on estimating wetting geometries under trickle irrigation. The models were evaluated using the mean absolute error (MAE) and the  $R^2$  value. The MAE ranged from 1 to 58.1 cm for WetUp, 0.87 to 10.43 cm for HYDRUS-2D, and 1.34 to 12.24 cm for the selected empirical models. The study obtained good  $R^2$  values that ranged from 0.71 – 0.84 for all models. Cook et al. (2006) assessed point source trickle irrigation wetting dimensions using HYDRUS-2D and WetUp. The findings revealed the models' equal capacity in estimating wetted dimensions, however HYDRUS-2D had difficulties in estimating wetted dimensions for soils with low hydraulic conductivity. Kanda et al. (2020c) numerically and experimentally estimated soil wetting dimensions under



MTI. Elmaloglou et al. (2013) developed a numerical model for simulation of soil water distribution under line source SDI considering hysteresis.

Despite their simplicity, empirically models can also be applied to help answer design and management questions in soil water movement and irrigation water management. Schwartzman and Zur (1986) developed an empirical model that simulated horizontal and vertical wetting geometries for line source water application under Gilat loam and Sinai sand soils. The wetting geometries were dependent on emitter discharge, total soil water volume and soil characteristics. Dabral et al. (2012) modified the Schwartzman and Zur (1986) equations and modelled the horizontal width ( $W$ ) and vertical depth ( $Z$ ) from a point source emitter.. The models' versatility were closely similar to those by Schwartzman and Zur (1986) and Keller and Bliesner (1990); however, a lack of the emitter placement depth variable potentially limited the accuracy of the model.

Amin and Ekhmaj (2006) developed an empirical model that estimated horizontal ( $R$ ) and vertical downward ( $Z$ ) distances of the wetting front from the surface drip emitter, whereas Singh et al. (2006) applied the dimensional analysis to determine the wetted width ( $W$ ) and wetted depth ( $D$ ) of sandy loam soils under subsurface drip irrigation. Kandolous et al. (2008) employed Singh's (Singh et al., 2006) method to develop an empirical model that estimated the horizontal ( $W$ ), vertical upward ( $Z_+$ ), and vertical downward ( $Z_-$ ) wetting distances.

Literature presents evidence on the exhaustive use of analytical and numerical models for estimating soil wetting geometries or dimensions under point source and line source surface and subsurface irrigation. However limited literature exists on empirical model that estimate wetting geometries under a relatively new SPM MTI porous lateral. Empirical models tend to bring about simplicity and ease of application without the need for extensive data sets and, at times, proprietary software.

MTI flow approximates a semi-permeable porous line source two-dimensional flow and the water flow process is best described by Richards Equation. Flow simulation models utilize the van Genuchten-Mualem constitutive relationships to estimate the soil hydraulic parameters and aid in the plotting of soil water retention curves that are subsequently used to determine soil water content at various water potential head ( $h$ ). The van Genuchten-Mualem constitutive variables can be potentially incorporated in empirical model development to accommodate the

soil hydraulic properties, this subsequently provides an actual representation of the soil water movement component in the flow or wetting geometry simulation.

The Buckingham  $\pi$  theorem or dimensional analysis is a powerful and useful tool in developing empirical simulation models (Eddey, 1945). The Buckingham  $\pi$  theorem is premised on the concept that physical laws are independent of the units that define the variables (Curtis et al., 1982). The method allows for simplification of processing by reducing dimensional quantities that describe physical terms into a few and manageable non-dimensional quantities called  $\pi$  terms (Tillotson and Nielsen, 1984). Tillotson and Nielsen (1984) applied the  $\pi$  theorem to derive scale factors for soil properties, whilst studies by Singh et al. (2006) and Dabral et al. (2012) applied dimensional analysis to successfully develop soil wetting simulation models. Despite the development of empirical models for simulating soil wetting under surface and sub-surface drip irrigation using the  $\pi$  theorem; however, the concept has not been extended to MTI.

Whilst Kanda et al. (2020) used HYDRUS 2/3D to simulate the wetting fronts of a sandy-clay-loam and loamy sand under MTI, this paper adds to the body of knowledge by developing an empirical model that simulates the horizontal and vertical wetting geometry of line source water application for a silty clay loam and a coarse sand soil under MTI – the two soils were deliberately selected to cover the two extremes of fine-textured and coarse-textured soils, and attempt to establish the operational boundaries of the empirical model developed. Several studies (Schwartzman and Zur, 1986; Risse and Chesness, 1989; Moncef et al., 2002; Singh et al., 2006; Malamos, 2007; Ainechee et al., 2009) have developed soil wetting geometry simulating models under point source or trickle source, however, there is limited knowledge on the wetting geometries of porous irrigation pipes such as MTI in particular. We hypothesized that soil hydraulic properties influenced the horizontal and vertical soil water movement. The objective of the current study was therefore to develop and test soil wetting empirical models' for silty clay loam and sandy soils.

## 5.2 Materials and Methods

### 5.2.1 Model description

The horizontal ( $W$ ) and vertical ( $Z$ ) wetting geometry of the semi-permeable porous line source water application MTI were assumed to be a function of the total volumetric soil water content per unit length of the MTI lateral ( $V$ ), emitter discharge per unit length of MTI lateral ( $q$ ), hydraulic conductivity of the soil ( $k$ ), and placement depth ( $D$ ) (Singh et al., 2006). The relationship was modelled according to Equation 5.1.

$$(W, Z) = f(V, q, k, D) \quad 5.1$$

Equation 5.1 reduces to Equation 5.2

$$f(V, q, k, W, Z, D) = 0 \quad 5.2$$

Using the Buckingham  $\pi$  theorem (Singh et al., 2006; Dabral et al., 2012) four  $\pi$ s were derived as presented in Equations 5.3 to 5.7. The four  $\pi$ s were derived because the Buckingham  $\pi$  theorem states that if there is a physically meaningful equation involving a certain number,  $n$ , of physical variables in a problem and these variables contain 'm' primary dimensions, the equation relating all variables will have  $(n - m)$  dimensionless groups. In this case there were 6 variables with 2 primary variables, namely  $W$  and  $Z$ , which resulted in 4 dimensionless groups.

$$f(\pi_1, \pi_2, \pi_3, \pi_4) = 0 \quad 5.3$$

where:

$$\pi_1 = \frac{Z}{D} \quad 5.4$$

$$\pi_2 = \frac{W}{D} \quad 5.5$$

$$\pi_3 = \frac{V}{D^2} \quad 5.6$$

$$\pi_4 = \frac{kD}{q} \quad 5.7$$

Multiplying the  $\pi_3$  and  $\pi_4$  yielded the dimensionless soil water content per unit length of MTI ( $V^*$ ) as presented by Equation 5.8.

$$V^* = V \left( \frac{k}{qD} \right) \quad 5.8$$

By taking the square root of the product of  $\pi_4$  and  $(\pi_2)^2$  yielded the dimensionless wetted width ( $W^*$ ) as presented by Equation 5.9.

$$W^* = W \left( \frac{k}{qD} \right)^{0.5} \quad 5.9$$

The square root of the product of  $\pi_4$  and  $(\pi_1)^2$  yielded the dimensionless wetted depth ( $Z^*$ ) as presented by Equation 10.

$$Z^* = Z \left( \frac{k}{qD} \right)^{0.5} \quad 5.10$$

Schwartzman and Zur (1986) and Singh et al. (2006) postulated that there exists a relationship amongst dimensionless parameters. For this research, the relationships are as presented in Equations 5.11 and 5.12;

$$W^* = A_1 V^{*b_1} \quad 5.11$$

$$Z^* = A_2 V^{*b_2} \quad 5.12$$

where:  $A_1$ ,  $A_2$ ,  $b_1$ , and  $b_2$  are constants for a 2-dimensional flow model. The constants  $A_1$  and  $b_1$ , were determined from the graphical plot of  $V^*$  and  $W^*$  whereas the constants  $A_2$  and  $b_2$  were determined from the graphical plot of  $V^*$  and  $Z^*$ .

Combining Equations 5.8 and 5.9 and Equations 5.8 and 5.11 yielded the wetted width ( $W$ ) and wetted depth ( $Z$ ) functions presented in Equations 5.13 and 5.14, respectively.

$$W = A_1 V^{b_1} \left( \frac{k}{qD} \right)^{(b_1-0.5)} \quad 5.13$$

$$Z = A_2 V^{b_2} \left( \frac{k}{qD} \right)^{(b_2-0.5)} \quad 5.14$$

### 5.3 Experimental Design and Data Collection

#### 5.3.1 Soil hydraulic parameters and textural characteristics

The silty clay loam (34 % clay, 58% silt, 8% sand) was obtained from University of KwaZulu-Natal's Ukulinga Research Farm in Pietermaritzburg, KwaZulu-Natal, South Africa (29°39'44.8"S 30°24'18.2"E, altitude: 636 m). The coarse sand soil (98% sand and 2% gravel)

was obtained from Genie sand in Pinetown, KwaZulu-Natal, South Africa (29°48'08.7"S 31°00'37.8"E). Soil samples were subjected to soil textural analyses using the hydrometer method. The experiment sampled five depths for textural analysis and the resultant textural data was fed into the SPAW model (Saxton and Willey, 2005) to determine saturated hydraulic conductivity ( $k_s$ ) was derived. Other soil hydraulic parameters total porosity ( $\theta_r$ ), residual soil water content ( $\theta_s$ ), and shape fitting parameters ( $n$ ,  $m$ , and  $\alpha$ ) (Table 5.1) were laboratory determined using the soil-water retention pressure method (Klute, 1986; Cresswell et al., 2008; Kanda, 2019). The 50 cm depth soil sample for the silty clay loam was used to fit the van Genuchten parameters because the 50 cm plot provided a smooth curvilinear shape and the resultant parameters closely aligned with Rawls et al. (1982). The sandy soil was commercially acquired hence the absence of varied sampling depths. The methods were selected on the basis of reliability of results and also equipment availability.

Table 5.1 Soil textural and soil hydraulic parameters (van Genuchten-Mualem model)

Textural class	Depth (cm)	$\theta_r (cm^3 \cdot cm^{-3})$	$\theta_s (cm^3 \cdot cm^{-3})$	$n$	$k_s (cm \cdot d^{-1})$	$\alpha$	$m$	BD ( $g \cdot cm^{-3}$ )
Silty loam	clay 10	0.11	0.52	1.35	62.67	0.01	0.26	0.52
Silty loam	clay 20	0.267	0.58	1.646	62.67	0.01	0.39	1.10
Silty loam	clay 30	0.4	0.49	1.35	62.67	0.01	0.26	1.36
Silty loam	clay 40	0.04	0.51	1.11	62.67	0.011	0.10	1.29
Silty loam	clay 50	0.04	0.59	1.18	62.67	0.01	0.15	1.36
Sand	NIL	0.020	0.54	2.68	513.21	0.03	0.63	1.22

\*BD = Bulk Density,  $n$  and  $m$  = shape factors for the soil water retention curve, where  $m = 1 - n^{-1}$ .

### 5.3.2 Measurement of soil wetted front

The soil was air dried, crushed and sieved through a 2 mm sieve. Thereafter, the soil was loaded into a soil bin measuring 1 m (H)  $\times$  1 m (W)  $\times$  0.5 m (B). The soil bin had transparent plexiglass walls and soil loading was done gently to avoid compaction and possible crushing of the MTI tubing. To prevent MTI collapse under the soil surcharge the MTI was supplied with water prior to loading the soil till it was turgid. To prevent MTI smearing and potential nano-pore blocking, the water was supplied upon reaching the MTI burying level. The MTI lateral was placed at a depth of 0.2 m below the soil surface and upon soil loading, MPS-2 sensors were simultaneously installed at prescribed depths (Table 5.2). The initial soil-water content for the silty clay loam was  $1.02 \cdot 10^{-6} m^3 \cdot m^{-3}$  and  $6.64 \cdot 10^{-7} m^3 \cdot m^{-3}$  for the sandy soil. Both soils were packed at a bulk density of  $1.4 g \cdot cm^{-3}$ .

Table 5.2 MPS-2 sensors placement depths and lateral spacing for the respective soils

Soil texture	MPS-2 placement depth (m)	MPS-2 lateral spacing (m)
Silty clay loam	0.1, 0.2, 0.25, and 0.3	0.05, 0.15, 0.20, and 0.25
Sand	0.1, 0.15, 0.2, 0.3, 0.4, 0.5, 0.6, 0.7, and 0.8	0.1, 0.2, and 0.3

The MPS-2 sensors measured water potential (-10 to -500 kPa) and temperature and they were calibrated by soaking them in de-ionised water for a period of 72 h before installation. Water to the MTI lateral was supplied at a pressure head of 150 kPa, which gave a discharge of 2.39 l.hr<sup>-1</sup>.m<sup>-1</sup> (Table 5.3).

The experiment was carried out in two phases, the first dataset of measured variables was used for model calibration whilst the measured variables from the second phase dataset was used for model validation. The measured variables are summarised in Table 4. Both the first and second phase were carried under identical conditions. Soil water-retention curves derived from the soil-water retention experiment were used to determine the volumetric soil water content. The experimental equipment set-up is shown in Figure 5.1.

Table 5.3 Models' inputs

Parameter	Value	
	Silty clay loam soil	Sandy soil
$k$ (cm.d <sup>-1</sup> )	62.67	513.21
$q$ (l.hr <sup>-1</sup> .m <sup>-1</sup> )	2.39	2.39
$D$ (m)	0.2	0.2
$V$	Volumetric soil water content	
$W$ and $Z$	Measured physically	

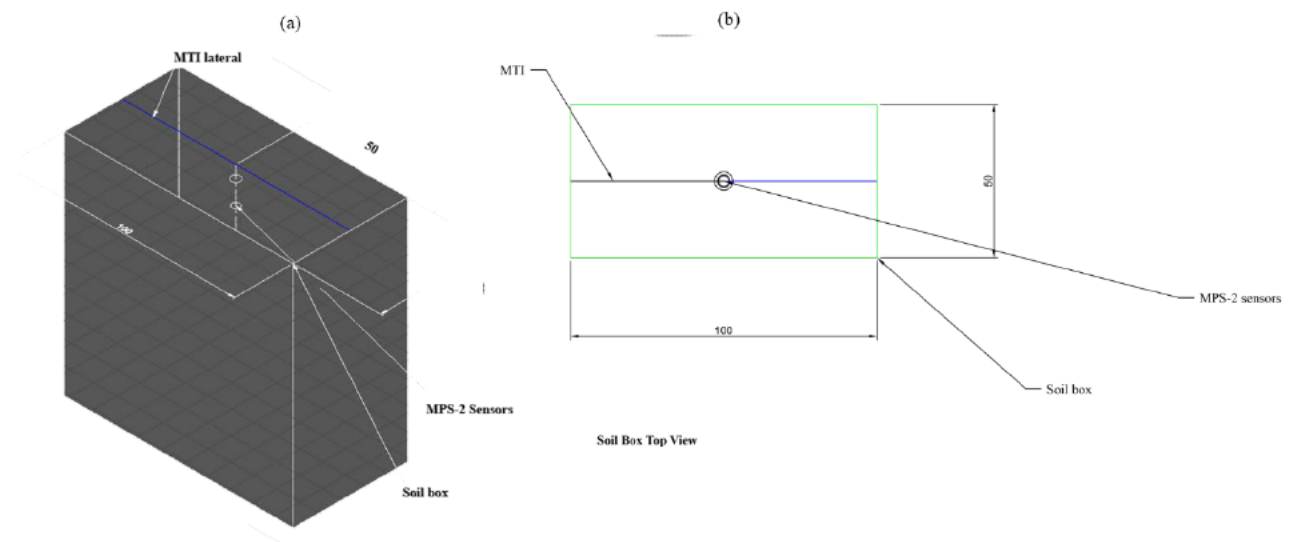


Figure 5.1 Soil bin experimental set-up (a) 3-D view and (b) orthographic top view. Dimensions in cm (Scale = 1:1 cm).

### 5.3.3 Models' calibration

The models' calibration was done on the first phase of the experiment. The calibration process was done in order to determine the models' constants  $A_1$ ,  $A_2$ ,  $n_1$ , and  $n_2$ . To improve the models' precision and accuracy, iterations were carried out on constants  $A_1$  and  $A_2$ .

### 5.3.4 Models' validation

The parameter variability – sensitivity analysis (PV-SA) method was employed for the models' validation (Sargent, 2013). A sensitivity analysis was carried out to assess the effects of  $k$ ,  $q$ , and  $D$  on both  $W$  and  $Z$ . The sensitivity analysis was done by holding all the other variables constant and assessing the functional relationship a particular “active variable” had with  $W$  and  $Z$ . Table 5.4 summarise the two independent experimental phases and their respective purposes.

Table 5.4 The experiments used for models' calibration and validation

Phase	Description	Use
1	Determining the constants $A_1$ , $A_2$ , $n_1$ and $n_2$	Calibration
2	Testing the models' predictive capacity	Validation

### 5.3.5 Models' evaluation

The study applied the normalised root mean square error ( $nRMSE$ ), index of agreement ( $d$ ), Nash-Sutcliffe efficiency ( $NSE$ ), and percentage bias ( $PBIAS$ ) for the assessment of the empirical models'. The selected evaluation statistics are defined by Equations 5.15 – 5.18 (Karandish and Šimůnek, 2019; Kanda et al., 2020). Moriasi et al. (2007) recommended the  $NSE$  and  $PBIAS$  for model evaluation because of their robust performance rating of simulating models.

$$nRMSE = \frac{\sqrt{\frac{1}{x} \sum_{i=1}^x (O_i - P_i)^2}}{O_{mean}} \quad 5.15$$

$$NSE = 1 - \left[ \frac{\sum_{i=1}^x (O_i - P_i)^2}{\sum_{i=1}^x (O_i - O_{mean})^2} \right] \quad 5.16$$

$$d = 1 - \left[ \frac{\sum_{i=1}^x (P_i - O_i)^2}{\sum_{i=1}^x (|P_i - O_{mean}| + |O_i - O_{mean}|)^2} \right] \quad 5.17$$

$$PBIAS = \frac{\sum_{i=1}^x (O_i - P_i) * 100}{\sum_{i=1}^x O_i} \quad 5.18$$

Where  $O_i$  and  $P_i$  = observed and predicted value(s), respectively,  $\bar{O}_i$  = mean observed data, and  $x$  = number of observations.  $nRMSE$  defined the developed model's accuracy whilst  $PBIAS$  defined the bias provided by the developed model. The error index  $nRMSE$  showed the performance of the model but did not clearly indicate the degree of over or under-estimation hence the use of the  $NSE$  and  $PBIAS$  statistical tools in the analysis. The  $NSE$  statistic measured the residual variance vs the measured data variance and it ranges from  $-\infty$  to 1.  $NSE$  values between 0.0 and 1.0 are considered acceptable.

$PBIAS$  measured the tendency of the simulated data to either under-estimate or overestimate the observed values. Low magnitudes presented optimal model simulation whilst positive values represented model under-estimation and negative values represented model over estimation (Moriasi et al., 2007). A summarised performance rating for the recommended statistics is shown in Table 5.5.

Table 5.5 General performance rating for model evaluation statistics

Performance rating	$NSE$	$PBIAS$ (%)	$d$
Very good	$0.75 < NSE < 1.00$	$PBIAS < \pm 15$	$0.8 < d < 1.0$
Good	$0.65 < NSE < 0.75$	$\pm 15 < PBIAS < \pm 30$	$0.6 < d < 0.8$
Satisfactory	$0.50 < NSE < 0.65$	$\pm 30 < PBIAS < \pm 55$	$0.3 < d < 0.6$
Unsatisfactory	$NSE \leq 0.50$	$PBIAS \geq \pm 15$	$d < 0.2$



## 5.4 Results and Discussion

### 5.4.1 Model calibration

The calibration steps for the four wetting geometry models' are outlined below.

#### Silty clay loam soil

The study followed the outlined steps below to determine the values for the constants  $A_1$ ,  $A_2$ ,  $b_1$ , and  $b_2$  (Singh et al., 2006). Recorded volumetric soil water content and observed wetted distance values were used to calibrate the developed soil wetting geometry models. The wetted  $W$  and  $Z$  were physically measured using grids demarcated onto the transparent plexiglass whilst the volumetric soil water content was measured using the MPS-2 sensors.

Step 1: The dimensionless variables  $V^*$ ,  $W^*$ , and  $Z^*$  were estimated using Equations 5.8 to 5.10 utilising observed values of the requisite variables from the soil bin experiments.

Step 2:  $W^*$  was plotted against  $V^*$ , similarly  $Z^*$  was plotted against  $V^*$  and the resultant power functions yielded Equations 5.19 and 5.20, with  $R^2 = 0.84$  and  $R^2 = 0.71$ , respectively (see Figure 5.2).

$$W^* = 0.03V^{*0.56} \quad 5.19$$

$$Z^* = 0.71V^{*0.16} \quad 5.20$$

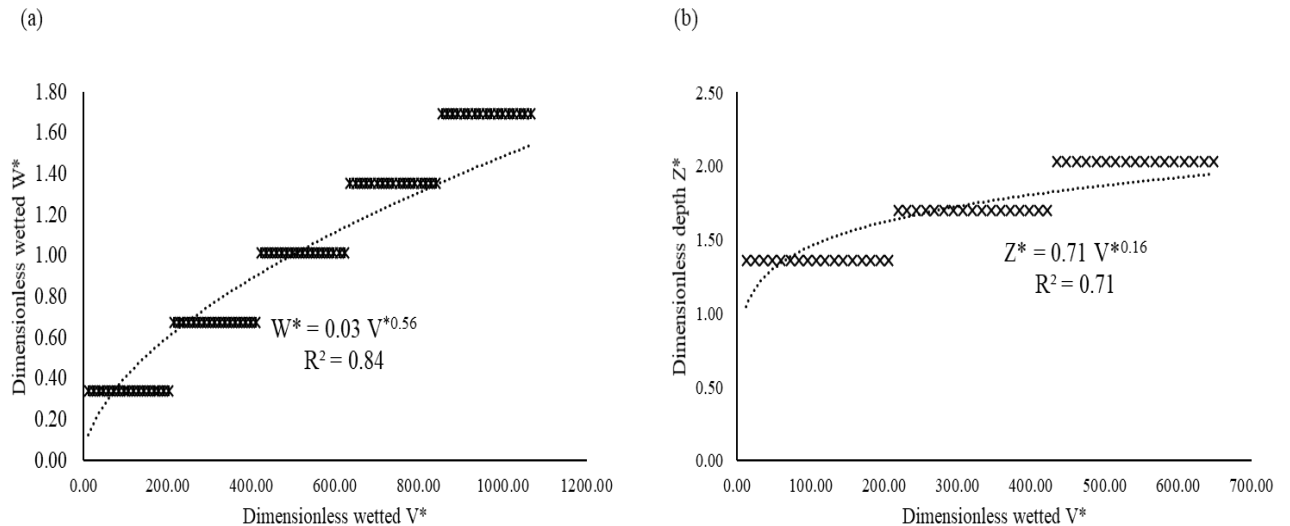


Figure 5.2 Relationship between (a) dimensionless wetted volume ( $V^*$ ) and dimensionless wetted width ( $W^*$ ) and (b) dimensionless wetted volume ( $V^*$ ) and dimensionless wetted depth ( $Z^*$ ) for silty clay loam (The bars represent a cluster of data points).

From Equations 19 and 20, values for  $A_1 = 0.03$ ,  $A_2 = 0.71$ ,  $b_1 = 0.56$ , and  $b_2 = 0.16$  were derived and these were inputted into Equations 13 and 14 to yield Equations 5.21 and 5.22.

$$W = 0.03V^{0.56} \left( \frac{k}{qD} \right)^{0.06} \quad 5.21$$

$$Z = 0.71V^{0.16} \left( \frac{k}{qD} \right)^{-0.34} \quad 5.22$$

In order to improve the models' accuracy and precision the calibration step performed iterations on the constants  $A_1$  and  $A_2$  and the resultant equations are shown in Equations 5.23 and 5.24.

$$W = 0.09V^{0.56} \left( \frac{k}{qD} \right)^{0.06} \quad 5.23$$

$$Z = 0.59V^{0.16} \left( \frac{k}{qD} \right)^{-0.34} \quad 5.24$$

For the silty clay loam soil,  $b_1 > b_2$ . This signified a high-water content in the lateral direction as compared to vertical direction. This is typical in fine textured soils (Bouma, 1984). Conversely, the calibration results yielded a scenario where  $A_1 < A_2$ , which subsequently resulted in a  $W < Z$ , an observation atypical of fine textured soils. This was because the application times during the experiment promoted the border effect within the confined soil bin.

### **Sandy soil**

The simulation steps for the sandy soil followed similar steps as those described for the silty clay loam soil. The relationships between the dimensionless volumetric soil water content per unit length of MTI ( $V^*$ ) and the dimensionless wetted width ( $W^*$ ) and wetted depth ( $Z^*$ ) are depicted in Figure 5.3. The resultant wetted width ( $W$ ) and wetted depth ( $Z$ ) for the soil are shown in Equations 5.21 and 5.22.

$W^*$  was plotted against  $V^*$ , similarly  $Z^*$  was plotted against  $V^*$  and the resulting power relationships yielded Equations 5.25 and 5.26 with  $R^2 = 0.72$  and  $R^2 = 0.84$ , respectively (see Figure 4).

$$W^* = 0.11V^{*0.44} \quad 5.25$$

$$Z^* = 0.27V^{*0.41} \quad 5.26$$

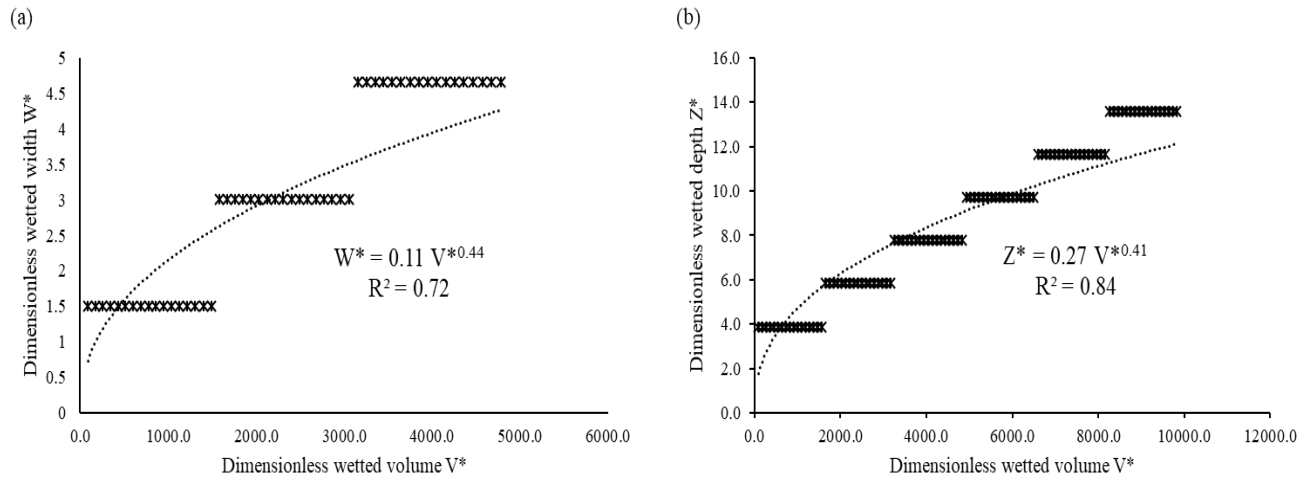


Figure 5.3 Relationship between (a) dimensionless wetted volume ( $V^*$ ) and dimensionless wetted width ( $W^*$ ) and (b) dimensionless wetted volume ( $V^*$ ) and dimensionless wetted depth ( $Z^*$ ) for sandy soil.

Similarly, from Equations 5.25 and 5.26, the values for  $A_1 = 0.11$ ,  $A_2 = 0.27$ ,  $b_1 = 0.44$ , and  $b_2 = 0.41$ , respectively, were obtained and these were inputted into Equations 5.13 and 5.14 to yield Equations 5.27 and 5.28.

$$W = 0.11V^{0.44} \left( \frac{k}{qD} \right)^{-0.06} \quad 5.27$$

$$Z = 0.27V^{0.41} \left( \frac{k}{qD} \right)^{-0.09} \quad 5.28$$

In order to improve the models' accuracy and precision the calibration step performed iterations on the constants  $A_1$  and  $A_2$  and the resultant equations are shown in Equations 5.29 and 5.30.

$$W = 0.07V^{0.44} \left( \frac{k}{qD} \right)^{-0.06} \quad 5.29$$

$$Z = 0.92V^{0.41} \left( \frac{k}{qD} \right)^{-0.09} \quad 5.30$$

The power indices for the sandy soil,  $b_1$  and  $b_2$  were approximately equal. However, the constant  $A_1 < A_2$ , which resulted in a  $Z > W$ , a phenomenon attributed to soil hydraulic characteristics. Gravity forces dominated the soil water movement mechanism in the coarse textured soil.

It is worth noting that the data in Figures 2 and 3 were modelled against a linear, logarithmic and power functions, and the power function produced satisfactory results based on the respective  $R^2$  values. Thabet and Zayani (2008) and Dabral et al. (2012) in their respective soil

wetting geometry studies opted for power functions to relate  $W$ ,  $Z$  and  $V$ . The findings were also consistent with other wetting front and infiltration studies by Xue et al. (2013), Zhang et al. (2017), and Zhanga et al. (2019).

## 5.5 Sensitivity Analysis

To evaluate the sensitivity of the soil wetted width ( $W$ ) and wetted depth ( $Z$ ) to  $k$  the parameters  $V$ ,  $q$  and  $D$  were kept constant. This yielded Equations 5.31 and 5.32.

$$\text{Silty clay loam soil } \begin{cases} W \sim k^{0.06} \\ Z \sim k^{-0.34} \end{cases} \quad 5.31$$

$$\text{Sandy soil } \begin{cases} W \sim k^{-0.06} \\ Z \sim k^{-0.09} \end{cases} \quad 5.32$$

Considering Equation 5.31, a decrease in  $k$  by an order of magnitude i.e., migrating to fine textured soil yielded a 24 % decrease in  $W$  and a 119 % increase in  $Z$ . Likewise, in Equation 5.32, a decrease in  $k$  by an order of magnitude i.e., migrating to fine textured soils resulted in approximately 15% increase in  $W$  and an approximately 23% increase in  $Z$ .

To assess the sensitivity of the soil wetting geometry with respect to discharge ( $q$ ) the parameters  $V$ ,  $D$ , and  $k$  are held constant and the resultant relationships are outlined by Equations 5.33 and 5.34.

$$\text{Silty clay loam soil } \begin{cases} W \sim q^{-0.06} \\ Z \sim q^{0.34} \end{cases} \quad 5.33$$

$$\text{Sandy soil } \begin{cases} W \sim q^{0.06} \\ Z \sim q^{0.09} \end{cases} \quad 5.34$$

Doubling  $q$  for the silty clay loam soil resulted in a 5 % decrease in  $W$  and a 27 % increase in  $Z$ . Similarly, for the sandy soil when  $q$  was doubled there was a 4 % increase in  $W$  and a 6 % increase in  $Z$ . Table 6 presents a summarized sensitivity evaluation containing hypotheticals and the resultant wetted horizontal and vertical wetted distances. MTI exhibited an increase in both  $W$  and  $Z$  in sandy soil whilst it exhibited an increase in  $Z$  and a decrease in  $W$  for silty clay loam. Regarding the silty clay loam soil, the findings were in contradiction to Schwartzman and Zur (1986) who posited that an increase in  $q$  results in an increase in  $W$  and a decrease in  $Z$  of a Gilat loam soil under sub-surface drip irrigation. The difference in

behaviour is attributed to the porous nature of MTI wherein discharge is not of a point source nature.

Table 5.6 Sensitivity analysis evaluation of  $W$  and  $Z$  to model parameters

Eqn	Adjusting parameters						Wetted Distances			
	$k_o$ (cm.d <sup>-1</sup> )	$\Delta k$ (cm.d <sup>-1</sup> )	$q_o$ (cm <sup>3</sup> .s <sup>-1</sup> )	$\Delta q$ (cm <sup>3</sup> .s <sup>-1</sup> )	$D_o$ (cm)	$\Delta D$ (cm)	$W_o$ (cm)	$\Delta W$ (cm)	$Z_o$ (cm)	$\Delta Z$ (cm)
5.31	100	10	-	-	-	-	1.15	NC	1	1.19
5.32	100	10	-	-	-	-	1	1.15	1	1.23
5.33	-	-	1	2	-	-	1	NC	1	1.27
5.34	-	-	1	2	-	-	1	1.04	1	1.06
5.35	-	-	-	-	20	30	1.10	1.07	0.59	0.90
5.36	-	-	-	-	20	30	1	1.04	1	1.06

\*\* $k_o$  = initial hydraulic conductivity,  $\Delta k$  = order of magnitude incremental hydraulic conductivity  $q_o$  = starting discharge,  $\Delta q$  = incremental discharge,  $D_o$  = initial MTI placement depth,  $\Delta D$  = change in MTI placement depth,  $W_o$  = initial wetted width  $\Delta W$  = change in soil wetted width,  $Z_o$  = initial wetted depth,  $\Delta Z$  = change in soil wetted width, and NC = No significant change.

The sensitivities of  $W$  and  $Z$  to placement depth  $D$  for the respective soils was characterised by Equations 5.35 and 5.36.

$$\text{Silty clay loam } \begin{cases} W \sim D^{-0.06} \\ Z \sim D^{0.34} \end{cases} \quad 5.35$$

$$\text{Sandy soil } \begin{cases} W \sim D^{0.06} \\ Z \sim D^{0.09} \end{cases} \quad 5.36$$

An increase in  $D$  by a unit magnitude (from 0.2 m to 0.3 m) for the silty clay loam soil resulted in approximately 3 % decrease in  $W$  and an approximately 53 % increase in  $Z$ . For the sandy soil a unit increase in  $D$  resulted in a 4% increase in  $W$  and a 6% increase in  $Z$ . According to Bresler (1978)  $W$  increases for low  $k$  values (fine textured soils) and  $Z$  increases by a high magnitude for soils with a high  $k$  value (coarse textured soils).

To gauge the sensitivity of  $W$  and  $Z$  to  $V$ , the parameters  $D$ ,  $q$  and  $k$  were assumed constant. This yielded Equations 5.37 and 5.38.

$$\text{Silty clay loam soil } \begin{cases} V \sim W^{1.79} \\ Z \sim V^{0.16} \end{cases} \quad 5.37$$

$$\text{Sandy soil } \begin{cases} V \sim W^{2.27} \\ Z \sim V^{0.41} \end{cases} \quad 5.38$$

Doubling  $V$  under silty clay loam soil resulted in a 47 % increase in  $W$  and an approximately 12% increase in  $Z$ . For the sandy soil, a doubling  $V$  resulted in a 36 % increase in  $W$  and a 33 % increase in  $Z$ .

In order to obtain simulated wetted distances ( $W$  and  $Z$ ), an estimation of a range of values for  $V$  was made using the sensitivity analysis relationships in Equations 5.37 and 5.38, and the resultant simulated  $Z$  and  $W$  for the semi-permeable porous wall line source 2-D flow model were computed. A correlation test based on the  $R^2$  was carried out on a plot of simulated  $W$  and  $Z$  against observed  $W$  and  $Z$  (Figure 5.4). The correlation coefficients  $R^2 > 0.75$  showed a good agreement between the observed and simulated.

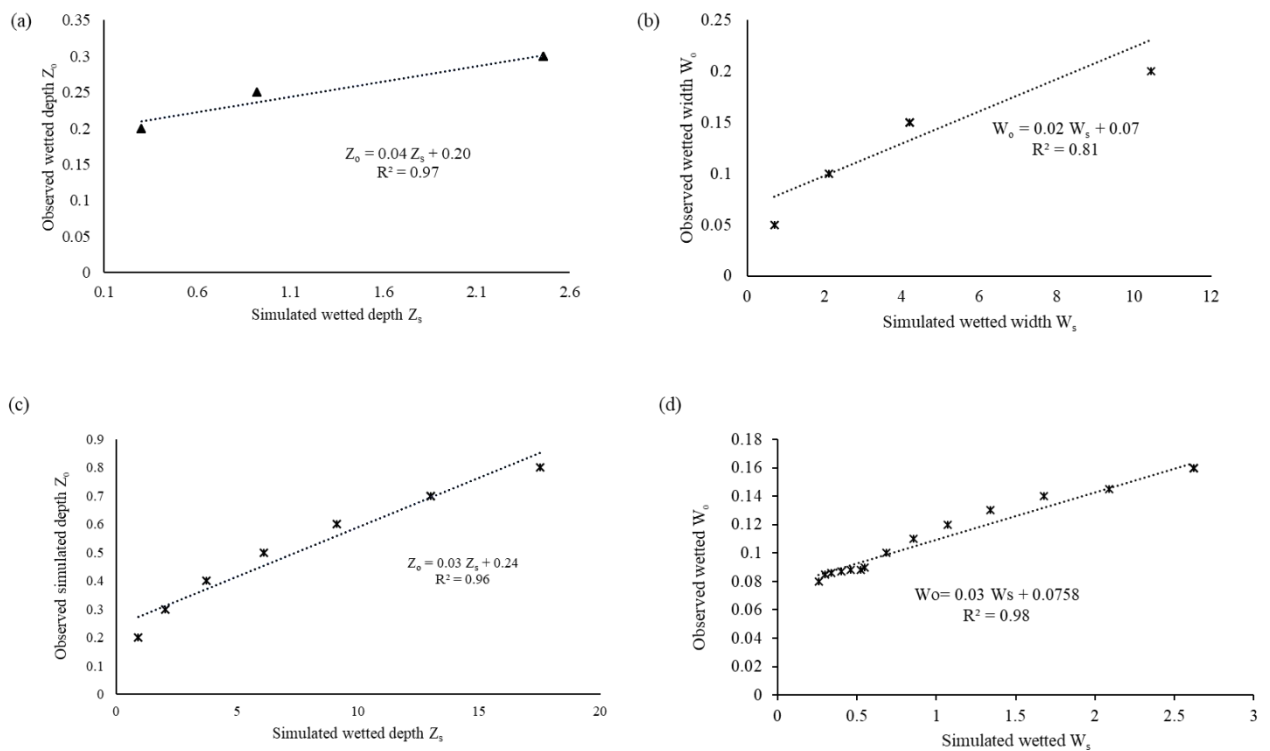


Figure 5.4 Comparison of observed  $W_o$  and  $Z_o$  vs simulated  $W_s$  and  $Z_s$  from estimated  $V$  for silty clay loam (a and b) and sandy soil (c and d).

### 5.5.1 Models' validation

The silty clay loam soil exhibited a wetting pattern on the soil surface, so for that reason the experimental data from the MPS-2 sensor buried at 0.1 m was excluded. The soil surface wetting phenomenon was observed on both phases of the experiment. A similar observation

was made by Kanda et al. (2020) for a MTI tubing buried at a depth of 0.2 m. Fan et al. (2018b) also made a similar observation and posited that shallow buried depth facilitate upward water movement, a phenomenon observed in fine textured soils.

The models evaluation revealed a satisfactory performance, for instance the silty clay loam models' had a  $nRMSE$  of 0.84 % and 8.80 % for  $W$  and  $Z$ , respectively, a  $NSE > 0.5$ , a  $PBIAS < \pm 25$  % and an index of agreement ( $d$ ) of 1 and 0.98 for  $W$  and  $Z$ , respectively (Figures 5.5 and 5.6). The sandy soil exhibited a satisfactory performance as evidence by a  $nRMSE$  of 0.3 % and 2.5 % for  $W$  and  $Z$  respectively, a  $NSE > 0.75$ , a  $PBIAS < \pm 15$  % and an index of agreement ( $d$ ) of 0.6 and 0.3 for  $W$  and  $Z$ , respectively.

The model underestimated the wetted depth ( $Z$ ) for the sandy soil whilst it overestimated the wetted width ( $W$ ). A one-way ANOVA revealed a statistically significant difference ( $p < 0.05$ ) in both the observed and simulated wetted  $W$  and  $Z$  under sandy soil. For the silty clay loam soil there was no statistically significant difference ( $p > 0.05$ ) between observed  $W$  and simulated  $W$ , similarly there was no statistically significant difference ( $p > 0.05$ ) between observed  $Z$  and simulated  $Z$ .

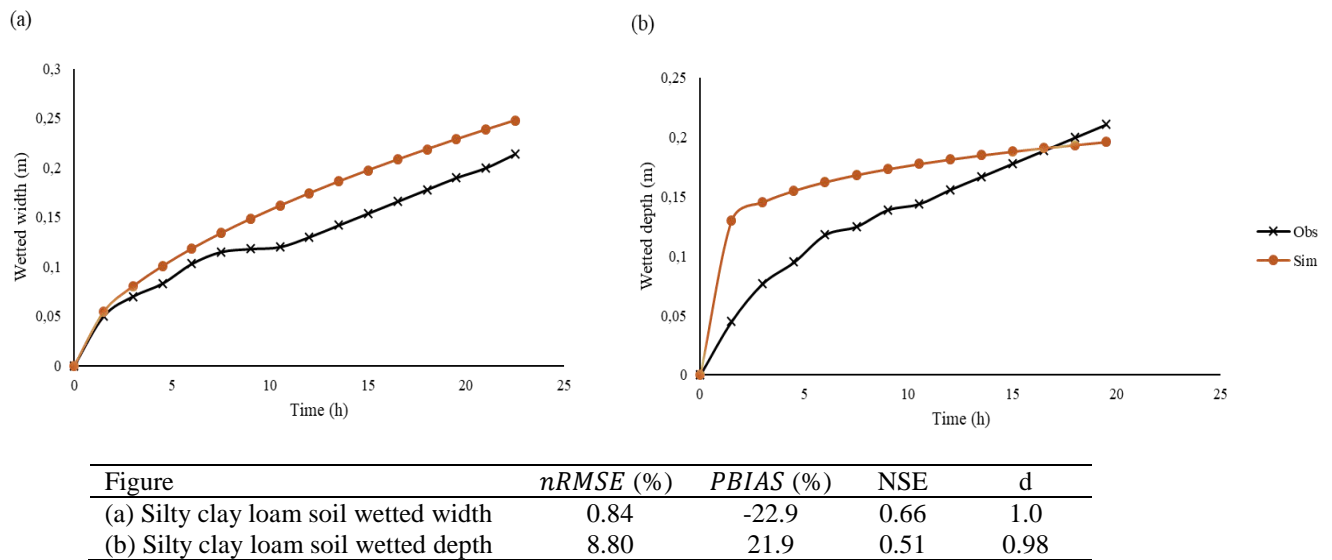


Figure 5.5 Observed vs simulated wetted distances for silty clay loam soil.

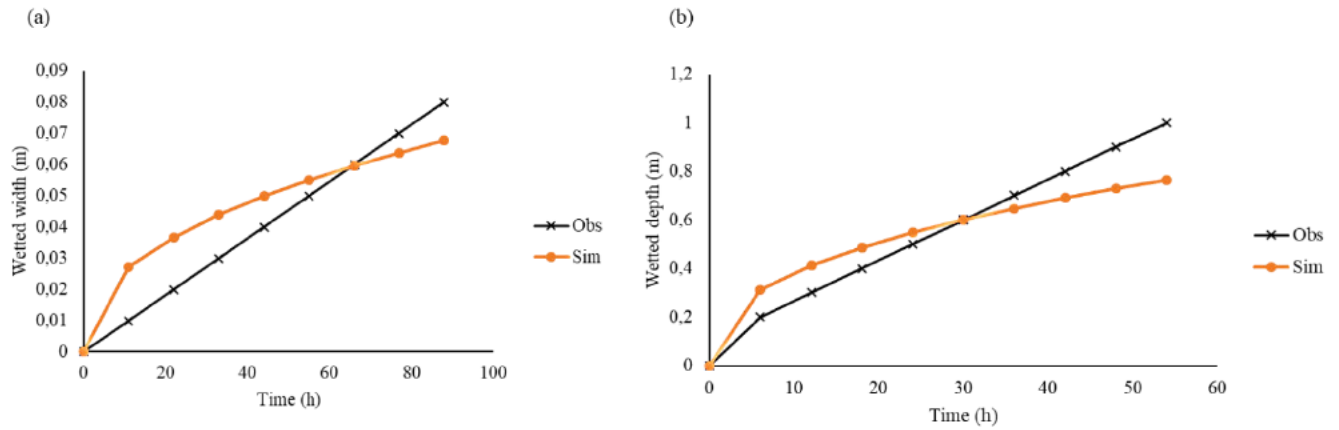


Figure	<i>nRMSE</i> (%)	<i>PBIAS</i> (%)	NSE	d
(a) Sandy soil wetted width	0.3	-12.2	0.82	0.6
(b) Sandy soil wetted depth	2.5	3.9	0.78	0.3

Figure 5.6 Observed vs simulated wetted distances for sandy soil.

Soil texture influenced water movement ( $p < 0.05$ ). The silty clay loam soil recorded pronounced lateral and upward water movement than downward movement (Figure 5.7) whereas the sandy soil exhibited a pronounced vertical movement compared to lateral movement (Figure 5.8). There was a notable difference in wetting patterns between the two soils. The silty clay loam soil exhibited an ellipsoidal shape of the wetting geometry. The observed and simulated wetting depths for the silty clay loam soil were lower than the observed and simulated wetted depths for the sandy soil. The observation can be attributed to a high clay content in the former. The finding concurs with Fan et al. (2018a) who postulated that wetted depth is low in high clay content soils. In addition, a wetting front experiment by Cote et al. (2003) attributed the fine textured soil wetting pattern to dominance of capillarity and matric tension. Saefuddin et al. (2019) observed pronounced radial soil water movement in a silt profile under a multiple outlet ring-shaped emitter.



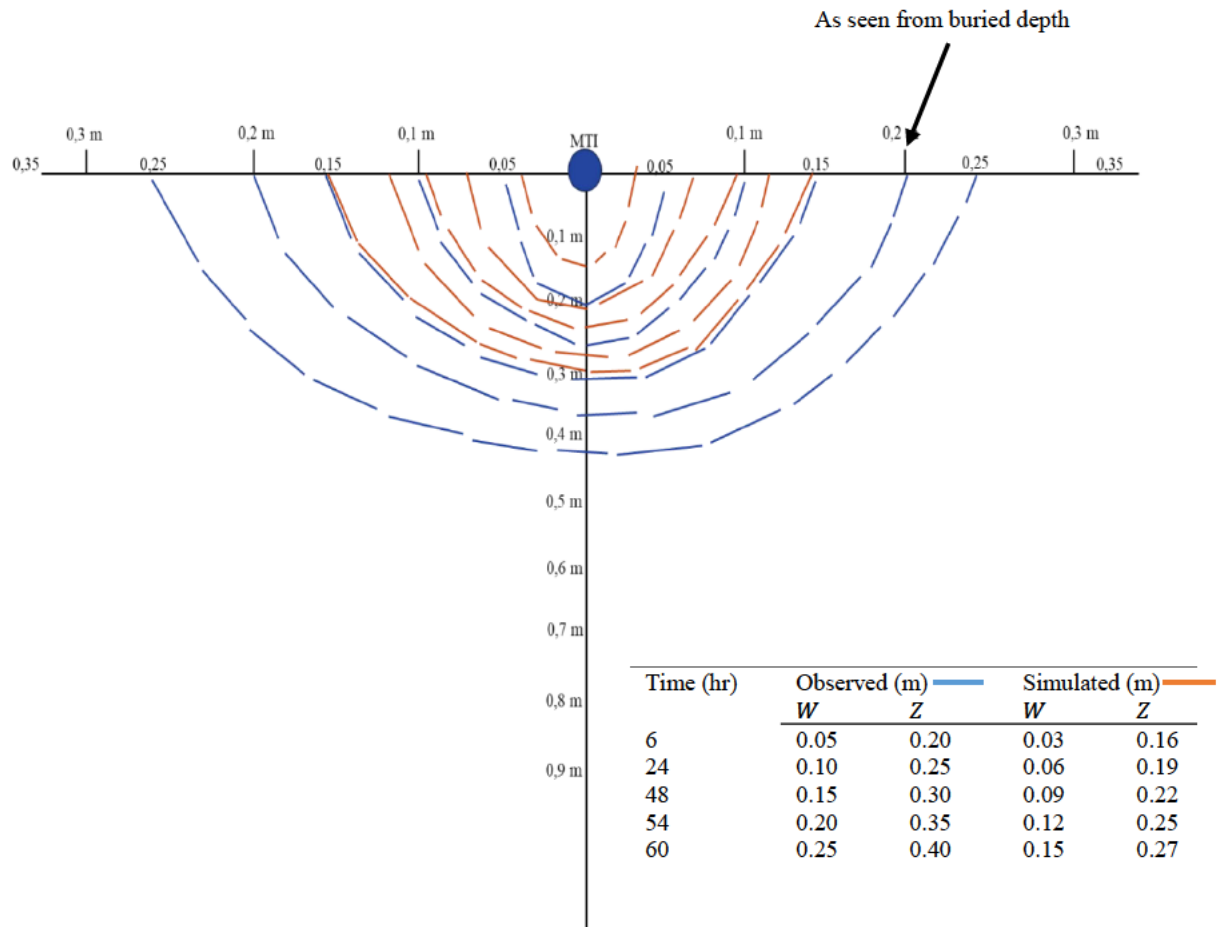


Figure 5.7 Observed and simulated wetting geometries for silty clay loam under MTI as seen from the front view.

Fan et al. (2018a) in their MTI wetting front experiment observed a slow lateral water movement after initial wetting of the silt-loam soil after 48 h, much similar to this study timeline. Granular soils exhibit a high vertical water movement due to the presence of granular pores and dominant gravitational forces (Figure 5.8), thus the sandy soil had a greater wetted depth compared to the silty clay loam soil. The findings concur with a study by Cote et al. (2003) who performed a wetting front experiment with a sandy soil under a trickle source emitter. Ghumman et al. (2018) attributed the high wetted depths in sandy soils to porosity. Although this study used a line source porous pipe, the findings relate due to the soil hydraulic characteristics factor. Another attribute to high Z in sandy soils is the low macroscopic capillary length in sand which favours gravity as compared to lateral or upward movement. Siyal and Skaggs (2009) observed a similar phenomenon in their modelling of a sandy soil using HYDRUS 2D.

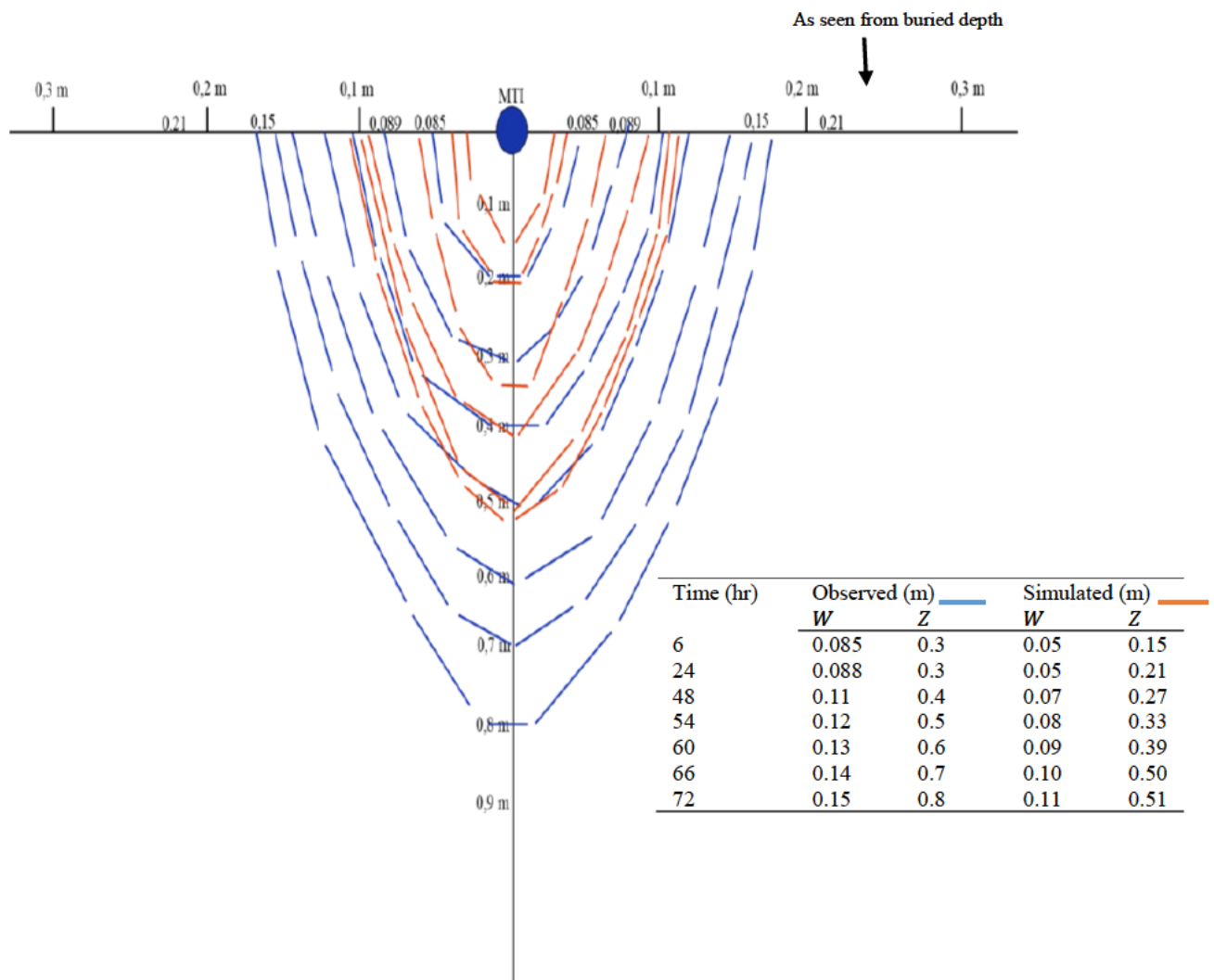


Figure 5.8 Observed and simulated wetting geometries for sandy soil under MTI as seen from the front view.

## 5.6 Irrigation Implication

The developed soil wetting geometry models can be adopted to estimate soil wetting geometries for particular soils in question, thus ensuring optimal placement depth and spacing of MTI laterals. Knowledge on wetting geometries can potentially aid irrigators in adopting optimal lateral placement depth and spacing. Application of the wetting depth models can inform irrigators on irrigation application times thus availing optimal volume to the root-zone thus minimizing deep percolation and soil water loss due to evaporation. For fine textured soil, shallow buried depth avails water to the soil surface that will be lost due to soil evaporation. The lateral waterfront for fine textured soils expanded faster than that of coarse textured soils hence lateral placement under fine texture soils should be strategically placed to promote an

optimal overlap between row crop whereas for coarse texture close lateral placement will be require to create an optimal wetting front overlap.

## 5.7 Limitations

Application of Equations 5.20 – 5.21 and 5.24 – 5.25 may require testing in different geographical locations and assess their universal suitability. The study was carried out for 20 hours under a silty clay loam and 96 hours for the sandy soil. The testing times for silty clay loam were limited by the soil bin's lateral dimension (width). The implication was the influence of border effects on soil water movement if the experimental times went beyond 20 hours. Likewise, for the macroscopic sandy soil the experimental times were limited to 96 hours because of the restrictions imposed by the soil bin's depth. Models' development was also limited to the following constant inputs; placement depth ( $D = 0.2$  m) and discharge ( $q = 2.39$  l.h<sup>-1</sup>.m<sup>-1</sup>). The wetted depth  $Z$  is not entirely an independent variable as factors such as crop specific root water uptake influence the vertical soil-water movement.

## 5.8 Conclusions and Recommendations

The study adopted the Buckingham  $\pi$  theorem or dimensional analysis to develop, calibrate and validate models' that simulate soil wetting geometries for MTI as a function of soil hydraulic conductivity ( $k$ ), placement depth ( $D$ ), emitter discharge ( $q$ ), and soil water content ( $V$ ). Soil texture significantly affected the wetting geometry under MTI. The models satisfactorily simulated the wetting geometries for the two soils (silty clay loam and sandy soil). The *PBIAS* showed the degree of over and under-estimation of the wetted width and depth for the two soils. The *nRMSE* and the *NSE* were satisfactory for the models developed for the two soil types and the results showed that the models' can be used to simulate wetting geometries for a porous wall line source MTI system placed at a depth of 0.2 m. The empirical models satisfactorily estimated the wetting depths and widths of the respective soils.

The study also noted, judging from the wetting pattern of the fine textured soil, there is potential in MTI to provide plants with water with minimized deep percolation loses. The study was done in a soil bin on a bare homogenous soil. The researchers recommend the study be carried under field conditions for both cropped and un-cropped soils and test the suitability of the developed models. Furthermore, the experiment was carried on dry soil, thus an investigation on the soil wetted pattern under an initially moist soil should be carried out and compare the

findings to the current study. Future studies are required to understand the wetting geometries in layered soils.

## 5.9 References

- Ainechee, G, Boroomand-Nasab, S & Behzad, M. 2009. Simulation of soil wetting pattern under point source trickle irrigation. *Journal of Applied Sciences* 9 (6): 1170-1174.
- Amin, M and Ekhmaj, A. 2006. DIPAC-drip irrigation water distribution pattern calculator. *7th International Micro Irrigation Congress*, Kuala Lumpur, Malaysia.
- Besharat, S, Barão, L & Cruz, C. 2020. New strategies to overcome water limitation in cultivated maize: Results from sub-surface irrigation and silicon fertilization. *Journal of Environmental Management* 263: 110398.
- Bouma, J., 1984, August. Using soil morphology to develop measurement methods and simulation techniques for water movement in heavy clay soils. In *Proceedings of the ISSS Symposium on Water and Solute Movement in Heavy Clay Soils* (pp. 298-310). Wageningen: International Institute for Land Reclamation and Improvement. Wageningen, Netherlands.
- Bresler, E. 1975. Two-dimensional Transport of Solutes During Nonsteady Infiltration from a Trickle Source 1. *Soil Science Society of America Journal* 39 (4): 604-613.
- Bresler, E. 1978. Analysis of trickle irrigation with application to design problems. *Irrigation Science* 1 (1): 3-17.
- Cook, FJ, Fitch, P, Thorburn, PJ, Charlesworth, PB and Bristow, KL. 2006. Modelling trickle irrigation: Comparison of analytical and numerical models for estimation of wetting front position with time. *Environmental Modelling Software* 21 (9): 1353-1359.
- Cote, CM, Bristow, KL, Charlesworth, PB, Cook, FJ & Thorburn, PJ. 2003. Analysis of soil wetting and solute transport in subsurface trickle irrigation. *Irrigation Science* 22 (3-4): 143-156.
- Cresswell, H, Green, T & McKenzie, N. 2008. The adequacy of pressure plate apparatus for determining soil water retention. *Soil Science Society of America Journal* 72 (1): 41-49.
- Curtis, W, Logan, JD & Parker, W. 1982. Dimensional analysis and the pi theorem. *American Journal of Physics* 40 (1815): 117-126.
- Dabral, P, Pandey, P, Pandey, A, Singh, K & Singh, MS. 2012. Modelling of wetting pattern under trickle source in sandy soil of Nirjuli, Arunachal Pradesh (India). *Irrigation Science* 30 (4): 287-292.
- Eddey, EE. 1945. *Some Engineering Applications of the Buckingham Pi Theorem*. Ohio State University, College of Engineering Ohio, USA.
- Elmaloglou, S, Soulis, KX and Dercas, N. 2013. Simulation of soil water dynamics under surface drip irrigation from equidistant line sources. *Water Resources Management* 27 (12): 4131-4148.
- Fan, Y-W, Huang, N, Zhang, J & Zhao, T. 2018a. Simulation of Soil Wetting Pattern of Vertical Moistube-Irrigation. *Water* 10 (5): 601-621.
- Fan, Y, Zhao, T, Bai, G & Liu, W. 2018b. HYDRUS-2D simulation of soil wetting pattern with horizontal moistube-irrigation and analysis of its influencing factors. *Transactions of the Chinese Society of Agricultural Engineering* 34 (4): 115-124.
- Fwa, T, Tan, S & Chuai, C. 1998. Permeability measurement of base materials using falling-head test apparatus. *Transportation Research Record* 1615 (1): 94-99.

- Ghumman, AR, Iqbal, M, Ahmed, S & Hashmi, HN. 2018. Experimental and numerical investigations for optimal emitter spacing in drip irrigation. *Irrigation and Drainage* 67 (5): 724-737.
- Kanda, E. 2019. Soil water dynamics and response of cowpea under Moistube irrigation. Unpublished PhD Thesis. Bioresources Engineering, University of KwaZulu-Natal, Pietermaritzburg, South Africa.
- Kanda, EK, Senzanje, A & Mabhaudhi, T. 2020. Soil water dynamics under Moistube irrigation. *Physics and Chemistry of the Earth, Parts A/B/C* 115 (2020): 102836. <https://doi.org/10.1016/j.pce.2020.102836>
- Kandelous, MM & Šimůnek, J. 2010. Numerical simulations of water movement in a subsurface drip irrigation system under field and laboratory conditions using HYDRUS-2D. *Agricultural Water Management* 97 (7): 1070-1076. <https://doi.org/10.1016/j.agwat.2010.02.012>
- Karandish, F & Šimůnek, J. 2019. A comparison of the HYDRUS (2D/3D) and SALTMED models to investigate the influence of various water-saving irrigation strategies on the maize water footprint. *Agricultural Water Management* 213 (2019): 809-820.
- Keller, J & Bliesner, RD. 1990. *Sprinkle and trickle irrigation*. Blackburn Press, Caldwell, New Jersey, USA.
- Klute, A. 1986. *Water retention: laboratory methods*. American Society of Agronomy-Soil Science Society of America, Madison, USA.
- Lamm, FR. 2005. SDI for conserving water in corn production. In: *Impacts of Global Climate Change*. 1-12, Kansas, USA.
- Lamm, FR, O'Brien, DM, Rogers, DH & Dumler, TJ. 2006. Using the K-State center pivot sprinkler and SDI economic comparison spreadsheet. *Proceedings for 2006 Central Plains Irrigation Conference, Colby, Kansas, Feb 21-22*. Kansas, USA.
- Lamm, FR, Trooien, TP, Clark, GA, Stone, LR, Alam, M, Rogers, DH & Schlegel, AJ. 2002. Using beef lagoon wastewater with SDI. *Proc. Irrig. Assoc. Int'l. Irrigation Technical Conf., October*. New Orleans, Louisiana, USA.
- Malamos, N. 2007. Estimation of width and depth of the wetted soil volume under a surface emitter, considering root water-uptake and evaporation. *Water Resources Management* 21 (8): 1325-1340.
- Moncef, H, Hedi, D, Jelloul, B & Mohamed, M. 2002. Approach for predicting the wetting front depth beneath a surface point source: theory and numerical aspect. *Irrigation and Drainage* 51 (4): 347-360.
- Moriasi, DN, Arnold, JG, Van Liew, MW, Bingner, RL, Harmel, RD & Veith, TL. 2007. Model evaluation guidelines for systematic quantification of accuracy in watershed simulations. *Transactions of the ASABE* 50 (3): 885-900.
- Provenzano, G. 2007. Using HYDRUS-2D simulation model to evaluate wetted soil volume in subsurface drip irrigation systems. *Journal of Irrigation and Drainage Engineering* 133 (4): 342-349.
- Ragab, R. 2002. A holistic generic integrated approach for irrigation, crop and field management: the SALTMED model. *Environmental Modelling & Software* 17 (4): 345-361.
- Rawls, WJ, Brakensiek, DL & Saxton, K. 1982. Estimation of soil water properties. *Transactions of the ASAE* 25 (5): 1316-1320.
- Risse, L & Chesness, J. 1989. A simplified design procedure to determine the wetted radius for a trickle emitter. *Transactions of the ASAE* 32 (6): 1909-1914.
- Saefuddin, R, Saito, H & Šimůnek, J. 2019. Experimental and numerical evaluation of a ring-shaped emitter for subsurface irrigation. *Agricultural Water Management* 211: 111-122.

- Saxton, K.E. and Willey, P.H., 2005. The SPAW model for agricultural field and pond hydrologic simulation. *Watershed Models*, pp.400-435.
- Schaap, MG, Leij, FJ & Van Genuchten, MT. 2001. Rosetta: A computer program for estimating soil hydraulic parameters with hierarchical pedotransfer functions. *Journal of Hydrology* 251 (3-4): 163-176.
- Schaap, MG & Van Genuchten, MT. 2006. A modified Mualem–van Genuchten formulation for improved description of the hydraulic conductivity near saturation. *Vadose Zone Journal* 5 (1): 27-34.
- Schwartzman, M & Zur, B. 1986. Emitter spacing and geometry of wetted soil volume. *Journal of Irrigation and Drainage Engineering* 112 (3): 242-253.
- Singh, D, Rajput, T, Sikarwar, H, Sahoo, R & Ahmad, T. 2006. Simulation of soil wetting pattern with subsurface drip irrigation from line source. *Agricultural Water Management* 83 (1-2): 130-134.
- Siyal, A & Skaggs, TH. 2009. Measured and simulated soil wetting patterns under porous clay pipe sub-surface irrigation. *Agricultural Water Management* 96 (6): 893-904.
- Thabet, M & Zayani, K. 2008. Wetting patterns under trickle source in a loamy sand soil of south Tunisia. *American-Eurasian Journal of Agricultural & Environmental Sciences* 3 (01): 38-42.
- Tillotson, PM & Nielsen, DR. 1984. Scale factors in soil science. *Soil Science Society of America Journal* 48 (5): 953-959.
- Van Genuchten, MT. 1980. A closed-form equation for predicting the hydraulic conductivity of unsaturated soils 1. *Soil Science Society of America Journal* 44 (5): 892-898.
- Vogel, T, Van Genuchten, MT & Cislerova, M. 2000. Effect of the shape of the soil hydraulic functions near saturation on variably-saturated flow predictions. *Advances in Water Resources* 24 (2): 133-144.
- Wilkinson, W. 1968. Constant head in situ permeability tests in clay strata. *Geotechnique* 18 (2): 172-194.
- Xue, G and Liu D. 2013. Effects of the tomato growth and water use efficiency in sunlight greenhouse by moistube irrigation. *Water Saving Irrigation*, 25(6) :61 – 66.
- Zhang, M, Niu, W, Lu, Z, Li, Y, Wang, J, and Qui, X. 2017. Effect of moistube-irrigation on crop yield and water use efficiency. *Chinese Journal of Eco-Agriculture*, 25: 1671 – 1683.
- Zhanga, Z.Y., Qi, W. and Wang, C. 2019. Effect of alternate irrigation on water and salt movement under moistube irrigation. 3<sup>rd</sup> World Irrigation Forum (WIF3), 1 - 7 September 2019. Bali, Indonesia.

## 6 TWO DIMENSIONAL MODELLING OF NITRATE TRANSPORT FOR CANOLA (*BRASSICA NAPUS* L.) GROWN UNDER MOISTUBE IRRIGATION USING HYDRUS 2D/3D

This chapter was submitted for review to the Irrigation Science Journal on the 7<sup>th</sup> May 2021.

**Dirwai, TL**, Senzanje, A, Mabhaudhi, T (with editor). Two Dimensional Modelling of Nitrate Transport for Canola (*Brassica Napus* L.) Grown Under Moistube Irrigation Using Hydrus 2D/3D. *Irrigation Science*.

### Abstract

The study sought to demonstrate nitrate distribution in the soil profile and nitrate leaching under MTI. It was hypothesised that MTI emission results in no nitrate leaching. The experiment was conducted in a 20 m by 8 m naturally ventilated greenhouse under three water application regimes, namely, (i) full irrigation at 100%  $ET_c$ , (ii) deficit irrigation (DI) at 75%  $ET_c$ , and (iii) 55%  $ET_c$ . Each irrigation regime had four plots measuring 2 m  $\times$  1 m. Each plot accommodated 18 plants at 90 000 plants.ha<sup>-1</sup>. A 1 m buffer physically and hydrologically separated the plots. Also, a 250-micron plastic sheeting was entrenched in each buffer plot to a depth of 1 m. Twelve neutron probe access tubes for soil moisture measurement were installed in each plot to a depth of 1 m. Fertiliser was applied at a rate of 210 ppm over two split applications. Soil samples for fertility analysis were collected at the emitter and 15 cm from the emitter at depths of 20-, 30-, 40-, and 50-cm before and after 2 h, 4 h, 24 h, 48 h, and 72 h of each fertigation exercise. HYDRUS 2D/3D was used to simulate solute transport under two scenarios: cropped scenario and no cropping scenario under the irrigation regimes. The partial factor productivity of applied N ( $PFP_N$ ) was used as a proxy for nitrogen use efficiency (NUE). The extreme deficit irrigation regime (55%  $ET_c$ ) had a pronounced leaching effect compared to the other two regimes. The yield for the full irrigation (100%  $ET_c$ ) and optimal deficit irrigation (75%  $ET_c$ ) were 1.48 ton.ha<sup>-1</sup> and 1.15 ton.ha<sup>-1</sup> and  $PFP_N$  of 1.72 kg.kg<sup>-1</sup> and 1.29 kg.kg<sup>-1</sup>, respectively. HYDRUS 2D/3D successfully simulated solute movement under full and optimal DI [(100%  $ET_c$ : nRMSE = 0.13, EF = 0.54, PBIAS = -0.22%) (75%  $ET_c$ : nRMSE = 0.24, EF = 0.23, and a PBIAS = -7.41%.)] and performed poorly under extreme DI regime. HYDRUS 2D/3D active root nutrient uptake simulations revealed the readily available

assimilate for plant uptake under full and optimal DI strategies, whilst the extreme DI strategy exhibited increased leaching. It was concluded that fertigation events under optimal deficit MTI could be employed without the farmer incurring yield penalties. It is recommended that the experiment be done under field conditions that include rainfall fluxes and assess the solute movement.

**Keywords:** diffusion, hydrodynamic dispersion, leaching, nitrogen use efficiency,

## 6.1 Introduction

The burgeoning world population requires intensified agriculture to maintain and increase food security. Irrigation and fertilisation are important factors that facilitate intensified crop production (Bar-Yosef, 1999). Fertigation has reported advantages over the conventional broadcasting methods, and these advantages include flexibility in nutrient application, minimal fluctuations under fertigation systems to ensure uniform nutrient application. Precise application using micro-irrigation technology avoids excesses in the application and targets points where there is high root density (Bar-Yosef, 1999). Irrigation and fertilisation are intrinsically linked. Thus, improved irrigation technology promotes efficient liquid nutrient application. Gärdenäs et al. (2005) posited that micro-irrigation systems such as drip emitters, drip tape and micro-sprinklers could potentially apply water and nutrients with precision, thus promoting uniformity.

Vadose zone contamination due to nitrates poses a threat to groundwater sources. This requires fertigation technologies that minimise nitrate leaching. Literature has revealed that drip fertigation significantly reduces nitrogen (N) leaching by 90% compared to conventional flood irrigation (Lv et al., 2019). Some studies by Clothier and Sauer (1988) and Mmolawa and Or (2000a) have investigated fertiliser distribution around a dripline, whilst Hanson et al. (2006) modelled fertiliser distribution under surface drip, and subsurface drip tape and Ajdary et al. (2007) investigated nitrogen leaching from an onion field under drip fertigation.

Sun et al. (2019) performed a soil bin experiment to investigate the infiltration capacity of fertilizer solution in mixing waste biomass and the distribution characteristics of water-fertilizer in wetted soil under MTI fertigation and revealed that (i) the soil-biomass mixture improved infiltration rate, and (ii) the functional relationship between the cumulative



infiltration of fertilizer solution and infiltration time followed the Kostiakov infiltration model. Another study by Liu et al. (2017) investigated MTI water salinity distribution under different soils and different pressure heads. Although numerous irrigation technologies have been used for fertigation, there exists a gap in data on fertigated industrial crop production such as canola using MTI under field conditions.

Understanding nitrate movement in the vadose zone facilitates controlled fertiliser application and groundwater remediation. Anthropogenic activities such as industrialisation and intensified crop production have promoted N's excessive and perpetual input into the soil, consequently promoting groundwater contamination (Xin et al., 2019). Modelling tools such as HYDRUS 2D/3D have been used and adapted to develop irrigation and fertigation support tools for farmers (Šimůnek et al., 1999; Gärdenäs et al., 2005; Hanson et al., 2006). Modelling tools are time-saving and break down the complex dynamics of water and nutrient uptake and movement in the vadose zone (Hanson et al., 2006).

MTI is a relatively new semi-permeable membrane (SPM) irrigation technology. Hence, this study's objective was to demonstrate the nitrate distribution in the soil profile and nitrate leaching under MTI. Furthermore, there exist few soil guidelines for designing and managing fertigation under MTI. The study applied HYDRUS 2D/3D to model solute movement in the soil profile. The study was based on the hypothesis that MTI emission results in no nitrate leaching.

## **6.2 Materials and Methods**

### *6.2.1 Model description*

HYDRUS-2D was used to model the solute movement in the variably saturated soil profile zone. HYDRUS-2D robustness facilitates the simultaneous modelling of multiple independent solutes or nitrogen species whose solutes go through first-order degradation reactions (Hanson et al., 2006). Coupled water flow and solute transport equations were applied. Richards equation (Equation 6.1) was used to compute the spatially distributed soil moisture and the subsequent volumetric fluxes. For this study, we adopted the  $x$  (lateral)-  $z$  (vertical) spatial directions.

$$\frac{\partial \theta(h)}{\partial t} = \frac{\partial}{\partial x_i} \left[ K_{ij}(h) \frac{\partial h}{\partial x_j} + K_{iz}(h) \right] - S(h) \quad 6.1$$

Where:  $\theta$  = volumetric water content [ $L^3.L^{-3}$ ],  $h$  = pressure head [L],  $S$  = sink term [ $L^3.L^{-3}.T^{-1}$ ] representing root water uptake as a function of spatial position and time,  $x_i$  = spatial coordinates [L],  $t$  = time [T], and  $K_{ij}$  and  $K_{iz}$  = components of the hydraulic conductivity tensor [ $L.T^{-1}$ ]. The root water uptake was determined by the Vrugt model (Vrugt et al., 2001). Chemical transport of solutes in a variably saturated zone is governed by the linear partial differential Equations 6.2 and 6.3.

$$\frac{\partial \theta c_1}{\partial t} + \rho \frac{\partial s_1}{\partial t} = \frac{\partial}{\partial x_i} \left( \theta D_{ij,1} \frac{\partial c_1}{\partial x_j} \right) - \frac{\partial q_i c_1}{\partial x_i} - \mu_{w,1} \theta c_1 - \mu_{s,1} \rho s_1 - S C_{r,1} \quad 6.2$$

$$\frac{\partial \theta c_k}{\partial t} + \rho \frac{\partial s_k}{\partial t} = \frac{\partial}{\partial x_i} \left( \theta D_{ij,k} \frac{\partial c_k}{\partial x_j} \right) - \frac{\partial q_i c_k}{\partial x_i} - \mu_{w,1} \theta c_k - \mu_{s,k} \rho s_k + \mu_{w,k-1} \theta c_{k-1} + \mu_{s,k-1} \rho s_{k-1} - S C_{r,k} \quad 6.3$$

$$S_k = K_{d,k} C_k \quad 6.4$$

Where:  $c_i$  and  $s_i$  = solute concentrations in the liquid [ $M.L^{-3}$ ] and solid [ $M.M^{-1}$ ] phase respectively,  $q_i$  =  $i$ th component of volumetric flux density [ $L.T^{-1}$ ],  $\mu_w$  and  $\mu_s$  = first order rate constants for solutes in the liquid and solid phase [ $T^{-1}$ ] respectively,  $\rho$  = soil bulk density [ $M.L^{-3}$ ],  $S$  = sink term [ $L^3.L^{-3}.T^{-1}$ ] in the water flow equation,  $C_r$  = concentration of the sink term [ $M.L^{-3}$ ],  $D_{ij}$  = dispersion coefficient tensor [ $L^2.T^{-1}$ ] for the liquid phase,  $k$  =  $k$ th chain number,  $n_s$  = number of solutes involved in the reaction,  $K_{d,k}$  = distribution coefficient of species  $k$  [ $L^3.M^{-1}$ ], and  $c_k$  and  $s_k$  = adsorption isotherms.

## 6.3 Experimental Design

### 6.3.1 Study site and soil hydraulic properties

The experiment was conducted at the Ukulinga Research Farm at the University of KwaZulu-Natal in Pietermaritzburg, South Africa (29°39'44.8"S 30°24'18.2"E, 636 m a.s.l.). The site had a predominantly silty clay loam soil (39 % clay, 44% silt, 17% sand). The soil was sampled at depths of 10-, 20-, 30-, 40-, and 50 cm. The maximum selected depth was informed by literature (Gan et al., 2011; Cutforth et al., 2013; Luce et al., 2016). A study by Kanda et al. (2020c) at

the Ukulinga Research Farm sampled to a similar depth because of an impermeable layer at a depth of 60 cm. The soil hydraulic characteristics are shown in Table 6.1.

Table 6.1 Soil textural and soil hydraulic parameters

Depth (cm)	Textural class	$\theta_r(cm^3.cm^{-3})$	$\theta_s(cm^3.cm^{-3})$	$n$	$k_s(cm.h^{-1})$	$m$	BD (g.cm <sup>-3</sup> )
10	Silty clay	0.33	0.52	1.35	0.21	0.26	1.28
20	Silty clay	0.28	0.52	1.64	0.40	0.39	1.27
30	Silty clay	0.33	0.55	1.35	0.57	0.26	1.19
40	Silty clay	0.27	0.60	1.11	1.59	0.10	1.07
50	Silty clay	0.32	0.56	1.18	0.78	0.15	1.16

\*BD = Bulk density,  $n$  and  $m$  = shape factors for the soil water retention curve, where  $m = 1 - n^{-1}$

Saturated hydraulic conductivity was determined by the constant head permeability apparatus (Wilkinson, 1968; Fwa et al., 1998), whilst other hydraulic parameters ( $\theta_r$ ,  $\theta_s$ ,  $n$ ,  $k_s$  and  $\alpha$ ) were determined using the soil-water retention pressure method (Klute, 1986; Cresswell et al., 2008; Kanda et al., 2020b). The methods were selected based on the reliability of results and also equipment availability. The soil hydraulic properties closely concurred with those of Rawls et al. (1982) and Vogel et al. (2000) for silty clay soils.

### 6.3.2 Field experiment

The study was a one-factor experiment: with three water application treatments. The canola was irrigated at 100% ET<sub>c</sub>, 75% ET<sub>c</sub>, and 55% ET<sub>c</sub>. Each water treatment consisted of four plots measuring 2 m × 1 m. Each plot was hydrologically separated from another by a 1 m buffer wherein 250-microns thick plastic film buried vertically to a depth of 1.0 m. The plot separation ensured the creation of irrigation management specific zones (IMSZ). For each water application treatment, one plot was dedicated for destructive sampling. The study applied a mix of two fertilisers, namely CALMAG N and new generation coastal blend fertiliser obtained from GROMOR fertilisers in Cato Ridge South Africa (29°42'53.7"S 30°28'33.3"E). The nutrient composition of each fertiliser is summarised in Table 6.2.

Table 6.2 Nutrient composition of the applied fertilisers

Nutrient	Fertiliser	
	CALMAG g.kg <sup>-1</sup>	Coastal blend g.kg <sup>-1</sup>
N	148	68
P	-	52
K	-	245
Ca	177	-
Mg	14	14
Fe	700	0.689
S	-	79
Mn	0.161	0.229
Zn	0.141	0.273
Cu	0.0175	0.014
B	0.21	0.442
Mo	0.028	0.091

The fertilisers were mixed in 1000 litres of solution to obtain: N 210 ppm, P 44 ppm, K 245 ppm, Ca 117 ppm, Mg 28 ppm, S 79 ppm, Fe 1.39 ppm, Mn 0.46 ppm, Zn 0.41 ppm, Cu 0.03 ppm, B 0.65 ppm, and Mo 0.12 ppm. Recommended canola fertilisation rates range from 90 kg N ha<sup>-1</sup> to 150 kg N ha<sup>-1</sup> applied over three split applications (Coetzee, 2017). The dilute fertiliser was applied continuously for one hour at a rate of 0.2 L.min<sup>-1</sup>. Thus, each fertigation exercise applied 12 litres of fertiliser solution per hour per lateral, which amounted to 36 litres of fertiliser solution per plot.

#### 6.4 Data Collection

Soil samples were collected from various depths 10-, 20-, 30-, 40-, and 50 cm, 15 – 30 cm at the emitter and vertical planes 15 cm away from the MTI. The observed data represented the spatial and temporal solute movement during the growing season under MTI. The soil samples were air-dried and analysed using the Leco Carbon/Nitrogen/Sulphur analyser (Leco TRUMAC CNS Model No: 630-300-400, Serial No: 4093, St Joseph, Michigan, USA). The tube auger was used to collect soil samples after 2-, 4-, 24-, 48- and 72 h of fertigation. Above ground plant samples were also collected, oven-dried and analysed for N. Upon destructive sampling for biomass analysis, the canola stalk, leaves and the seed were dried at 30°C and ground to pass through a 1 mm sieve. Total N concentration was determined by dry combustion using the MICRO cube equipment (Elementer Americas).

## 6.5 Modelling Domain and Nitrogen Reactions

MTI is a porous line source irrigation method; thus, the modelling domain assumed a rectangular geometry (Hanson et al., 2006) (Figure 6.1). Since the fertigation occurred under active plant uptake, the modelling domain consisted of the area occupied by roots. The effective maximum root zone depth for canola was 1.0 m (FAO, 2002). The transport domain consisted of 33 cm by 100 cm with the MTI lateral buried at a depth of 20 cm. The 33 cm by 100 cm was selected as the space occupied by the fertigating MTI lateral within a single plot consisting of 3 evenly spaced laterals. The transport domain (finite element (FE) mesh) was discretized into 5000 nodes on the boundary curve and 200 000 FE-mesh nodes with finer grid around the Moistube lateral and coarser grid in the remaining surface. The default smoothing factor of 1.3 was adopted.

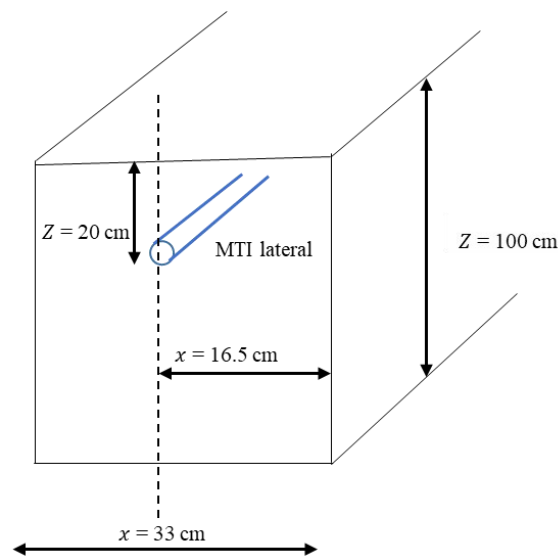


Figure 6.1 Modelling domains for MTI lateral

## 6.6 Model Calibration

The model was calibrated by adjusting the initial soil hydraulic properties (Table 6.1) and dispersivity values until the model closely matched the observed values (Kanda et al., 2020a). The dataset from the second fertigation exercise was used for model validation.

### 6.6.1 Parameter values

Since the fertiliser contained ammonium and nitrate, Equations 6.2 and 6.3 were considered for simulating nitrogen species. The nitrate were assumed to be available in the dissolved phase; hence distribution coefficient ( $K_d$ ) was assigned a value of  $0 \text{ cm}^3.\text{g}^{-1}$ , and ammonium was assumed to adsorb to the solid phase using an  $K_d$  of  $3.5 \text{ cm}^3.\text{g}^{-1}$ . The other parameter values are summarised in Table 6.3 below.

Table 6.3 Summarised model parameter values

Parameter	Values	Reference
Distribution coefficient ( $K_d$ )	$0 \text{ cm}^3.\text{g}^{-1}$	Lotse et al. (1992)
$\mu_w$	$0.38 \text{ day}^{-1}$	Ling and El-Kadi (1998) and Hanson et al. (2006)
Simulation of nitrification from the ammonium to nitrate	$0.2 \text{ day}^{-1}$	Hanson et al. (2006) and Jansson and Karlberg (2011)

The volatilization of ammonium and its gaseous diffusion was neglected for ease of modelling because the solutes were applied in full and variably saturated medium (underground). Thus, the study adopted the hydrodynamic solute dispersion phenomenon. Table 6.4 presents a summary of other parameter values. Longitudinal and transverse dispersivity values were initially set to 0.5 m and 0.1 m, respectively.

Table 6.4 Irrigation information and model parameters

	100% ET <sub>c</sub>	75% ET <sub>c</sub>	55% ET <sub>c</sub>
<b>Irrigation</b>			
Operating pressure (bars)	1	1	1
Discharge rate , $Q$ , (L.h <sup>-1</sup> .m <sup>-1</sup> )	1.82	1.82	1.82
Irrigation interval, $I_{int}$ (days)	continuous	See Table 6 in Appendix C	
Depth of emitter, $d$ (cm)	20	20	20
Emitter spacing, $w$ (cm)	33	33	33
<b>Water Demand</b>			
ET <sub>o</sub> (mm.day <sup>-1</sup> )	9.6	9.6	9.6
<sup>a</sup> Crop coefficient K <sub>c</sub>	0.98	0.98	0.98
<b>Simulated Domain</b>			
Width, $x$ (cm)	33	33	33
Depthz (cm)	100	100	100
<b><sup>b</sup>Solute transport parameters</b>			
Longitudinal dispersivity ( $\lambda_L$ ) (cm)	575	150	1000
Transverse dispersivity ( $\lambda_T$ ) (cm)	0.2	0.2	0.2
<b>Root water uptake</b>			
Critical water pressure in Feddes model	-10, -25, -200, -800, -8000 cm		
<b>Root zone</b>			
Root distribution model	Vrugt model (Vrugt et al., 2001)		
Maximum rooting depth $z$ (cm)	18	21	35
Depth with max root density, $z^*$ (cm)	15	10	25
Max rooting radius, $l_{max}$ (cm)	4	5.5	8
Empirical parameters, $p_z$ and $p_t$	1.0, 1.0	1.0, 1.0	1.0, 1.0

<sup>a</sup>K<sub>c</sub> values adopted were peak values when the canola crop was at the vegetative stage.

<sup>b</sup>Solute parameter  $\lambda_L$  was continuously fine-tuned until the simulated results matched the observed. The range of fine-tuning was done at a scale factor of 8800 (Schulze-Makuch, 2005), which gave the resultant  $\lambda_L$  range of 1000 – 10000 cm (Chakraborty and Das, 2018).

### 6.6.2 Initial and boundary conditions

The canola was first transplanted and irrigated for a continuous 30 days to prevent transplant shock and provide a pseudo-equilibrium condition. The first fertigation exercise took place after day 30 of irrigation which coincided with the tail end of the crop's vegetative stage. Initial NPK soil level measures were documented and adopted as the initial solute conditions. The variable flux boundary condition ( $q$ ) was placed at 20 cm, where the MTI lateral was buried. The  $q$  was defined by Equation 6.5 (Skaggs et al., 2004; Elashbah et al., 2019; Kanda et al., 2020a).

$$q = \frac{Q}{A} = \frac{1.5L.h^{-1}.m^{-1}}{0.1043m^2.m^{-1}length} = 14.38 \text{ cm.h}^{-1} \quad 6.5$$

Where  $q$  = variable flux,  $Q$  = MTI nominal discharge at 1 bar, and  $A$  = surface area.

All boundaries were considered to be no flow except for the bottom boundary of the soil profile and the boundary representing MTI lateral, which was considered a free drainage boundary (Figure 2). For purposes of generating the FE-mesh, the free drainage boundary was placed at  $z = 100$  cm. However, the observation nodes on the generated FE-mesh were scattered to a depth of 60 cm, thus rendering the drainage effect zero. During non-fertigation periods, the flux was kept at zero. Root distribution was assumed to follow the Vrugt model (Vrugt et al., 2001), and the root water uptake was also assumed to follow Feddes' model (Feddes, 1982).

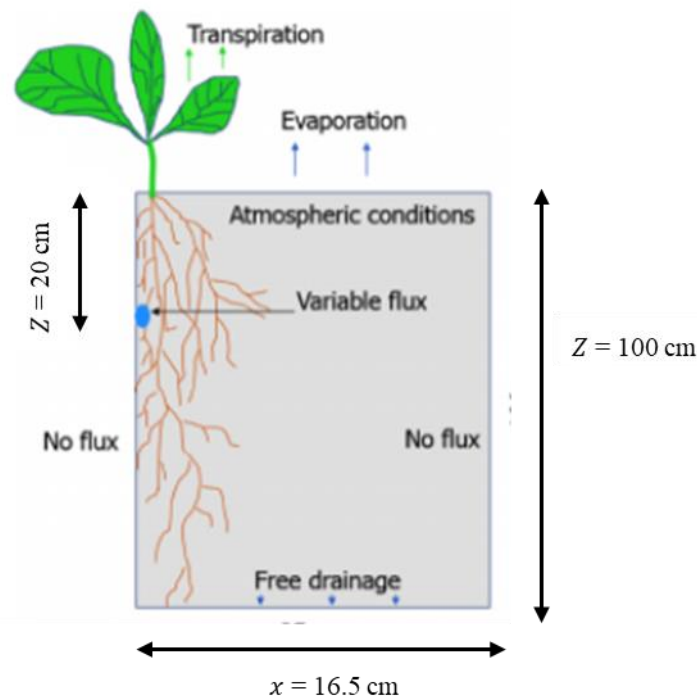


Figure 6.2 Boundary conditions adopted from Kanda et al. (2020a)

## 6.7 Nitrogen Use Efficiency

The partial factor productivity of applied N ( $PFP_N$ ) was used as a proxy for nitrogen use efficiency (NUE). The  $PFP_N$  was computed using Equation 6.6 (Dobermann, 2005).



$$PFP_N = \frac{Y_N}{F_N + S_i} \quad 6.6$$

Where:  $Y_N$  = crop yield with applied N ( $\text{kg} \cdot \text{ha}^{-1}$ ),  $F_N$  = amount of (fertilizer) N applied ( $\text{kg} \cdot \text{ha}^{-1}$ ), and  $S_i$  = average initial nitrogen concentration ( $\text{kg} \cdot \text{ha}^{-1}$ ) in the soil profile (0 – 60 cm).

The  $S_i$  for the 100%  $ET_c$ , 75%  $ET_c$ , and 55%  $ET_c$  plots were  $390.43 \text{ kg} \cdot \text{ha}^{-1}$ ,  $418.66 \text{ kg} \cdot \text{ha}^{-1}$ , and  $432.77 \text{ kg} \cdot \text{ha}^{-1}$ .

## 6.8 Model Validation

HYDRUS 2D/3D is a physical-based model (Simunek et al., 2012). The validation process was done over a split sampling approach whereby the dataset for the second fertigation exercise for each irrigation regime was used to assess the model's performance. The validation process maintained the “conservative” values (longitudinal dispersivity and soil hydraulic properties). The conservative and non-conservative parameters applied during model validation are summarised in Table 6.5.

Table 6.5 Summarised conservative and non-conservative parameters for model validation

	Irrigation regime		
	100% $ET_c$	75% $ET_c$	55% $ET_c$
<b><sup>a</sup>Conservative</b>			
$n$		1.11 – 1.64	
$m$		0.10 – 0.39	
$l$	0.05	0.05	0.05
$k_s (\text{cm} \cdot \text{h}^{-1})$		0.21 – 1.59	
$\lambda_L (\text{cm})$	575	150	1000
Bulk density ( $\text{g} \cdot \text{cm}^{-3}$ )		1.07 – 1.28	
<b>Non-conservative</b>			
% N concentration	0.19 – 0.28	0.13 – 0.28	0.18 – 0.28

<sup>a</sup> Values given in ranges are summarised in Table 6.1

## 6.9 Statistical Analyses and Model Evaluation

For the field experiment data, a normality test was undertaken on the yield and biomass data for each respective irrigation regimes using the Shapiro-Wilk normality test followed by a one-way ANOVA test. All statistical analyses were done using R Studio© (R-Core-Team, 2017). Model evaluation was done using the following criteria: normalised root mean square error (*nRMSE*), Model Efficiency (*EF*), and percentage bias (*PBIAS*). The selected criteria are presented in Equations 6.7 – 6.9. The performance evaluation statistics were selected based on robustness (Moriassi et al., 2007).

$$nRMSE = \frac{\sqrt{\left(\frac{1}{x} \sum_{i=1}^x (O_i - P_i)^2\right)}}{O_{mean}} \quad 6.7$$

$$EF = 1 - \left[ \frac{\sum_{i=1}^x (O_i - P_i)^2}{\sum_{i=1}^x (O_i - O_{mean})^2} \right] \quad 6.8$$

$$PBIAS = \frac{\sum_{i=1}^x (O_i - P_i) * 100}{\sum_{i=1}^x O_i} \quad 6.9$$

Where  $O_i$  and  $P_i$  = observed and predicted value(s), respectively,  $\bar{O}_i$  = mean observed data, and  $x$  = number of observations. *nRMSE* defined the simulation model's accuracy, whilst the *EF* statistic measured the residual variance vs the measured data variance. The statistic (*EF*) ranges from  $-\infty$  to 1 (Moriassi et al., 2007), however, Yang et al. (2014) asserted there exists a positive and scattered correlation between *EF* and the index of agreement thus when estimating soil water content, a satisfactory agreement can be considered when  $EF \geq -1$ . *PBIAS* measured the tendency of the simulated data to either under-estimate or overestimate the observed values. Table 6.6 summarises the general performance rating for the selected evaluation criteria.

Table 6.6 General performance rating for model evaluation statistics (Moriassi et al., 2007)

Performance rating	EF	<i>PBIAS</i> (%)
Very good	$0.75 < EF < 1.00$	$PBIAS < \pm 15$
Good	$0.65 < EF < 0.75$	$\pm 15 < PBIAS < \pm 30$
Satisfactory	$0.50 < EF < 0.65$	$\pm 30 < PBIAS < \pm 55$
Unsatisfactory	$EF \leq 0.50$	$PBIAS \geq \pm 15$

## 6.10 Results and Discussion

### 6.10.1 Effects of different irrigation regimes on solute mobility under canola crop

Under the full irrigation regime (100%  $ET_c$ ), maximum solute movement occurred at  $t = 2$  h. The depth ( $D$ ) vs solute movement curves followed a similar trajectory under the respective times, as exhibited by Figures 6.3 (a) and (b). There, however, was a significant variation in N concentration at  $t = 24$  h and  $t = 72$  h at  $D = 40$  cm and 50 cm, respectively ( $p < 0.05$ ). The respective  $NH_4^+ - N, NO_3^- - N$  concentrations were  $0.05 \text{ g.kg}^{-1}$  and  $0.10 \text{ g.kg}^{-1}$ . Maximum  $NH_4^+ - N, NO_3^- - N$  accumulation (approx.  $0.13 \text{ g.kg}^{-1}$ ) was uniform at  $D = 20$  cm both at the emitter ( $E$ ) and away from the emitter ( $Ae$ ) localities. This could be potentially attributed to the MTI lateral placement depth of 20 cm that influenced solute accumulation at the near placement depth.

Under the optimal deficit irrigation (DI) regime (75%  $ET_c$ ), maximum  $NH_4^+ - N, NO_3^- - N$  concentration ( $0.17 \text{ g.kg}^{-1}$ ) was at  $D = 30$  cm after  $t = 24$  h (Figure 6.3c). Under 55%  $ET_c$ , the solute movement curves at  $E$  and  $Ae$  followed a similar trajectory. Maximum  $NH_4^+ - N, NO_3^- - N$  accumulation was at  $D = 30$  cm for all irrigation regimes at localities  $E$  and  $Ae$ , albeit at different times. This implied that full irrigation (100%  $ET_c$ ) and the optimal irrigation (75%  $ET_c$ ) had no significant effect on solute movement both at  $E$  and  $Ae$  in the variably saturated zones ( $p > 0.05$ ).

Under 100%  $ET_c$ , peak  $NH_4^+ - N, NO_3^- - N$  accumulation at the  $E$  scenario occurred at  $t = 55$  h (approx.) at  $D = 30$  cm (Figure 6.4a) whereas under the  $Ae$  locality, peak accumulation occurred at  $t = 20$  h at  $D = 20$  cm and it plateaued at  $NH_4^+ - N, NO_3^- - N$  -concentration of  $0.12 - 0.13 \text{ g.kg}^{-1}$  (Figure 6.4b). There was no significant difference between the concentrations at the respective depth ( $p > 0.05$ ). This observation can be attributed to the soil characteristics. However, fine-textured soils exhibit lateral movement (Fan et al., 2018), the soil in question did not have pronounced lateral movement than the vertical movement. Active root nutrient uptake (RNU) could have also potentially influenced the lag in peak concentration at the  $E$  locality compared to  $Ae$ . Mmolawa and Or (2000b) noted a solute concentration decline under a cropped field compared to an uncropped one under drip irrigation.

For the three irrigation regimes, the solute infiltration rate was high at the initial phase ( $t = 1$  h to approx.  $t = 2.5$  h) at both locations ( $E$  and  $Ae$ ). This could be attributed to the availability of micro and macro pores that could accommodate solutes during the initial phases of fertigation. The availability of pore space in fully irrigated plots was potentially made possible by gravity-assisted drainage. There was a significant difference ( $p < 0.05$ ) in concentration at various depths under the 100%  $ET_c$  regime between localities  $E$  and  $Ae$ . The highest concentration levels were recorded at  $D = 30$  cm and 20 cm respectively at  $E$  and  $Ae$  during  $t = 50$  h (approx.) (see Figures 4a and 4b). Gravity assisted solute movement was experienced at  $E$ ; thus, a high  $NH_4^+ - N, NO_3^- - N$  concentration at  $D = 30$  cm, whereas the effect of lateral buried depth acted on the high  $NH_4^+ - N, NO_3^- - N$  concentrations at location  $Ae$ ,  $D = 20$  cm.

Under the 75%  $ET_c$  DI at the  $E$  locality, peak  $NH_4^+ - N, NO_3^- - N$  accumulation at  $D = 30$  cm occurred at  $t = 25$  h (Figure 6.4c), which was half the time it took for the 100%  $ET_c$  irrigation regime to reach peak salt accumulation at the same depth. Similarly, under the 55%  $ET_c$  irrigation regime, peak salt accumulation occurred at  $t = 25$  h and  $D = 20$  cm. The phenomenon revealed how DI potentially aided the imbibition of the nitrate solutes, thus promoting mobility. Partially dry soils imbibe solutes as compared to their saturated counterparts (Youngs and Leeds-Harrison, 1990).

Under the extreme DI regime (55%  $ET_c$ ) , nitrate concentration levels were uniform and  $D = 30$  cm and  $D = 40$  cm at  $t = 72$  h (Figure 6.4f). Nitrate mobility was not as pronounced because of imbibing water's unavailability – due to preferential vertical flow - to transport the solutes. Interestingly, the extreme DI regime had a high  $NH_4^+ - N, NO_3^- - N$  concentration accumulation at  $D = 40$  cm and 50 cm,  $t = 50$  h and at locality  $E$  where-as, at locality  $Ae$  the high concentration was recorded at  $t = 55$  h (Figures 4e and 4f), one would argue that preferential flow was dominant in the extreme DI regime resulting in a favoured vertical movement as compared to lateral. Merdun et al. (2008) argued that there is a preferential flow for a relatively dry soil favouring vertical solute movement compared to lateral movement.

Peak  $NH_4^+ - N, NO_3^- - N$  concentrations were observed in the depth range of  $D = 20$  cm and  $D = 30$  cm at time range of 20 h to 30 h (approx.) at both localities ( $E$  and  $Ae$ ) under the full irrigation regime ( $p > 0.05$ ,  $CV > 15\%$ ) and optimal irrigation regimes ( $p > 0.05$ ,  $CV > 15\%$ ). For both irrigation regimes, the concentration plateaued for  $t = 20$  h. This prolonged resident

time presented an opportunity for active nutrient utilisation by the canola. Thus, fertigation using MTI at optimal DI conditions (75%  $ET_c$ ) minimises nutrient leaching and promotes crop beneficial nutrient uptake.

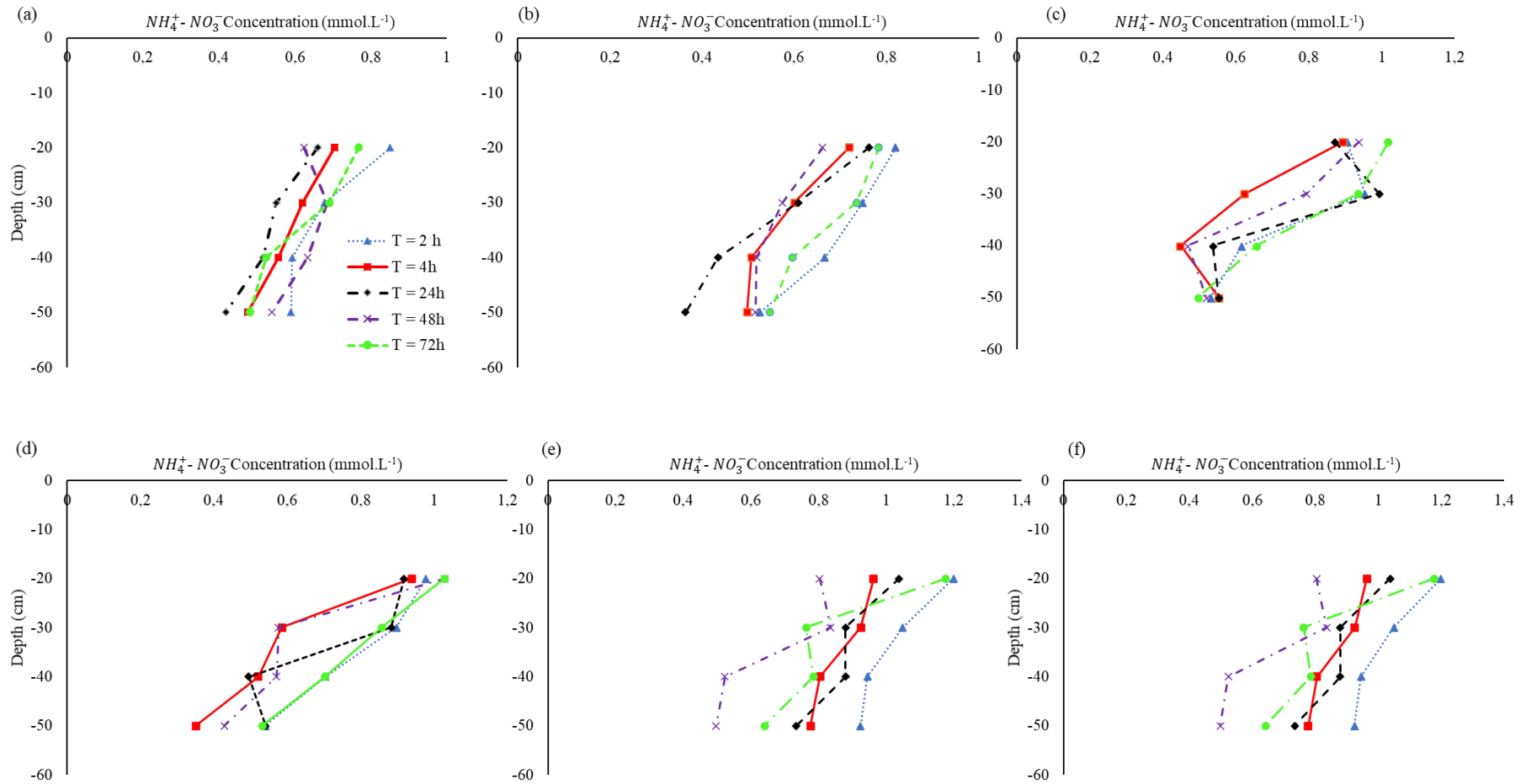


Figure 6.3 First fertigation exercise:  $NH_4^+ - N, NO_3^- - N$  vertical movement at (a) emitter at 100% ET<sub>c</sub>, (b) 15 cm away from emitter at 100% ET<sub>c</sub>, (c) emitter at 75% ET<sub>c</sub>, (d) 15 cm away from emitter at 75% ET<sub>c</sub>, (e) emitter at 55% ET<sub>c</sub>, and (f) 15 cm away from emitter at 55% ET<sub>c</sub>

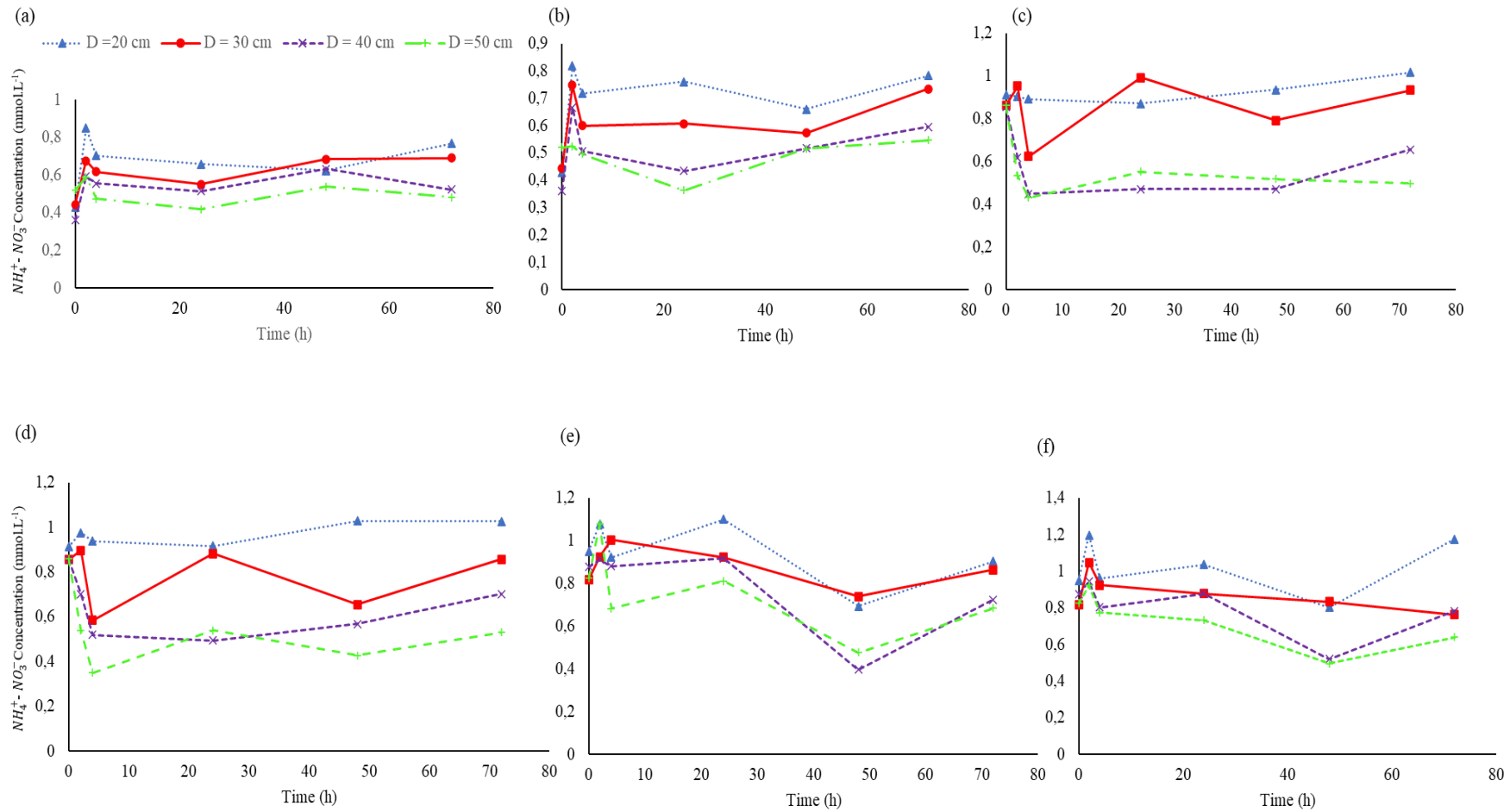


Figure 6.4 Cumulative  $NH_4^+ - N, NO_3^- - N$  breakthrough curves at (a) 20-, 30 -,40-, 50 cm at emitter at 100% ET<sub>c</sub> irrigation regime, (b) 20-, 30 -,40-, 50 cm at 15 cm away from emitter at 100% ET<sub>c</sub> irrigation regime, (c) at 20-, 30 -,40-, 50 cm at emitter at 75% ET<sub>c</sub> irrigation regime, (d) 20-, 30 -,40-, 50 cm at 15 cm away from emitter at 75% ET<sub>c</sub> irrigation regime, (e) 20-, 30 -,40-, 50 cm at emitter at 55% ET<sub>c</sub> irrigation regime, and (f) 20-, 30 -,40-, 50 cm at 15 cm away from emitter at 55% ET<sub>c</sub> irrigation regime. The plots include active root nutrient uptake.

### 6.10.2 Modelling results: MTI solute movement without active root water uptake

The fertigation wetting pattern was ellipsoid in shape, similar to what was reported by Sun et al. (2019) under MTI fertigation. Under the 100%  $ET_c$ , there were no solute contours observed from the period  $t = 0$  h - 60 h (Figure 6.5). The irrigation regime was characterised by continuous irrigation, hence there was potential  $NH_4^+ - N, NO_3^- - N$  dilution. Nitrate concentrations can be increasingly diluted for irrigation scenarios that have prolonged post-fertigation freshwater application (Gärdenäs et al., 2005). Solute concentrations were minimal ( $0.953 \text{ mmol.cm}^{-3}$ ) at  $t = 120$  h and  $t = 156$  h under the 100%  $ET_c$  irrigation regime. The low concentrations resulted from the continuous solute dilution. Under the 100%  $ET_c$  the model successfully simulated the solute movement under MTI (nRMSE = 0.13, EF = 0.54), although it slightly over-estimated solute mobility (PBIAS = -0.22%). This shows that HYDRUS 2D/3D can simulate solute movement under full MTI regimes.

Under the 75%  $ET_c$  irrigation regime, the model successfully simulated the  $NH_4^+ - N, NO_3^- - N$  observed breakthrough curve (Figure 6.6). There was also an over-estimation instance. The simulation results revealed a nRMSE = 0.24, EF = 0.23, and a PBIAS = -7.41%. HYDRUS 2D/3D can simulate MTI solute mobility under optimal DI strategies. Solute movement was pronounced during the  $t = 12$  h to  $t = 96$  h. Moisture infiltration rates in a partially wet/dry soil profile are pronounced during a similar period (Shen et al., 2020). The solute concentration became more dilute at  $t = 120$  h and  $t = 168$  h, this phenomenon can be attributed to the dilution effect that was similarly observed under the 100%  $ET_c$  irrigation regime.

Under the 55%  $ET_c$  DI strategy, the model poorly simulated nitrate leaching at the *E* locality (nRMSE = 0.77, EF = -2.05, and PBIAS = 76%) as compared to the *Ae* locality (nRMSE = 0.35, EF = -1, and PBIAS = 18.78%) (see Figures 6.7 and 6.8). Similar to the 75%  $ET_c$  irrigation regime, solute infiltration was high, albeit less pronounced under the 75%  $ET_c$  irrigation regime. The 55%  $ET_c$  irrigation regime plots exhibited pronounced lateral nitrate movement. The observed contour map revealed high leachate concentration beyond the 40 cm depth. The high  $NH_4^+ - N, NO_3^- - N$  mobility was attributed to availability of air-filled micro and macropores in a partially dry soil. The air-filled pores effected preferential flow in the extreme DI plots. The 55%  $ET_c$  showed horizontal dispersivity of solutes. The lateral dispersivity can



be described as a function of the relatively low initial soil moisture ( $0.353 \text{ m}^3.\text{m}^{-3}$ ) as compared to the 75% ETc ( $0.363 \text{ m}^3.\text{m}^{-3}$ ) and 100% ETc ( $0.408 \text{ m}^3.\text{m}^{-3}$ ).

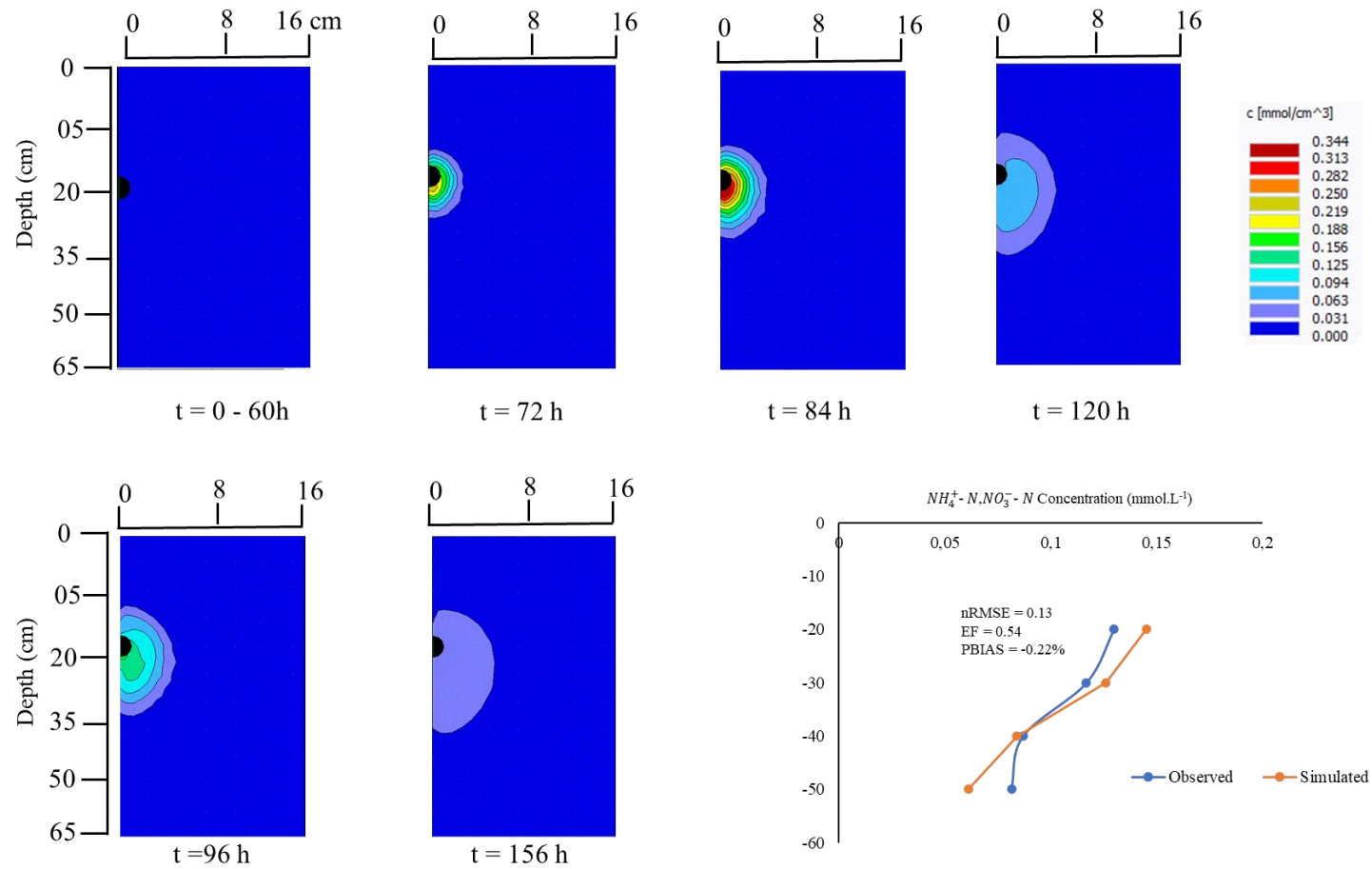


Figure 6.5 Simulated distribution of  $NH_4^+ - N, NO_3^- - N$  at 100%  $ET_c$  irrigation regime from  $t = 12$  h to  $t = 156$  h

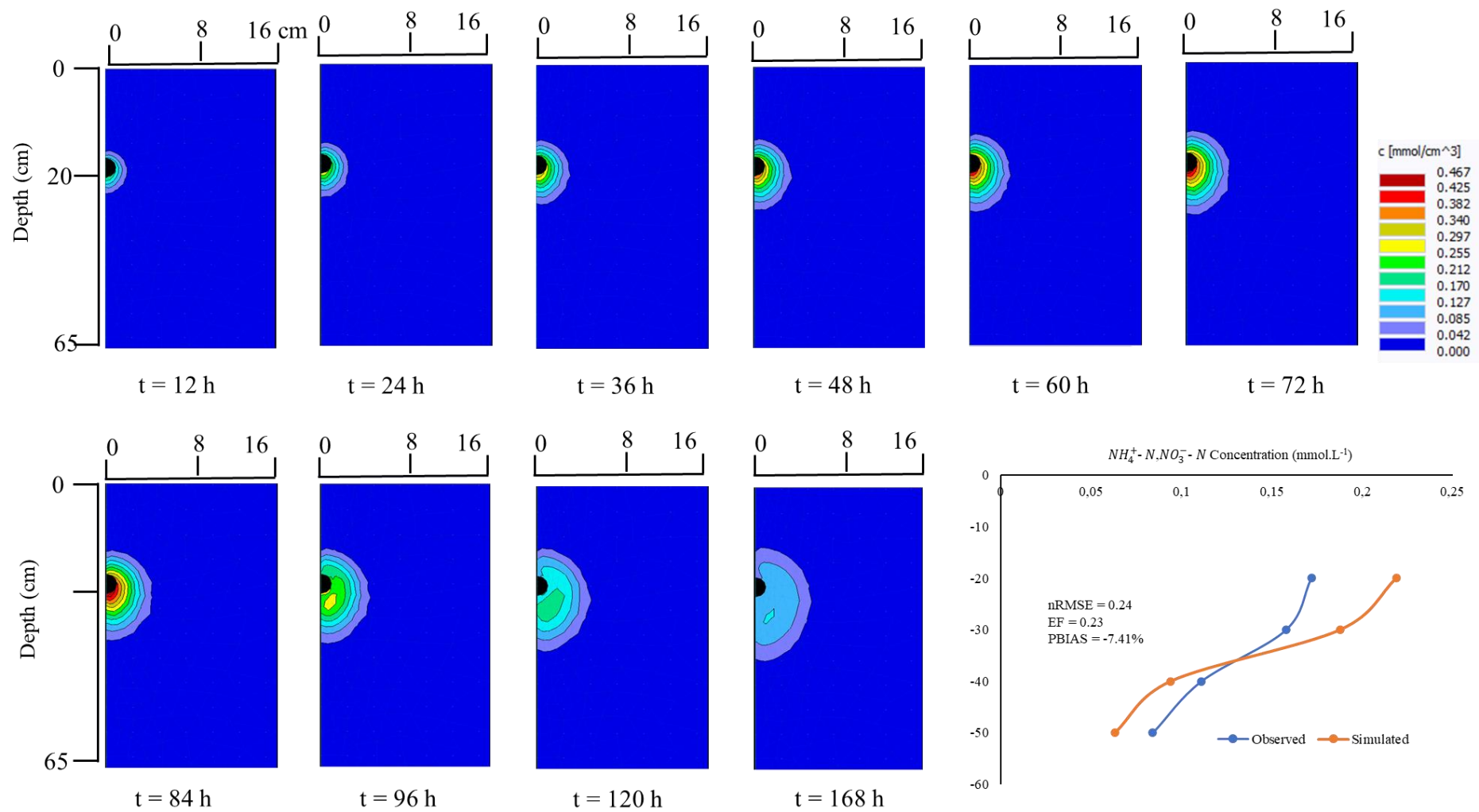


Figure 6.6 Simulated distribution of  $NH_4^+ - N, NO_3^- - N$  at 75%  $ET_c$  irrigation regime from  $t = 12$  h to  $t = 168$  h

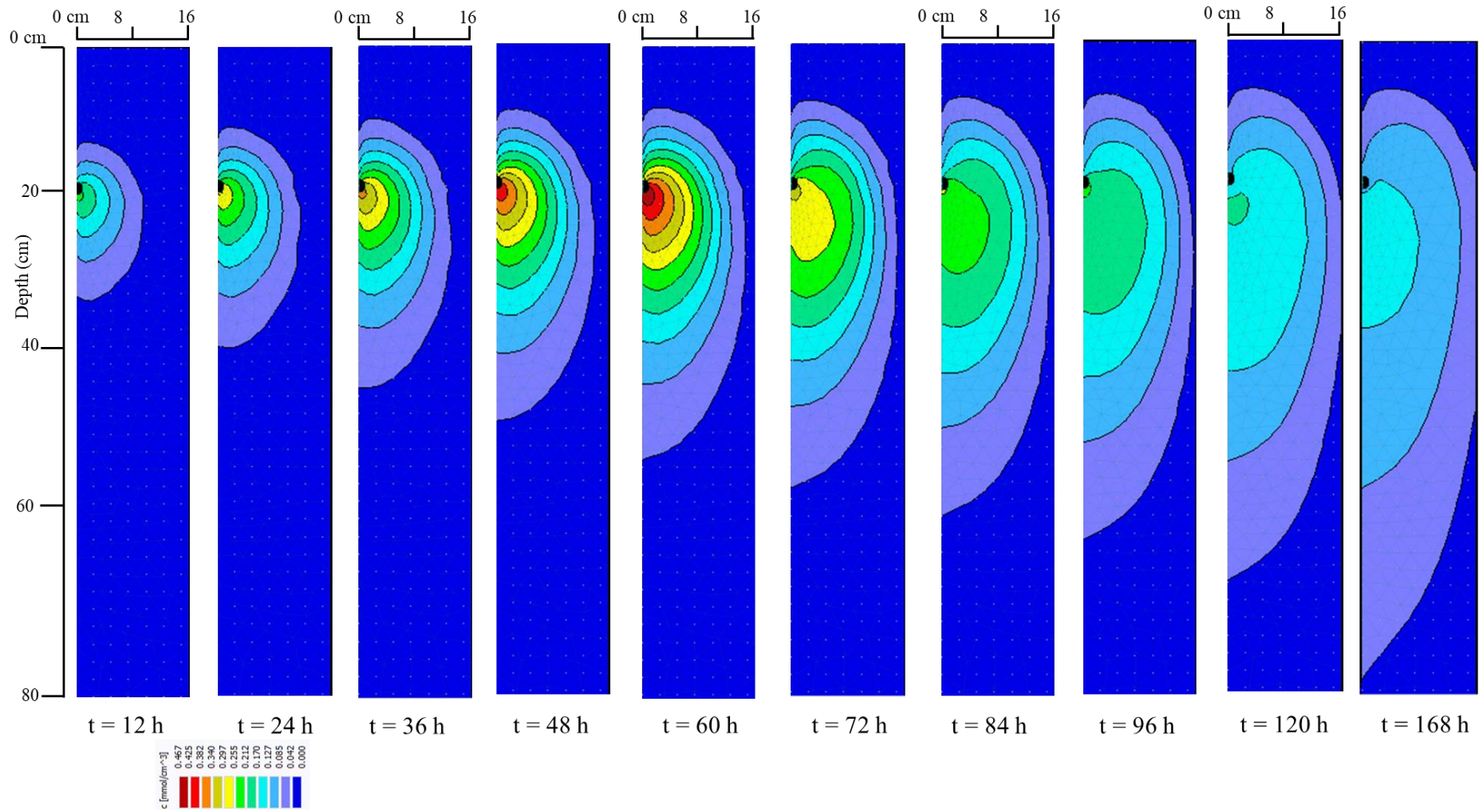


Figure 6.7 Simulated distribution of  $NH_4^+ - N, NO_3^- - N$  at 55%  $ET_c$  irrigation regime from  $t = 12$  h to  $t = 168$  h.

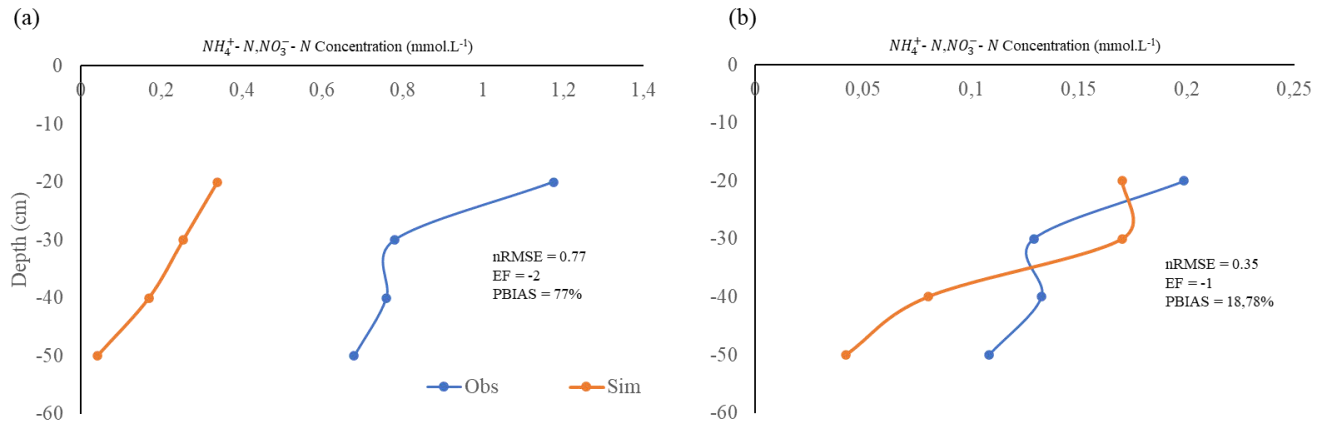


Figure 6.8  $NH_4^+ - N, NO_3^- - N$  observed vs simulated calibration results for the 55%  $ET_c$  irrigation regime over a 72 h period (a) at emitter and (b) 15 cm away from the emitter.

### 6.11 Second Fertigation Exercise and Model Validation

There was no significant difference ( $p > 0.05$ ) between solute concentrations at localities *E* and *Ae* for the 100%  $ET_c$  and 75%  $ET_c$  irrigation regimes. However, there was a significant difference ( $p < 0.05$ ) in solute concentrations at locality *E* between the extreme DI regime and the other two irrigation regimes (full irrigation and optimal DI). There was also a significant difference ( $p < 0.05$ ) at locality *Ae* between the full irrigation regime and the extreme irrigation regime, the latter had high solute concentrations at  $D = 20$  cm and  $D = 40$  cm. This was attributed to drier conditions in the 55%  $ET_c$  irrigation regime. The solute movement curves at *E* for all irrigation regimes were generally smoother than the *Ae* solute curves.

Under the 100%  $ET_c$  and 75%  $ET_c$ , the solute curves followed a similar trajectory (Figures 6.9a and 6.9b). Under the 55%  $ET_c$  irrigation regime, locality *E*'s solute movement was a near-perfect vertical line. In contrast, the movement at locality *Ae* was curvilinear (Figure 6.9e). The observed phenomenon under the 55%  $ET_c$  was attributed to the extreme deficit irrigation conditions imposed on the treatment, which presented available air spaces that could accommodate solutes.

A separate second fertigation dataset was used to validate the model. The HYDRUS 2D/3D validation results are shown in Figures 6.9d – 6.9e. The model successfully simulated the solute

movement under the three irrigation regimes (100% ET<sub>c</sub>, 75% ET<sub>c</sub>, and 55% ET<sub>c</sub>). The model showed an overestimation instance under the 100% ET<sub>c</sub> and 75% ET<sub>c</sub> irrigation regime with a *PBIAS* of -8.79% and 3.53%, respectively. The model under-estimated solute concentration across the 55% ET<sub>c</sub> irrigation regime (*PBIAS* = 11.34%). The *nRMSE* ( $nRMSE \leq 26\%$ ) was within acceptable ranges. However, the model efficiency (*EF*) was average for the 100% ET<sub>c</sub> irrigation regime and poor for the two DI regimes (75% ET<sub>c</sub> and 55% ET<sub>c</sub>). This was potentially due to the DI strategy (75% ET<sub>c</sub> and 55% ET<sub>c</sub>) under the heavy clay Ukulinga soils. Javadzadeh et al. (2017) revealed how HYDRUS 2D/3D poorly simulated solute movement in clay textured soils. Considering that this experiment was carried out under field conditions, the effect of the inherent heterogeneity of the Ukulinga soil profile cannot be ignored in contributing to the poor *EF*. Also, model fitting procedures potentially affect the model performance. Merdun (2012) also attributed the low coefficient of model efficiency (CME) of HYDRUS to parameter value determination and fitting procedures.

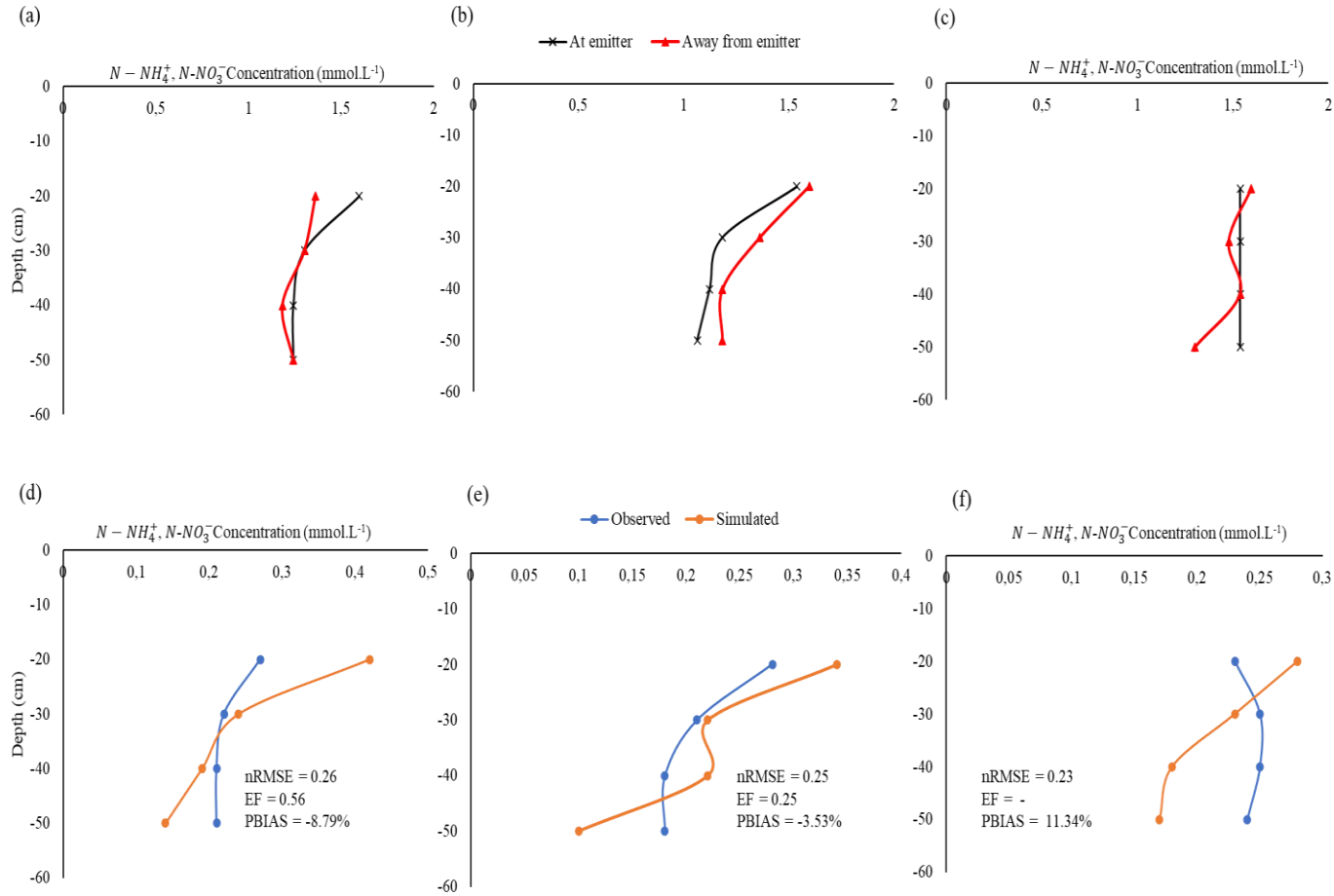


Figure 6.9 Second fertigation exercise  $NH_4^+ - N, NO_3^- - N$  movement at  $E$  and  $A_e$  for (a) 100% ET<sub>c</sub> -, (b) 75% ET<sub>c</sub> -, and (c) 55% ET<sub>c</sub> irrigation regimes after  $t = 72$  h and observed vs simulated  $NH_4^+ - N, NO_3^- - N$  movement at (d) 100% ET<sub>c</sub> -, (e) 75% ET<sub>c</sub> -, and (f) 55% ET<sub>c</sub> irrigation regimes.

## 6.12 Root Nutrient Uptake

The relative plant root distributions and the subsequent solute ( $N - NH_4^+, N - NO_3^-$ ) concentrations are shown in Figure 6.10. The simulation was extended beyond the  $t = 72$  h mark to  $t = 168$  h. It is worth mentioning that actual field measurements were done up to  $t = 72$  h. The 100% ET<sub>c</sub> irrigation regime's solute concentration was the highest in the 0 – 10 cm depth profile. For the 75% ET<sub>c</sub> irrigation regime, the solutes were concentrated in the 5 -15 cm depth range. Under the 55% ET<sub>c</sub> irrigation regime, active solute uptake went beyond the emitter placement depth. The implication is for a fully saturated soil (100% ET<sub>c</sub>). Most of the applied

nutrients are readily available at optimal deficit irrigation strategies (75%  $ET_c$ ). The plant actively takes them because active RNU happens in the canola plant's effective rooting zone depth (ERD). The active water uptake occurs in the default 40%, 30%, 20%, and 10% pattern of the top surface to the lower ends of the ERD (Steduto et al., 2009; Kanda et al., 2020a). The study observed that the rootzones for the respective irrigation regimes (100%  $ET_c$  and 75%  $ET_c$ ) were concentrated in the 0 - 20 cm region close to the MTI emitter. Thus, irrigators need to take note of lateral placement depth as deep-buried lateral can potentially limit RNU. Under the 55%  $ET_c$ , solutes mobility was pronounced due to preferential flow. Partially dry soils exhibit pronounced solute infiltration (Figure 6.10c).

Minute solute concentration leached beyond the emitter placement depth. The lateral movement was pronounced under the 100%  $ET_c$  and 55%  $ET_c$  irrigation regimes, a phenomenon consistent with fine-textured soils. The model also displayed a wider root distribution pattern under the 100  $ET_c$  and 55%  $ET_c$  irrigation regimes (Figure 6.10). Sun et al. (2019), in their MTI laboratory experiment, observed high solute concentrations within the horizontal distance range of 5 – 13 cm. Interestingly, the observed lateral spread of solute concentration was minimal under the 75%  $ET_c$  irrigation. The observation mimicked a well-drained soil scenario. Continued fertigation under extreme DI strategies (55%  $ET_c$ ) promotes solute leaching, leading to salinization. For high fertiliser demand crops, full and optimal DI under MTI requires periodic flushing to prevent near-surface salinization, potentially affecting directly sown crops. Also, the two irrigation regimes present an opportunity to maintain fertiliser concentrations at the near-surface and below the emitter to reduce the risk of groundwater contamination.



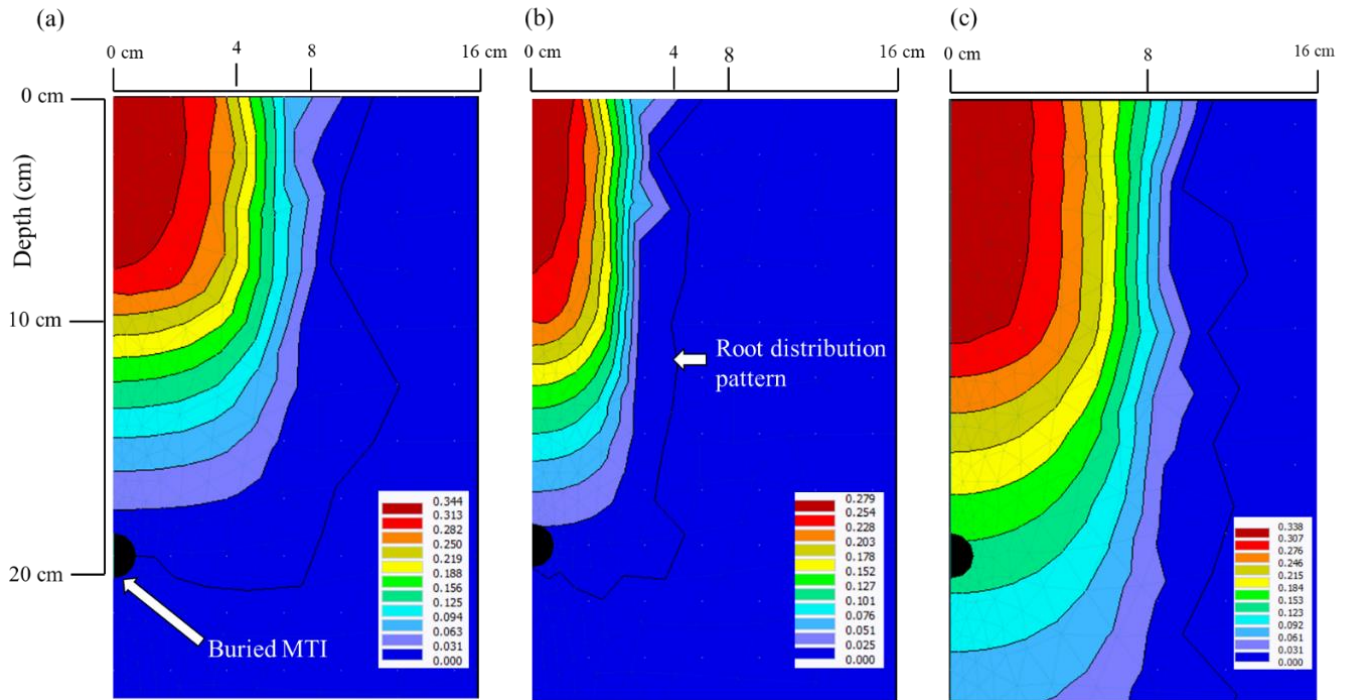


Figure 6.10  $NH_4^+ - N, NO_3^- - N$  concentration ( $\text{mmol.cm}^{-3}$ ) contours during active RNU by plants at (a) 100%  $ET_c$ , (b) 75%  $ET_c$ , and (c) 55%  $ET_c$ .

#### 6.12.1 Partial Factor Productivity (NUE)

The observed  $NH_4^+ - N, NO_3^- - N$  concentrations in the plant material were 27-, 28-, and 32  $\text{mmol.L}^{-1}$  for the 100%  $ET_c$ , 75%  $ET_c$ , and 55%  $ET_c$  irrigation regimes. The plant samples were collected on day 7 after the last fertigation exercise. The crops grown under deficit irrigation (DI) scenarios had high  $NH_4^+ - N, NO_3^- - N$  concentrations. The phenomenon can be attributed to the plants triggering a stress-coping mechanism that facilitates maximum storage of nutrients to counter the loss of turgor pressure and maintains transpiration. This concurs with a study by Eissa and Roshdy (2018) that revealed high fertiliser concentration in maize plant grown under optimal deficit (75%  $ET_c$ ) drip irrigation conditions. Table 6.7 summarises nitrogen concentrations and the subsequent yield and biomass values for each respective irrigation regime. Another possible explanation could be that the deep penetrating roots under the extreme DI regime (55%  $ET_c$ ) had access to the leached fertiliser in the deep wetter parts of the soil.

Table 6.7 Plant  $NH_4^+ - N$ ,  $NO_3^- - N$  concentrations and the resultant yields and biomass

Irrigation regime	Yield ton.ha <sup>-1</sup>	Biomass ton.ha <sup>-1</sup>	Fertiliser concentration Mmol.L <sup>-1</sup> .plant <sup>-1</sup>
100% ET <sub>c</sub>	1.48 (0.1) <sup>a</sup>	4.20 (2.20) <sup>a</sup>	27
75% ET <sub>c</sub>	1.15 (0.15) <sup>a</sup>	1.15 (1.50) <sup>a</sup>	28
55% ET <sub>c</sub>	0.75 (0.05) <sup>b</sup>	0.75 (1.50) <sup>a</sup>	32

Yield and biomass values in the same column, followed by the same superscript letter, do not significantly differ at 5% significance using the one-way ANOVA. Data in parenthesis are the standard deviations

The partial factor productivity of applied N (PFP<sub>N</sub>) used as a proxy for NUE was computed as per Equation 6.5. The PFP<sub>N</sub> values are summarised in Table 6.8. The PFP<sub>N</sub> values ranged from 0.83 – 1.72 kg of grain.kg<sup>-1</sup> of N. Similar values were obtained by Ma and Herath (2016) for spring canola planted under Canada's drought conditions. Yield penalties were incurred under the 55% ET<sub>c</sub> irrigation regime because of the imposed deficit irrigation (DI). This means that extreme MTI DI strategies are not suitable for canola production, as water stress reduces the mobility of the  $NH_4^+ - N$  and the  $NO_3^- - N$  assimilate. Full irrigation (100% ET<sub>c</sub>) and optimal DI (75% ET<sub>c</sub>) recorded relatively high yields compared to the 55% ET<sub>c</sub> irrigation regime. The observation is attributed to the availability of irrigation water for improved N utilisation. Maaz et al. (2016) attributed good canola oilseed yield to optimal irrigation strategies.

Table 6.8 PFP<sub>N</sub> as a proxy to NUE for the respective irrigation regimes

Irrigation regimes	Yield	$F_N$	$S_i$	$F_N + S_i$	PFP <sub>N</sub>
			kg.ha <sup>-1</sup>		kg.kg <sup>-1</sup>
100% ET <sub>c</sub>	1480	470.40	390.43	860.83	1.72
75% ET <sub>c</sub>	1150	470.40	418.66	889.06	1.29
55% ET <sub>c</sub>	750	470.40	432.77	903.17	0.83

### 6.13 Conclusion and Recommendations

The study sought to demonstrate nitrate distribution in a silty clay soil profile and nitrate leaching under MTI. The study further employed HYDRUS 2D/3D to simulate solute mobility under three irrigation regimes, namely, full irrigation (100% ET<sub>c</sub>) and two deficit irrigation (DI) regimes (75% ET<sub>c</sub> and 55% ET<sub>c</sub>). The study revealed that under full irrigation and optimal DI strategies, maximum nutrient utilisation is evidenced by high yields. Under extreme DI conditions, the canola crop absorbs the fertiliser as a coping mechanism. The coping mechanism is a trade-off for yield and biomass accumulation. The study concluded that nitrate

distribution under full and optimal irrigation regimes provided nutrients for the plants, whereas the extreme DI strategy promotes nutrient leaching.

HYDRUS 2D/3D successfully simulated the solute movement under full irrigation (100%  $ET_c$ ) and optimal irrigation (75%  $ET_c$ ) conditions [(100%  $ET_c$ :  $nRMSE = 0.13$ ,  $EF = 0.54$ ,  $PBIAS = -0.22\%$ ) (75%  $ET_c$ :  $nRMSE = 0.24$ ,  $EF = 0.23$ , and a  $PBIAS = -7.41\%$ .)], whereas the extreme DI strategy poorly simulated solute movement at locality *E* ( $nRMSE = 0.77$ ,  $EF = -2$ ,  $PBIAS = 76\%$ ). The extreme DI scenario exhibited high leaching as compared to the other two irrigation regimes (100%  $ET_c$  and 75%  $ET_c$ ). Varying soil water content before the fertigation exercise contributed to solute mobility, for instance, the low soil water content conditions under the 55%  $ET_c$  irrigation regime promoted solute imbibition.

The study employed the partial factor productivity of applied N ( $PFP_N$ ) as a proxy to measuring nitrogen use efficiency (NUE). This study also revealed that the small  $PFP_N$  variations produced statistically insignificant yield differences between full MTI and the optimal DI strategy (75%  $ET_c$ ). The study was carried out under a controlled environment; therefore, the authors recommend it be done under rainfed field conditions and assess the relative solute mobility for the respective irrigation regimes.

## 6.14 References

- Ajdary, K, Singh, D, Singh, AK and Khanna, M. 2007. Modelling of nitrogen leaching from experimental onion field under drip fertigation. *Agricultural Water Management* 89 (1-2): 15-28.
- Bar-Yosef, B. 1999. Advances in fertigation. *Advances in Agronomy*. 65: 1-77.
- Chakraborty, P and Das, BS. 2018. Measurement and Modeling of Longitudinal Dispersivity in Undisturbed Saturated Soil: An Experimental Approach. *Soil Science Society of America Journal* 82 (5): 1117-1123.
- Clothier, B and Sauer, T. 1988. Nitrogen transport during drip fertigation with urea. *Soil Science Society of America Journal* 52 (2): 345-349.
- Coetzee, A. 2017. Rate and timing of nitrogen fertilisation for canola production in the Western Cape of South Africa. Unpublished MSc thesis, Agronomy, Stellenbosch University, Stellenbosch, South Africa.
- Cresswell, HP, Green, TW and McKenzie, NJ. 2008. The Adequacy of Pressure Plate Apparatus for Determining Soil Water Retention. *Soil Science Society of America Journal* 72 (1): 41-49.
- Cutforth, H, Angadi, S, McConkey, B, Miller, P, Ulrich, D, Gulden, R, Volkmar, K, Entz, M and Brandt, S. 2013. Comparing rooting characteristics and soil water withdrawal

- patterns of wheat with alternative oilseed and pulse crops grown in the semiarid Canadian prairie. *Canadian Journal of Soil Science* 93 (2): 147-160.
- Dobermann, AR. 2005. *Nitrogen use efficiency-state of the art*. Agriculture and Horticulture Department, University of Nebraska - Lincoln., Nebraska, USA.
- Eissa, MA and Roshdy, NMK. 2018. Effect of nitrogen rates on drip irrigated maize grown under deficit irrigation. *Journal of Plant Nutrition* 42 (2): 127-136.
- Elasbah, R, Selim, T, Mirdan, A and Berndtsson, R. 2019. Modeling of Fertilizer Transport for Various Fertigation Scenarios under Drip Irrigation. *Water* 11 (5): 893-908.
- Fan, Y-W, Huang, N, Zhang, J and Zhao, T. 2018. Simulation of Soil Wetting Pattern of Vertical Moistube-Irrigation. *Water* 10 (5): 601-621.
- FAO. 2002. Sprinkler irrigation systems planning, design, operation and maintenance. In: eds. Savva, A, Stoutjesdijk, J, Regnier, P and Hindkjaer, S, *FAO Irrigation Manuals*. FAO, Harare, Zimbabwe.
- Feddes, RA. 1982. *Simulation of field water use and crop yield*. Pudoc, Wageningen, The Netherlands.
- Fwa, T, Tan, S and Chuai, C. 1998. Permeability measurement of base materials using falling-head test apparatus. *Transportation Research Record* 1615 (1): 94-99.
- Gan, Y, Liu, L, Cutforth, H, Wang, X and Ford, G. 2011. Vertical distribution profiles and temporal growth patterns of roots in selected oilseeds, pulses and spring wheat. *Crop Pasture Science* 62 (6): 457-466.
- Gärdenäs, A, Hopmans, J, Hanson, B and Šimůnek, J. 2005. Two-dimensional modeling of nitrate leaching for various fertigation scenarios under micro-irrigation. *Agricultural Water Management* 74 (3): 219-242.
- Hanson, BR, Šimůnek, J and Hopmans, JW. 2006. Evaluation of urea–ammonium–nitrate fertigation with drip irrigation using numerical modeling. *Agricultural Water Management* 86 (1-2): 102-113.
- Jansson, P and Karlberg, L. 2011. *Coupled heat and mass transfer model for soil-plant-atmosphere systems*. Royal Institute of Technology, Dept of Civil and Environmental Engineering, Stockholm, Sweden.
- Javadzadeh, F, Khaledian, M, Navabian, M and Shahinrokhshar, P. 2017. Simulations of both soil water content and salinity under tape drip irrigation with different salinity levels of water. *Geosystem Engineering* 20 (4): 231-236.
- Kanda, EK, Senzanje, A and Mabhaudhi, T. 2020a. Modelling soil water distribution under Moistube irrigation for cowpea (*VIGNA unguiculata* (L.) Walp.) crop. *Irrigation and Drainage* 69 (5): 1116-1132.
- Kanda, EK, Senzanje, A and Mabhaudhi, T. 2020b. Soil water dynamics under Moistube irrigation. *Physics and Chemistry of the Earth, Parts A/B/C* 115(2020): 102836
- Kanda, EK, Senzanje, A and Mabhaudhi, T. 2020c. Soil water dynamics under Moistube irrigation. *Physics and Chemistry of the Earth* 115(2020): 102836.
- Klute, A. 1986. *Water retention: laboratory methods*. American Society of Agronomy-Soil Science Society of America, Madison, USA.
- Ling, G and El-Kadi, AI. 1998. A lumped parameter model for nitrogen transformation in the unsaturated zone. *Water Resources Research* 34 (2): 203-212.
- Liu, X, Zhu, Y, Yu, X, Li, Y, Tang, J and Yu, L. 2017. Water-salinity distribution characteristics in wetted soil of moistube irrigation under different pressure heads and soil bulk densities. *Trans. Chin. Soc. Agric. Mach* 48: 194-202.
- Lotse, E, Jabro, J, Simmons, K and Baker, D. 1992. Simulation of nitrogen dynamics and leaching from arable soils. *Journal of Contaminant Hydrology* 10 (3): 183-196.
- Luce, MS, Grant, CA, Ziadi, N, Zebbarth, BJ, O'Donovan, JT, Blackshaw, RE, Harker, KN, Johnson, EN, Gan, Y and Lafond, GP. 2016. Preceding crops and nitrogen fertilization

- influence soil nitrogen cycling in no-till canola and wheat cropping systems. *Field Crops Research* 191: 20-32.
- Lv, H, Lin, S, Wang, Y, Lian, X, Zhao, Y, Li, Y, Du, J, Wang, Z, Wang, J and Butterbach-Bahl, K. 2019. Drip fertigation significantly reduces nitrogen leaching in solar greenhouse vegetable production system. *Environmental Pollution* 245: 694-701.
- Ma, BL and Herath, AW. 2016. Timing and rates of nitrogen fertiliser application on seed yield, quality and nitrogen-use efficiency of canola. *Crop and Pasture Science* 67 (2): 167-180.
- Maaz, T, Pan, W and Hammac, W. 2016. Influence of Soil Nitrogen and Water Supply on Canola Nitrogen Use Efficiency. *Agronomy Journal* 108 (5): 2099-2109.
- Merdun, H. 2012. Effects of Different Factors on Water Flow and Solute Transport Investigated by Time Domain Reflectometry in Sandy Clay Loam Field Soil. *Water Air Soil Pollution* 223 (8): 4905-4923.
- Merdun, H, Meral, R and Riza Demirkiran, A. 2008. Effect of the initial soil moisture content on the spatial distribution of the water retention. *Eurasian Soil Science* 41 (10): 1098-1106.
- Mmolawa, K and Or, D. 2000a. Root zone solute dynamics under drip irrigation: A review. *Plant Soil Science* 222 (1-2): 163-190.
- Mmolawa, K and Or, D. 2000b. Water and Solute Dynamics under a Drip-Irrigated Crop: Experiments and Analytical Model. *Transactions of the ASAE* 43 (6): 1597-1608.
- Moriasi, DN, Arnold, JG, Van Liew, MW, Bingner, RL, Harmel, RD and Veith, TL. 2007. Model evaluation guidelines for systematic quantification of accuracy in watershed simulations. *Transactions of the ASABE* 50 (3): 885-900.
- R-Core-Team. 2017. *R: A language and environment for statistical computing*. R Foundation for Statistical Computing, Vienna, Austria.
- Rawls, WJ, Brakensiek, DL and Saxton, K. 1982. Estimation of soil water properties. *Transactions of the ASAE* 25 (5): 1316-1320.
- Schulze-Makuch, D. 2005. Longitudinal dispersivity data and implications for scaling behavior. *Ground Water* 43 (3): 443-56.
- Shen, L, Zhang, Y, Yang, M and Liu, R. 2020. Effects of alternate moisture-irrigation on soil water infiltration. *International Journal of Agricultural and Biological Engineering* 13 (4): 151-158.
- Šimůnek, J, Šejna, M and Van Genuchten, MT. 1999. *The HYDRUS-2D software package for simulating to-dimensional movement of water, heat, and multiple solutes in variable saturated media. Version 2.0*. IGWMC-TPS-53, International Ground Water Modeling Center, Colorado School of Mines, Colorado, USA.
- Simunek, J, van Genuchten, R and Šejna, M. 2012. HYDRUS: Model Use, Calibration, and Validation. *Transactions of the ASABE* 55 (4): 1263-1276.
- Skaggs, TH, Trout, TJ, Šimůnek, J and Shouse, PJ. 2004. Comparison of HYDRUS-2D Simulations of Drip Irrigation with Experimental Observations. *Journal of Irrigation and Drainage Engineering* 130 (4): 304-310.
- Steduto, P, Hsiao, TC, Raes, D and Fereres, E. 2009. AquaCrop-The FAO Crop Model to Simulate Yield Response to Water: I. Concepts and Underlying Principles. *Agronomy Journal* 101 (3): 426-437.
- Sun, G, Li, Y, Liu, X, Cui, N, Gao, Y and Yang, Q. 2019. Effect of Moisture Fertigation on Infiltration and Distribution of Water-Fertilizer in Mixing Waste Biomass Soil. *Sustainability* 11 (23): 6757-6773.
- Vogel, T, Van Genuchten, MT and Cislerova, M. 2000. Effect of the shape of the soil hydraulic functions near saturation on variably-saturated flow predictions. *Advances in water resources* 24 (2): 133-144.

- Vrugt, J, Hopmans, J and Šimunek, J. 2001. Calibration of a two-dimensional root water uptake model. *Soil Science Society of America Journal* 65 (4): 1027-1037.
- Wilkinson, W. 1968. Constant head in situ permeability tests in clay strata. *Geotechnique* 18 (2): 172-194.
- Xin, J, Liu, Y, Chen, F, Duan, Y, Wei, G, Zheng, X and Li, M. 2019. The missing nitrogen pieces: A critical review on the distribution, transformation, and budget of nitrogen in the vadose zone-groundwater system. *Water Research* 165: 114977.
- Yang, J, Yang, J, Liu, S and Hoogenboom, G. 2014. An evaluation of the statistical methods for testing the performance of crop models with observed data. *Agricultural Systems* 127 (2014): 81-89.
- Youngs, EG and Leeds-Harrison, PB. 1990. Aspects of transport processes in aggregated soils. *Journal of Soil Science* 41 (4): 665-675

## 7 CALIBRATION AND EVALUATION OF THE FAO AQUACROP MODEL FOR CANOLA (*Brassica Napus. L*) UNDER VARIED MOISTUBE IRRIGATION REGIMES

This Chapter was published as:

**Dirwai, TL**, Senzanje, A, Mabhaudhi, T. (2021). Calibration and Evaluation of the FAO AquaCrop Model for Canola (*Brassica napus*) Under Varied Moistube Irrigation Regimes. *Agriculture* 2021, 11, 410. <https://doi.org/10.3390/agriculture11050410>

### Abstract

The AquaCrop model was calibrated and validated for canola (*Brassica napus*) under Moistube irrigation (MTI) and various water regimes [(i)100%, (ii) 75%, and (iii) 55% of crop water requirement ( $ET_c$ )] over two seasons, 2019 and 2020. The normalised root mean square (nRMSE), Model Efficiency (EF),  $R^2$ , and the Willmot's index of agreement ( $d$ ) statistics were used to evaluate the model's efficiency in simulating biomass (B), canopy cover (CC), yield (Y) and harvest index (HI). The calibration results indicated the model simulated with accuracy the  $CC_x$  (under 100%  $ET_c$   $R^2 = 0.99$ ,  $EF = 0.92$ ,  $nRMSE = 6.4\%$ ,  $d = 0.98$ ) and 75%  $ET_c$  ( $R^2 = 0.99$ ,  $EF = 0.92$ ,  $nRMSE = 10.3\%$ ,  $d = 0.98$ ). The model simulated CC well for validation for 100%  $ET_c$  ( $R^2 = 0.97$ ,  $EF = 0.93$ ,  $nRMSE = 22.5\%$ ,  $d = 0.98$ ) and 75%  $ET_c$  ( $R^2 = 0.84$ ,  $EF = 0.45$ ,  $nRMSE = 59.2\%$ ,  $d = 0.86$ ) irrigation regimes. Final biomass simulations were reasonably good under 100%  $ET_c$ , 75%  $ET_c$ , and 55%  $ET_c$  irrigation regimes ( $R^2 > 0.90$ ,  $d > 0.65$ ). The study showed the usefulness of AquaCrop for assessing yield response of canola to full and deficit irrigation scenarios under MTI. The researchers recommend that the experiment be done under field conditions and perform a comparative analysis of the findings

**Keywords:** biomass, crop modelling, water productivity, water regimes, yield

## 7.1 Introduction

The global agricultural water consumption utilises 70% of the world's freshwater. Water is a finite resource, and climate variability and change have exacerbated the natural resource's depletion. Burgeoning populations have also increased per capita water use, thus compounding the global freshwater water scarcity situation (Mustafa et al., 2020). Modern agricultural practices in sub-Saharan Africa (SSA) are a dualistic exercise that meets the poor's food security needs and is also a primary economic driver (Chimonyo et al., 2020). As such, using advanced irrigation techniques will maximise water productivity (WP) and subsequently increase yields. Climate variability and change threaten food security, and industrial crops are not spared. An increase in global temperatures will lead to high carbon concentrations and warmer temperature; this consequently impacts cool climate C3 (canola, flax, wheat, and soybean) industrial crops (Korres et al., 2016). Expanding irrigation land under current irrigation technologies and strategies can accelerate water scarcity, i.e., an increase in demand will lead to water scarcity under the present climate change variability scenarios (Fujihara et al., 2008; Kang et al., 2009). Henceforth, adopting efficient irrigation techniques and strategies can ameliorate the accelerated demand on the finite water resource (Zhang et al., 2019).

Canola is a C3 crop of economic importance. The crop produces oilseed that is processed into oil products for human consumption (Raymer, 2002), and it is also used for forage production and phytoremediation (Bañuelos et al., 2002). Canola is considered a “healthy” trade oil. It contains no cholesterol, thus reducing cardiovascular diseases (Lordkipanidze et al., 1998). This has subsequently increased its demand, leading to expanded irrigated canola hectareage worldwide. Efficient irrigation technology is required for improved yield, water productivity (WP) and water use efficiency (WUE). Several researchers have investigated canola production under various drip irrigation technologies and deficit irrigation strategies. For example, Katuwal et al. (2020) investigated and assessed the soil water extraction pattern and water use efficiency of spring canola under drip irrigation. Their study (Katuwal et al., 2020) revealed that deficit irrigated canola at the vegetative stage extracted the same amount of water as the fully irrigated canola. Safi et al. (2019) investigated the effects of deficit irrigation (DI) on transplanted and directly sown spring canola and revealed that directly sown cultivars had low grain yield.



Hergert et al. (2016) performed full and deficit drip irrigation trials on spring canola and revealed that deficit irrigation accelerated crop maturity. The study also showed a high WUE of  $7.6 \text{ kg.ha}^{-1}.\text{mm}^{-1}$ , thus proving that deficit irrigation is attractive for canola growth. Another study by Bañuelos et al. (2002) investigated the vegetative production of canola under drip irrigation in central California, and the study argued that optimal yields were obtained by irrigating at 125%  $\text{ET}_c$ . Interestingly, the study by Bañuelos et al. (2002) contradicted finding by Safi et al. (2019) and Hergert et al. (2016) despite employing near-similar DI strategies. Taylor et al. (1991) also used drip irrigation to assess the effects of irrigation and nitrogen fertilizer on yield, oil content, nitrogen accumulation, and canola crop efficiency. The study revealed that the WUE for grain production and biomass were 7.5 and  $23 \text{ kg.ha}^{-1}.\text{mm}^{-1}$ , respectively. Other studies also performed different investigations on canola under different irrigation technologies and irrigation management processes (Khalili et al., 2012; Majnooni-Heris et al., 2014; Hergert et al., 2016; Pavlista et al., 2016; Katuwal et al., 2018; Safi et al., 2019).

Moistube irrigation (MTI) is a relatively new subsurface semi-permeable membrane irrigation technology (Yang et al., 2008). Discharge is facilitated by a response to soil water potential and system pressure (Yang et al., 2008; Kanda et al., 2019). The matric potential effect can only be utilised for 44 hours; thereafter, external pressure is required to drive the system (Kanda et al., 2019; Dirwai et al., 2021). MTI is a subsurface irrigation technology hence it minimises non-beneficial water such as deep percolation, run-off and soil evaporation (Locascio, 2005; Kanda et al., 2019) and it has a reported high water use efficiency (WUE) compared to other technologies such as sprinkler and drip irrigation (Kanda et al., 2019).

MTI has been used in China's arid regions and for legume production in some parts of SSA (Kanda et al., 2020b). Kanda et al. (2020b) applied deficit irrigation techniques under MTI for cowpea production and the resultant WUE for grain production at 100%  $\text{ET}_c$  and 70%  $\text{ET}_c$  irrigation were  $0.92$  and  $0.95 \text{ kg.m}^{-3}$ , respectively. The study by Kanda et al. (2020b) was a comparative study between MTI and subsurface drip irrigation (SDI), and MTI exhibited a high WUE ( $100\% \text{ ET}_c = 0.95 \text{ kg.m}^{-3}$ ) as compared to SDI ( $100\% \text{ ET}_c = 0.82 \text{ kg.m}^{-3}$ ). MTI presents an opportunity for canola production under various irrigation regimes. Despite the extensive research on irrigated canola, there is a gap in canola production under MTI. MTI can potentially offer realistic matric potential informed irrigation schedules for maximised irrigation water use.

Crop modelling is a cost-effective method for quantifying crop yields and crop WP (Foster et al., 2017). Crop modelling tools are either carbon driven models, radiation use efficiency (RUE), and water-driven models (Bauböck, 2014). Various studies have applied crop modelling techniques to canola production. For example, He et al. (2017) used Agricultural Production Systems Simulator (APSIM), a radiation driven model to simulate canola phenology. The study revealed that APSIM accurately simulated canola phenology under different growing environments. However, the study also revealed that APSIM required extensive data for accurate canola phenology simulation during the vernalisation sensitivity, photoperiod sensitivity phases which subsequently influence grain yield formation. Robertson and Kirkegaard (2003) used APSIM to simulate rainfed canola grain yields accurately. Qian et al. (2019) carried out a comparative study to assess two C3 crops' simulation performance: canola and wheat under rainfed conditions. CROPGRO was used to simulate canola yields, whilst Crop Environment Resources Synthesis (CERES) was used to simulate wheat yields. The study results showed that both models successfully simulated yields with the  $R^2 > 0.90$  and nRMSE range of 5% -18.2%.

AquaCrop is a water-driven model that simulates yield, biomass production and beneficial water use (Raes et al., 2009; Steduto et al., 2009; Todorovic et al., 2009). Water-driven models are an attractive option compared to their counterparts because of the ease of use. They facilitate easy normalisation of WP parameter under different climatic conditions (evaporative demand and atmospheric carbon dioxide). AquaCrop use has been applied to different crops such as cowpea (Kanda et al., 2020a), groundnuts (Chibarabada et al., 2020), wheat (Andarzian et al., 2011; Iqbal et al., 2014; Jin et al., 2014; Kumar et al., 2014; Toumi et al., 2016), maize (Heng et al., 2009; Abedinpour et al., 2012; Ahmadi et al., 2015), and much recently on leafy vegetables (Nyathi et al., 2018). Zeleke et al. (2011) used the AquaCrop to simulate canola yields under rainfed and irrigated conditions. The percentage relative difference (%D) between the observed and simulated yield was 2.2%. This signified AquaCrop's capability in simulating canola grain yield. This study investigated the capability of MTI for canola production under full and deficit irrigation scenarios. Identifying optimal DI strategies can potentially save water without imposing yield penalties on the canola grower. To extend the study's applicability beyond location-specific results, the experiment adopted AquaCrop modelling software (Raes et al., 2009). The model has been used in numerous studies (eg. Farahani et al., 2009; Heng et al., 2009; Araya et al., 2010a; Araya et al., 2010b; Andarzian et al., 2011; Abedinpour et al., 2012; Iqbal et al., 2014; Mabhaudhi et al., 2014; Maniruzzaman et al., 2015; Toumi et al., 2016;

Nyathi et al., 2018; Chibarabada et al., 2020; Kanda et al., 2020a) to assess yield response to water stress, however, there is a need to calibrate and test the AquaCrop model for industrial crops such as canola under MTI. As mentioned prior, there is a gap in how canola performs under MTI water stress conditions. The study was premised on the hypothesis that AquaCrop cannot effectively simulate canola crop performance under varying MTI water regimes.. The specific objectives for this study were to (i) calibrate AquaCrop for canola under MTI water stress conditions, (ii) evaluate its ability to simulate CC, biomass, yield and evapotranspiration (ET) under local South African conditions.

## 7.2 Material and Methods

### 7.2.1 Model description

AquaCrop is a water-driven modelling software used to simulate plant growth processes such as canopy cover (CC), biomass accumulation and yield (Raes et al., 2009). The model simulates yield response to water, i.e., water productivity (Nyathi et al., 2018). Water productivity ( $WP^*$ ) is one of the crucial variables together with simulated transpiration ( $T_r$ ), and reference evapotranspiration ( $ET_o$ ) required to compute daily biomass ( $B$ ) production (Equation 7.1) (Zeleeke et al., 2011). For this study, canola biomass referred only to the above-ground component. AquaCrop's calculation scheme includes simulating the water stored in the root zone. The water stress coefficient is instrumental in determining the harvest index (HI). Once  $B$  is determined, the crop yield ( $Y$ ) is then computed as per Equation 7.2.

Equation 7.2.

$$WP^* = \frac{B}{\sum(T_r/ET_o)} \quad 7.1$$

$$Y = B \times HI \quad 7.2$$

Where:  $WP^*$  = water productivity ( $\text{g.m}^{-3}$ ),  $B$  = biomass ( $\text{g.m}^{-2}$ ),  $T_r$  = transpiration (mm),  $ET_o$  = reference evapotranspiration (mm),  $HI$  = harvest index, and  $Y$  = yield ( $\text{kg.ha}^{-1}$ ).

AquaCrop simulates water use as a function of four stress factors, namely (1) canopy expansion, (2) stomatal closure, (3) early canopy senescence, and (4) aeration stress (Mabhaudhi et al., 2014; Vanuytrecht et al., 2014; Nyathi et al., 2018). The model is relatively easy to use as it requires few explicit parameters and largely-intuitive input variables (Steduto et al., 2009). AquaCrop is underpinned by two sets of parameters: conservative parameters and

non-conservative parameters. The former does not change with time management and are applicable on a large spatial variation scale, whereas the latter change with time, management and location (Montoya et al., 2016; Nyathi et al., 2018).

## Experimental Design

### 7.2.2 Study site and description of field experiment

The experiment was conducted at Ukulinga farm at the University of KwaZulu-Natal in Pietermaritzburg, South Africa (29°39'44.8"S 30°24'18.2"E, altitude: 636 m). The experiment was run over two growing seasons, 2019 (July – September) and 2020 (September – November), in a tunnel, which was not temperature controlled but was designed to exclude rainfall. The 2019 growing season was used to calibrate the AquaCrop model, and the 2020 season was used for model validation. The experiment was a split-plot design that consisted of three MTI regimes, namely 100%, 75% ET<sub>c</sub> and 55% crop water requirement (ET<sub>c</sub>), under tunnel conditions measuring 30 m by 10 m. The ET<sub>c</sub> was computed according to Equation 7.3:

$$ET_c = K_c \times ET_o \quad 7.3$$

where ET<sub>c</sub> = crop water requirement (mm.day<sup>-1</sup>), K<sub>c</sub> = crop coefficient, and ET<sub>o</sub> = evapotranspiration (mm.day<sup>-1</sup>).

In order to compute the CWR under the deficit irrigation regimes, Equation 7.4 was used:

$$ET_{c-deficit} = ET_{c-100\%} \times \text{Deficit fraction} \quad 7.4$$

Each MTI regime comprised of 4 experimental plots measuring 2 m by 1 m. The MTI AquaCrop deficit irrigation schedules followed the procedure by Geerts et al. (2010) and Savva and Frenken (2002). The varied irrigation scheduling is summarized in Table 7.1.

Table 7.1 Irrigation frequencies and application times

Irrigation regime	100% ET <sub>c</sub>			75% ET <sub>c</sub>			55% ET <sub>c</sub>		
	M 1	M 2	M 3	M 1	M 2	M 3	M 1	M 2	M 3
IF (days)	4.5	2.5	2.8	6.0	3.3	3.7	8.2	4.5	5.0
AT (h)	1.3	2.4	2.1	1.0	1.8	1.6	0.7	1.3	1.2

\*M = Month, IF = Irrigation frequency, and AT = Application times

The experiment was done under a tunnel to facilitate better control of water fluxes and exclude of rainfall. A 1 m buffer hydrologically separated each experimental plot; a 250-micron plastic sheeting was vertically inserted to a depth of 1 m in each buffer space. PR2/6 profile probe access tubes were installed in each plot for soil water measurement at depths 10-, 20-, 30-, 40-, 60-, and 100- cm. Soil water content (SWC) measurements were done weekly using a PR2/6 profile probe connected to an HH2 handheld moisture meter (Delta-T, UK). Kanda et al. (2020a) performed weekly SWC measurements for cowpea production under MTI and showed that there was minimal temporal and spatial SWC variability. The canola was nursed at the University of KwaZulu-Natal – Pietermaritzburg (UKZN – PMB) (29°37'34.0"S 30°24'11.9"E) Controlled Environment Facilities (CEF) for two months before transplanting at Ukulinga farm. Soil water measurements commenced two weeks before transplanting. Each plot accommodated 18 plants resulting in 9 plants.m<sup>-2</sup>. Heng et al. (2009) adopted plant densities of 6 – 8 plants.m<sup>-2</sup> to prevent canola lodging.

### **7.3 Model Parameters and Input Data**

The following data were collected during the 07/2019 -10/2019 and the 10/2020 – 12/2020 growing season.

#### *7.3.1 Weather data*

HOBO temperature and relative humidity (RH) sensors (Onset Computer Corporation, USA) were installed in the greenhouse for additional data collection (Figures 1 and 2 and Table 2). The ET<sub>o</sub> for the local conditions (within) the greenhouse were calculated using the evapotranspiration (ET<sub>o</sub>) calculator, (FAO, 1998). Some variables required for calculating ET<sub>o</sub> were obtained from the automatic weather station (AWS) situated 100 m away from the greenhouse. The AWS uses the CS-500 Vaisala probe (Campbell Scientific, Unites States of America, Logan, UT) to measure temperature and relative humidity (converted into vapour pressure deficit), L1-200 pyranometer (Campbell Scientific, Unites States of America, Logan, UT) to measure solar radiation, and the Penman-Monteith equation to calculate reference evapotranspiration. The signal was transmitted wirelessly, and downloadable files made available from the South African Sugarcane Research Institute (SASRI) weather data portal.

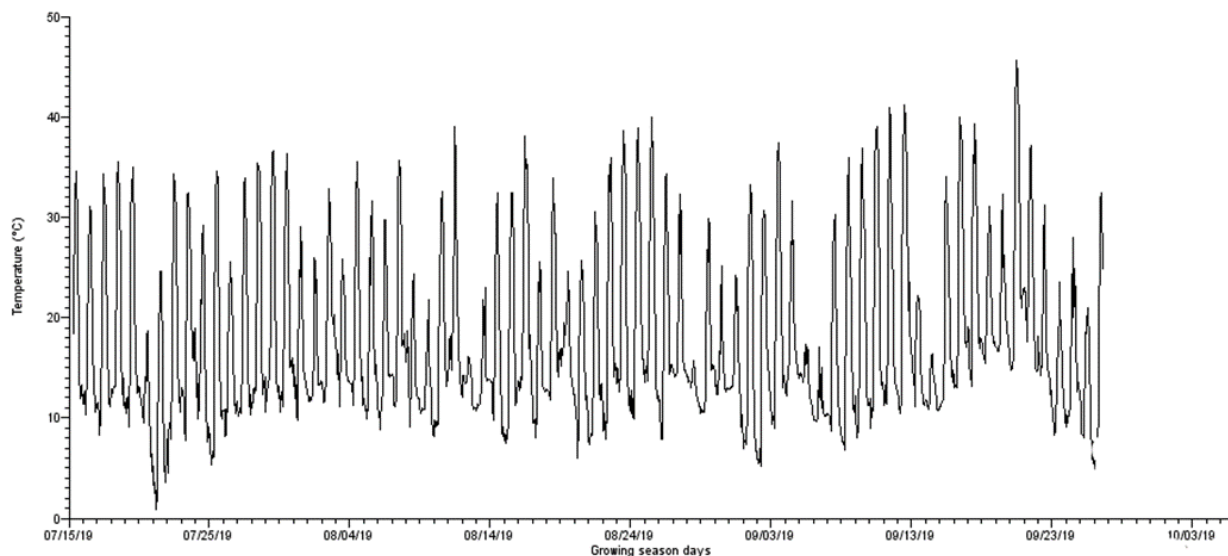


Figure 7.1 Average maximum and minimum temperatures recorded in the greenhouse during the 2019 growing season.

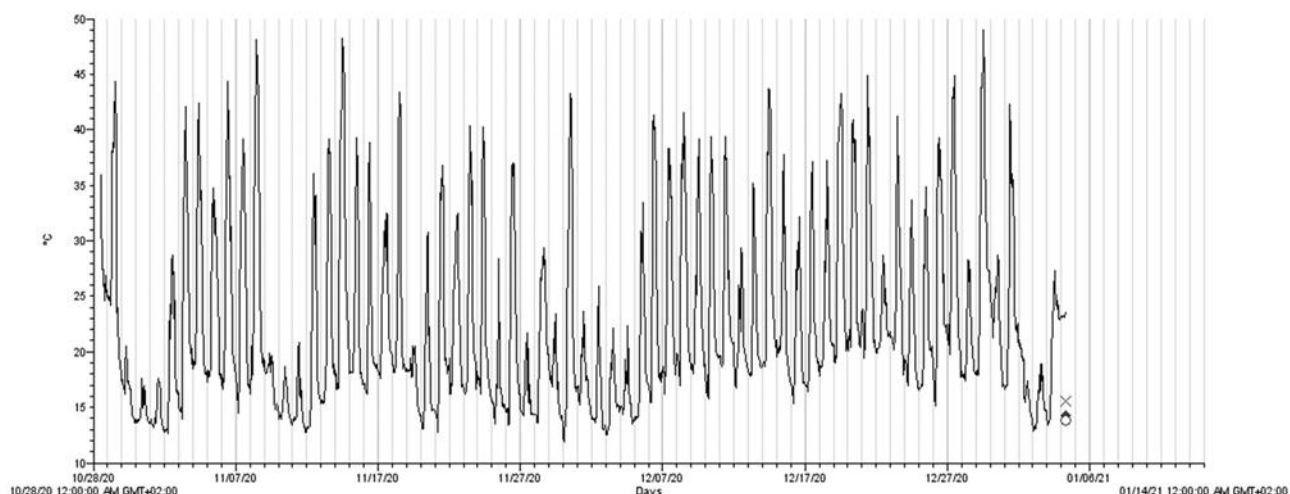


Figure 7.2 Average maximum and minimum temperatures recorded in the greenhouse during the 2020 growing season.

The weather data were used to create the climate file (.CLI) in AquaCrop consisting of  $ET_o$  (.ETO), daily minimum and maximum temperature (.TMP). Solar radiation data was input into the  $ET_o$  calculator (FAO, 1998) for computing  $ET_o$ . There was no daily rainfall file (.PLU).

Table 7.2 Summarised meteorological conditions for the respective growing seasons (S<sub>i</sub>)

Month	$T_{max}$ (°C)		$T_{min}$ (°C)		Solar radiation (J.m <sup>-2</sup> )		ET <sub>o</sub> (mm.d <sup>-1</sup> )	
	S 1	S 2	S 1	S 2	S 1	S 2	S 1	S 2
1	33.0	44.3	9.2	13.5	201. 2	371. 5	7.4	9.6
2	36.0	48.1	10.0	12.7	246.6	416. 9	8.0	9.7
3	39.6	49.0	9.2	12.6	309.6	437. 0	8.7	9.7

### Canopy Cover (CC<sub>x</sub>)

The leaf area index (LAI) was measured every two weeks using the LAI 2200 Canopy Analyser (Li-Cor, USA & Canada). Since AquaCrop uses canopy cover (CC<sub>x</sub>), Equation 7.5 was used to convert LAI to CC<sub>x</sub>. Mabhaudhi et al. (2014) argued that diffuse non-interceptance (DIFN) (Equation 7.6), which is an output of the LAI 2200, can be used to compute CC. The DIFN utilises gap fractions to estimate the sections not “fully” obscured by the growing canopy (Rautiainen et al., 2009; Mabhaudhi et al., 2014). The DIFN value ranges from 0 (no sky visible to the sensor) to 1 (no canopy obscuring the sun).

$$CC = 1 - DIFN \quad 7.5$$

$$DIFN = 2 \int_0^{\frac{\pi}{2}} \overline{cgf}(\theta) \sin \theta \cos \theta d\theta \quad 7.6$$

Where:  $\overline{cgf}$  = canopy gap fraction at zenith angle  $\theta$  (averaged over azimuth angle and horizontal area) (Rautiainen et al., 2009). Since the seedlings were transplanted the initial canopy cover (CC<sub>o</sub>) was calculated by Equation 7.7. The computed CC<sub>o</sub> was 4.5%.

$$CC_o = [plant\ density\ (plants.m^{-2}) \times size\ of\ CC/seedling\ (m^2.plant^{-1})] \times 100 \quad 7.7$$

### Soil data

Soil samples were subjected to soil textural analyses using the hydrometer method. The experiment sampled five depths for textural analysis, and the resultant textural data was fed into the SPAW model (Saxton and Willey, 2005) to determine the saturated hydraulic conductivity ( $k_s$ ) and the bulk density (BD) (Table 7.3). Other soil hydraulic parameters total porosity ( $\theta_s$ ) and residual soil water content ( $\theta_r$ ) were laboratory determined using the soil-water retention pressure method (Klute, 1986; Cresswell et al., 2008; Kanda et al., 2020c). . Soil moisture data was measured weekly using the PR2/6 profile probe at depths of 10-, 20-, 30-, 40-, 60-, and 100 cm. The soil data was used to create the soil file in AquaCrop (.SOL).

Table 7.3 Soil textural and soil hydraulic parameters

Depth (cm)	$\theta_r (cm^3 \cdot cm^{-3})$	$\theta_s (cm^3 \cdot cm^{-3})$	$k_s (cm \cdot d^{-1})$	BD ( $g \cdot cm^{-3}$ )
10	0.52	0.33	5.1	1.28
20	0.52	0.28	9.7	1.27
30	0.55	0.33	13.7	1.19
40	0.60	0.27	38.1	1.07
50	0.56	0.32	18.6	1.16

\*Notes:  $\theta_r$  = residual soil water content (SWC),  $\theta_s$  = total porosity  $k_s$  = saturated hydraulic conductivity and BD = Bulk density.

### Field and water management practices

The experiment was done under greenhouse conditions; hence no rainfed systems were considered. The canola was subjected to optimal and deficit irrigation (DI) regimes. The optimal conditions consisted of irrigating at 100% of the crop water requirements (100%  $ET_c$ ), whereas the DI irrigation regimes consisted of 75%  $ET_c$  and 55%  $ET_c$ . The irrigation intervals were used to create the irrigation file (.IRR). The SWC data was one of the parameters used to create the observation file (.OBS). The .OBS file was used for calibration and validation, respectively. The experiment assumed zero fertility stress. Other field management practices considered were (i) no weeds, (ii) no mulch, and (iii) zero runoff.

### Biomass ( $B$ )

The above-ground biomass ( $B$ ) ( $g \cdot m^{-2}$ ) was harvested three times during each growing season. To avoid border effects, the samples were collected from the middle row. The freshly collected leaves and stems were weighed, and then oven-dried at 85°C for four days until there was consistent mass. The harvest index (HI) was calculated as per Equation 7.8.

$$HI = \frac{Y}{B} \quad 7.8$$

Where:  $HI$  = Harvest index (no units),  $Y$  = yield ( $g \cdot m^{-2}$ ), and  $B$  = above ground biomass ( $g \cdot m^{-2}$ ).

Other crop parameters recorded were transplanting date, amount of irrigation water, agronomic practices, time to flowering, time to yield formation, time to senescence, and harvesting dates.

### Actual evapotranspiration ( $ET_a$ )

The water budget method (Equation 7.9) (Qin, 2015; Kanda et al., 2020a) was used to compute actual evapotranspiration for canola over the growing seasons.



$$ET_a = P_r + I + C - D_r - SR \pm \Delta S \quad 7.9$$

where  $ET_a$  = actual evapotranspiration (mm),  $P_r$  = rainfall/precipitation (mm),  $I$  = irrigation (mm),  $C$  = capillary rise (mm),  $SR$  = surface runoff (mm),  $D_r$  = drainage (mm), and  $\Delta S$  = change in soil water storage (mm).

The experiments were carried out in a greenhouse; hence rainfall was zero. MTI is a subsurface irrigation method; therefore, surface runoff assumed a zero value. The impermeable layer at Ukulinga farm lies at a depth of 60 cm; thus, it prevented drainage and capillary rise (Kanda et al., 2020a).  $ET_a$  was converted from mm to  $m^3.ha^{-1}$  by multiplying Equation 7.8 by 10 (Allen et al., 1998).

### **Water productivity ( $WP_{ET}$ )**

Water productivity ( $WP_{ET}$ ) was computed by Equation 7.10 (Andarzian et al., 2011).

$$WP_{ET} = \frac{Y}{ET_a} \quad 7.10$$

Where  $WP_{ET}$  = water productivity ( $kg.m^{-3}$ ).

## **7.4 Model calibration**

The calibration involved fine-tuning the non-conservative parameters for the canola crop. Table 4 presents summarised conservative and non-conservative values derived from the experiment. The parameters were adopted by Zeleke et al. (2011) for calibrating and testing the FAO AquaCrop model for canola in Wagga Wagga, Australia. The study adopted the canola crop files calibrated by researchers from Lethbridge University Alberta, Canada (LeithbridgeUni, 2020). The crop file was calibrated for warmer and drier climates in Swift Current, Saskatchewan, Canada.

The study destructively measured the seedling leaf area ( $4.50 \text{ cm}^2$ ) of the canola shoots at 90% emergence. Other input parameters were minimum rooting depth at 90% emergence (5 cm) and maximum rooting depth at harvesting. The average maximum rooting depths were 15.69 cm, 16.24cm, 20.41 cm for the 100%  $ET_c$ , 75%  $ET_c$ , and 55%  $ET_c$  irrigation regimes. The

reference harvest index ( $HI_o$ ) was computed using Equation 2. Fine-tuning the  $HI_o$  resulted in adopting a value of 25% for good simulations.

The calibration involved adjusting the non-conservative parameters  $HI_o$ , initial canopy cover ( $CC_o$ ), canopy growth coefficient (CGC) until the simulated CC, B and Y closely matched the observed data. The time to flowering was measured from the day of transplanting, and it was defined as the time when 50% of the plants had visible yellow flowering. Length of the flowering stage was the date after 50% flowering to the date when 50% of the plants had formed pods (Brink, 1997; Kanda et al., 2020a). The maximum rooting depth was measured from the fully matured harvestable plants.

1 Table 7.4 Conservative and non-conservative parameters for canola.

Parameter	Determination	Value		
<b>Conservative</b>				
Base temperature ( $^{\circ}C$ )	Obtained from <a href="#">Zeleeke et al. (2011)</a>	0		
Upper temperature ( $^{\circ}C$ )	Obtained from <a href="#">Zeleeke et al. (2011)</a>	30		
Canopy growth coefficient CGC ( $\% \cdot day^{-1}$ )	Derived by the model using time to reach $CC_x$ and value of $CC_x$	8.9		
Canopy decline coefficient CDC ( $\% \cdot day^{-1}$ )	Derived by the model using time to reach senescence	5.2		
Canopy expansion	Derived by the model using time to reach $CC_x$ and value of $CC_x$	Very fast		
Soil water depletion factor for canopy expansion, upper limit	$P_{upper}$	0.10		
Soil water depletion factor for canopy expansion, lower limit	$P_{lower}$	0.45		
Shape factor for Water stress coefficient for canopy expansion	Obtained from <a href="#">Zeleeke et al. (2011)</a>	3.5		
Soil water depletion factor for stomatal closure	$P_{upper}$	0.45		
Shape factor for Water stress coefficient for stomatal closure	Derived by the model	2.5		
Soil water depletion factor for early canopy senescence	$P_{upper}$	0.70		
Shape factor for Water stress coefficient for canopy senescence	Derived by the model 1	5		
Normalized water productivity $WP^*$ ( $g \cdot m^{-2}$ )	Calibrated from regression of biomass accumulation and $\Sigma Tr/ET_o$	15.0		
Adjustment for yield formation (%)	Obtained from <a href="#">Zeleeke et al. (2011)</a>	100		
Basal crop coefficient (maximum) ( $K_{cb}(x)$ )	Obtained from <a href="#">Zeleeke et al. (2011)</a>	0.95		
<b>Non-conservative</b>		100% $ET_c$	75% $ET_c$	55% $ET_c$
Plant density (plants.m <sup>-2</sup> )	Using intra- and inter-row spacing	9	9	9
Initial canopy cover $CC_o$ (%)	Derived by the model using initial seedling leaf area and plant density	1.25	1.25	1.25
Maximum canopy cover $CC_x$ (%)	Consistent maximum cover read from observed canopy cover curve	93.1	91.1	74.4
Time to maximum canopy cover (d)	Time to reach peak canopy cover converted from LAI data using Equation 3	72	72	72
Time to flowering (d)	Time taken to 50% of the plants to form flowers	32	38	44
Length of the flowering stage (d)	Date after 50% flowering to when 50% of the plants had formed pods	17	19	15
Time to senescence (d)	Time to when no new leaves are formed and at least 10% of plants turn yellow	90	90	51
Maximum rooting depth (m)	Destructive measurement of full-grown plant at harvesting	1.57	1.62	2.04
Minimum effective rooting depth (m)	Destructive measurement of seedling root depth at 90% emergence	0.05	0.05	0.05
Reference harvest index $HI_o$ (%)	Determined from initially from optimum irrigation conditions and calibrated until simulated yield closely matched observed	25	25	25

2

#### 7.4.1 Model validation and evaluation statistics

The model was validated using an independent data set from the 2020 growing season. The data consisted of optimum irrigation (100% ET<sub>c</sub>) and two DI regimes of 75% ET<sub>c</sub> and 55% ET<sub>c</sub>. It was validated, similar to calibration, for SWC, CC<sub>x</sub>, final *B*, *Y* and *WP<sub>ET</sub>*. Statistical analyses were employed to assess the model's ability to simulate canola crop growth and yield under MTI. The study applied the following criteria; normalised root mean square error (*nRMSE*), Wilmott's index of agreement (*d*), Model efficiency (*EF*), and the *R*<sup>2</sup> value to assess the model's performance. The selected criteria are defined by Equations 7.11 – 7.14 (Karandish and Šimůnek, 2019; Kanda et al., 2020c).

$$RMSE = \frac{\sqrt{(\frac{1}{m} \sum_{i=1}^m (O_i - P_i)^2)}}{O_{mean}} \quad 7.11$$

$$d = 1 - \left[ \frac{\sum_{i=1}^m (P_i - O_i)^2}{\sum_{i=1}^m (|P_i - O_{mean}| + |O_i - O_{mean}|)^2} \right] \quad 7.12$$

$$EF = 1 - \left[ \frac{\sum_{i=1}^m (O_i - P_i)^2}{\sum_{i=1}^m (O_i - O_{mean})^2} \right] \quad 7.13$$

$$R^2 = \left[ \frac{\sum_{i=1}^m (O_i P_i) - \sum_{i=1}^m (O_i) \sum_{i=1}^m (P_i)}{\sqrt{[\sum_{i=1}^m O_i^2 - \sum_{i=1}^m (O_i)^2][\sum_{i=1}^m P_i^2 - \sum_{i=1}^m (P_i)^2]}} \right]^2 \quad 7.14$$

Where *O<sub>i</sub>* and *P<sub>i</sub>* = observed and predicted value(s), respectively,  $\bar{O}_i$  = mean observed data, and *m* = number of observations. The error index *nRMSE* showed the model's performance but did not clearly indicate the degree of over or under-estimation, hence using the *EF* statistical tool in the analysis. The *EF* statistic measured the residual variance vs the measured data variance, and it ranges from  $-\infty$  to 1. *EF* values between 0.0 and 1.0 are considered acceptable (Table 7.5); however, Yang et al. (2014) asserted there exists a positive and scattered correlation between *EF* and *d*; thus, when estimating soil water content, a satisfactory agreement can be considered when *EF* is greater than or equal to -1 and when *d* is greater than or equal to 0.60. *R*<sup>2</sup> represents the goodness of fit between the observed and simulated values (Kanda et al., 2020a). For *R*<sup>2</sup>, a range of 0.5 – 1.0 represents good collinearity between observed and simulated values (Moriasi et al., 2007).

Table 7.5 General performance rating for model evaluation statistics

Performance rating	$d$	$EF$
Very good	$0.8 < d < 1.0$	$0.75 < EF < 1.00$
Good	$0.6 < d < 0.8$	$0.65 < EF < 0.75$
Satisfactory	$0.3 < d < 0.6$	$0.50 < EF < 0.65$
Unsatisfactory	$d < 0.2$	$EF \leq 0.50$

$B$ , yield and ET differences were computed as percentage relative differences (%D) using Equation 7.15. Relative differences of  $\pm 10\%$  were considered accurate, whilst differences of  $\pm 20\%$  were deemed acceptable (Farahani et al., 2009; Steduto et al., 2009; Chibarabada et al., 2020).

$$\%D = [(P_i - O_i) / O_i] \times 100 \quad 7.15$$

## 7.5 Results and Discussion

### 7.5.1 Effects of water regimes on growth, yield, and water productivity of canola

The leaf area index, represented by  $CC_x$ , was significantly high for the 100%  $ET_c$  treatment (Figure 7.3).  $CC_x$  under 100%  $ET_c$  was reached after approximately nine weeks after transplanting. Pavlista et al. (2016) reached  $CC_x$  after ten weeks of planting under optimal irrigation conditions. The 75%  $ET_c$  treatment recorded a 91%  $CC_x$  and 85.7%  $CC_x$  for season 1 (S1) and season 2 (S2), respectively. The 55%  $ET_c$  treatment recorded a low 74%  $CC_x$  during S1 and  $CC_x$  of 86% for S2. The 55%  $ET_c$  S2 observation contradicted the norm since severe deficit irrigation is reported to yield a reduced canopy cover. The  $CC_x$  was reached at week eight and week seven after transplanting under 75%  $ET_c$  and 55%  $ET_c$ , respectively. Deficit irrigation allows early crop maturity and small canopy cover as a form of drought avoidance mechanism. Small canopy development occurs to minimise water losses through transpiration (Prasad et al., 2008; Kanda et al., 2020a).

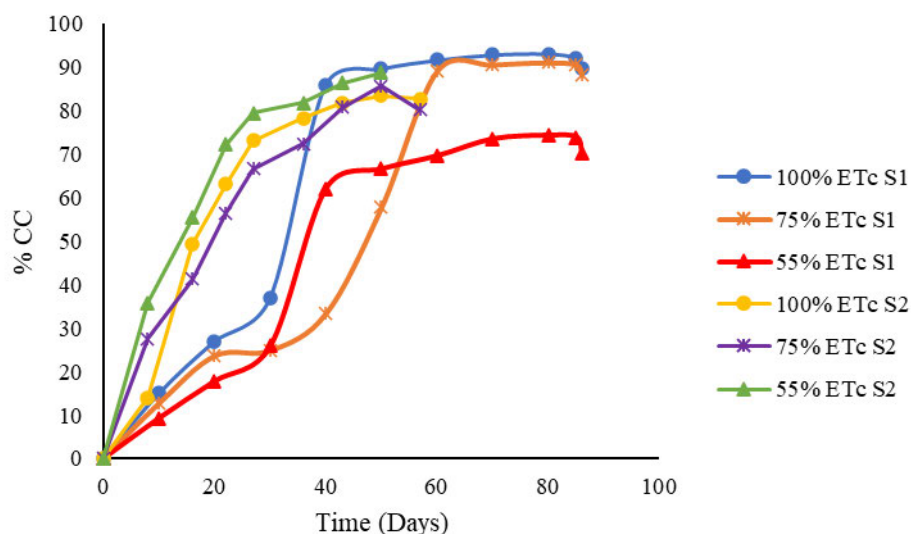


Figure 7.3 Variation in canopy cover for the (a) 100% ET<sub>c</sub>, (b) 75% ET<sub>c</sub>, and (c) 55% ET<sub>c</sub> irrigation regimes over two seasons (S<sub>i</sub>).

Soil water content (SWC) varied across the irrigation regimes (Table 6). Soil water content between the 100% ET<sub>c</sub> and 75% ET<sub>c</sub> did not differ significantly ( $p > 0.05$ ). There was no significant difference between the 75% ET<sub>c</sub> and the 55% ET<sub>c</sub> irrigation regime.

Table 7.6 Effects of irrigation regime on the soil water content

Irrigation regime	Mean water content (mm)
100% ET <sub>c</sub>	413.6 (37.67) <sup>a</sup>
75% ET <sub>c</sub>	416.4 (39.35) <sup>ab</sup>
55% ET <sub>c</sub>	363.1(62.89) <sup>c</sup>
LSD	55.5
CV (%)	12.3

Notes: Mean values in the same column followed by the same superscript letter do not significantly differ at 5% significance by LSD using Duncan's Multiple Test Range. Data in parenthesis are the standard deviations (SD).

Under the 100% ET<sub>c</sub> irrigation regimes, the recorded yields were 1.32 ton.ha<sup>-1</sup>, whilst under the 75% ET<sub>c</sub> and 55% ET<sub>c</sub>, the yield was 0.73 ton.ha<sup>-1</sup> and 0.56 ton.ha<sup>-1</sup>, respectively, during S1. The recorded yields during S2 for the 100% ET<sub>c</sub>, 75% ET<sub>c</sub>, and the 55% ET<sub>c</sub> irrigation regimes were 1.48 ton.ha<sup>-1</sup>, 1.15 ton.ha<sup>-1</sup>, and 0.75 ton.ha<sup>-1</sup>, respectively (Table 7.7).

Table 7.7 Summarised observed yields and biomass accumulation over two growing seasons

Irrigation regime	Season 1		Season 2	
	Yield (ton.ha <sup>-1</sup> )	Biomass (ton.ha <sup>-1</sup> )	Yield (ton.ha <sup>-1</sup> )	Biomass (ton.ha <sup>-1</sup> )
100% ET <sub>c</sub>	1.32	8.26	1.37	4.70
75% ET <sub>c</sub>	0.73	6.51	1.15	3.21
55% ET <sub>c</sub>	0.56	4.43	0.75	3.23

The recorded yields under 100% ET<sub>c</sub> were approximately consistent with Zeleke et al. (2011), who obtained canola yields of about 1.75 ton.ha<sup>-1</sup> using the Bln3343-Co0401 cultivar. Also, Zeleke et al. (2014) recorded canola grain yields of 0.77 ton.ha<sup>-1</sup> – 1.51 ton.ha<sup>-1</sup> under stressed irrigation and final biomasses in the range of 4 ton.ha<sup>-1</sup> – 10.47 ton.ha<sup>-1</sup> for irrigated and stressed canola in Wagga Wagga, Australia. Pavlista et al. (2016) recorded canola grain yields of 1.68 ton.ha<sup>-1</sup> under fully irrigated canola in Nebraska, whilst Safi et al. (2019) recorded a canola grain yield of 1.27 ton.ha<sup>-1</sup>. Majnooni-Heris et al. (2014) also reported a canola yield range of 1.12 ton.ha<sup>-1</sup> -1.78 ton.ha<sup>-1</sup> under full irrigation. Deficit irrigation imposed yield penalties because limited irrigation water supply inhibits canopy growth. Small canopy size results in low biomass, which consequently affects pod formation and grain yield. Biomass accumulation was also influenced by deficit irrigation. Extreme deficit irrigation strategies are not suitable for canola crop growth and yield development. It is worth mentioning that the yields attained were under tunnel conditions and the referenced literature performed the experiments under field conditions. Thus, this study reveals that there is no significant effect in growing canola under tunnel conditions compared to field conditions under full and optimal irrigation.

## 7.6 Calibration

### Soil Water Content

Since AquaCrop is a water-driven model, the model was firstly calibrated for soil water content (SWC). SWC simulations, if done accurately, will improve the accuracy of the simulated biomass and yield (Kanda et al., 2020a). The model satisfactorily simulated the SWC under the 100% ET<sub>c</sub> irrigation regime ( $R^2 = 0.99$ ,  $nRMSE = 16.3\%$ , and  $d = 0.44$ ), thus the model was successfully calibrated for SWC (Figure 4d). The *EF* was significantly low, considering that the model successfully simulated CC<sub>x</sub> under the 100% ET<sub>c</sub> regime. The low *EF* can potentially be attributed to inherent errors experienced during the calibration for CC<sub>x</sub>. Under 100% ET<sub>c</sub>, it is evident that the model over-estimated the SWC. This could be potentially attributed to discrepancies in initiating drainage under the continuous irrigation regime. Furthermore, MTI is a slow-release irrigation

technology hence the delay in wetting the soil to field capacity. Zeleke et al. (2011) attributed the same phenomenon to the lag in AquaCrop to initiate drainage. The model simulated the SWC under the 55% ET<sub>c</sub> regime well ( $R^2 = 0.98$ ,  $EF = 0.93$ ,  $nRMSE = 4.5\%$ , and  $d = 0.98$ ) (Figure 7.4f). Despite having simulated the CC<sub>x</sub> under the 75% ET<sub>c</sub> irrigation regimes well, the model yielded average simulation statistics for SWC ( $R^2 = 0.30$ ,  $EF = 0$ ,  $nRMSE = 15.1\%$ , and  $d = 0.53$ ). Inherent modelling errors in simulating CC<sub>x</sub> can be attributed to the poor  $R^2$  value under the 75% ET<sub>c</sub> irrigation regime (Figure 7.4e).

### **Canopy Cover (CC)**

The model successfully simulated the canopy cover for the 100% ET<sub>c</sub> treatment ( $R^2 = 0.99$ ,  $EF = 0.92$ ,  $nRMSE = 6.4\%$ , and  $d = 0.98$ ) (Figure 7.4a). Under the 75% ET<sub>c</sub> deficit irrigation regime (Figure 7.4b) the model performed well ( $R^2 = 0.99$ ,  $EF = 0.92$ ,  $nRMSE = 10.3\%$ , and  $d = 0.98$ ). The finding concurred with Zeleke et al. (2011) who observed a  $nRMSE = 8.4\% - 12.4\%$ ,  $EF = 0.72 - 0.82$ , and  $d = 0.90 - 0.97$  during AquaCrop calibration for canola grown in Wagga Wagga, Australia. However, under the 55% ET<sub>c</sub> irrigation regime the model under-estimated the CC, the evaluation statistics were:  $R^2 = 0.50$ ,  $nRMSE = 66.3\%$ , and  $d = 0.50$ ). The  $R^2$  and  $d$ -index were within the acceptable range; however, the  $EF$  was very low, and the  $nRMSE$  was significantly high. This resulted from the model capturing poor plant establishment and poor crop development after the transplanting exercise. Zeleke et al. (2011) noted a poor CC<sub>x</sub> whenever AquaCrop picked poor crop establishment and development. A careful calibration for C3 crops under extreme water deficit is required to produce a smooth and fitting CC<sub>x</sub> curve. AquaCrop has simulation inaccuracies when predicting CC<sub>x</sub> under water stress conditions (Zeleke et al., 2011; Ahmadi et al., 2015).



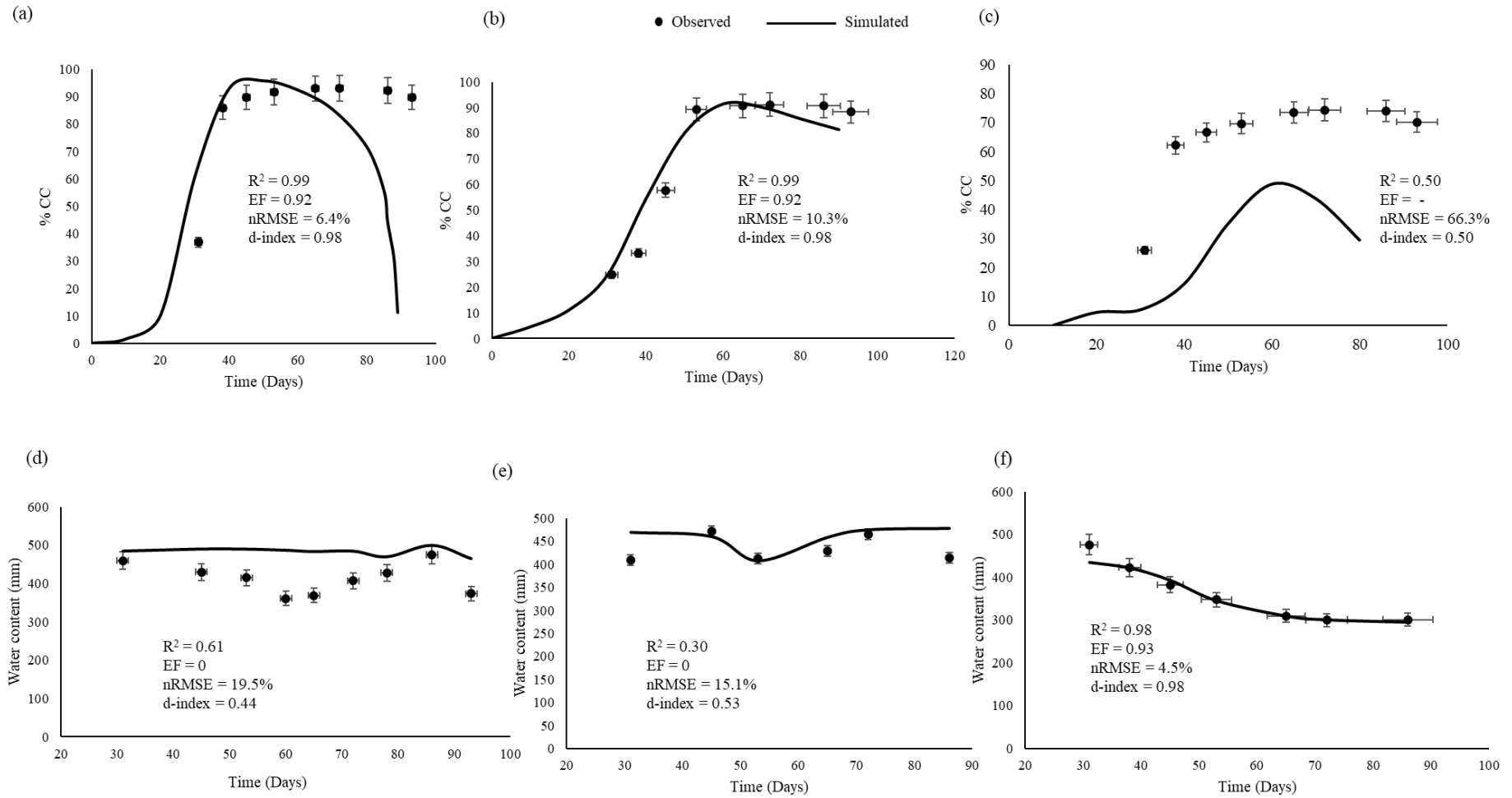


Figure 7.4 Canopy cover (CC) for (a) 100%  $ET_c$ , (b) 75%  $ET_c$ , and (c) 55%  $ET_c$  and soil water content (SWC) for (c) 100%  $ET_c$ , (d) 75%  $ET_c$ , and (e) 55%  $ET_c$  irrigation regimes during calibration.

## Biomass and Yield

The model generally simulated the biomass well (Table 7.8). The model satisfactorily simulated the biomass accumulation for the 100%  $ET_c$  and 75%  $ET_c$  irrigation regimes ( $R^2 > 0.90$ ,  $EF > 0.50$ , and  $d > 0.89$ ). The  $nRMSE$  under 100  $ET_c$  was 6.1%, and under 75%  $ET_c$  was 37.3%, signifying a high residual variance in estimating the biomass. The model simulated the biomass under the 55%  $ET_c$  irrigation regime well ( $R^2 = 0.90$ ,  $EF = 0.30$ ,  $nRMSE = 26.9\%$ , and  $d = 0.75$ ) (Figure 7.5). The  $nRMSE = 26.9\%$  was seemingly high; however, Ahmadi et al. (2015) asserted that an  $nRMSE < 30\%$  could be acceptable for crop simulation models. Thus, AquaCrop was successfully calibrated for biomass accumulation. It is worth noting that under the 55%  $ET_c$  irrigation regime, the model under-estimated biomass by 25.50% (Figure 7.5c). This is a common phenomenon with AquaCrop under deficit irrigation scenarios (Kanda et al., 2020a). On the contrary, Zeleke et al. (2011) showed that AquaCrop over-estimated the canola biomass because of heat stress. This study, however, was carried out during the winter (cool) season. The model simulated biomass with deviations of -27.48%, -2.30%, and 20.31%. The deviations fell within the acceptable ranges; thus, further asserting that the model was successfully calibrated for biomass under MTI.

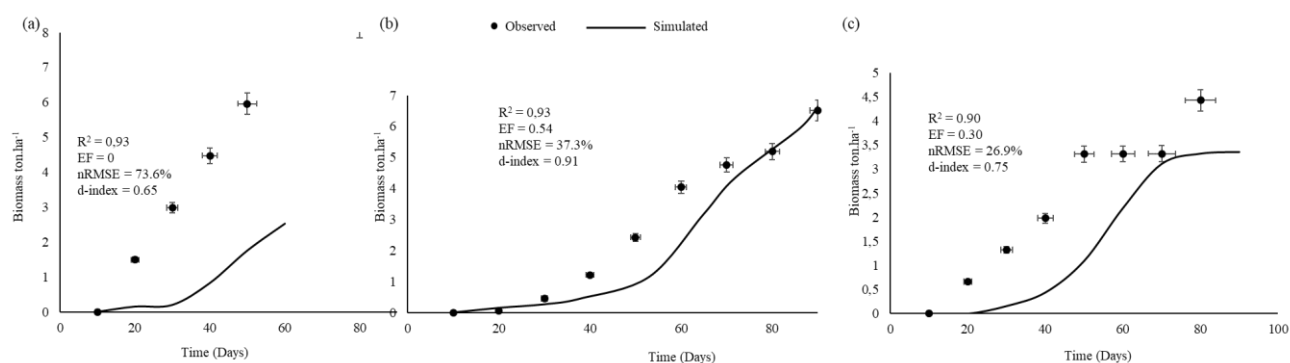


Figure 7.5 Observed and simulated biomass under (a) 100%  $ET_c$ , (b) 75%  $ET_c$ , and (c) 55%  $ET_c$  irrigation regimes.

The model over-estimated yield simulations despite having simulated CC well. Yield simulations were in the over-estimation range of  $\pm 34\%$  -  $\pm 97\%$  and an under-estimation under the 100%  $ET_c$  water regime, all of which are deemed unacceptable (Table 7.8). The inability of AquaCrop to simulate yield can be attributed to the low heat units available during the winter season in which the experiment was run. Spring canola cultivar is a cool-season crop that

requires a substantial amount of heat units for optimal growth (Pavlista et al., 2016). Hergert et al. (2016) also attributed low grain yield for canola to frost.

Table 7.8 Observed and simulated yield and final biomass during calibration

Irrigation regime	Yield (ton.ha <sup>-1</sup> )			Biomass (ton.ha <sup>-1</sup> )		
	Observed	Simulated	D (%) <sup>a</sup>	Observed	Simulated	D (%) <sup>a</sup>
100% ET <sub>c</sub>	1.32 (0.34)	0.87	34.17	8.26 (2.58)	4.01	51.45
75% ET <sub>c</sub>	0.73 (0.12)	1.44	-97.26	6.51 (2.32)	6.46	0.77
55% ET <sub>c</sub>	0.56 (0.12)	0.89	-58.9	4.43 (1.44)	3.35	20.31

<sup>a</sup> Data in parenthesis are the standard deviations, Deviation (D) =  $[(O_i - P_i) \div O_i] \times 100$

### Water productivity (WP<sub>ET</sub>)

The model successfully predicted the grain WP<sub>ET</sub> under 100% ET<sub>c</sub> and 75% ET<sub>c</sub> irrigation regimes and, more interestingly, under 55% ET<sub>c</sub> since the yield was low. Under the 100% ET<sub>c</sub> the observed WP<sub>ET</sub> was 0.42 kg.m<sup>-3</sup> whilst the simulated was 0.36 kg.m<sup>-3</sup> (D = 14.29%). Under the 75% ET<sub>c</sub>, the observed and simulated WP<sub>ET</sub> were 0.48 and 0.49 kg.m<sup>-3</sup>, respectively, whilst under the 55% ET<sub>c</sub>, the observed and simulated WP<sub>ET</sub> was 0.26 kg.m<sup>-3</sup>. The WP<sub>ET</sub> under the 55% ET<sub>c</sub> represented an optimal calibration scenario, whilst under the 100% ET<sub>c</sub> irrigation regime, the model under-estimated the WP<sub>ET</sub> by 13% and over-estimated WP<sub>ET</sub> by 2.1% under the 75% ET<sub>c</sub> irrigation regime. The observed WP<sub>ET</sub> under the 100% ET<sub>c</sub> and 75% ET<sub>c</sub> irrigation regimes slightly matched those reported by Kumar et al. (2014) for potatoes (C3 crop) grown in saline soils. The reported WP<sub>ET</sub> were in the range of 0.63 kg.m<sup>-3</sup> – 0.98 kg.m<sup>-3</sup>, although the model exhibited a low *EF* of 0.27.

## 7.7 Model validation

Model validation was done after the calibration exercise. An independent dataset from the 2020 growing season was used to validate the model. Canola was transplanted on 27/10/2020 and harvested on 04/01/2021.

### Soil water content

The model successfully simulated the SWC under the 100% ET<sub>c</sub> irrigation regime ( $R^2 = 0.90$ ,  $EF = 0.37$ ,  $nRMSE = 8.7\%$ , and  $d = 0.83$ ) and 75% ET<sub>c</sub> irrigation regime ( $R^2 = 0.91$ ,  $EF = 0.17$ ,  $nRMSE = 4.1\%$ , and  $d = 0.79$ ) (Figures 7.6d and 7.6e). The *EF* was relatively low, but it signified a generally good model performance for crop models (Yang et al., 2014). The model reasonably simulated the SWC under the 55% ET<sub>c</sub> irrigation regime ( $R^2 = 0.55$ ,  $EF = 0.05$ ,  $nRMSE = 9.6\%$ , and  $d = 0.63$ ). The observation was attributed to the poor CC<sub>x</sub> simulations'

errors in which the model under-estimated the canopy growth (Figure 7.6c). The model successfully simulated SWC during the flowering and yield formation stages across all three irrigation regimes. The evidence revealed the capability of AquaCrop to simulate soil water content with reasonable accuracy for canola grown under MTI.

### Canopy cover (CC<sub>x</sub>)

The model successfully simulated the CC under the 100% ET<sub>c</sub> ( $R^2 = 0.97$ ,  $EF = 0.93$ ,  $nRMSE = 22.5\%$ , and  $d = 0.98$ ) (Figure 7.6a). Under the 75% ET<sub>c</sub> the successfully simulated canopy growth during the early stages of plant growth ( $R^2 = 0.84$ ,  $EF = 0.45$ ,  $nRMSE = 59.2\%$ , and  $d = 0.86$ ), but it however under-estimated the canopy growth (Figure 6b). The model poorly simulated the CC under the 55% ET<sub>c</sub> irrigation regime ( $R^2 = 0.61$ ,  $nRMSE = 87.9\%$ , and  $d = 0.40$ ). This finding is consistent with literature that states that AquaCrop inaccurately simulates CC<sub>x</sub> under water stress conditions for various crops such as sunflower Todorovic et al. (2009), maize Ahmadi et al. (2015), cotton Farahani et al. (2009), canola Zeleke et al. (2011), and cowpea Kanda et al. (2020a).

### Biomass and yield

The model simulated the yield with accuracy. The observed deviations (%D) were 7.43%, -25.22%, and 12.0% for the 100% ET<sub>c</sub>, 75% ET<sub>c</sub>, and 55% ET<sub>c</sub> irrigation regimes, respectively (Table 7.9). The findings concur with Zeleke et al. (2011), who found the  $D = -2.1\% - 12\%$  for spring canola cultivars grown in Wagga Wagga, Australia. The results obtained during validation were relatively accurate than those obtained during calibration.

Table 7.9 Observed and simulated yield and final biomass during validation

Irrigation regime	Yield (ton.ha <sup>-1</sup> )			Biomass (ton.ha <sup>-1</sup> )		
	Observed	Simulated	D (%) <sup>a</sup>	Observed	Simulated	D (%) <sup>a</sup>
100% ET <sub>c</sub>	1.48 (0.20)	1.37	7.43	4.70 (2.20)	7.26	-54.47
75% ET <sub>c</sub>	1.15 (0.29)	1.44	-25.22	3.21(1.50)	6.46	-100
55% ET <sub>c</sub>	0.75 (0.10)	0.66	12	3.23(1.50)	2.58	20.12

<sup>a</sup> Data in parenthesis are the standard deviations, Deviation (D) =  $[(O_i - P_i) \div O_i] \times 100$

The model over-estimated the final biomass under 100% ET<sub>c</sub> and the 75% ET<sub>c</sub> irrigation regimes giving  $D \geq \pm 54.47\%$  deviations. The model reasonably simulated the biomass data under the 55% ET<sub>c</sub> irrigation regime ( $D = 20.12\%$ ). The presented evidence demonstrates that AquaCrop can confidently simulate crop yields and biomass for canola under various MTI regimes with necessary adjustments.

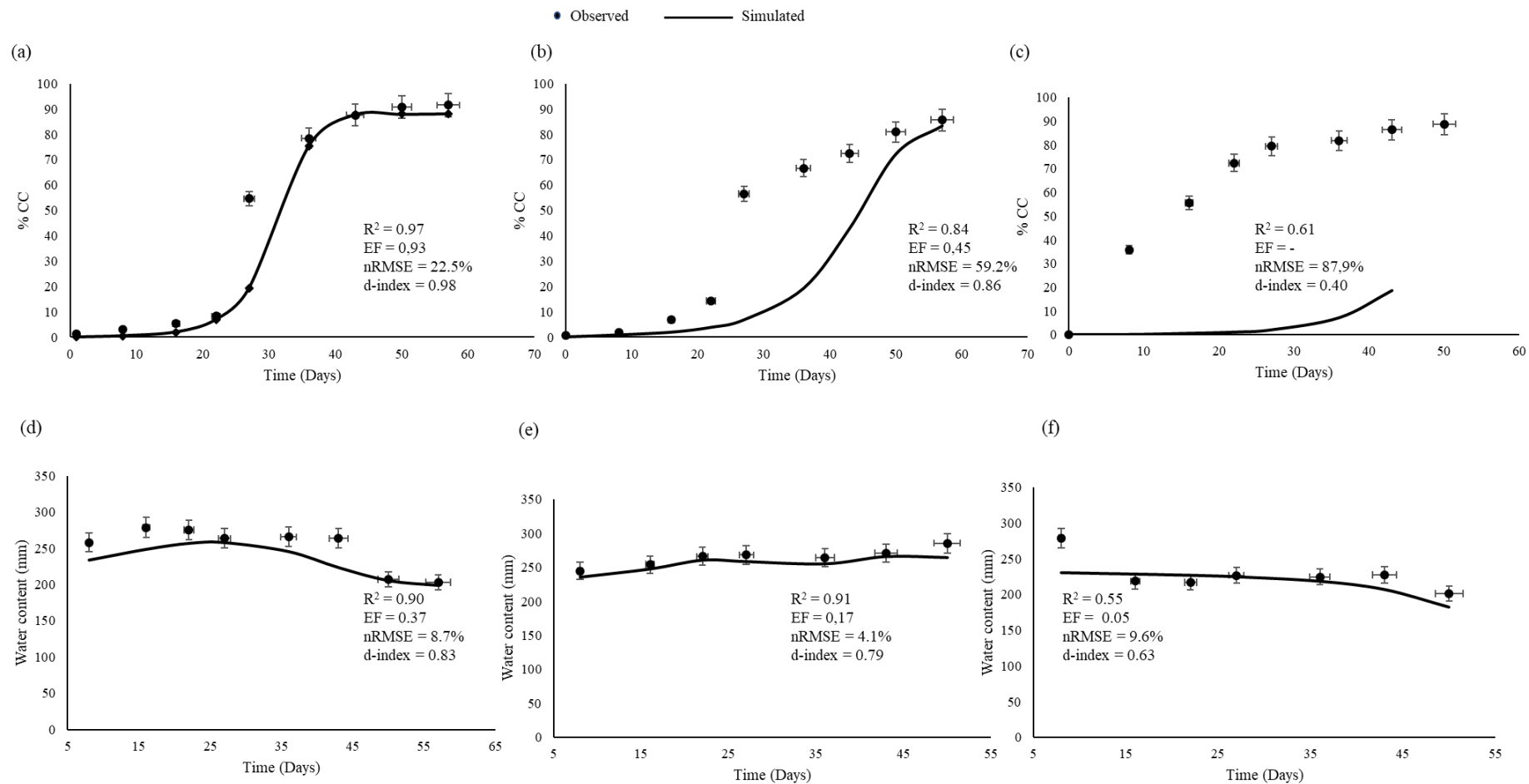


Figure 7.6 Canopy cover (CC) for (a) 100%  $ET_c$ , (b) 75%  $ET_c$ , and (c) 55%  $ET_c$  and soil water content (SWC) for (c) 100%  $ET_c$ , (d) 75%  $ET_c$ , and (e) 55%  $ET_c$  irrigation regimes during validation

### **Water productivity ( $WP_{ET}$ )**

The simulated  $WP_{ET}$  across the three irrigation regimes matched those obtained during calibration; thus, AquaCrop was successfully calibrated and validated for simulating  $WP_{ET}$ . Under the 100%  $ET_c$  the observed  $WP_{ET}$  was  $0.42 \text{ kg.m}^{-3}$  whilst the simulated was  $0.36 \text{ kg.m}^{-3}$  ( $D = 14.29\%$ ). Under the 75%  $ET_c$ , the observed and simulated  $WP_{ET}$  were 0.48 and 0.49  $\text{kg.m}^{-3}$ , respectively, whilst under the 55%  $ET_c$ , the observed and simulated  $WP_{ET}$  was 0.26  $\text{kg.m}^{-3}$ . The D values were within the good range ( $D \leq \pm 15\%$ ).  $WP_{ET}$  was high under the 75%  $ET_c$ , signifying that optimal yields and  $WP_{ET}$  can be achieved with optimal deficit irrigation management practices.

### **7.8 Conclusions and Recommendations**

The study sought to calibrate and validate the FAO AquaCrop model for canola grown under MTI and local South Africa conditions. The study was premised on the hypothesis that AquaCrop cannot effectively simulate yield response of canola under varying irrigation regimes. The study thus failed to reject the null hypothesis for the 100%  $ET_c$  and 75%  $ET_c$  and rejected the hypothesis for the 55%  $ET_c$  irrigation regime... The model was successfully calibrated and validated for soil water content, canopy cover, biomass accumulation, final biomass, yield and water productivity under 100%  $ET_c$  and 75%  $ET_c$  irrigation regimes. AquaCrop poorly simulated the canopy cover and the SWC under the extreme deficit irrigation regime (55%  $ET_c$ ). The poor simulation results can potentially be attributed to canola's sensitivity to extreme deficit irrigation scenarios. The study revealed that good deficit irrigation regimes could achieve optimum canola growth. The 75%  $ET_c$  irrigation regime had an optimal grain yield and relatively high water productivity ( $WP_{ET}$ ) compared to the 100%  $ET_c$  irrigation regime. Thus, appropriate deficit management practices can produce high biomass and lower yield penalties. The study revealed the capability of the AquaCrop model to simulate canola response to various irrigation regimes. It is recommended that the study be done in open field conditions and assess the reliability of the reported results in this study. Also, the authors recommend the study be carried over several DI regimes and investigate the  $WP_{ET}$  and yield correlation. In addition, the field experiments will generate an independent data set that will be used to further test AquaCrop.

## 7.9 References

- Abedinpour, M, Sarangi, A, Rajput, T, Singh, M, Pathak, H and Ahmad, T. 2012. Performance evaluation of AquaCrop model for maize crop in a semi-arid environment. *Agricultural Water Management* 110 55-66.
- Ahmadi, SH, Mosallaeepour, E, Kamgar-Haghighi, AA and Sepaskhah, AR. 2015. Modeling maize yield and soil water content with AquaCrop under full and deficit irrigation managements. *Water Resources Management* 29 (8): 2837-2853.
- Allen, RG, Pereira, LS, Raes, D and Smith, M. 1998. *Crop evapotranspiration-Guidelines for computing crop water requirements-FAO Irrigation and drainage paper 56*. FAO, Rome, Italy.
- Andarzian, B, Bannayan, M, Steduto, P, Mazraeh, H, Barati, M, Barati, M and Rahnema, A. 2011. Validation and testing of the AquaCrop model under full and deficit irrigated wheat production in Iran. *Agricultural Water Management* 100 (1): 1-8.
- Araya, A, Habtu, S, Hadgu, KM, Kebede, A and Dejene, T. 2010a. Test of AquaCrop model in simulating biomass and yield of water deficient and irrigated barley (*Hordeum vulgare*). *Agricultural Water Management* 97 (11): 1838-1846.
- Araya, A, Keesstra, S and Stroosnijder, L. 2010b. Simulating yield response to water of Teff (*Eragrostis tef*) with FAO's AquaCrop model. *Field Crops Research* 116 (1-2): 196-204.
- Bañuelos, GS, Bryla, DR and Cook, CG. 2002. Vegetative production of kenaf and canola under irrigation in central California. *Industrial Crops Products* 15 (3): 237-245.
- Bauböck, R. 2014. Simulating the yields of bioenergy and food crops with the crop modeling software BioSTAR: the carbon-based growth engine and the BioSTAR ET<sub>0</sub> method. *Environmental Sciences Europe* 26 (1): 1-9.
- Brink, M. 1997. Rates of progress towards flowering and podding in bambara groundnut (*Vigna subterranea*) as a function of temperature and photoperiod. *Annals of Botany* 80 (4): 505-513.
- Chibarabada, T, Modi, A and Mabhaudhi, T. 2020. Calibration and evaluation of aquacrop for groundnut (*Arachis hypogaea*) under water deficit conditions. *Agricultural Forest Meteorology* 281: 107850.
- Chimonyo, VGP, Wimalasiri, EM, Kunz, R, Modi, AT and Mabhaudhi, T. 2020. Optimizing traditional cropping systems under climate change: a case of maize landraces and bambara groundnut. *Frontiers in Sustainable Food Systems* 4:153-171.
- Cresswell, H, Green, T and McKenzie, N. 2008. The adequacy of pressure plate apparatus for determining soil water retention. *Soil Science Society of America Journal* 72 (1): 41-49.
- Dirwai, TL, Mabhaudhi, T, Kanda, EK and Senzanje, A. 2021. Moistube irrigation technology development, adoption and future prospects: A systematic scoping review. *Heliyon* 7 (2): e06213.
- FAO. 1998. *Crop evapotranspiration - Guidelines for computing crop water requirements*. FAO Irrigation and Drainage paper 56. FAO, Rome, Italy.
- Farahani, HJ, Izzi, G and Oweis, TY. 2009. Parameterization and evaluation of the AquaCrop model for full and deficit irrigated cotton. *Agronomy Journal* 101 (3): 469-476.
- Foster, T, Brozović, N, Butler, AP, Neale, CMU, Raes, D, Steduto, P, Fereres, E and Hsiao, TC. 2017. AquaCrop-OS: An open source version of FAO's crop water productivity model. *Agricultural Water Management* 181: 18-22.
- Fujihara, Y, Tanaka, K, Watanabe, T, Nagano, T and Kojiri, T. 2008. Assessing the impacts of climate change on the water resources of the Seyhan River Basin in Turkey: Use of

- dynamically downscaled data for hydrologic simulations. *Journal of Hydrology* 353 (1-2): 33-48.
- Geerts, S, Raes, D and Garcia, M. 2010. Using AquaCrop to derive deficit irrigation schedules. *Agricultural Water Management* 98 (1): 213-216.
- He, D, Wang, E, Wang, J, Lilley, J, Luo, Z, Pan, X, Pan, Z and Yang, N. 2017. Uncertainty in canola phenology modelling induced by cultivar parameterization and its impact on simulated yield. *Agricultural and Forest Meteorology* 232: 163-175.
- Heng, LK, Hsiao, T, Evett, S, Howell, T and Steduto, P. 2009. Validating the FAO AquaCrop model for irrigated and water deficient field maize. *Agronomy Journal* 101 (3): 488-498.
- Hergert, G, Margheim, J, Pavlista, A, Martin, D, Isbell, T and Supalla, R. 2016. Irrigation response and water productivity of deficit to fully irrigated spring camelina. *Agricultural Water Management* 177: 46-53.
- Iqbal, MA, Shen, Y, Stricevic, R, Pei, H, Sun, H, Amiri, E, Penas, A and del Rio, S. 2014. Evaluation of the FAO AquaCrop model for winter wheat on the North China Plain under deficit irrigation from field experiment to regional yield simulation. *Agricultural Water Management* 135: 61-72.
- Jin, X-l, Feng, H-k, Zhu, X-k, Li, Z-h, Song, S-n, Song, X-y, Yang, G-j, Xu, X-g and Guo, W-s. 2014. Assessment of the AquaCrop model for use in simulation of irrigated winter wheat canopy cover, biomass, and grain yield in the North China Plain. *PloS one* 9 (1): e86938.
- Kanda, EK, Niu, W, Mabhaudhi, T and Senzanje, A. 2019. Moistube Irrigation Technology: A Review. *Agricultural Research* 9 (2): 139-147.
- Kanda, EK, Senzanje, A and Mabhaudhi, T. 2020a. Calibration and validation of the AquaCrop model for full and deficit irrigated cowpea (*Vigna unguiculata* (L.) Walp). *Physics Chemistry of the Earth, Parts A/B/C* 115(2020): 102941.
- Kanda, EK, Senzanje, A and Mabhaudhi, T. 2020b. Effect of Moistube and subsurface drip irrigation on cowpea (*Vigna unguiculata* (L.) Walp) production in South Africa. *Water SA* 46 (2): 197-204.
- Kanda, EK, Senzanje, A and Mabhaudhi, T. 2020c. Soil water dynamics under Moistube irrigation. *Physics Chemistry of the Earth, Parts A/B/C* 115 102836.
- Kang, Y, Khan, S and Ma, X. 2009. Climate change impacts on crop yield, crop water productivity and food security—A review. *Progress in Natural Science* 19 (12): 1665-1674.
- Karandish, F and Šimůnek, J. 2019. A comparison of the HYDRUS (2D/3D) and SALTMED models to investigate the influence of various water-saving irrigation strategies on the maize water footprint. *Agricultural Water Management* 213: 809-820.
- Katuwal, KB, Angadi, SV, Singh, S, Cho, Y, Begna, S and Umesh, M. 2018. Growth-Stage-Based Irrigation Management on Biomass, Yield, and Yield Attributes of Spring Canola in the Southern Great Plains. *Crop Science* 58 (6): 2623-2632.
- Katuwal, KB, Cho, Y, Singh, S, Angadi, SV, Begna, S and Stamm, M. 2020. Soil water extraction pattern and water use efficiency of spring canola under growth-stage-based irrigation management. *Agricultural Water Management* 239:106232.
- Khalili, M, Aboughadareh, AP, Naghavi, MR and Talebzadeh, S. 2012. Response of spring canola (*Brassica napus* L.) genotypes to water deficit stress. *Int. J. Agric. Crop Sci* 4: 1579-1586.
- Klute, A. 1986. *Water retention: laboratory methods*. American Society of Agronomy-Soil Science Society of America, Madison, USA.
- Korres, NE, Norsworthy, JK, Tehranchian, P, Gitsopoulos, TK, Loka, DA, Oosterhuis, DM, Gealy, DR, Moss, SR, Burgos, NR and Miller, MR. 2016. Cultivars to face climate



- change effects on crops and weeds: a review. *Agronomy for Sustainable Development* 36 (1): 12-34.
- Kumar, P, Sarangi, A, Singh, D and Parihar, S. 2014. Evaluation of AquaCrop model in predicting wheat yield and water productivity under irrigated saline regimes. *Irrigation and Drainage* 63 (4): 474-487.
- LeithbridgeUni. 2020. Canola Swift Current Dataset. University, L. Leithbridge University. Alberta, Canada.
- Locascio, SJ. 2005. Management of Irrigation for Vegetables: Past, Present, and Future. *HortTechnology* 15 (3): 482-485.
- Lordkipanidze, N, Epperson, J and Ames, G. 1998. An Economic Analysis of the Import Demand for Canola Oil in the United States. *Journal of International Food & Agribusiness Marketing* 9 (4): 23-34.
- Mabhaudhi, T, Modi, AT and Beletse, YG. 2014. Parameterisation and evaluation of the FAO-AquaCrop model for a South African taro (*Colocasia esculenta* L. Schott) landrace. *Agricultural Forest Meteorology* 192: 132-139.
- Majnooni-Heris, A, Nazemi, AH and Sadraddini, AA. 2014. Effects of deficit irrigation on the yield, yield components, water and irrigation water use efficiency of spring canola. *Biodivers. Environ. Sci* 5 44-53.
- Maniruzzaman, M, Talukder, M, Khan, M, Biswas, J and Nemes, A. 2015. Validation of the AquaCrop model for irrigated rice production under varied water regimes in Bangladesh. *Agricultural Water Management* 159: 331-340.
- Montoya, F, Camargo, D, Ortega, J, Córcoles, J and Domínguez, A. 2016. Evaluation of Aquacrop model for a potato crop under different irrigation conditions. *Agricultural Water Management* 164: 267-280.
- Moriasi, DN, Arnold, JG, Van Liew, MW, Bingner, RL, Harmel, RD and Veith, TL. 2007. Model evaluation guidelines for systematic quantification of accuracy in watershed simulations. *Transactions of the ASABE* 50 (3): 885-900.
- Mustafa, M, Mabhaudhi, T, Avvari, M and Massawe, F. 2020. Transition toward sustainable food systems: a holistic pathway toward sustainable development. In: ed. Galanakis, C, *Food Security and Nutrition*. Academic Press, London, United Kingdom.
- Nyathi, M, Van Halsema, G, Annandale, J and Struik, P. 2018. Calibration and validation of the AquaCrop model for repeatedly harvested leafy vegetables grown under different irrigation regimes. *Agricultural Water Management* 208: 107-119.
- Pavlista, A, Hergert, G, Margheim, J and Isbell, T. 2016. Growth of spring canola (*Brassica napus*) under deficit irrigation in Western Nebraska. *Industrial Crops Products* 83: 635-640.
- Prasad, P, Staggenborg, S and Ristic, Z. 2008. Impacts of drought and/or heat stress on physiological, developmental, growth, and yield processes of crop plants. In: eds. Ahuja, LR, Reddy, VR, Saseendran, SA and Yu, Q, *Response of crops to limited water: Understanding and Modelling Water Stress Effects on Plant Growth Processes*. American Society of Agronomy, Wisconsin, USA.
- Qian, B, Jing, Q, Zhang, X, Shang, J, Liu, J, Wan, H, Dong, T, De Jong, R and Naeth, MA. 2019. Adapting estimation methods of daily solar radiation for crop modelling applications in Canada. *Canadian Journal of Soil Science* 99 (4): 533-547.
- Qin, W. 2015. Exploring options for improving water and nitrogen use efficiency in crop production systems. Unpublished thesis, Wageningen University, Wageningen, The Netherlands.
- Raes, D, Steduto, P, Hsiao, TC and Fereres, E. 2009. AquaCrop—the FAO crop model to simulate yield response to water: II. Main algorithms and software description. *Agronomy Journal* 101 (3): 438-447.

- Rautiainen, M, Möttöus, M and Stenberg, P. 2009. On the relationship of canopy LAI and photon recollision probability in boreal forests. *Remote Sensing of Environment* 113 (2): 458-461.
- Raymer, PL. 2002. Canola: an emerging oilseed crop. In: eds. Janick, J and Whipkey, A, *Trends in new crops new uses*. ASHS Press, Alexandria, Virginia, USA.
- Robertson, M and Kirkegaard, J. 2003. Crop modelling for the Australian canola industry: a review. In: ed. Edwards, J, *13th Australian research assembly on Brassicas*, 8-12. NSW Agriculture, Tamworth Regional Entertainment Centre, Tamworth, New South Wales.
- Safi, S, Kamgar-Haghighi, A, Zand-Parsa, S, Emam, Y and Honar, T. 2019. Evaluation of yield, actual crop evapotranspiration and water productivity of two canola cultivars as influenced by transplanting and seeding and deficit irrigation. *International Journal of Plant Production* 13 (1): 23-33.
- Steduto, P, Hsiao, TC, Raes, D and Fereres, E. 2009. AquaCrop—The FAO crop model to simulate yield response to water: I. Concepts and underlying principles. *Agronomy Journal* 101 (3): 426-437.
- Taylor, A, Smith, C and Wilson, I. 1991. Effect of irrigation and nitrogen fertilizer on yield, oil content, nitrogen accumulation and water use of canola (*Brassica napus* L.). *Fertilizer Research* 29 (3): 249-260.
- Todorovic, M, Albrizio, R, Zivotic, L, Saab, MTA, Stöckle, C and Steduto, P. 2009. Assessment of AquaCrop, CropSyst, and WOFOST models in the simulation of sunflower growth under different water regimes. *Agronomy Journal* 101 (3): 509-521.
- Toumi, J, Er-Raki, S, Ezzahar, J, Khabba, S, Jarlan, L and Chehbouni, A. 2016. Performance assessment of AquaCrop model for estimating evapotranspiration, soil water content and grain yield of winter wheat in Tensift Al Haouz (Morocco): Application to irrigation management. *Agricultural Water Management* 163: 219-235.
- Vanuytrecht, E, Raes, D and Willems, P. 2014. Global sensitivity analysis of yield output from the water productivity model. *Environmental Modelling Software* 51 323-332.
- Yang, J, Yang, J, Liu, S and Hoogenboom, G. 2014. An evaluation of the statistical methods for testing the performance of crop models with observed data. *Agricultural Systems* 127 (2014): 81-89.
- Yang, W, Tian, L, Du, T, Ding, R and Yang, Q. 2008. Research Prospect of the Water-saving Irrigation by Semi-permeable Film [J]. *Journal of Water Resources and Water Engineering* 6:16.
- Zeleeke, K, Luckett, D and Cowley, R. 2014. Response of canola (*Brassica napus* L.) and mustard (*B. juncea* L.) to different watering regimes. *Experimental Agriculture* 50 (4): 573.
- Zeleeke, KT, Luckett, D and Cowley, R. 2011. Calibration and testing of the FAO AquaCrop model for canola. *Agronomy Journal* 103 (6): 1610-1618.
- Zhang, B, Fu, Z, Wang, J and Zhang, L. 2019. Farmers' adoption of water-saving irrigation technology alleviates water scarcity in metropolis suburbs: A case study of Beijing, China. *Agricultural Water Management* 212: 349-357.

## **8 SUMMARY, CONCLUSIONS AND RECOMMENDATIONS**

A knowledge gap exists around the MTI subject area. For instance how does the MTI discharge mechanism influence water and solute movement in the variably saturated zone (vadose zone). Understanding the wetting characteristics and solute movement or nutrients migration for MTI under field crops production is essential for MTI design. Treated waste water is an alternative source of irrigation water since it reduce the demand for fresh water irrigation and it contains nutrients from human excreta. Thus, this thesis carried out a systematic characterisation on MTI discharge and its application to field crops production under chemigation. The modelling approach adopted in this study (especially Chapters 6 and 7) provided real time insights of solute movement or nutrient migration and the subsequent periodic moisture movement during and after the chemigation event. The soil in question was a silty clay soil.

### **8.1 Summary**

MTI characterisation informs the irrigation knowledge body by informing the operation and maintenance of MTI under specific conditions. For example, in this study, MTI performance under induced negative pressure can potentially inform irrigators on realistic matric potential informed irrigation schedules. In addition, knowledge on membrane degradation provides insights on whether irrigators should adopt full or intermittent MTI operations. On soil wetting geometries, soil texture influences the wetting pattern of MTI. Full irrigations and optimal deficit irrigation strategies irrigation minimise leaching as compared to the extreme deficit irrigation strategy. Full and optimal deficit MTI readily availing nutrients for plant uptake. The following sections provide concise conclusions and key recommendation for the specific research work carried out on MTI.

### **8.2 Conclusions**

#### *8.2.1 Evaporative demand*

Realistic matric potential informed irrigation schedules are essential in maximising water use efficiency and managing energy requirements for irrigation water conveyance. When MTI is exposed to an artificially induced evaporative demand, a negative pressure develops that induces discharge. The induced discharge facilitates moisture release in minute quantities that

match crop water requirements. The concept is relevant as it assists irrigators cope with CC driven unstable planned crop water use patterns. The research work concluded that MTI can effect discharge under an artificial evaporative demand. The implication being high matric potential soils can induce a high MTI discharged for a specified period of time.

#### 8.2.2 *Moistube irrigation plugging*

The study also investigated MTI plugging under two effluent namely, anaerobic filtered (AF) and horizontal flow constructed wetland (HFCW) effluent. The study experimentally deduced potential plugging coefficients ( $\alpha$ ). The experiment revealed that the HFCW effluent clogged faster than the AF effluent. The study also revealed that the effluents were unsuitable for MTI irrigation as the plugging occurred in 8 days of intermittent operation. The study thus, rejected the null hypothesis. The two effluents exhibited different characteristics, for example, HFCW had a higher degree of clogging (DC) and it showed a quick decline in relative discharge ( $q_{rel}$ ). Anaerobic and wetland filtration promotes accelerated MTI plugging hence further filtration is required before using the water for irrigation purposes. Period flushing can be a potential anti-foulant. The study therefore concluded that the two effluents are not suitable for MTI as they promote membrane degradation under intermittent operation.

#### 8.2.3 *Moistube soil wetting geometries*

Soil wetting geometries under sub-surface irrigation depend on irrigation technology and soil type. The study developed an empirical model that estimated the wetted width and wetted depths for two soil namely, silty clay loam and sandy soil. The two soils were deliberately selected to cover the two extremes of fine-textured and coarse-textured soils and attempt to establish the operational boundaries of the empirical model developed. The findings revealed that for fine textured soils, shallow buried depths promote capillary rise and promotes non-beneficial water loss through soil evaporation. For sandy soils, MTI lateral spacing should allow the wetting fronts to have the desired overlap. Fine textured soils can supply plant water with minimised deep percolation under MTI. The study concluded that soil texture influences the MTI wetting pattern, hence the study rejected the null hypothesis.

#### 8.2.4 *Solute movement*

The study applied the HYDRUS 2D/3D model to simulate solute movement under MTI. The model successfully simulated solute movement under the full irrigation regime (100%  $ET_c$ )

and optimal deficit irrigation (DI) regime (75%  $ET_c$ ). The extreme DI regime (55%  $ET_c$ ) showed high rates of nutrient leaching. The Partial Factor Productivity ( $PFP_N$ ) was used to assess the nitrogen use efficiency (NUE) under each irrigation regime. The  $PFP_N$  for the 100%  $ET_c$ , 75%  $ET_c$  and 55%  $ET_c$  was 1.72, 1.29, and 0.83 kg of grain.kg<sup>-1</sup> of N. This revealed that the full and optimal deficit irrigation strategies can potentially promote N utilisation and extreme deficit MTI causes leaching thus leading to yield penalties. The study therefore rejected the null hypothesis. The study concluded that HYDRUS 2D/3D is a powerful modelling tool that can be used to simulate solute fluxes under MTI. The study recommended that the experiment be done under field conditions and assess the effect of rainfall fluxes on solute movement under the variably saturated zone.

#### 8.2.5 Calibration and validation of AquaCrop

The study investigated the response of canola to varied irrigation water regimes. Canola is an industrial crop of economic importance. The model was successfully calibrated and validated for soil water content, canopy cover, biomass accumulation, final biomass, yield and water productivity under 100%  $ET_c$  and 75%  $ET_c$  irrigation regimes. The study also revealed that the 75%  $ET_c$  irrigation regime had an optimal grain yield and a relatively high water productivity ( $WP_{ET}$ ) compared to the 100%  $ET_c$  irrigation regime. This revealed that moderate deficit irrigation regimes could improve  $WP_{ET}$ . The research work concluded that AquaCrop is powerful crop modelling tool that can be used to simulate yield, biomass and water productivity for canola (*Brassica napus*) grown under full and optimal deficit MTI.

### 8.3 Recommendations

The study sought to characterise MTI, which is a relatively new irrigation technology. The following recommendations can be drawn from the study:

1. The evaporative demand study was an open-air experiment. It is recommended that the study be carried on a buried MTI lateral where actual soil matric potential forces are present.
2. Additional filtering is required for both effluents and assess the MTI plugging capacity under the respective effluents. The study recommends a continuous MTI experiment be done and assess the degree of clogging under the two effluents. Secondary to that, the study also recommends that a comparative analysis be done on the two irrigation methods (continuous vs intermittent) under the respective effluents.

3. The study recommends that the soil wetting geometry be carried under field conditions under cropped and un-cropped scenarios. The study further recommends that the experiment be carried out on an initially moist soil.
4. The study recommended that the canola be grown under open filed conditions and assess the reliability of the HYDRUS 2D/3D and AquaCrop calibration and validation results presented in this thesis. Furthermore, the study recommends that similar experiment be carried out under MTI and rainfed scenarios and gain insights on the effects of rainfall fluxes on solute movement.

#### **8.4 Statement of Originality**

This study contributed to new and additional knowledge aspect of MTI in the following aspects:

Firstly, the study induced a MTI discharge under an artificial evaporative demand ( $E_d$ ). Secondly, the study calibrated and validated an MTI empirical power function for soil wetting geometries under heavy clay and coarse sandy soils. This knowledge will aid in the design of MTI for specified soil textures. The study developed plugging coefficients for AF and HFCW effluents which can be incorporated into the MTI emitter discharge equation. The study revealed MTI solute movement in the variably saturated zone (vadose) for canola grown under different irrigation regimes. Such knowledge is essential, as it will minimise vadose zone contamination. The study provided new knowledge on the ability of MTI to satisfy various crop water requirements (CWR) under varying climatic conditions. Furthermore, the study provided insights on canola response or performance to continuous and deficit irrigation under MTI.

## 9 Appendices

### 9.1 Appendix A: Data for the computed $q_{Ave}$ values using Equation 3.7

Region	Evaporating power (ET <sub>o</sub> ) mm.d <sup>-1</sup>	Computed $q_t$ l.h <sup>-1</sup> .m <sup>-1</sup>
<b>Humid</b>	1	0.13
	2	0.28
	3	0.43
<b>Sub-Humid</b>	3.5	0.51
	4	0.58
	5	0.73
<b>Semi-Arid</b>	5.5	0.81
	6	0.88
	7	1.03
<b>Arid</b> (> 7 mm.d <sup>-1</sup> )	7.5	1.11
	8	1.18
	9	1.33
	10	1.48

## 9.2 Appendix B: R Script for DS and ABF from AF and HFCW

```

coefficients: Named num [1:2] 3.12 1.19
... attr(*, "names")= chr [1:2] "(Intercept)" "indAF"
residuals: Named num [1:31] -1.98 -2.6 -2.59 -2.47 10.18 ...
... attr(*, "names")= chr [1:31] "1" "2" "4" "5" ...
effects: Named num [1:31] -20.82 3.31 -1.97 -1.86 10.79 ...
... attr(*, "names")= chr [1:31] "(Intercept)" "indAF" "" "" ...
rank: int 2
fitted.values: Named num [1:31] 3.12 3.12 3.12 3.12 3.12 ...
... attr(*, "names")= chr [1:31] "1" "2" "4" "5" ...
assign: int [1:2] 0 1
qr: list of 5
..$ qr: num [1:31, 1:2] -5.57 0.18 0.18 0.18 0.18 ...
... attr(*, "dimnames")=List of 2
... ..$ : chr [1:31] "1" "2" "4" "5" ...
... ..$ : chr [1:2] "(Intercept)" "indAF"
... attr(*, "assign")= int [1:2] 0 1
... attr(*, "contrasts")=List of 1
... ..$ ind: chr "contr.treatment"
..$ graux: num [1:2] 1.18 1.16
..$ pivot: int [1:2] 1 2
..$ tol: num 1e-07
..$ rank: int 2
... attr(*, "class")= chr "qr"
df.residual: int 29
na.action: 'omit' Named int [1:5] 3 6 12 23 26
... attr(*, "names")= chr [1:5] "3" "6" "12" "23" ...
contrasts: List of 1
..$ ind: chr "contr.treatment"
xlevels: List of 1
..$ ind: chr [1:2] "HFCW" "AF"
call: language aov(formula = values ~ ind, data = stacked_groups1)
terms:Classes 'terms', 'formula' language values ~ ind
... attr(*, "variables")= language list(values, ind)
... attr(*, "factors")= int [1:2, 1] 0 1
... .. attr(*, "dimnames")=List of 2
... .. ..$ : chr [1:2] "values" "ind"
... .. ..$ : chr "ind"
... attr(*, "term.labels")= chr "ind"
... attr(*, "order")= int 1
... attr(*, "intercept")= int 1
... attr(*, "response")= int 1
... attr(*, ".Environment")=environment: R_GlobalEnv
... attr(*, "predvars")= language list(values, ind)
... attr(*, "dataclasses")= Named chr [1:2] "numeric" "factor"
... attr(*, "term.labels")= chr "ind"
... attr(*, "order")= int 1
... attr(*, "intercept")= int 1
... attr(*, "response")= int 1
... attr(*, ".Environment")=environment: R_GlobalEnv
... attr(*, "predvars")= language list(values, ind)
... attr(*, "dataclasses")= Named chr [1:2] "numeric" "factor"
... attr(*, "names")= chr [1:2] "values" "ind"
model: 'data.frame': 31 obs. of 2 variables:
..$ values: num [1:31] 1.14 0.527 0.537 0.653 13.303 ...
..$ ind: Factor w/ 2 levels "HFCW","AF": 1 1 1 1 1 1 1 1 ...
... attr(*, "terms")=Classes 'terms', 'formula' language values ~ ind
... .. attr(*, "variables")= language list(values, ind)
... .. attr(*, "factors")= int [1:2, 1] 0 1
... .. .. attr(*, "dimnames")=List of 2
... .. .. ..$ : chr [1:2] "values" "ind"
... .. .. ..$ : chr "ind"
... .. attr(*, "term.labels")= chr "ind"
... .. attr(*, "order")= int 1
... .. attr(*, "intercept")= int 1
... .. attr(*, "response")= int 1
... .. attr(*, ".Environment")=environment: R_GlobalEnv
... .. attr(*, "predvars")= language list(values, ind)
... .. attr(*, "dataclasses")= Named chr [1:2] "numeric" "factor"
... .. .. attr(*, "names")= chr [1:2] "values" "ind"
... .. .. attr(*, "na.action")= 'omit' Named int [1:5] 3 6 12 23 26
... .. .. attr(*, "names")= chr [1:5] "3" "6" "12" "23" ...
... attr(*, "class")= chr [1:2] "aov" "lm"

AF: num [1:18] 0.265 0.455 0.38 0.635 NA ...
anova_results: List of 14
coefficients: Named num [1:2] 2.723 0.514
... attr(*, "names")= chr [1:2] "(Intercept)" "indAF"
residuals: Named num [1:49] -2.07 -2.09 -2.26 -2.24 11.84 ...
... attr(*, "names")= chr [1:49] "1" "2" "4" "5" ...
effects: Named num [1:49] -20.97 1.8 -1.79 -1.76 12.32 ...
... attr(*, "names")= chr [1:49] "(Intercept)" "indAF" "" "" ...
rank: int 2
fitted.values: Named num [1:49] 2.72 2.72 2.72 2.72 2.72 ...
... attr(*, "names")= chr [1:49] "1" "2" "4" "5" ...
assign: int [1:2] 0 1
qr: List of 5
..$ qr: num [1:49, 1:2] -7 0.143 0.143 0.143 0.143 ...
... attr(*, "dimnames")=List of 2
... ..$ : chr [1:49] "1" "2" "4" "5" ...
... ..$ : chr [1:2] "(Intercept)" "indAF"
... attr(*, "assign")= int [1:2] 0 1
... attr(*, "contrasts")=List of 1
... ..$ ind: chr "contr.treatment"
..$ graux: num [1:2] 1.14 1.13
..$ pivot: int [1:2] 1 2
..$ tol: num 1e-07
..$ rank: int 2
... attr(*, "class")= chr "qr"
df.residual: int 47
na.action: 'omit' Named int [1:5] 3 6 8 15 41
... attr(*, "names")= chr [1:5] "3" "6" "8" "15" ...
contrasts: List of 1
..$ ind: chr "contr.treatment"
xlevels: List of 1
..$ ind: chr [1:2] "HFCW" "AF"
call: language aov(formula = values ~ ind, data = stacked_groups)
terms:Classes 'terms', 'formula' language values ~ ind
... attr(*, "variables")= language list(values, ind)
... attr(*, "factors")= int [1:2, 1] 0 1
... .. attr(*, "dimnames")=List of 2
... .. ..$ : chr [1:2] "values" "ind"
... .. ..$ : chr "ind"
... attr(*, "term.labels")= chr "ind"
... attr(*, "order")= int 1
... attr(*, "intercept")= int 1
... attr(*, "response")= int 1
... attr(*, ".Environment")=environment: R_GlobalEnv
... attr(*, "predvars")= language list(values, ind)
... attr(*, "dataclasses")= Named chr [1:2] "numeric" "factor"
... .. attr(*, "names")= chr [1:2] "values" "ind"
model: 'data.frame': 49 obs. of 2 variables:
..$ values: num [1:49] 0.65 0.63 0.46 0.485 14.565 ...
..$ ind: Factor w/ 2 levels "HFCW","AF": 1 1 1 1 1 1 1 1 ...
... attr(*, "terms")=Classes 'terms', 'formula' language values ~ ind
... .. attr(*, "variables")= language list(values, ind)
... .. attr(*, "factors")= int [1:2, 1] 0 1
... .. .. attr(*, "dimnames")=List of 2
... .. .. ..$ : chr [1:2] "values" "ind"
... .. .. ..$ : chr "ind"
... .. attr(*, "term.labels")= chr "ind"
... .. attr(*, "order")= int 1
... .. attr(*, "intercept")= int 1
... .. attr(*, "response")= int 1
... .. attr(*, ".Environment")=environment: R_GlobalEnv
... .. attr(*, "predvars")= language list(values, ind)
... .. attr(*, "dataclasses")= Named chr [1:2] "numeric" "factor"
... .. .. attr(*, "names")= chr [1:2] "values" "ind"
... .. .. attr(*, "na.action")= 'omit' Named int [1:5] 3 6 8 15 41
... .. .. attr(*, "names")= chr [1:5] "3" "6" "8" "15" ...
... attr(*, "class")= chr [1:2] "aov" "lm"

```

## 9.3 Appendix C: Irrigation Schedule

Irrigation regime	100% ET <sub>c</sub>			75% ET <sub>c</sub>			55% ET <sub>c</sub>		
	M 1	M 2	M 3	M 1	M 2	M 3	M 1	M 2	M 3
IF (days)	4.5	2.5	2.8	6.0	3.3	3.7	8.2	4.5	5.0
AT (h)	1.3	2.4	2.1	1.0	1.8	1.6	0.7	1.3	1.2

\*M = Month, IF = Irrigation frequency, and AT = Application times.